Extensional Evolution of the Central East Greenland Caledonides

by

Arthur P. White

B.A. Earth and Planetary Sciences

Harvard College, 1994

SUBMITTED TO THE DEPARTMENT OF EARTH, ATMOSPHERIC, AND PLANETARY SCIENCES IN PARTIAL FULFILLMENT OF THE REQUIREMENTS FOR THE DEGREE OF

DOCTOR OF PHILOSOPHY
AT THE
MASSACHUSETTS INSTITUTE OF TECHNOLOGY

SEPTEMBER 2001

© 2001 Massachusetts Institute of Technology. All rights reserved.

Signature of Author: _____
Department of Earth, Atmospheric and Planetary Sciences
August 17, 2001

Certified by: _____
Kip V. Hodges
Thesis Supervisor

Accepted by: _____
Ronald G. Prinn
Department Head

Lindgren

MASSACHUSETTS INSTITUTE OF TECHNOLOGY
WITHDRAWN
NOV 28 2001
FROM
MIT LIBRARIES


26°30'W
26°W
25°30'W
25°W
72°30'N
72°N
Kempes Fjord
Kong Oscars Fjord
Pohlems Dal
Segelsällskapets Fjord
Forsblad Fjord
Alpefjord
Høgedal
Tærskedal

Table of Contents

ABSTRACT

This thesis addresses the complexity of both syn- and post-orogenic extension in the overriding plate during Caledonian continental collision through field and laboratory investigations in the central East Greenland Caledonides. During the course of this work, attempts were made to answer some of the outstanding regional and local questions in East Greenland geology. Structural, U-Pb and $^{40}Ar/^{39}Ar$ geochronologic, petrographic and thermobarometric data were combined to constrain and reconstruct a portion of the tectonic history of this orogen. Most extension was accommodated along a system of orogen-parallel, N-S striking normal faults known as the Fjord Region Detachment (FRD) system. The FRD system comprises two temporally distinct, but overlapping, splays just south of 73° N. The lowermost splay is called the Høgedal detachment was active from ca. 417 to 380 Ma, and was active for a second time as recently as ca. 357 Ma. The uppermost splay is the Tindern detachment. This fault was active from ca. 425-423 Ma, exhuming material at rates as fast as ~6.5 mm/year. Continued extension in the hanging-wall of this fault accounts for additional denudation at much slower rates over a 25 my time-period. In-between activity on these faults, there is evidence to suggest that middle-crustal thickening continued to occur. Thus, the East Greenland Caledonides preserve evidence for crustal thickening (minimum ~16 km) and orogen parallel shear, followed by rapid upper-middle crustal thinning (~13 km), followed by coeval middle-crustal thickening (unknown amount) and upper-crustal thinning (~5 km), and ending with crustal collapse (~16 km thinning). This is the first time that an alternation between thrusting and normal faulting has been observed in an over-riding plate during continent-continent collision, and only the second time that it has ever been documented in a collisional orogen. The data imply that there was a fundamental cyclicity between crustal

thickening and thinning, consistent with dynamical models of orogenesis in which plate-forces responsible for contraction and gravitational forces responsible for extension, oscillate between periods where one dominates. Furthermore, given the established relationship between topography and synorogenic extension in active mountain belts, it is likely that activity along the Tindern detachment, the earliest splay of the FRD, was controlled by Caledonian paleotopography that formed during the initial stages of orogenesis. The fact that most middle- and upper-crustal extension was restricted to the FRD implies that a localized inherent crustal weakness may have developed after initial movement along the Tindern detachment. Given that late-stage Devonian activity on the FRD may have played a prominent role in the formation of the Devonian basins, which themselves likely controlled the geometry and location of subsequent Mesozoic extension and formation of the North Sea basins, the implication is that the position of rifting of the north Atlantic ocean was partially [pre-determined] inherited from the initial Caledonian paleotopography.

Acknowledgements

Until I sat down to write this section, I did not realize the shear size of the collective group of people that have contributed to the creation of this thesis. First and foremost is my advisor Kip Hodges, who conceptualized the thesis and was instrumental in every step of its creation from start to finish. Not only has Kip been accessible throughout my entire tenure at MIT, he has been both a teacher and a friend in the classroom, laboratory and field. He has excelled as a mentor and provided a stream of valuable inspiration. His honest yet constructive criticism has kept me on track along an exciting and upward learning curve.

I also thank Sam Bowring, my "academic advisor". Sam was instrumental in my coming to MIT, and has been a source of sage advice throughout my entire time here. Thanks also for the use of his laboratory facilities for U-Pb work.

This thesis would not have been possible without the logistical generosity, scientific knowledge and friendship that Arild Andresen (University of Oslo) contributed as our principle collaborator in East Greenland. And also Ebbe Hartz (both as a student and a post-doc) who provided invaluable logistical and scientific aid as well as friendship both in and out of the field.

Also, thanks to the rest of my thesis committee, Clark Burchfiel, Peter Crowley, and Nafi Toksoz for their helpful guidance and comments. I also would like to thank professors Kelin Whipple, Tim Grove, John Southard, John Grotzinger, Wiki Royden, and Rob Van der Hilst for their teaching and/or use of facilities throughout my MIT years, and Mike Williams and Mike Jercinovic for their help and the use of their laboratory at UMass Amherst.

Field work would not have been possible without the assistance of José Hurtado, Lindsay Schoenbohm, and Josh Kaufman in the field, and the generosity and support of Niels Henriksen and the Greenland Geological Survey, the Sirius Patrol, and the Danish Polar Center. While working in remote places like East Greenland, the importance of open and friendly relationships, even across the radio-waves, cannot be overstated. In this vein, I am honored to have shared science and become acquainted with the following people who enriched both the experience and the thesis, Thomas Rasmussen, "Carsten" and "Niels" (Mestersvig Radio Controllers), and all the other DPC workers and Sirius soldiers, Tormod, Bjorn, Berre, Poul Caspersen (*in memoriam*), Paul Smith, Steve

Robertson (*in memoriam*), Gordon Watt, Niels Henriksen, Synnøve Elvevold, Kristine Thrane, Johan Friderichsen, Kasper Frederiksen, Jane Gilotti, Jan Escher, Graham Leslie, Tony Higgins, Kevin Jones, Feiko Kalsbeek, other members of the Greenland Geological Survey, and members of the Cambridge Arctic Shelf Program, and Frissi and the pilots of Iceland Air.

I also wish to thank the following people for their help and advice in the laboratories at MIT: Bill Olszewski, Neel Chatterjee, Mike Kroll, Mark Martin, Kathy Keefe, Jahan Ramezani, Greg Hoke.

Perhaps most important during the entire learning process at MIT, are the other graduate students who made the past 5 years fun and altogether formed an invaluable resource of knowledge. This includes of course, the "gang-of-four": José Hurtado, Eric Kirby and Noah Snyder. Also, Kip's other students: Anke Friedrich, Audrey Huerta, José Hurtado, Karen Viskupic, Jeremy Boyce, Cam Wobus. And all the rest of the wonderful graduate students that I overlapped with that make MIT such a terrific place: Simon Brocklehurst, Sinan Akciz, Lindsay Schoenbohm, Julie Baldwin, Mark Schmitz, Jenny Matzel, Dave Hawkins, Kirsten Nicolaysen, C.J Northrup, Jim Van Orman, Odin Smith, Steve Parman, Steve Singletary, John Thurmond, Marin Clark, , Shane Pelachety, Chris Studnicki-Gizbert, Blair Schoene, Ben Crosby, Steve Dibenedetto, Bill Lyons, Peter Dodds, Frederik Simons, Hrafnell Karason, Mark Behn (I apologize if I have left anybody out inadvertently).

Last but most importantly, I wish to thank my family. This includes my extremely patient, and lovely wife (as of August 4th, 2001), Inna Raiskin White. Having met during Spring break of the first year of graduate school, she has been patiently making the New York-Boston commute every other weekend for the past 4 years. I could not have completed this thesis without her love and support, and her dedicated reminder that "there is life outside of school", and the deadline of our marriage which came just 2 weeks after the thesis defense. Now we have to go to Greenland together.

And finally, my parents, Joan and Donald White, who instilled in me a sense of curiosity and a desire for adventure which has fueled my scientific interest, as well as the support and discipline to complete this project. Thanks Mom and Dad for always being with me through the adventures.

Funding for this study was provided by National Science Foundation grant EAR 930072 (to K.V. H.).

1. INTRODUCTION

The iconoclastic identification of large extensional faults in the central East Greenland Caledonides during the 1970s-90s (e.g. Caby, 1976; Hartz and Andresen, 1995; McClay et al., 1986), permanently altered the way in which geologists view the evolution of this orogen, and established a new set of geological problems related to orogenic deformation in the over-riding plate during oblique continental collision. Already well known for its unrivaled exposures that span a wide breadth of structural levels, the East Greenland Caledonides provide an unusual opportunity to examine the development of extensional structures that formed both during and after orogenesis. This is because there are multiple, well-defined generations of normal faults interspersed with fabrics and features related to crustal thickening. These are preserved at a variety of structural levels that deform or are cross-cut by granitic rocks and are associated with metamorphic rocks with mineral assemblages that are suitable for geochronology and metamorphic petrology. At the time this thesis was conceptualized, it had just been discovered that the most prominent N-S striking Caledonian fault system was not a thrust, but rather a normal fault (Hartz and Andresen, 1995). This finding was important because it indicated that the role of extension during deformation of the over-riding Laurentian plate, as it collided with Baltica, might be more significant than previously suspected. Given the growing interest among Earth scientists to better understand the complexities of continent-continent collision, this thesis focuses on resolving a portion of the syn- and post-orogenic deformation preserved in East Greenland in order to contribute to and refine our overall understanding of the multitude of processes that govern collisional orogenesis.

The original motivation for this work was to test the application of dynamical models developed in the Himalayas where the interactions between contractional and extensional deformation have been well documented (e.g. Burchfiel and Royden, 1985; Burchfiel et al., 1992; Hodges et al., 1996). There, it had been proposed by Hodges (1998) that a constantly evolving balance between the plate-forces that drive crustal thickening and the gravitational forces that drive crustal thinning, resulted in alternating episodes of thrusting and normal faulting during continental collision. This model predicts several testable hypotheses (see appendix for details in original proposal): first, there must be synorogenic normal faulting; in addition, there is an expected relationship between anatexis, leucogranite formation and faulting based on our understanding of melt formation with respect to the increasing amount of radioactive heat production during crustal thickening and dehydration reaction melting during crustal thinning; furthermore, there are characteristic pressure-temperature-time histories associated with different portions of the crust depending on the structural position with respect to the contractional and extensional faults; finally, there ought to be evidence for alternating episodes of thrusting and normal faulting during continental collision.

Bearing this in mind, the investigations of this thesis began with defining the various distinguishable episodes of extensional faulting associated with the principal Caledonian normal fault system in central East Greenland, known as the Fjord Region Detachment (Andresen et al., 1998). The next step was to determine absolute age constraints on the timing of this deformation in order to place these events into a tectonic context with respect to the Baltica-Laurentia collision. Having constrained the timing of deformation, an effort was made to quantify the amount of tectonic exhumation attributable to the various modes of crustal thinning using a combination of P-T and structural data. The final results of these analyses were used to reconstruct the tectonic

evolution of extension in the central East Greenland Caledonides; and in so-doing, to document when extensional activity was important with respect to crustal thickening during orogenesis and what role extension may have played.

The thesis includes work from four separate projects that are presented in five chapters, written as papers intended for submission to professional journals. As such, there is some overlap from chapter to chapter. This material represents the ongoing accumulation of results from research over the past 5 years. An evolving progression of thought is evidenced from chapter to chapter as iteration between annual field-season and laboratory investigations took place. However, the four projects build upon each other to support the final tectonic model that is presented in Chapter 6.

The Forsblad Fjord region (72.5° N) was chosen for the site of the field work because it provides a natural transect perpendicular to the orogen that penetrates from the basement Archean-Paleoproterozoic orthogneisses through the Neoproterozoic sedimentary rocks that comprise the Eleonore Bay Supergroup and the overlying Devonian conglomerates. This transect forms a natural cross-section that cuts both the lowermost splay of the Fjord Region Detachment (Høgedal detachment), and the uppermost splay (Tindern detachment), permitting access to a near-complete middle- and upper-crustal Caledonian section exposed in central East Greenland.

Outline of chapters 2 through 6

The work in Chapter 2 serves to establish a sequence of deformation in each of the three allochthons juxtaposed by movement along the Fjord Region Detachment. From west to east and structurally lowest to highest, these are the Hagar Niggli-Spids, Høgedal and Tindern allochthons. The principle goal of this project was to determine the relative

timing of deformational fabrics that developed at amphibolite facies in the Høgedal allochthon, including structures that formed during E-W contraction and N-S orogen parallel shear, as well as E-W extension along the Tindern detachment. Results from U-Pb geochronology on monazite from granitic material used to bracket the timing of this activity indicate that the two modes of deformation were coeval (ca. 425 Ma) within the resolution of the geochronology. Given that the Baltica-Laurentia collision is not thought to have ceased until ca. 402 Ma (Fossen and Dallmeyer, 1998) these new data indicate that extension was synkinematic with respect to orogenic activity. An additional, important finding was circumstantial evidence for an underlying thrust fault that placed the Høgedal allochthon on top of the Hagar Niggli-Spids allochthon sometime after movement on the Tindern detachment and prior to movement on the Høgedal detachment.

Building upon the U-Pb geochronology, Chapter 3 presents results of $^{40}Ar/^{39}Ar$ geochronology of muscovite, biotite, K-feldspar and pseudotachylite from samples that extend across the Høgedal allochthon, and include the footwall of the Høgedal detachment and the hanging-wall of the Tindern detachment. Three important findings came out of this work. First, the muscovite data serve to constrain deformation along the Tindern detachment at temperatures above ca. 450° C, to have been short lived from ca. 425-423 Ma. This is a critical constraint because the field evidence indicates that the majority of deformation along this fault was ductile, and therefore occurred over that 2 million year interval. In addition, the biotite data combined with K-feldspar data indicate that the Høgedal detachment was active between ca. 417 and 380 Ma. Moreover, *in situ* UV laser microprobe data on pseudotachylite from this shear zone indicate that it was reactivated as recently as ca. 357 Ma. Altogether, these findings are important because they indicate extension was partitioned along two discrete, overlapping faults that were

active during at least two separate time-intervals, syn- and post-orogenic with respect to the Baltica-Laurentia collision. As opposed to previously reported data that was interpreted to suggest the FRD was active continuously for ca. 80 million years, the new data imply that discrete episodes of extension could have been separated by as many as 60 million years.

Having established that the Tindern and Høgedal detachments were far from coeval, the next goal was to quantify the amount of displacement along these faults. Chapter 4 presents the results of petrographic observations and semi-quantitative constraints from the petrogenetic grid combined with quantitative thermobarometry using the geothermometer GARB (Ferry & Spear, 1978) and the geobarometer GASP (Ghent, 1976). Having first established a sequence of metamorphism, these data were interwoven with the deformational data and placed into a tectonic context. The results were used to reconstruct a pressure-temperature history of rocks from the Krummedal Sequence at a variety of structural levels within the footwall of the Tindern detachment. The data follow a clockwise loop in P-T space. Assuming a lithostatic gradient of 250 b/km, the data indicate that initial burial of at least ~16 km was followed by exhumation at rates approaching ~9 millimeters of denudation per year. Roughly 18 km of exhumation was accommodated by the TD and various hanging wall splays investigated in Chapter 5. By combining these new data with previously published results (Vold, 1997), tectonostratigraphic throw on the Høgedal detachment was also estimated to be ~16 km.

The next logical step was to place this pressure-temperature history into a temporal context. The geochronologic data from Chapters 2 and 3 were sufficient to constrain most of the P-T path; however, no previously reported geochronologic data constrained the earliest deformation and metamorphism in the Krummedal Sequence.

Previous workers have suggested that these early events could be attributed to the Grenvillian orogeny (e.g. Kalsbeek *et al.*, 1998; Thrane *et al.*, 1999; Watt & Thrane, 1999); however, this is inconsistent with the rest of the geochronologic data from the Høgedal allochthon. For this reason, Chapter 4 introduces new, *in situ,* preliminary U-Pb-monazite chemical ages (determined with an electron microprobe) from armored inclusions in the earliest phase of garnet growth that pre-dates the earliest deformational fabrics. Despite some calibration issues, these data leave no doubt that this early metamorphism occurred during Caledonian orogenesis.

The final project focused on the role of upper crustal extension during Caledonian orogenesis. In particular, Chapter 5 presents new structural observations from the hanging wall of the Tindern detachment, which preserves multiple generations of W-dipping normal faults that are antithetic to the dip of the main E-dipping shear zones that comprise the FRD normal-fault system. Retro-deformed cross-sections are used to indicate that the Tindern allochthon underwent an additional 22% extension (5 km of thinning, or 1/7 of the exhumation on the FRD system) as a result of movement along these faults. Furthermore, new $^{40}Ar/^{39}Ar$ data from K-feldspar was utilized to constrain the timing of these structures. Time-temperature models of ^{39}Ar loss during step-heating experiments suggest that tectonic denudation was associated with steady cooling from ca. 420 to ca. 400 Ma. These results indicate that 13 km of tectonostratigraphic throw on the Tindern detachment occurred rapidly from ca. 425 to 423 Ma, while a remaining 5 km of exhumation was accomplished over ca. 25 million years.

Altogether, the data from these four projects provide the basis for proposing a new tectonic model that describes the evolution of extensional deformation in the central East Greenland Caledonides. Chapter 6 outlines this model, and focuses on two of the

important implications of the overall work that may be of universal interest. The first is a demonstrable cyclicity between crustal thickening and thinning in the central East Greenland Caledonides. Not only are both syn- and post-orogenic extensional structures present in East Greenland, but there is a clear alternation between significant episodes of thrusting and normal faulting during orogenesis. Furthermore, the data indicate that upper crustal extension and middle crustal thickening were coeval during the latter part of orogenesis.

In addition, the established links between topography and upper crustal extension in active mountain belts are used to suggest that the location of the Tindern detachment may have been related to paleotopography. Furthermore, the fact that much of the middle and upper crustal extension in the East Greenland Caledonides reactivated portions of the Tindern detachment implies that the initial topography formed during orogenesis may have played a crucial role in controlling the geometry and location of subsequent extensional deformation. This includes the formation of the Devonian basins, which themselves played an integral role in determining the geometry of the Mesozoic North Sea basin formation (McClay et al., 1986). Thus, the location of crustal anisotropies that led to rifting in the North Atlantic ocean may be an inherited effect, left over from Caledonian paleotopography.

The following five chapters have been written for publication in journals. Co-authors are listed on the first page of each chapter. Chapter 2 has been accepted by the International Journal of Earth Science, Chapter 3 has been submitted to Tectonics. Chapter 4 is intended to be submitted to the Journal of Metamorphic Geology, Chapter 5 is for the Journal of Geology, and Chapter 6 is for Geology.

References:

Andresen, A., Hartz, E.H., and Vold, J., 1998, A late orogenic extensional origin for the infracrustal gneiss domes of the East Greenland Caledonides (72-74 N): Tectonophysics, v. 285, p. 353-369.

Burchfiel, B.C., and Royden, L.H., 1985, North-south extension within the convergent Himalayan region.: Geology, v. 13, p. 679-682.

Burchfiel, B.C., Zhiliang, C., Hodges, K.V., Yuping, L., Royden, L.H., Changrong, D., and Jiene, X., 1992, The South Tibetan detachment system, Himalayan Orogen; extension contemporaneous with and parallel to shortening in a collisional mountain belt: Special Paper - Geological Society of America, v. 269, p. 41.

Caby, R., 1976, Tension structures related to gliding tectonics in the Caledonian superstructure of Canning Land and Wegener Halvø, central East Greenland: Rapport Grønlands geologiske Undersøgelse, v. 72, p. 1-24.

Ferry, J.M., and Spear, F.S., 1978, Experimental calibration of the partitioning of Fe and Mg between biotite and garnet.: Contrib. Mineral. Petrol., v. 66, p. 113-117.

Fossen, H., and Dallmeyer, R.D., 1998, (super 40) Ar/ (super 39) Ar muscovite dates from the nappe region of southwestern Norway; dating extensional deformation in the Scandinavian Caledonides: Tectonophysics, v. 285, p. 119-133.

Ghent, E.D., 1976, Plagioclase-garnet-Al2SiO5-quartz: a potential geobarometer-geothermometer: Am. Min., v. 61, p. 710-714.

Hartz, E., and Andresen, A., 1995, Caledonian sole thrust of central East Greenland: A crustal-scale Devonian extensional detachment?: Geology, v. 23, p. 637-640.

Hodges, K.V., Parrish, R.R., and Searle, M.P., 1996, Tectonic evolution of the central Annapurna Range, Nepalese Himalayas: Tectonics, v. 15, p. 1264-1291.

Hodges, K.V., Treloar, P.J.e, and O'Brien, P.J.e, 1998, The thermodynamics of Himalayan orogenesis: What drives metamorphism and metamorphic relations?: Geological Society Special Publications, v. 138, p. 7-22.

Kalsbeek, F., Nutman, A.P., and Jepsen, H.F., 1998, Granites in the Caledonian fold belt, East Greenland, *in* Frederiksen, K.S., and Thrane, K., eds., Symposium on

Caledonian geology - abstract volume, Volume 46: Denmark, Danmarks og Grønlands Geologiske Undersøgelse Rapport, p. 43-44.

McClay, K.R., Norton, M.G., Coney, P., and Davis, G.H., 1986, Collapse of the Caledonian orogen and the Old Red Sandstone: Nature, v. 323, p. 147-149.

Thrane, K., Kalsbeek, F., and Watt, G.R., 1999, Evidence for a Grenvillian event in the East Greenland Caledonian fold belt, *in* Frederiksen, K.S., and Thrane, K., eds., Second symposium on East Greenland geology, mainly Caledonian: Abstract volume, Volume 21: Denmark, Danmarks og Grønlands Geologiske Undersøgelse Rapport, p. 64.

Vold, J., 1997, Et studie av den tectonomatemorphe utviklingen av gneisserne i liggblokken til "The Fjord Region Detachment Zone" på Kap hedlund, sentrale Øst Grønland [Cand. Scient Thesis]: Oslo, University of Oslo.

Watt, G.R., and Thrane, K., 1999, The nature of the Grenvillian orogeny in central East Greenland, *in* Frederiksen, K.S., and Thrane, K., eds., Second symposium on East Greenland geology, mainly Caledonian: Abstract volume, Volume 21: Denmark, Danmarks og Grønlands Geologiske Undersøgelse Rapport, p. 64.

Geologic constraints on middle-crustal behavior during broadly synorogenic extension in the central East Greenland Caledonides

Arthur P. White*, Kip V. Hodges*, Mark W. Martin*, Arild Andresen**

** Department of Earth, Atmospheric and Planetary Sciences, Massachusetts Institute of Technology, Cambridge, MA, 02139,USA. apwhite@mit.edu tel (617)-253-8445 fax (617) 252-1800*

*** Department of Geology, University of Oslo, P.O. Box 1047, Blindern, 0316 Oslo, Norway (47) 22856689*

Abstract

Structural and U-Pb geochronologic data from the Forsblad Fjord area of East Greenland (72° 30' N) indicate close spatial and temporal ties between orogen-parallel shear and extensional deformation during Caledonian orogenesis. This territory is composed of three tectonostratigraphic units separated by two splays of the Fjord Region Detachment System (FRDS), a principal extensional fault system of the East Greenland Caledonides that was active in Silurian time. The oldest Caledonian fabrics in Forsblad Fjord, which developed at upper amphibolite facies metamorphic conditions, indicate that there was north-south, lateral extrusion of ductile middle-crustal material synchronous with approximately east-west shortening. U-Pb dating of synkinematic granitic leucosomes in migmatitic schists and gneisses demonstrates that this process was underway at ca. 425 Ma. Subsequently, east-west extension along the two splays of the FRDS truncated the older fabrics; the structurally highest of these shear zones – the Tindern detachment – was active as early as ca. 424 Ma. This implies either that there was a rapid transition from Caledonian shortening and possible transpressional

deformation to post-orogenic collapse, or our preferred interpretation that extension was synorogenic.

The FRDS shares many structural characteristics with the South Tibetan Detachment System of the Cenozoic Himalayan orogen but exhibits two important differences. First, while the South Tibetan system developed in the down-going Indian plate during India-Eurasia collision, the Fjord Region system developed in the overriding Laurentian plate during the collision of Laurentia with Baltica. Second, whereas the exposed extensional structures in the Himalaya developed in the upper crust and are only inferred to have extended to deeper levels, those in the Forsblad Fjord area were demonstrably active at middle-crustal levels. Evidence for broadly coeval extension and contraction at different structural levels in both mountain belts emphasizes the general importance of crustal decoupling in the collisional orogenic process, and implies that synorogenic extensional deformation is not strictly an upper crustal phenomenon.

Introduction

Extensional structures formed during collisional orogenesis provide important insights into the processes that build and destroy mountains. For example, evidence of contemporaneous thrusting and normal faulting in the Himalaya has been attributed to the episodic, gravitational collapse of high topographic gradients formed during the India-Eurasia collision (Burchfiel et al., 1992; Hodges et al., 1996). This type of extension, distinctive from post-orogenic collapse (Dewey, 1988), may occur anytime after the initial onset of crustal thickening once a critical thickness has been achieved. In a simplified model, extensional faults are triggered in the upper crust when local gravitational potential energy gradients, driven by changing topographic relief, reach

critical values such that vertical body forces due to gravity exceed horizontal deviatoric stresses applied by the converging plates (Burchfiel and Royden, 1985). Additional factors — such as changes in crustal rheology caused by variations in composition and temperature, as well as rates of plate convergence — can affect this transition. Given that the compressional stress regime associated with plate convergence during orogenesis is transferred laterally beyond areas of localized, upper-crustal extension as demonstrated in 2-sided orogens like the Himalayan-Tibetan system, lower-crustal contraction and upper-crustal extension must be decoupled at some unknown depth. Unfortunately, our understanding of this process is limited by the narrow spectrum of observational evidence that is available. Current models of synorogenic extension have been significantly influenced by Himalayan studies (e.g. Burchfiel and Royden, 1985; Burchfiel, 1990; Hodges, 2000; Hurtado et al., 2001), which have revealed a large component of orogen-perpendicular normal faulting. At present, an extensive system of N-dipping normal faults termed the South Tibetan Detachment System remains both the type-example and the primary evidence for these kinds of decoupling zones. Despite the fact that scientists have proposed similar models for synorogenic extension in other places, such as the Grenville and Variscan orogens (e.g. Mezger et al., 1991; Inger et al., 1994; Vanderhaeghe et al., 1999), more direct observations in other orogens are necessary to improve our understanding of the process.

The East Greenland Caledonides provide an excellent opportunity to examine middle-crustal levels of an overriding plate in a collisional orogen. As suggested by other researchers (e.g. Jain et al., 1991; Andersen et al., 1998; Hartz, 1998), the Caledonian orogen, produced by convergence between Baltica and Laurentia, has regional dimensions and geometries similar to those of the modern Himalayan-Tibetan system; in which case, the Kunlun or Tian Shan mountains on the north side of the plateau might be

analogous to orogenic activity preserved in East Greenland. Erosion and tectonic denudation over the past 425 Ma have exposed large tracts of high-grade metamorphic rocks in East Greenland, which preserve middle-deep crustal structures formed during Caledonian orogenesis.

The E-W-trending Forsblad Fjord transect (72° 30' N) exposes a tilted, yet relatively simple tectonic stratigraphy that consists of three distinct allochthons of regional extent that are separated by E-dipping faults. From west to east, and structurally lowest to highest, we term them the Hagar-Niggli Spids allochthon, the Høgedal allochthon, and the Tindern allochthon (Plate 1a). Although Higgins et al. (1981) proposed that these allochthons were emplaced by westward thrusting, Hartz and Andresen (1995) and Andresen et al. (1998a), have interpreted the kinematic indicators in the shear zone separating the Hagar-Niggli Spids and Høgedal allochthons as a record of top-to-the-east displacement relative to present-day horizontal. Given that the hanging wall in the northward continuation of this fault consists of upright, E-dipping Neoproterozoic sedimentary rocks, they argue from their kinematic reinterpretation and the juxtaposition of young on old rocks that this was a normal fault.. In this paper, we focus on the Høgedal allochthon and its upper bounding fault contact; this allochthon preserves evidence for having undergone amphibolite facies metamorphism that was synkinematic with early N-S flow and E-W shortening. These shortening structures were subsequently overprinted by structures related to E-W extension on the Fjord Region Detachment System (FRDS). Monazite and xenotime U-Pb dates for igneous and metamorphic rocks are used to constrain the timing of these deformational events and the temporal relationship between orogen parallel flow, contraction and extension.

Geologic Setting: Scandinavian and East Greenland Caledonides

Paleomagnetic evidence suggests that the continental landmass of Baltica collided into that of Laurentia with a component of counterclockwise rotation during the Middle to Late Silurian (Torsvik et al., 1996); this led to the development of the North Atlantic Caledonides. Whilst Baltica is thought to have been the down-going plate during collision (Gee, 1975; Sturt and Thon, 1978; Hodges et al., 1982; Henriksen, 1985; Andresen and Steltenpohl, 1994), large-displacement deformational structures were developed in both plates; fold and thrust belts verge eastwards in Scandinavia and westwards in East Greenland (Figure 1). In addition to the well-known Caledonian shortening features, detailed field studies in western Norway and eastern Greenland have led to the identification of major normal-sense faults and shear zones of Caledonian and post-Caledonian age (e.g. Andersen and Jamtveit, 1990; Cashman, 1990; Fossen and Rykkelid, 1992; Fossen et al., 1992; Northrup and Burchfiel, 1993; Gee et al., 1994; Rykkelid and Andresen, 1994; Hartz et al., 1994; Fossen and Holst, 1995; Hartz and Andresen, 1995; Northrup, 1997; Hartz and Andresen, 1997; Andresen et al., 1998a; Andersen et al., 1998; Fossen, 2000; Hartz, 2001; Strachan et al., In Press). Mapping in the East Greenland Caledonides from 1935 to 1958 revealed Archean-Paleoproterozoic basement complexes structurally overlain by nappes of Mesoproterozoic-Neoproterozoic metasedimentary rocks, Neoproterozoic sedimentary rocks, and Devonian-Carboniferous basin sequences (Figure 1), all of Laurentian affinity (e.g. Koch and Haller, 1971; Haller, 1971; Higgins et al., 1981; Peucat et al., 1985; Henriksen, 1985). The metamorphism and deformation of these N-S trending structures has been attributed to multiple events ranging from Proterozoic to Middle Paleozoic (Caledonian) age (e.g. Backlund, 1930; Wegmann, 1935; Haller, 1970; Henriksen and Higgins, 1976; Rex et al., 1976; Rex and Gledhill, 1981). Important thrust faults have been remapped recently north of the study

area by Leslie and Higgins (1999) in Eleonore Sø and Målebjorg and by Escher and Jones (1999) in Niggli Spids, as well as south of the study area in Charcot Land and Gåseland (mapped by the Greenland Geological Survey and appearing on the map by Christoffersen, 1984). These faults surround tectonic windows (Figure 1) that contain Early to Middle Proterozoic basement crystalline rocks. It is probable that the thrusts in the north may be correlated with thrusts in the south and projected beneath the ice cover west of our study area ca. 72° 30'. In addition to shortening structures, there is an important family of N-S striking, E-directed normal faults known as the Fjord Region Detachment System (FRDS) (Hartz and Andresen, 1995; Andresen et al., 1998a). Mapped most extensively in Kajser Franz Joseph Fjord, Kempes Fjord and Forsblad Fjord (e.g. Hartz and Andresen, 1995; Vold, 1997; White et al., 1998; Rasmussen and Andresen, 1998; Escher and Jones, 1999), it is reported that these ductile shear zones are overprinted by geometrically similar brittle fault surfaces, consistent with exhumation under decreasing temperature conditions. Aside from the juxtaposition of greenschist facies metamorphism in the hanging wall with amphibolite facies metamorphism in the footwall, there are no quantitative constraints on the amount of displacement along these faults.

Local Tectonostratigraphy

The study area (Figure 1, Plate I) may be subdivided into three tectonostratigraphic units separated by east-dipping extensional shear zones of the FRDS. Rocks of the lowest package have been mapped traditionally as amphibolite and granulite facies gneisses of the Gletscherland Complex, those of the middle package as amphibolite facies metasedimentary rocks of the Krummedal Sequence, and those of the upper package as lower amphibolite facies to unmetamorphosed units of the Eleonore

Bay Supergroup (Haller, 1971; Henriksen, 1985). Progressively deeper structural levels are exposed from east to west along Forsblad Fjord; unfortunately, the substratum of the Gletscherland Complex is covered by the Inland Ice of Greenland. Comparisons with the tectonostratigraphy farther north, however, suggests that the Gletscherland Complex at Forsblad Fjord correlates to other Archean/Paleoproterozoic rocks in the Niggli Spids and/or Hagar thrust sheets mapped by Escher and Jones (1999) at latitudes ca. 73°N. For this reason, we refer to the structurally deepest tectonostratigraphic unit in Forsblad Fjord as the Hagar-Niggli Spids allochthon. We introduce local names for the two splays of the FRDS exposed in the area: the lowest, separating the lower and middle tectonostratigraphic packages, is the Høgedal detachment, and the shear zone separating the middle and upper packages is the Tindern detachment. Following standard convention, the middle and upper tectonostratigraphic packages are named the Høgedal and Tindern allochthons (respectively) after their underlying fault zones.

Hagar-Niggli Spids allochthon

The crystalline rocks of the Hagar-Niggli Spids allochthon are exposed only on the western edge of the study area. This composite of orthogneisses, paragneisses, and amphibolites is characterized in Forsblad Fjord by extensive migmatization and amphibolite facies metamorphism. Amphibolites, rich in hornblende ± biotite, occur both as concordant lenses and discordant dikes. Foliated and folded leucocratic gneisses cut across the darker hornblende and hornblende-biotite gneisses (Higgins et al., 1981). The Gletscherland Complex which reaches a structural thickness of at least 5 km at the inner end of Forsblad Fjord, is unconformably overlain to the north and west by packages of supracrustal rocks (Haller, 1971; Henriksen and Higgins, 1976) while the eastern contact is defined by the Høgedal detachment.

Rb-Sr whole rock "ages" were interpreted to suggest that the amphibolite facies metamorphism in this unit was as old as the Late Archean and Paleoproterozoic, ca. 2450 to 1705 Ma (Rex et al., 1976; Rex et al., 1977; Rex and Gledhill, 1981). The same researchers inferred from their Rb-Sr and K-Ar data that these rocks experienced low temperature Caledonian thermal overprinting (but not regional metamorphism) from the Middle Ordovician to the Early Carboniferous. Zircon U-Pb dates from Thrane et al. (1999a) support a protolith age ca. 3000-2500 Ma followed by Paleoproterozoic metamorphism ca. 1800-1700 Ma. An additional Pb-Pb age of 1600 Ma was published by Rasmussen and Andresen (1998) for porphyroblastic allanite growing in rocks from the uppermost Gletscherland Complex.

Høgedal allochthon

The Høgedal allochthon, with an estimated structural thickness in Forsblad Fjord of ca. 11 km, is composed of the Krummedal Sequence, amphibolite facies, banded biotite-garnet-sillimanite/kyanite gneisses with secondary garnet- and hornblende-bearing calc-silicate lenses and garnet amphibolite lenses. Compositional layering strikes north-south and dips moderately to steeply eastward. No primary sedimentary features are preserved. From north to south, there is variation in the composition of gneisses. In the Forsblad Fjord transect, the sequence is rich in biotite-garnet-sillimanite/kyanite-pelitic schists and gneisses. Just to the south, in Schaffhauserdalen, exposures are more psammitic, with significantly more quartz and fewer metamorphic index minerals.

Previous Rb-Sr dates from this sequence suggested a Middle to Late Proterozoic age (ca. 1245 Ma to 750 Ma) for deformation and amphibolite facies metamorphism (Rex et al., 1976; Rex et al., 1977; Rex and Gledhill, 1981). These authors suggested that scatter in their data was related to Caledonian metamorphism and plutonism based on a

ca. 430 Ma Rb-Sr errorchron obtained from a concordant leucogranite sill. Support for this interpretation comes from recently obtained zircon U-Pb SHRIMP data from similar metasedimentary rocks outside of the study area (e.g. Thrane et al., 1999a; Watt and Thrane, 1999). Within Forsblad Fjord, an upper intercept date of 995 Ma from discordant zircon U-Pb analyses by Andresen et al. (1998b) suggests that at least some magmatic activity occurred during the Middle Proterozoic. These authors also published a U-Pb age of ca. 425 Ma for a presumably metamorphic monazite from a metapelitic rock collected from the Høgedal allochthon in Forsblad Fjord.

Tindern allochthon

The Tindern allochthon comprises a very thick sequence of generally east-dipping sedimentary and metasedimentary rocks. The basal part of the section (at least 3km-thick) includes chlorite-biotite-garnet bearing schists and phyllites, with interstratified garnet-amphibole bearing calc-silicate rocks. Although Smith and Robertson (1999) reported the presence of sillimanite porphyroblasts in metapelitic rocks near the base of the section, we cannot corroborate their observation. The grade of metamorphism decreases progressively upward as the metasedimentary rocks give way to a thick (> 6km) succession of interlayered siltstones, sandstones and mudstones of the predominately Proterozoic (post-Riphean) Nathorst Land Group (Vidal, 1976; Vidal, 1979), which represents the lower of the two groups comprising the Eleonore Bay Supergroup (Sønderholm and Tirsgaard, 1993; Smith and Robertson, 1999). Whether the basal metasedimentary rocks are part of the Eleonore Bay succession or a low-grade stratigraphic equivalent of the Krummedal Sequence is unknown. However, three observations lead us to join Smith and Robertson (1999) in assigning these rocks to the lowermost Nathorst Land Group. First, unlike the Krummedal Sequence rocks of the

Høgedal allochthon, these rocks preserve primary sedimentary structures, such as cross-beds, similar to those found in the overlying Nathorst Land Group units. Second, the Krummedal Sequence is rich in amphibolite lenses whilst these rocks have none. Finally, the medium-grade metamorphism of the metasedimentary rocks is most likely to be a local phenomenon related to the intrusion of one large granitic pluton and a stockwork of meter- to decameter-thick granitic pegmatites and aplites in the immediate hanging wall of the Tindern detachment.

Granitic Rocks

A variety of dikes, sills and plutons of different ages are found in the Forsblad Fjord area. The oldest of these are foliated, biotite-granite sheets that intruded sub-parallel to the compositional layering of the Høgedal allochthon. On the basis of field relations and the preliminary Middle Proterozoic, U-Pb zircon age of Andresen et al. (1998b) for one of these intrusions, they are interpreted to be pre-Caledonian. However, our U-Pb geochronologic data (presented below) suggest that most of the granitic rocks in the Høgedal and Tindern allochthons are of Caledonian age. They comprise four categories: centimeter-scale, anatectic leucosomes in the Krummedal Sequence, concordant to the regional foliation; centimeter-scale leucosomes discordant to the dominant schistosity of the Høgedal allochthon; a variably deformed, foliated granite pluton (Caledonia Ø Granite) which intruded synkinematically into the Tindern detachment (discussed below); and an undeformed two-mica leucogranite pluton (Klosterbjerg Granite) which intruded into the base of the Nathorst Land Group. There are also late Caledonian pegmatite and pegmatite-aplite dikes and sills that transect regionally prominent structural fabrics in the Krummedal Sequence, the lowermost Nathorst Land Group, and older granitic plutons.

Centimeter-scale, medium grained leucosomes, concordant to the regional schistosity, are common within the Krummedal Sequence. These bodies are uniformly white to light gray in hand sample. Their principle mineralogy consists of plagioclase + K-feldspar + quartz + muscovite ± biotite ± garnet ± fibrous sillimanite. The preservation of magmatic crystallization and melt segregation textures in these rocks are indicative of *in-situ* anatexis (Figure 2a). Preliminary unpublished PT data from garnets that grew synkinematically with respect to these deformational fabrics indicates prograde garnet growth (at conditions up to ca. 725° C at 9 kBar using the GARB-GASP thermobarometers; White and Hodges, manuscript in preparation).

The leucosomes that cut across the regional schistosities are conspicuously undeformed. These centimeter-scale, medium-grained stringers of granite attest to the mobilization of some anatectic melts. Compared to the concordant leucosomes, they have less muscovite and contain no sillimanite. Their micas have no preferred orientation; and no garnet is present.

On a much larger scale, the Caledonia Ø Granite intruded synkinematically into the high strain zone between the Høgedal and Tindern allochthons. The pluton has a sheet-like geometry and ranges up to several kilometers in thickness. It separates the migmatitic Krummedal Sequence from the low-grade Eleonore Bay Supergroup. This pluton is characterized by extreme strain heterogeneity; some outcrops display only magmatic crystallization textures, while others exhibit solid state, ductile deformational fabrics. Constituent minerals include K-feldspar + plagioclase + chlorite + muscovite ± biotite ± cordierite. In places, the K-feldspar forms megacrysts up to 10 cm across. Most outcrops contain schlieren of altered biotite-rich, melanocratic rocks that probably represent autoliths or partially consumed xenoliths of the pluton's host rocks.

Even more regionally extensive is a two-mica leucogranite pluton, the Klosterbjerg Granite, that is restricted to the base of the Tindern allochthon. This granite is similar to other plutons that have been mapped at the base of the Eleonore Bay Supergroup outside of the study area. These plutons were regarded collectively as representing a regionally extensive batholith by Haller (1970). Light gray in color with an equigranular medium to coarse grained matrix, this granite bears superficial resemblance to undeformed regions of the Caledonia Ø Granite, although it contains none of the xenoliths that are common in the other pluton. The contact (Tindern detachment) between the two granites is very subtle when viewed from a distance, and difficult to reach on foot, which may explain why past workers thought the Tindern detachment was obscured by a large granite intrusion (Higgins et al., 1981). The contact is marked by a sudden change from solid-state ductile deformation fabrics in the Caledonia Ø Granite of the footwall to magmatic crystallization fabrics in the Klosterbjerg Granite of the hanging wall, The Klosterbjerg Granite contains the assemblage K-feldspar + plagioclase + quartz + muscovite + biotite. Published dates for this and similar plutons range from Late Ordovician to Early Silurian (e.g. Rex and Gledhill, 1981; Andresen et al., 1998b; this paper).

Structural Geology

Each of the three tectonostratagraphic units exposed in the study area experienced separate and distinct thermal and deformational histories. We use the following terminology for describing structures. Deformational phase (D) is based on relative age determined whilst in the field. To indicate this, we append a D number to each structure: fold (F); schistosity (S); lineation (L). We append a N (Hagar-Niggli Spids allochthon), H (Høgedal allochthon) or T (Tindern allochthon) to the numbering scheme to distinguish

which allochthon is associated with the structure. Therefore, a fold associated with the first phase of deformation in the Høgedal allochthon would be recorded as F_{1H}. Appended to this paper are both a geologic and a structural map of the study area (Plate 1.) These structural relationships are discussed in order from lowest structural allochthon in the west to highest in the east.

Hagar-Niggli Spids allochthon and fault contact with Høgedal allochthon

Since the Gletscherland Complex lies just on the edge of the study area, our observations were limited to reconnaissance trips. Scattered from north to south throughout the unit are tight to isoclinal, sometimes recumbent, F_{2N} folds with E-W trending hinges, which deform S_{1N} gneissic fabrics (Haller, 1971). These are attributed to early phases of deformation (D_{1N} and D_{2N}). Haller (1971) reported that the F_{2N} folds were refolded during a third stage of deformation (D_{3N}) by broad, north-south oriented antiforms and synforms (F_{3N}). This third phase of folding was most likely associated with W-directed Caledonian thrusting.

The upper contact (eastern margin) of this allochthon is marked by a 2 km-wide zone of high strain (D_{4N}). Within this shear zone, mylonitization overprints D_{3N} fabrics and structures with increasing intensity structurally upwards (Rasmussen and Andresen, 1998). In thin section, K-feldspar grains reveal subgrain boundaries, deformation banding, undulatory extinction, and are locally broken apart, whilst the quartz has been dynamically recrystallized into ribbons (Figure 2b). Strain asymmetries preserved in this ductile fabric (i.e. mica fish surrounding strained feldspar) provide evidence for non-coaxial shear with a top-to-the-east sense of motion. Superimposed onto and parallel to these mylonites are low- and high-angle N-S striking, E-dipping brittle faults. They display SE-plunging slickenlines that are subparallel to lineations associated with ductile

D_{4N} non-coaxial shear. The sequence is capped by a several-meter-thick cataclasite zone in which partially devitrified pseudotachylites are found. The geometric similarities of both the ductile and brittle structures, combined with their close spatial relationship have been interpreted by Rasmussen and Andresen (1998) to signify continuous fault movement under decreasing metamorphic conditions due to structural exhumation of the footwall. Previously, this D_{4B} shear zone has been mapped as a W-vergent thrust fault (Higgins et al., 1981). However, based on our observations and those of Andresen et al. (1998a) and Rasmussen and Andresen (1998), the most recent sense-of-shear indicators in the mylonites (e.g. asymmetric boudins, shear bands, asymmetric folds, winged porphyroclasts, shear bands, asymmetric pressure shadows) in Forsblad Fjord record normal-sense hanging wall transport to the east.

Høgedal allochthon

The oldest planar fabric in the Høgedal allochthon is a well-defined compositional layering (S_{0H}). We regard centimeter to meter scale layers of alternating felsic and mafic migmatitic material as having formed during *in-situ* partial melting. The first phase of deformation, D_{1H}, formed a prominent schistosity, S_{1H}, defined by biotite ± muscovite ± kyanite. Heterogeneities in rheology and/or strain during subsequent deformation preserved intrafolial F_{1H} folds.

The dominant structures of the Høgedal allochthon belong to D_{2H}. Defined by biotite ± muscovite, the S_{0H} and the S_{1H} schistosities were transposed by D_{2H} such that the two lie parallel to a predominant S_{2H} schistosity with an average strike of 007°, and dip of 52°E (Plate Ib). Commonly observed F_{2H} folds have axes with a mean trend of 172° and plunge of 27° . These F_{2H} folds commonly form W-vergent fold trains with wavelengths that range from centimeters to kilometers in scale. They are seen to refold F_{1H} folds

(Figure 2c). A pronounced mineral lineation (L_{2H}) is defined by prismatic sillimanite, pseudomorphed after kyanite, and a stretching lineation defined by recrystallized quartz rods. L_{2H} parallels the trend of F_{2H}, but plunges shallowly to both the north and the south (Plate Ib), suggesting that they may have been subsequently deformed. Alternatively, given the lack of other evidence to suggest later deformation and the fact that most of the lineations plunge to the south, we prefer a simpler interpretation: that the variation in the plunge of these lineations reflects minor heterogeneities in the regional strain field during D_{2H}. Offset shear bands, asymmetric, folded lenses and leucocratic layers and asymmetric, rotated boudins (Figures 2d and 2e) provide evidence for both top-to-the-south (dextral) and top-to-the-north (sinistral) non-coaxial shear during N-S, orogen-parallel flow. Additional evidence for N-S flow is suggested by the N-S L_{2H} stretching lineations that accompany the above mentioned shear structures Orogen-parallel flow has been reported to the north by Holdsworth and Strachan (1991), Strachan et al. (1992), Friderichsen et al. (1994), Strachan et al. (1995), Vold (1997), and Andresen et al. (1998a) and in middle-crustal rocks of the Scandinavian Caledonides by Fossen (2000). Holdsworth and Strachan (1991) proposed that the N-S lineations with top-to-the-N sense of shear that they observed in NE Greenland resulted from an early phase of strike-slip deformation followed by transpression associated with the sinistrally oblique nature of the Baltica-Laurentia collision. We cannot corroborate this hypothesis in our field area because we did not observe a preferred top-to-the-N sense-of-shear in the fabrics preserved in the rocks. Given the published kinematics in NE Greenland (Holdsworth and Strachan, 1991), the paleomagnetic data constraining the Baltica-Laurentia collision (Torsvik et al., 1996), and the fact that orogen parallel flow fabrics are synkinematic with E-W contractional fabrics in the field area, it is likely that there was a significant component of transpression recorded in the Høgedal allochthon. However, the most

simple interpretation from data presented in this paper is that generalized N-S flow was synchronous with E-W compression. Unfortunately, strain indicators were not available to quantify the amount of E-W shortening and N-S flow. We note the preservation of D_{2H} ductile shear bands that cut across concordant leucosomes during this stage of deformation. Preliminary petrologic data from syn-D_{2H} garnet porphyroblasts indicate that deformation occurred during prograde metamorphic conditions (White and Hodges, in preparation).

D_{3H} locally overprints D_{2H} near the base (D_{3aH}) and top (D_{3bH}) boundaries of the Høgedal allochthon. Deformation near the base is associated with movement along the Høgedal detachment while deformation near the top with movement along the Tindern detachment. There is no structural evidence to constrain the relative timing of D_{3aH} and D_{3bH}. There is a prominent schistosity, S_{3bH}, near the allochthon's upper boundary which is defined by phyllosilicates, and has a mean strike of 039° and a dip of 37°E (Plate Ib). L_{3bH} stretching lineations defined by recrystallized quartz lie within this fabric with a mean trend of 092° and plunge of 54° (Plate Ib). As with the shear zone at the top of the Hagar-Niggli Spids allochthon, strain increased upwards, through the shear zone located at the top of the Høgedal allochthon.

Høgedal allochthon-Tindern allochthon fault contact

The eastern margin of the Krummedal Sequence (exposed west of Randenæs and south of Caledonia Ø in Forsblad Fjord) is marked by a series of normal fault splays with top-to-the-east sense of shear. We regard the main metamorphic discontinuity within the 2-4 km thick zone of high strain as the Tindern detachment (*sensu stricto*). The splay of D_{3H} fault slivers that lies above this contact bears a close spatial and geometric correlation to the Tindern detachment. They define the structural transition from lowermost Eleonore

Bay Supergroup to the rest of the Tindern allochthon and truncate the network of garnetiferous dikes that invaded these rocks.

The Tindern detachment crops out in three localities within the study area. It has been intruded by multiple generations of two-mica leucogranite plutons which are pre- to synkinematic with respect to motion along the shear zone. On the north side of Forsblad Fjord, the fault truncates a large (1 km amplitude) F_{2H} fold in the footwall. The fault can be traced along the east side of the Tindern glacier in the hanging valley west of Randenæs. It disappears beneath a talus-covered slope, projecting downhill into the fjord. The fault may be traced on the south side of the fjord as the boundary between the Caledonia Ø granite and the Klosterbjerg granite. Within the Caledonia Ø Granite that intruded the Tindern detachment footwall, wispy strands of Krummedal Sequence metasedimentary rocks are seen strung out and boudinaged parallel to the detachment (Figure 2f). Structurally higher, just beneath the Tindern detachment *sensu stricto*, the Caledonia Ø granite contains rounded xenoliths of the Nathorst Land Group. The best exposures of the fault are found in Schaffhauserdalen where the shear zone is ca. 700 meters thick; 500 meters of Krummedal Sequence sillimanite-migmatites that experienced strong ductile deformation are overlain by 200 meters of equally strained schists from the base of the Nathorst Land Group. A network of partially sheared, interconnected sills and dikes intruded across these highly deformed, quartz-rich, low-grade sedimentary rocks. Overprinting the zone of ductile deformation and bounding the top of the shear zone is a brittle fault marked by a ca. 2 meter-thick cataclasite layer that was intruded by synkinematic pink granite sheets partially brecciated during brittle deformation.

All shear sense indicators–such as the mylonitic fabric in the Caledonia Ø granite, asymmetric, rotated boudins, asymmetric pinch-swell tails, shear bands and S-C cataclasite fabrics (in the sense described by Lin, 1999) in Schaffhauserdalen (average strike/dip of C plane equals 351°/31E) – indicate top-to-the-east transport. Thus, the kinematic indicators, the juxtaposition of low-grade sedimentary rocks in the hanging wall with high-grade metasedimentary rocks in the footwall, and the truncation of large D_{2H} structures in the footwall are consistent with a low-angle normal fault with significant E-W displacement, orthogonal to the trend of the Caledonian orogen.

Tindern allochthon

The basal section of the Nathorst Land Group at Randenæs in Forsblad Fjord displays a spaced cleavage (S_{1T}) that overprints the primary bedding S_{0T} without significant transposition. In most outcrops, S_{1T} is subparallel to S_{0T}, striking N-S with a dip 30°-40° east. This relationship extends upwards within the Tindern allochthon where both schistosities are folded by macroscopic F_{2T} folds, the largest of which is a ca. 1 kilometer-amplitude, E-plunging recumbent fold exposed at the mouth of Schaffhauserdalen. North-striking normal faults in the Tindern allochthon (N_{3T}) include shallowly E-dipping and steeply W-dipping structures that we interpret as an extensional fan complex associated with the Tindern detachment.

Post-D3 Structures Present in All Three allochthons

After juxtaposition during extensional deformation along the FRDS, the three allochthons experienced similar deformational histories. A generation of low-angle brittle normal faults (N_{5N}, N_{4H}, N_{4T}) that strike WNW-ESE and dip SSW, cross-cut the Tindern detachment and associated brittle faults. The later structures transported hanging wall material westward. Additional high-angle, E-W striking faults with uncertain, but minor

displacement traverse from the Hagar-Niggli Spids allochthon to the Høgedal allochthon, across the Høgedal detachment. Similar faults appear at the base of the Tindern allochthon along the Randenæs peninsula. We have no age constraints on these faults.

Geochronology

Granitic rocks found at Forsblad Fjord display a wide range of relative age relationships with respect to deformational structures, suggesting that their absolute ages might provide important constraints on the timing and duration of deformation in this part of the East Greenland Caledonides. To determine absolute ages, we have used the U-Pb method on monazite, [(Ce,La,Y,Th)PO_4], and xenotime, [YPO_4], mineral fractions separated from critical granitic rock samples. Reconnaissance petrography using an optical microscope and backscattered electron (BSE) imagery revealed single-phase monazite crystals growing along the margins of prograde metamorphic mineral sub-assemblages that define fabrics observed in the field and in thin section. BSE imagery of monazite and xenotime populations demonstrated that there are a variety of compositional zoning patterns in addition to the single-phase compositions seen in thin-section. The results and interpretation of geochronologic data for each sample are discussed in the following section, whilst the implications of this data are discussed later in the text.

Anatectic Leucosome of the Høgedal allochthon

Sample **97GR14** comes from a concordant leucosome in the Krummedal Sequence that was ductilely deformed during high-temperature deformation and preserves a magmatic foliation. It is interpreted as synkinematic with respect to D_{2H}. Reconnaissance BSE imaging and EDS analysis of a thin section from this leucosome

revealed two varieties of monazite *in situ*. One variety is subhedral and appears to have grown in equilibrium with the other igneous minerals in the matrix. The other variety is anhedral with complex boundaries that are partially overgrown by the surrounding igneous minerals which suggests that it is xenocrystic with respect to crystallization of this leucosome. Magnified images of individual monazites selected from mineral separates reveal four classes of grains, distinguished by their zoning patterns (Figure 3a - d): 1) unzoned, single-phase grains; 2) multiphase, partially resorbed grains with small inclusions; 3) unzoned, single-phase grains with single-phase overgrowths; 4) multiphase, partially resorbed grains with single-phase overgrowths.

We analyzed 11 individual monazite crystals from this sample. They varied in size from 75 μm to 150 μm. Most were relatively clear with a pale yellow color and round, subhedral grain boundaries. Exceptions were one small, oblong-shaped, subhedral crystal and one, round anhedral grain with several inclusions. Analyses M11 and M16 yield $^{207}Pb/^{206}Pb$ dates of 766 and 822 Ma, respectively, and are interpreted to be xenocrystic monazite scavenged from the metapelitic host rocks, possibly having grown during a "Grenvillian" aged magmatism or metamorphism (Thrane et al., 1999a; Watt and Thrane, 1999). The remaining analyses generally disperse along concordia between 428 and 418 Ma (Figure 4). Such behavior, typical of monazites found in rocks produced by the anatexis of aluminous protoliths in regional metamorphic settings (Parrish, 1990; Hawkins and Bowring, 1997; Hawkins and Bowring, 1999), is extremely difficult to interpret unambiguously. In **97GR14**, it may reflect high-temperature Pb-loss and/or multiple periods of monazite precipitation. If the monazite is polygenetic, at least some of the younger grains may reflect post-magmatic mineral-fluid interactions during retrograde metamorphism; such an origin is consistent with the complex BSE imaging characteristics of the monazite in this sample. The possibility that this leucosome

crystallized after 424 Ma can be dismissed because the Caledonia Ø Granite – which has more easily interpretable U-Pb monazite systematics; (see below) cross-cuts structures that deform these concordant leucosomes and is interpreted to be no younger than 423.8 ± 1.5 Ma. On the basis of these relationships we believe the best estimate of the crystallization age of **97GR14** to be the weighted mean of the $^{207}Pb/^{235}U$ dates of analyses M15 and M19 which is 425.3 ± 0.3 (MSWD = 0.4) Ma. This is consistent with the BSE image of grain M19 which showed no evidence for a composite crystal growth history (Figure 3a).

Cross-cutting Leucosome of the Høgedal allochthon

Monazites were separated from a leucosome, sample **97GR13**, that cuts across the E-W contraction-related structural fabrics preserved in the Krummedal Sequence and places a minimum age constraint on D_{2H}. Individual monazite crystals from this sample were a cloudy, pale yellow color with round, subhedral grain boundaries and had a mottled surface texture. Due to the limited quantity of monazite recovered from this sample, we were unable to make BSE images of any grains. Five single crystals were analyzed and yielded a normally discordant linear array with an upper intercept of 425.8 ± 2.1 Ma (MSWD = .4) (Figure 4), which we interpret as the crystallization age of **97GR13**. Because the lower intercept of this regression is indistinguishable from 0 Ma, we consider it to be indicative of modern Pb-loss.

Caledonia Ø Granite

Efforts to determine the age of the Tindern detachment involved the dating of monazite and xenotime from two samples of the Caledonia Ø Granite collected 500m apart (locations plotted in Plate 1a). Both samples came from outcrops where the strongly heterogeneous magmatic foliation defined by alignment of feldspar and mica and equally

heterogeneously strained schlieren of biotite suggested that intrusion of the granite was syntectonic with respect to movement along the Tindern detachment.

Sample 97GR18 yielded both monazite and xenotime that ranged in size from 75 μm to 200 μm and were clear with a pale yellow color. The monazite contained a few dark inclusions and well-defined, euhedral crystal faces, whereas the xenotime had a more mottled surface texture with dark inclusions and rounded, subhedral crystal forms. Two types of xenotime were identified through BSE imagery: single-phase grains with some inclusions (Figure 3e), which made up the bulk of the separate, and less-abundant two-phase mixtures with single-phase overgrowths (Figure 3f). No monazites from this sample were examined with BSE imagery. Five xenotime U-Pb analyses define a normally discordant linear array that has an upper intercept of 427.2 ± 0.8 Ma and a lower intercept near 0 Ma, MSWD = 0.4 (Figure 4). Five monazite crystals from 97GR18 also yielded a normally discordant, quasi-linear array on a concordia diagram (MSWD = 5.9) with an upper intercept of 423.9 ± 3.8 Ma and a lower intercept indistinguishable from 0 Ma.

Six individual monazite crystals were analyzed from sample **98GR23**, These crystals, were ca. 50 to 100 μm in diameter, and were less cloudy and mottled than those of **97GR18**. BSE images of thin sections from this sample show monazite growing along the boundaries of matrix biotite, quartz and K-feldspar. Trains of monazite and zircon crystals lie adjacent and parallel to the phyllosilicates that define S_{3H} in the rock (Figure 5). Magnified BSE images of individual monazite crystals from the mineral separates revealed 4 distinct patterns of compositional zoning (Figure 3g - j): 1) single-phase, homogeneous crystals with few inclusions; 2) two-phase, partially resorbed crystals with complex boundaries and inclusions of zircon; 3) two-phase, partially resorbed complex

cores with single-phase, anhedral mantles; 4) two-phase, partially resorbed complex cores with mantles that preserve oscillatory zoning parallel either to relict or preserved crystal faces. Grains M7 and M9, which displayed the third zoning pattern, are reversely discordant and distinctly older than the remaining three analyses (Figure 4); we interpret these two grains as xenocrysts with magmatic overgrowths. Of the remaining four analyses, three cluster on or near concordia at 422-423 Ma and the fourth is normally discordant.

Excluding **98GR23**-M7 and -M9, all of the monazite analyses from **97GR18** and **98GR23** define a quasi-linear array (MSWD = 3.5) suggestive of a consistent upper intercept with concordia at 423.8 ± 1.5 Ma whilst the linear array of xenotime analyses from sample 97GR18 yields an upper intercept age of 427.2 ± 0.8 Ma. Although it is unclear which of these mineral ages best represents the age of crystallization of the Caledonia Ø granite, our favored interpretation is that the xenotimes are xenocrysts derived from the source region or country rocks of the Caledonia Ø Granite while the monazites best represent the crystallization age (423.8 ± 1.5 Ma) of this pluton which was emplaced syntectonically with respect to motion along the Tindern detachment.

Klosterbjerg Granite

Sample **98GR17** comes from the undeformed and unmetamorphosed two-mica leucogranite pluton near the base of the Tindern allochthon, along the south side of Forsblad Fjord. It places a maximum age constraint on the latest movement on the Tindern detachment. Subhedral monazite crystals, clear with a pale yellow color and ranging in size from 70 to 150 μm were separated from the sample. BSE images (Figures 3k – m) showed that these grains took the form of 1) single-phase, non-zoned monazite; 2) two-phase, partially resorbed monazite with complex boundaries; and 3) single-phase

crystals with oscillatory zoning. Five single crystal analyses are dispersed along concordia between 432 and 424.5 Ma. Given these data, two possible interpretations exist for the timing of crystallization of this pluton. The first is that it crystallized at 432 Ma and the monazite subsequently experienced high-temperature Pb-loss and/or precipitation from a high-temperature fluid phase. The second is that crystallization occurred at 424.5 Ma and this granite contains a xenocrystic monazite component scavenged from the granite's source region. We favor the latter scenario because there is no field or petrographic evidence to indicate that this intrusion experienced high-temperature, post-crystallization metamorphism or significant fluid-rock interaction.

Structural Synthesis

Unraveling the polyphase deformational history preserved in the Forsblad Fjord region is complicated by the fact that each of the Hagar-Niggli Spids, Høgedal and Tindern allochthons was separate prior to juxtaposition by the FRDS . As shown in Figure 6, the geometric and temporal similarities in the allochthons when they were separate suggest that some pre-emplacement deformational events may be correlated.

Evidence for the earliest deformation is found in the Hagar-Niggli Spids allochthon. There, E-W trending folds, that are seen only below the Høgedal detachment, deform the gneisses. These E-W trending folds are overprinted by N-S trending folds that are geometrically consistent with the structures documented in the overlying allochthons. Thus, there is an apparent angular inconsistency between the orientation of these E-W trending folds with all other shortening structures in the field area and with models for E-W Caledonian compression or transpression. Given the record of Archean-Proterozoic metamorphism (e.g. Rex et al., 1976; Rex and Gledhill, 1981; Thrane et al., 1999a)

preserved in these rocks, the simplest interpretation is that the E-W trending, F_{2N} fold structures in the Gletscherland Complex formed before the Caledonian Orogeny. Direct evidence for correlative deformation in the Høgedal and Tindern allochthons has not been found.

The data necessary to constrain the absolute timing and duration of D_{1H} structures are not available. The transposition of D_{1H} structures by D_{2H} fabrics has made it impossible to determine whether deformation occurred in two discrete episodes or as a protracted event. Because the possibility of additional rotation of D_{1H} structures during subsequent deformation cannot be ruled out, the simplest interpretation is that D_{1H} resulted from early Caledonian contraction that continued into D_{2H}.

The geochronologic data necessary to constrain the timing and duration of D_{1T} are also not yet available. This deformation must have occurred after the youngest age of detrital zircons (1100 Ma) dated in the Nathorst Land Group by Thrane et al. (1999b). D_{1T} fabrics near the base of the Nathorst Land Group also affect some of the garnetiferous pegmatite-aplite dikes mapped there. $^{40}Ar/^{39}Ar$ data from Hartz (1998), and White and Hodges (in preparation) implies that these are Caledonian pegmatites.

Abundant N-S trending F_{3N} folds preserved in the Gletscherland Complex are similar in geometry to the F_{2H} and F_{2T} fold structures, and indicate there was significant E-W shortening. D_{2H} fabrics in the ductiley deformed gneisses of the Krummedal Sequence preserve kinematic indicators that show there was substantial N-S transcurrent, flow of material. Taken together, these structures indicate that orogen-parallel flow was synchronous with E-W contraction. Although the amount of E-W shortening and N-S ductile flow is not constrained in this study, the age of the event is constrained by our

new U-Pb age on concordant leucosomes in the Krummedal Sequence (**97GR14**) of 425.3 ± 0.3 Ma.

Extension along the FRDS (D_{4N}, D_{3H}, D_{3T}) juxtaposed the three allochthons in their current structural relationship. Our geochronologic data for the synkinematic Caledonia Ø Granite demonstrate that the Tindern detachment was active at ca. 424 Ma, but we have no direct constraints on the timing of the Høgedal detachment. Although the Høgedal structure is at a substantially deeper structural level than the Tindern detachment, it displays much better developed low-temperature deformational fabrics than the structurally higher fault, perhaps indicating that it experienced somewhat later movement.

Subsequent to displacement on the FRDS , all three allochthons developed conjugate fracture patterns 500 – 1000 m long consistent with N-S compression, E-W extension. In addition to these faults, there are west-dipping, brittle normal faults of uncertain displacement and prominent, near-vertical, N-S striking faults which may be traced for several km along strike; these were also mapped by Haller (1970). These faults cross-cut even the late, discordant dikes (**97GR13**). Thus, these late-stage faults could not have been active until after 425.8 ± 2.1 Ma.

"Age" of orogen parallel flow, E-W contraction and E-W extension

Monazite and xenotime U-Pb dates presented here for igneous and metamorphic rocks associated with N-S flow, E-W contraction and E-W extension are indistinguishable within error and imply that crustal exhumation was occurring at the same time as extensive orogen-parallel flow and E-W contraction at ca. 424-425 Ma. Centrally positioned between an Early Proterozoic package of amphibolite facies orthogneisses (Gletscherland Complex) and a sequence of low-grade sedimentary rocks

(Nathorst Land Group), the Krummedal Sequence of amphibolite facies paragneisses unequivocally experienced Caledonian anatexis, metamorphism, and deformation. Prograde garnet growth synkinematic with respect to D_{2M}, was accompanied by *in-situ* anatexis. D_{2H} was characterized by N-S ductile flow and E-W shortening. The ages of pre- to syn-D_{2H} leucosomes formed during *in situ* anatexis constrain both orogen-parallel flow and orogen-perpendicular contraction to have occurred at and/or after 425 Ma. This date is supported by an additional monazite U-Pb age (425 Ma) for the metamorphism of the Krummedal Sequence paragneisses of Forsblad Fjord published by Andresen et al. (1998b).

D_{3H} fabrics associated with E-W extension, accommodated by motion along the Tindern detachment, developed synchronously with intrusion of the Caledonia Ø Granite at ca. 424 Ma. Therefore, given the resolution of our U-Pb geochronologic constraints, orogen-perpendicular extension occurred contemporaneously with or closely post-dated orogen-parallel flow and E-W contraction in this segment of the East Greenland Caledonides.

Implications for regional thrusting

Crustal thickening in East Greenland during the Baltica-Laurentia collision has been traditionally inferred from the presence of large-scale fold nappes and thrust faults. Early workers mapped nappes that were thrust in excess of 20 km westward over foreland blocks (e.g. Koch and Haller, 1971; Haller, 1971). The long, N-S striking fault system that transects the west end of Forsblad Fjord was thought to provide substantial evidence for Caledonian thrusting in our study area. Extensional faults mapped in East Greenland (e.g. Haller, 1971; Larsen and Bengård, 1991; Strachan, 1994), were traditionally attributed to post-Caledonian collapse. However, in our mapping of the Forsblad Fjord

area, we could not corroborate fold nappes of the scale described in other parts of East Greenland. Furthermore, the N-S striking fault system at the west end of Forsblad Fjord has been reinterpreted by recent workers (Andresen et al., 1998a) to have been a top-to-the-east normal fault, the Høgedal detachment. In light of these observations, it is important to ask: how *was* Caledonian crustal thickening accommodated in this region?

Although no thrust faults of mappable scale crop out within the Forsblad Fjord area, the crystalline units beneath the FRDS are thought to lie within a thickened thrust sheet that moved along a continuation of either the Hagar Thrust or the Niggli Spids Thrust mapped to the north by Escher and Jones (1999). This interpretation is supported by Higgins and Leslie (1999) who group all three allochthons discussed in this paper into their lower thrust sheet. However, Higgins and Leslie (1999) also suggested there is an upper thrust sheet which emplaced the Eleonore Bay Supergroup sedimentary rocks on top of Krummedal Sequence-type metasedimentary rocks and migmatitic gneisses. Leslie and Higgins (1999) reported a ductile thrust at the base of the Eleonore Bay Supergroup (exposed in eastern Bartholins Land, 74° 15' N) which had been reactivated by a co-planar top-down-to-the-east, brittle normal fault marked by zones of pseudotachylite. However, 2 degrees to the south, we observe that the Lower Eleonore Bay Supergroup sedimentary rocks at the base of the Tindern allochthon sit immediately on Krummedal Sequence rocks of the Høgedal allochthon. We see no structural evidence to suggest that the intervening Tindern detachment is a reactivated thrust fault. Given the kinematic indicators and the metamorphic relationship across the fault, we interpret the present geometry to be solely the result of simple normal faulting as drawn in the cross-section in Figure 7.

On the other hand, the Høgedal detachment may be an early Caledonian thrust fault that was reactivated as a strand of the FRDS. Although the youngest kinematic indicators suggest that the detachment moved most recently as a normal fault, such displacement does not satisfactorily explain the observation that the hanging wall metasedimentary sequence experienced Caledonian-aged amphibolite-facies metamorphism while the footwall gneisses apparently did not (Rex et al., 1976; Rex and Gledhill, 1981; Rasmussen and Andresen, 1998; Thrane et al., 1999a).

There are at least two geometric solutions to this problem. The first is that Krummedal Sequence rocks that now make up the Høgedal allochthon were initially thrust westward over Gletscherland Complex rocks that are now part of the Hagar-Niggli Spids allochthon, and that the Høgedal detachment subsequently down-dropped the thrust hanging wall relative to its footwall. This hypothesis implies that the offset thrust surface lies at depth beneath the study area, as drawn in Figures 7 and 8, a. The second hypothesis is that the Høgedal detachment itself marks the thrust surface and was reactivated as a normal-sense shear zone (Figure 8, b). Either scenario, if correct, has important implications for the rate of deformation in this part of the East Greenland Caledonides in Early Silurian time. In order to juxtapose rocks that experienced syn-D_{2H} amphibolite facies metamorphism with those that did not, the postulated thrust fault must be younger than ca. 425 Ma. If both the Høgedal and Tindern detachments are of similar ages (ca. 424 Ma), then the thrusting event is very tightly bracketed in time. Such a rapid transition from shortening to extension would be consistent with a lack of evidence for Caledonian-aged regional metamorphism in the Gletscherland Complex, but it would require extraordinarily fast thrust and detachment slip rates, on the order of tens of kilometers per million years. This leads us to question whether or not the Gletscherland Complex actually escaped Caledonian regional metamorphism, and we feel that more

data on the cooling history of the Hagar-Niggli Spids allochthon are necessary to resolve the issue.

Implications for the Role of Extension in the Development of Orogens

Our work adds to a growing database (e.g. Hartz, 1998; Hartz et al., 2000; Hartz, 2001) suggesting that crustal exhumation by extension accompanied the main phase of Caledonian orogenesis in East Greenland ca. 425 Ma. Until recently, extensional structures in the East Greenland Caledonides were interpreted to reflect post-Caledonian, Devonian-aged extension (e.g. McClay et al., 1986; Larsen and Bengård, 1991; Hartz and Andresen, 1995) mirroring evidence for widespread, post-orogenic extension in Scandinavia (e.g. Fossen et al., 1992; Fossen and Rykkelid, 1992; Fossen and Holst, 1995). Our results suggest that extension took place at middle and upper crustal levels and occurred synchronously with or very soon after the main phase of contraction. Additional field observations east of Frænkel Land (73 N) have been interpreted to suggest two cycles of crustal thickening and thinning (Escher and Jones, 1999). In this model, the second cycle of thinning corresponds to movement along the FRDS. Although Escher and Jones (1999) present no geochronologic constraints on their structures, their work suggests that Caledonian extension may have initiated even earlier than 424 Ma. We cannot corroborate multiple phases of extension at Forsblad Fjord, however, our observations pertain to a smaller area with less structural relief. Collectively, the data support the notion that some Caledonian extensional structures in East Greenland resulted from synorogenic extensional compensation that occurred in the upper to middle crust prior to wholesale post-orogenic collapse. On the other hand, if the extension associated with the FRDS seen in the Forsblad Fjord region actually indicates the onset of post-orogenic collapse, then the implication is that contractional orogenesis can make the

transition to extensional orogenesis extremely rapidly. Initiation of post-orogenic collapse at 424 Ma is problematic because it is usually associated with Devonian basin formation (i.e. deposition of the Old Red Sandstones e.g. McClay et al., 1986). Furthermore, evidence from the Scandinavian Caledonides suggests that crustal thickening due to convergence between Laurentia and Baltica continued until earliest Devonian followed by post-orogenic extension ca. 402 Ma (Fossen and Dallmeyer, 1998). Therefore, we prefer to interpret the extension at Forsblad Fjord as synorogenic.

Implications for models of synorogenic extension during crustal thickening

The Caledonides and modern analogs such as the Himalayan-Tibetan orogenic system resulted from continent-continent collisions affecting continental margins that stretch for thousands of kilometers. They both exhibit significant thrusting both near and far from their convergent margins. Furthermore, there is evidence for syncollisional orogen-perpendicular extension in the Caledonides just as in the Himalayas. While the obliquity of convergence may have been different, there are enough important similarities, that the two orogenic systems may be used as complimentary natural laboratories to improve our understanding of this orogenic process.

Orogens such as the Himalaya may be viewed as stable, tapering, topographic wedges which slide along their basal planes, allowing external deviatoric stresses to work against basal frictional resistance (Platt, 1986; Chapple, 1978; Davis et al., 1983). In this simplified model, internal deformation occurs when longitudinal forces along the cross-sectional area at the rear of the wedge exceed the material strength of the wedge causing internal shortening and thickening. By this process, gravitational potential energy is amassed as the topographic gradient of the wedge increases until a "steady-state" condition of balance between gravitational and compressional forces develops. Transient

deviations from this steady-state during which the wedge oversteepens can lead to episodes of internal extensional deformation (e.g. Platt, 1986). Examples of internal extension parallel to the direction of N-S convergence in the Himalaya, first identified by Caby et al. (1977) and Burg and Chen (1984), have been documented along the length of the orogen (Burchfiel et al., 1992) as the South Tibetan Fault System (Hodges, 2000). Evidence for alternating, thrust and normal faulting over millions of years led Hodges et al. (1996) to hypothesize that small deviations from the steady-state orogenic wedge configuration can lead to alternating episodes of shortening and extension over long periods of collisional orogenesis.

Geodynamic modeling to understand this process in the India-Eurasia collision has led to several untested predictions. In the model of Royden (1996), synorogenic extensional faults related to thrusting are predicted to occur on both sides of orogenic plateaux. In the case of the Himalaya-Tibetan system, there has been no documentation of extensional structures along the northern plateau margin as yet. Another prediction from such modeling is that localized extension in the topographic wedge must somehow be decoupled from the regional compression-related stress regime. Thus, in the Himalayas, the South Tibetan Fault System is thought to represent the surface manifestation of this decoupling horizon (Hodges, 2000). However, the nature of this horizon at depth remains poorly constrained. Bird (1991) hypothesized that lateral extrusion of ductile, lower crustal material beneath the Tibetan Plateau may have been driven by lateral pressure gradients due to topographic loads. Thus, he said that the lower crust will flow away from a topographic high toward a "pancake-shape" state. Royden (1996), suggested that a ductile zone beneath the Tibetan Plateau undergoing crustal shortening could serve to decouple the thickening of the orogenic wedge from regions of local, internal extension. If this is true, how do extensional structures like the South

Tibetan Fault interact with this ductile zone? The East Greenland Caledonides provide an opportunity to address this problem directly.

In East Greenland, geologic features associated with crustal thickening (i.e. folds, thrust faults, and anatectic melts) are truncated by extensional structures consistent with predictions for the synorogenic, gravitationally driven models of extension in the Himalayas. This implies that extensional deformation internal to the orogenic wedge can occur on either side of a two-sided orogenic system as predicted (Royden, 1996) (simple schematic cross-section in Figure 9).

In addition, the N-S ductile-flow (D_{2H}) fabrics preserved in the Krummedal Sequence in Forsblad Fjord, which are kinematically similar to features documented further north by Holdsworth and Strachan (1991), Strachan et al. (1992), Friderichsen et al. (1994), Strachan et al. (1995), Vold (1997) and Andresen et al. (1998a), are consistent with lateral extrusion of middle-crustal material as predicted by the Bird (1991), model. However, it is important to note that that flow was oriented N-S. Rather than flowing away from the topographic high down the ~E-W maximum gravitational potential energy gradient that we would expect to be perpendicular to a N-S trending orogen, this material flowed parallel to it. We suggest that given the presence of synkinematic E-W shortening and N-S flow structures, the simplest interpretation of this dataset is that the direction of orogen-parallel flow was constrained by orogen-perpendicular compression or transpression during plate convergence as predicted by the Royden (1996) model. Furthermore, we note that large allochthonous units of the Scandinavian Caledonides record similar middle-crustal orogen-parallel flow prior to 405 Ma (Fossen, 2000) which indicates that this was an orogen-scale phenomena. We have no quantitative measure on either the amount of E-W shortening or N-S extension within the Krummedal Sequence.

From data in this paper, we argue that the time of shearing along the Tindern detachment and formation of the N-S ductile fabrics (sampled 6-7 km structurally below the fault) are indistinguishable within analytical uncertainty. This suggests that the FRDS rooted directly into the ductilely deforming, weak middle crust that experienced regional E-W contraction and N-S flow associated with collisional orogenesis. Thus, the FRDS acted at depth as a decoupling horizon between regions experiencing coeval extensional and compressional-transpressional deformation for the duration of its slip history.

Conclusions

The Forsblad Fjord region of the East Greenland Caledonides comprises three allochthonous units now juxtaposed by normal faults. Monazite and xenotime U-Pb dates for igneous and metamorphic rocks from these allochthonous blocks indicate that Caledonian magmatism and metamorphism associated with contraction and extension occurred ca. 425 Ma. Integrated field and U-Pb geochronologic studies demonstrate that the Høgedal allochthon preserves a pervasive high-grade deformational fabric that formed at middle-crustal depths and is associated with N-S flow and E-W contraction at ca. 425 Ma. These structures have been overprinted by structural fabrics associated with E-W extension on the overlying Tindern detachment that was active ca. 424 Ma. The new age constraints are significant because they suggest either contemporaneous orogen-parallel flow, contraction and extension, or very rapid transitions from a regime dominated by N-S flow and E-W shortening to E-W extension at a specific structural level in an evolving orogen. In addition, if contraction and extension were protracted events, the temporal constraints presented in this paper may suggest that crustal thinning was occurring synchronously with crustal thickening at different structural levels.

We infer from the relative ages of high grade metamorphism in the Hagar-Niggli Spids allochthon and the Høgedal allochthon that a basal thrust fault probably underlies the study area and was either reactivated by the Høgedal detachment or offset by this fault to a deeper structural level that lies beneath current exposures. Because existence of this thrust fault is inferred on the basis of limited K-Ar and Rb-Sr data, we believe that the Hagar-Niggli Spids allochthon is a good candidate for further thermochronologic research.

The examples of synorogenic extensional structures described in this paper bear a marked similarity to orogen-perpendicular extensional structures in the Himalaya and probably had a similar origin. Our work in East Greenland builds on previous observations in the Himalaya by documenting the presence of large-displacement, synorogenic extensional structures on the side of an orogen opposite the primary subduction boundary. For example, the East Greenland Caledonides are broadly analogous to the Kunlun Mountains along the northern margin of the Tibetan Plateau. The evidence for middle-crustal ductile flow parallel to the Caledonian orogen provides strong observational data in support of geodynamic models that hypothesize the presence of a middle-crustal ductile regime within the core of contracting orogens. The flow anisotropies preserved in the Krummedal Sequence suggest that flow direction was influenced by regional, compressional or transpressional stresses. Field relationships and geochronologic constraints demonstrate that the Fjord Region Detachment System rooted directly into a zone of active ductile flow that accommodated contractional strains at middle-crustal levels. This implies that similar structures in other orogens also may have served to decouple deep-level zones of regional contraction from overlying zones of crustal thinning within the orogenic wedge.

Acknowledgements

This research was part of a collaborative effort between the Department of Earth, Atmospheric and Planetary Sciences at MIT and the University of Oslo in Norway. Funding for this study was provided by National Science Foundation grant EAR 930072 (to K.V. H.). We wish to thank the Greenland Geological Survey, Danish Polar Center, Sirius Patrol, E. Hartz, S. Bowring, N. Henriksen, F.D. Friderichsen, J. Hurtado, L. Schoenbohm, K. Keefe, N. Chatterjee and H. Jepsen for logistical assistance and E. Hartz for comments on the manuscript. This paper benefited enormously from thoughtful and constructive reviews for which we thank H. Fossen and R. Holdsworth.

References

Andersen TB, and Jamtveit B (1990) Uplift of deep crust during orogenic extensional collapse: A model based on field studies in the Sogn-Sunnfjord region, W. Norway. Tectonics, 9: 1097-1111

Andersen TB, Jolivet Le, and Gapais De (1998) Extensional tectonics in the Caledonides of Southern Norway, an overview. 8th meeting of the European Union of Geosciences symposium on Extensional tectonics and exhumation of metamorphic rocks in mountain belts, 285, Strasbourg, France: 333-351

Andresen A, Hartz EH, and Vold J (1998a) A late orogenic extensional origin for the infracrustal gneiss domes of the East Greenland Caledonides (72-74 N). Tectonophysics, 285: 353-369

Andresen A, and Steltenpohl MG (1994) A reevaluation of nappe sequences in the Ofoten-Troms region, north Norwegian Caledonides: Implications for terrane accretion, ophiolite obduction, and polyorogenic evolution. Tectonophysics, 231: 59-70

Andresen A, Walker N, and Hartz E (1998b) U-Pb and 40Ar/39Ar isotope constraints on Caledonian and Grenvillian orogenesis in the Kong Oscar Fjord region. Frederiksen KS and Thrane K, Symposium on Caledonian geology in East

Greenland: Abstract Volume, 46, Danmarks og Grønlands Geologiske Undersøgelse Rapport, Denmark: 55

Backlund HG (1930) Contributions to the geology of Northeast Greenland. Meddelser om Grønland, 74: 207-296

Bird P (1991) Lateral extrusion of lower crust from under high topography, in the isostatic limit. Journal of Geophysical Research, B, Solid Earth and Planets, 96: 10,275-10,286

Burchfiel BC (1990) The continental crust. In: Moores E (eds), Shaping the Earth: Tectonics of Continents and Oceans. W.H. Freeman and Company, New York, pp 5-21

Burchfiel BC, Chen Z, Hodges KV, Liu Y, Royden LH, Deng C, and Xu J (1992) The South Tibetan Detachment System, Himalayan Orogen: Extension Contemporaneous With and Parallel to Shortening in a Collisional Mountain Belt. Geological Society of America, Boulder, CO, pp 41

Burchfiel BC, and Royden LH (1985) North-south extension within the convergent Himalayan region. Geology, 13: 679-682

Burg JP, and Chen GM (1984) Tectonics and structural zonation of southern Tibet, China. Nature, 311: 219-223

Caby R, Kienast JR, Saliot P, and Jest Ce (1977) Modele d'evolution structurale des Alpes occidentales; Model of the structural evolution of the Western Alps Himalaya; sciences de la terre. Ecologie et geologie de l'Himalaya, Paris, France: 85-92

Cashman PH (1990) Evidence for extensional deformation during a collisional orogeny, Rombak window, North Norway. Tectonics, 9: 859-886

Chapple WM (1978) Mechanics of thin-skinned fold-and-thrust belts. Geological Society of America Bulletin, 889: 1189-1198

Christoffersen M (1984) Scoresby Sund. Grønlands Geologiske Undersøgelse, Denmark

Davis D, Suppe J, and Dahlen FA (1983) Mechanics of fold-and-thrust belts and accretionary wedges. J geophys Res, 88: 1153 - 1172

Dewey JF (1988) Extensional collapse of orogens. Tectonics, 7: 1123-1139

Escher JC, and Jones KA (1999) Caledonian geology of Frænkel Land and adjacent areas (73°00'-73°30'N), East Greenland. Higgins Ak and Frederiksen KS, Geology of East Greenland 72°-75°, mainly Caledonian: preliminary reports from the 1998 expedition, Danmarks og Grønlands Geologiske Undersøgelse Rapport, Denmark:

Fossen H (2000) Extensional tectonics in the Caledonides; synorogenic or postorogenic? Tectonics, 19: 213-224

Fossen H, Burg J-Pe, Mainprice De, and Petit J-Pe (1992) The role of extensional tectonics in the Caledonides of South Norway. Mechanical instabilities in rocks and tectonics; a selection of papers. International conference on Mechanical instabilities in rocks and tectonics, 14: 1033-1046

Fossen H, and Dallmeyer RD (1998) (super 40) Ar/ (super 39) Ar muscovite dates from the nappe region of southwestern Norway; dating extensional deformation in the Scandinavian Caledonides. Tectonophysics, 285: 119-133

Fossen H, and Holst TB (1995) Northwest-verging folds and the northwestward movement of the Caledonian Jotun Nappe, Norway. Journal of Structural Geology, 17: 3-15

Fossen H, and Rykkelid E (1992) Postcollisional extension of the Caledonide Orogen in Scandinavia; structural expressions and tectonic significance. Geology (Boulder), 20: 737-740

Friderichsen JD, Strachan RA, and Henriksen N (1994) Basement-cover relationships and regional structure in the Grandjean Fjord-Bessel Fjord region 72°-76° N, North-East Greenland. Rapport Grønlands geologiske Undersøgelse, 162: 17-33

Gee DG (1975) A tectonic model for the central part of the Scandinavian Caledonides. American Journal of Science, 275A: 468-515

Gee DG, Lobkowicz M, and Singh S (1994) Late Caledonian extension in the Scandinavian Caledonides; the Roragen detachment revisited. Tectonophysics, 231: 139-155

Haller J (1970) Tectonic map of East Greenland (1:500,000). An account of tectonism, plutonism, and volcanism in East Greenland. Meddelelser om Grønland, 171: 1-286

Haller J (1971) Geology of the East Greenland Caledonides. Interscience Publishers, New York, pp 413

Hartz E (1998) Late Orogenic Evolution of the East Greenland and Scandinavian Caledonides. Dissertation for the degree Doctor Scientiarum thesis, University of Oslo, Oslo,

Hartz E (2001) Syncontractional extension and exhumation of deep crustal rocks in the east Greenland Caledonides. Tectonics, 20: 58-77

Hartz E, and Andresen A (1995) Caledonian sole thrust of central East Greenland: A crustal-scale Devonian extensional detachment? Geology, 23: 637-640

Hartz E, Andresen A, Andersen TB, Andreasson P-Ge, and Andresen Ae (1994) Structural observations adjacent to a large-scale extensional detachment zone in the hinterland of the Norwegian Caledonides. Terranes in the Arctic Caledonides, 231, Lund, Sweden: 123-137

Hartz EH, and Andresen A (1997) From collision to collapse; complex strain permutation in the hinterland of the Scandinavian Caledonides. Journal of Geophysical Research, B, Solid Earth and Planets, 102: 24, 697-24, 711

Hartz EH, Andresen A, Martin MW, and Hodges KV (2000) U-Pb and (super 40) Ar/ (super 39) Ar constraints on the Fjord region detachment zone; a long-lived extensional fault in the central East Greenland Caledonides. Journal of the Geological Society of London, 157, Part 4: 795-809

Hawkins DP, and Bowring SA (1997) U-Pb systematics of monazite and xenotime: case studies from the Paleoproterozoic of the Grand Canyon, Arizona. Contributions to Mineralogy and Petrology, 127: 87-103

Hawkins DP, and Bowring SA (1999) U-Pb monazite, xenotime and titanite geochronological constraints on the prograde to post-peak metamorphic thermal history of Paleoproterozoic migmatites from the Grand Canyon, Arizona. Contributions to Mineralogy and Petrology, 134: 150-169

Henriksen N (1985) The Caledonides of central East Greenland 70 degrees -76 degrees N. In: Gee DG and Sturt BA (eds), The Caledonide Orogen — Scandinavia and Related Areas, vol. 2. John Wiley & Sons, Chichester, U.K., pp 1095-1113

Henriksen N, and Higgins AK (1976) East Greenland Caledonian fold belt. In: Escher A and Watt WS (eds), Geology of Greenland. The Geological Survey of Greenland, Copenhagen, DK, pp 183-246

Higgins AK, Friderichsen JD, and Thyrsted T (1981) Precambrian metamorphic complexes on the East Greenland Caledonides (72° -74° N) - their relationships to the Eleonore Bay Group, and Caledonian orogenesis. Rapport Grønlands geologiske Undersøgelse, 104: 1-82

Higgins AK, and Leslie AG (1999) Restoring thrusting in the southern East Greenland Caledonides. Frederiksen KS and Thrane K, Second symposium on East Greenland geology, mainly Caledonian: Abstract volume, 21, Danmarks og Grønlands Geologiske Undersøgelse Rapport, Denmark: 64

Hodges KV (2000) Tectonics of the Himalaya and southern Tibet from two perspectives. Geological Society of America Bulletin, 112: 324-350

Hodges KV, Bartley JM, and Burchfiel BC (1982) Structural evolution of an A-type subduction zone, Lofoten-Rombak area, northern Scandinavian Caledonides. Tectonics, 1: 441-462

Hodges KV, Parrish RR, and Searle MP (1996) Tectonic evolution of the central Annapurna Range, Nepalese Himalayas. Tectonics, 15: 1264-1291

Holdsworth RE, and Strachan RA (1991) Interlinked system of ductile strike slip and thrusting formed by Caledonian sinistral transpression in northeastern Greenland. Geology (Boulder), 19: 510-513

Hurtado JM, Jr., Hodges KV, and Whipple K (2001) Neotectonics of the Thakkhola Graben and implications for Recent activity on the South Tibetan fault system in the central Nepal Himalaya. Geological Society of America Bulletin, 113: 222-240

Inger S, Seranne Me, and Malavieille Je (1994) Magmagenesis associated with extension in orogenic belts; examples from the Himalaya and Tibet. Late orogenic extension in mountain belts, 238: 183-197

Jain AK, Singh S, Patel RC, Gee DG, Andresen Ac, Andreasson P-Gc, and Krogh EJc (1991) Extension tectonics in orogenic belts; comparative structures from the

Himalaya and Scandinavian Caledonides. Terranes in the Arctic Caledonides, 3: 20-21

Koch L, and Haller J (1971) Geologic map of East Greenland 72°-76° N. Lat. (1:250,000). Meddelelser om Grønland, 183: 1-26

Larsen PH, and Bengård HJ (1991) The Devonian basin initiation in East Greenland: A result of sinistral wrench faulting and Caledonian extensional collapse. Journal of the Geological Society of London, 148: 355-368

Leslie AG, and Higgins AK (1999) On the Caledonian (and Grenvillian) geology of Bartholin Land, Ole Rømer Land and adjacent nunataks, East Greenland. Higgins Ak and Frederiksen KS, Geology of East Greenland 72°-75°, mainly Caledonian: preliminary reports from the 1998 expedition, Danmarks og Grønlands Geologiske Undersøgelse Rapport, Denmark: 220

Lin A (1999) S-C cataclasite in granitic rock. Tectonophysics, 304: 257-273

McClay KR, Norton MG, Coney P, and Davis GH (1986) Collapse of the Caledonian orogen and the Old Red Sandstone. Nature, 323: 147-149

Mezger K, van der Pluijm BA, Essene EJ, and Halliday AN (1991) Synorogenic collapse; a perspective from the middle crust, the Proterozoic Grenville Orogen. Science, 254: 695-698

Northrup CJ (1997) Timing structural assembly, metamorphism, and cooling of Caledonian nappes in the Ofoten-Efjorden area, North Norway; tectonic insights from U-Pb and (super 40) Ar/ (super 39) Ar geochronology. Journal of Geology, 105: 565-582

Northrup CJ, and Burchfiel BC (1993) Emplacement of the Scandinavian allochthon, Scandinavian Caledonides: A-type subduction, syn-collisional extension, or both? Geological Society of America Abstracts with Programs, 25: A-340

Parrish R (1990) U-Pb dating of monazite and its application to geological problems. Canadian Journal of Earth Sciences, 27: 1431-1450

Peucat JJ, Tisserant D, Caby R, and Clauer N (1985) Resistance of zircons to U-Pb resetting in a prograde metamorphic sequence of Caledonian age in East Greenland. Canadian Journal of Earth Sciences, 22: 330-338

Platt JP (1986) Dynamics of orogenic wedges and the uplift of high-pressure metamorphic rocks. Geological Society of America Bulletin, 97: 1037-1053

Rasmussen TV, and Andresen A (1998) Kinematic indicators in Høgedal related to the "Fjord Region Detachment". Frederiksen KS and Thrane K, Symposium on Caledonian geology in East Greenland: Abstract Volume, 46, Danmarks og Grønlands Geologiske Undersøgelse Rapport, Denmark: 55

Rex DC, Gledhill A, and Higgins AK (1977) Precambrian Rb-Sr isochron ages from the crystalline complexes of inner Forsblads Fjord, East Greenland fold belt. Rapport Grønlands geologiske Undersøgelse, 85: 122-126

Rex DC, and Gledhill AR (1981) Isotopic studies in the East Greenland Caledonides (72°-74°N) — Precambrian and Caledonian ages. Rapport Grønlands geologiske Undersøgelse, 104: 47-72

Rex DC, Gledhill AR, and Higgins AK (1976) Progress report on geochronological investigations in the crystalline complexes of the East Greenland Caledonian fold belt between 72°N and 76°N. Rapport Grønlands geologiske Undersøgelse, 80: 127-133

Royden L (1996) Coupling and decoupling of crust and mantle in convergent orogens; implications for strain partitioning in the crust. Journal of Geophysical Research, B, Solid Earth and Planets, 101: 17,679-17,705

Rykkelid E, and Andresen A (1994) Late Caledonian extension in the Ofoten area, northern Norway. Tectonophysics, 231: 157-169

Smith MP, and Robertson S (1999) The Nathorst Land Group (Neoproterozoic) of East Greenland - lithostratigraphy, basin geometry and tectonic history. Higgins Ak and Frederiksen KS, Geology of East Greenland 72°-75°, mainly Caledonian: preliminary reports from the 1998 expedition, Danmarks og Grønlands Geologiske Undersøgelse Rapport, Denmark: 220

Sønderholm M, and Tirsgaard H (1993) Lithostratigraphic framework of the Upper Proterozoic Eleonore Bay Supergroup of East and North-East Greenland. Grønlands Geologiske Undersøgelse, 167

Strachan RA (1994) Evidence in North-East Greenland for Late Silurian - Early Devonian regional extension during the Caledonian orogeny. Geology, 22: 913-916

Strachan RA, Chadwick B, Friend CRL, Holdsworth RE, Hibbard JPe, van Staal CRe, and Cawood PAe (1995) New perspectives on the Caledonian Orogeny in Northeast Greenland. Current perspectives in the Appalachian-Caledonian Orogen. NUNA conference on New perspectives in the Appalachian-Caledonian Orogen, 41: 303-322

Strachan RA, Holdsworth RE, Friderichsen JD, and Jepsen HF (1992) Regional Caledonian structure within an oblique convergence zone, Dronning Louise Land, NE Greenland. Journal of the Geological Society of London, 149, Part 3: 359-371

Strachan RA, Martin MW, and Friderichsen JD (In Press) Evidence for contemporaneous yet contrasting styles of granite magmatism during extensional collapse of the northeast Greenland Caledonides. Tectonics

Sturt BA, and Thon A (1978) An ophiolite complex of probable early Caledonian age discovered on Karmoy. Nature (London), 275: 538-539

Thrane K, Kalsbeek F, and Watt GR (1999a) Evidence for a Grenvillian event in the East Greenland Caledonian fold belt. Frederiksen KS and Thrane K, Second symposium on East Greenland geology, mainly Caledonian: Abstract volume, 21, Danmarks og Grønlands Geologiske Undersøgelse Rapport, Denmark: 64

Thrane K, Watt GR, Kinny PD, Jones KA, and Escher JC (1999b) Early Neoproterozoic Rodinian rifting: SIMS U-Pb ages from the East Greenland Caledonides. Higgins Ak and Frederiksen KS, Geology of East Greenland 72°-75°, mainly Caledonian: preliminary reports from the 1998 expedition, Danmarks og Grønlands Geologiske Undersøgelse Rapport, Denmark: 220

Torsvik TH, Smethurst MA, Meert JG, Van der Voo R, McKerrow WS, Brasier MD, Sturt BA, and Walderhaug HJ (1996) Continental break-up and collision in the Neoproterozoic and Palaeozoic; a tale of Baltica and Laurentia. Earth-Science Reviews, 40: 229-258

Vanderhaeghe O, Burg J-P, Teyssier C, Ring Ue, Brandon MTe, Lister GSe, and Willett SDe (1999) Exhumation of migmatites in two collapsed orogens; Canadian Cordillera and French Variscides (eds), Exhumation processes; normal faulting,

ductile flow and erosion, vol. 154. Geological Society Special Publications, pp 181-204

Vidal G (1976) Late Precambrian acritarchs from the Eleonore Bay Group and Tillite Group in East Greenland; a preliminary report. Rapport - Groenlands Geologiske Undersoegelse, 19

Vidal G (1979) Acritarchs from the upper Proterozoic and Lower Cambrian of East Greenland. Bulletin - Grønlands Geologiske Undersøgelse, 37

Vold J (1997) Et studie av den tectonomatemorphe utviklingen av gneisserne i liggblokken til "The Fjord Region Detachment Zone" på Kap hedlund, sentrale Øst Grønland. Cand. Scient Thesis, University of Oslo, Oslo, 122

Watt GR, and Thrane K (1999) The nature of the Grenvillian orogeny in central East Greenland. Frederiksen KS and Thrane K, Second symposium on East Greenland geology, mainly Caledonian: Abstract volume, 21, Danmarks og Grønlands Geologiske Undersøgelse Rapport, Denmark: 64

Wegmann CE (1935) Preliminary report on the Caledonian orogeny in Christian X's Land (North-East Greenland). Meddelelser om Grønland, 128: 145-156

White AP, Hodges KV, and Davidek K (1998) Age constraints on metamorphism and deformation of the Krummedal Supracrustal Sequence in Forsblad Fjord, East Greenland. Geological Society of America, 1998 Annual Meeting, Toronto, 30: 191

York D (1969) Least-squares fitting of a straight line with correlated errors. Earth Planet Sci Lett, 5: 320-324

Appendix: U-Pb Analytical Methods

Samples were separated and analyzed at the Massachusetts Institute of Technology Thermal Ionization Mass Spectrometer Laboratory. Initial sample weights ranged from 1 to 4 kilograms. After being crushed, samples were sorted by density and magnetic susceptibility to isolate individual grains of monazite. Optical and back-scattered electron (BSE) images taken from the JEOL Superprobe 733 at the

Massachusetts Institute of Technology (operating with an accelerating voltage 15 to 20 kV and a beam current of 10 to 15 nA) were used to assess the internal compositional variations within the grains. Pb and U were extracted and analyzed from select crystals following the procedures of Hawkins and Bowring (1997). All analyses were performed on a VG Sector 54 mass spectrometer

Figure Captions

Figure 1: Simplified tectonic map of the central fjord region of the East Greenland Caledonides interpreted after Haller (1971), Henriksen and Higgins (1976), Peucat et al. (1985), Andresen et al. (1997), White et al. (1998), Smith and Robertson (1999), Leslie and Higgins (1999), Escher and Jones (1999), White and Hodges (1999). The following abbreviations have been used: Forsblad Fjord (FF); Alpefjord (AF); Kaiser Franz Joseph's Fjord (KFJF); Kong Oscar's Fjord (KOF); Furesø (F); Eleonore Sø (ES); Målebjorg (M); Niggli Spids (NS); Charcot Land (CL). *N.B.* Gåseland lies south to the south from this map. Box indicates area of Plate I. Question marks indicate unknown or enigmatic contacts, unexplained by past work in the region. We have interpreted the above thrust geometries based on correlations between the preliminary age relationships and fault contacts reported by the Greenland Geological Survey in 1999 and the earlier work of L. Koch, J. Haller and others as referenced above.

Figure 2: Fold structures that accommodate E-W shortening. a) Photograph of migmatitic leucosome in the Krummedal Sequence. Note the right-lateral, ductile shear-band that deforms the leucocratic melt. b) Photograph of mylonite from the Høgedal Detachment - facing N. Note the marked K-feldspar crystals: kfs2 has been separated from kfs1 during top-to-the-E deformation. Also note the presence of chlorite, biotite and

dynamically recrystallized quartz. c) Photograph of the Caledonia Ø granite facing north. Note the top-to-east mylonitic fabric macroscopically defined by sheared biotite schlieren. d) Photograph of an F_{2M} structure that folds the S_{1M} schistosity. This fold now forms the core of a D_{3M} boudin. The tail trailing off to the upper left corner, along with the biotite schlieren that are visible in the top right of the photograph, define the S_{3M} schistosity. e) Photograph (facing down, left to the north, right to the south) of deformed calc-silicate lense. The shear band just beneath the lense shows dextral, top-to-the-south sense-of-shear during D_{2H} N-S flow. f) Photograph (facing down, left corner is west, right corner is east) of asymmetric amphibolite lense showing sinistral, top-to-N sense-of-shear during D_{2H} N-S flow.

Figure 3: Back-scattered electron images of individual crystals from the concordant leucosome, 97GR14 (**a-d**), from the Caledonia Ø granite pluton (synkinematic to shearing along the Tindern detachment), 97GR18 (**e-f**), 98GR23 (**g-j**), from the undeformed two-mica leucogranite, 98GR17 (**k-m**) – these images indicate that some monazite preserve delicate zoning or lack thereof which may indicate *in situ* metamorphic growth while others preserve core-mantle relationships which may indicate some component of inheritance. **a** Subhedral monazite shows single domain, homogeneous composition with no significant Th variation from core to rim and some minor inclusions. **b** Subhedral monazite crystal with sector zoned domains indicating two phases: dominant phase with higher Th concentration, and secondary phase with lower Th concentration. **c** Euhedral, single crystal monazite with partially resorbed core showing multiple phases of varying Th concentrations with complex contacts, surrounded by a high Th, single phase mantle. **d** Subhedral monazite crystal showing a single phase core with a high Th concentration surrounded by a thick mantle with a low Th concentration. This core/mantle relationship suggests an inherited component of monazite

may be present within this sample. **e, f** Subhedral xenotime crystals showing single domain and two-phase mixture with single-phase rim overgrowth. **g** Subhedral, single domain monazite. **h** Partially resorbed, subhedral, two-domain monazite crystal. The boundaries between high and low Th concentration domains indicate overgrowth by the low-Th phase. There are inclusions of zircon and quartz. **i** Subhedral monazite crystal with partially resorbed core surrounded by simple, oscillatory zoning parallel to relict crystal faces. The high Th band just within the low Th rim has been partially resorbed. **j** Euhedral monazite crystal with partially resorbed core surrounded by a mantle with prominent, oscillatory zoning and inclusions of zircon. **k** Subhedral monazite with a single Th domain. **l** Subhedral monazite with two domains indicating significant resorbtion of darker, low Th domain which was overgrown by higher Th, lighter domain. **m** Subhedral monazite crystal displaying oscillatory zoning parallel to relict crystal faces.

Figure 4: Concordia diagrams for samples as marked. Curves with tic marks represent concordia with labels in units of Ma. M followed by a number indicates monazite fraction. X followed by a number indicates xenotime fraction. 2σ analytical uncertainties are represented by ellipses. Linear arrays determined by regression analysis after York (1969).

Figure 5: Back-scattered electron image of monazite growing in the matrix of sample 98GR23, the Caledonia Ø granite pluton. Note that the monazite and the zircon are growing parallel to the large biotite crystal in the lower left of the picture, next to K-feldspar and quartz, and parallel to the muscovite in the upper right. This relationship suggests that the monazite and zircon were growing at the same time as the other metamorphic minerals, and were preferentially aligned at the same time as the phyllosilicates.

Figure 6: Structural and temporal correlations between allochthons in the Forsblad Fjord region. Labeled rectangles indicate deformational events within a given allochthon. Circles indicate mapped tectonic structures that separate allochthons. H – Høgedal detachment, T – Tindern detachment. Shaded fields indicate deformational events and fabrics which are interpreted to be extensional. Solid horizontal lines indicate correlative deformational events in different allochthons. Dashed horizontal lines indicate inferred correlative deformational events in different allochthons. Age assignments are based on U-Pb geochronologic data presented or discussed in this paper.

Figure 7: Cross-section from **A-B** on Plate 1. Unit names correspond to those in the legend in Plate 1. Høgedal and Tindern detachments are inferred to merge onto a single plane based on the geometry of the FRDS around 73°N. The subsurface presence of a thrust fault is inferred from the regional map shown in Figure 1, timing of metamorphism and presence of contractional fabrics. The rationale is discussed in the "Implications for regional thrusting" section.

Figure 8: Simplified 3-D block diagram of the Forsblad Fjord region and surrounding areas. Two simple geometries are shown which could lead to the ambiguous field relationships in the current Forsblad Fjord exposures. Scenario A: low angle thrusting proceeded by folding or domal upwelling was followed by normal faulting along the FRDS. Extensional deformation was partitioned along two faults, the Høgedal detachment (HD) and the Tindern detachment (TD). Rupture along the HD truncated the thrust fault, sandwiching a remnant of the thrust plane between the TD and HD. Scenario B: a very similar situation except that extensional strain along the HD reactivated the plane of the original thrust fault. In either scenario, the Gletscherland Complex represents

the footwall of thrusting, a region which was not subjected to high-grade Caledonian metamorphism.

Figure 9: Simplified cartoon cross-section of Caledonian orogenesis. As Baltica subducted beneath Laurentia, crustal shortening due to synthetic and antithetic thrusting along the Laurentian margin raised up two symmetrical regions of high elevation and associated large topographic gradient – the Scandinavian Caledonides and the East Greenland Caledonides. Material at middle-crustal levels beneath this elevated orogen was flowing ductiley to both the north and south (in the present reference frame). At some point thereafter in modern-day East Greenland, synorogenic extension along orogen perpendicular normal faults acted in consort with the thrust faults to exhume a wedge of migmatitic gneisses preserving fabrics of middle-crustal E-W shortening and N-S flow in the Krummedal Sequence.

Plate I. a) Geologic Map of the Forsblad Fjord Region, East Greenland. Data for the topographic base was provided by the Geological Survey of Denmark and Greenland (GEUS). Fault lines are drawn with varying weights to indicate inferred importance. Note that the Klosterbjerg granite is included with the undifferentiated, Ordovician-Silurian granites. b) Structural Map of the Forsblad Fjord Region, East Greenland. Ice and sea level contacts are provided for reference to the geologic map. Structural data are statistical averages of 10 to 100 measurements for each symbol presented. Stereonet data (Schmidt net, Lower Hemisphere; contour interval = 2.0%/1% area; mean great circle and mean vector as indicated): poles to the S_{1H} and S_{2H} planes, 95% confidence cone = 1.3°; poles to the S_{3H} planes, 95% confidence cone = 1.7°; L_{2H} lineations, 95% confidence cone = 2.4°; L_{3H} lineations, 95% confidence cone = 5.9°.

Figure 1


Ice Cover
74
27
ES
M
7
KFJF
NS
73°
20 km
KF
KOF
Ice Cover
FF
CL
72°
N
ICE COVER
CALEDONIAN FOLD BELT
0 500 km
Fjord Region Detachment System
Normal Fault
Thrust Fault
Inferred Fault Contact
Lithologic Contact
Inferred Lithologic Contact
Devonian Carboniferous Basins
Caledonian Granitoid Plutons and Migmatitic Rocks
Neoproterozoic Eleonore Bay Supergroup
Mesoproterozoic - Neoproterozoic Metasedimentary Rocks
Archean - Paleoproterozoic Basement Complex

Figure 2

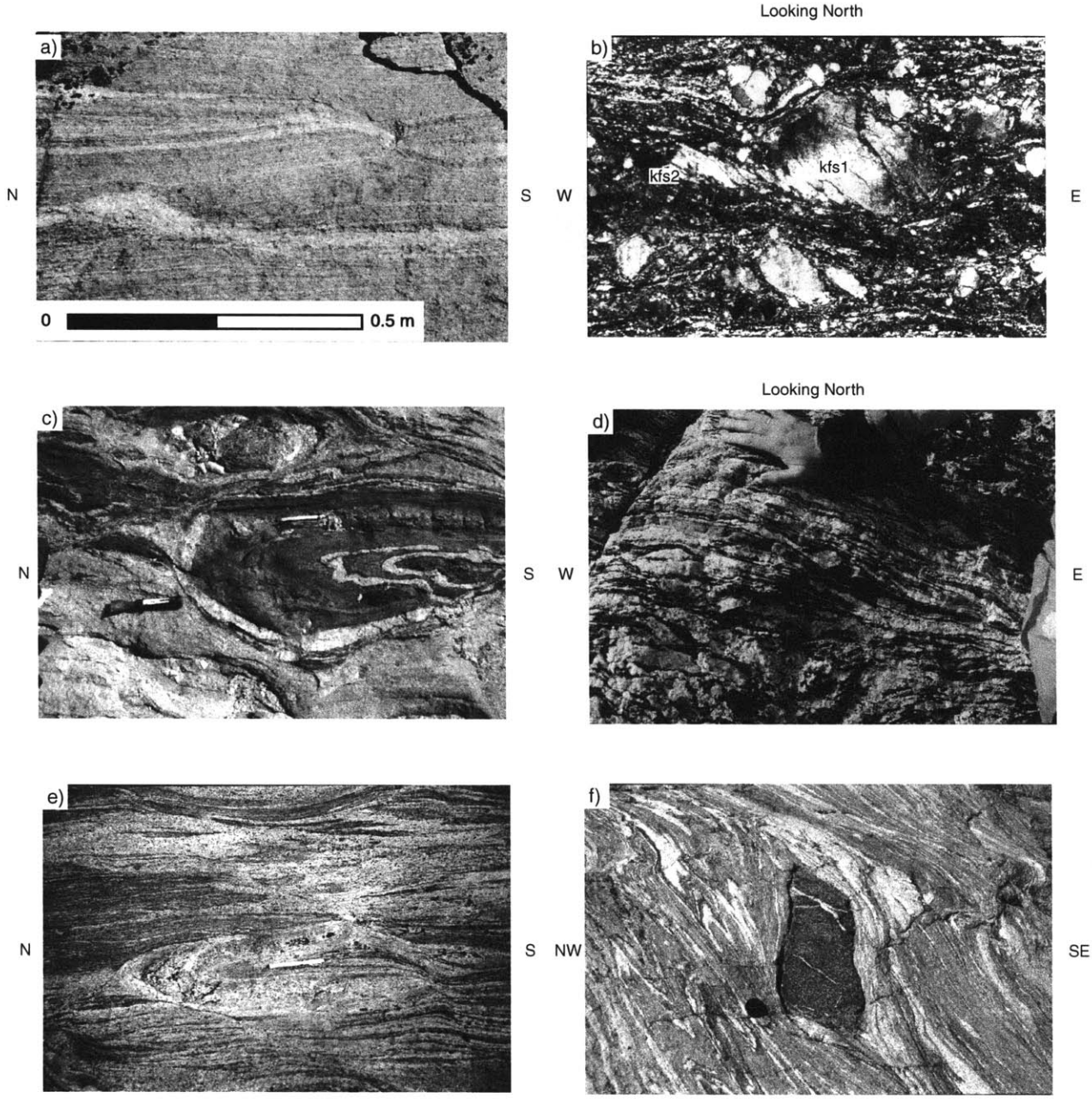
a)
0
0.5 m
N
S
Looking North
b)
kfs2
kfs1
W
E
c)
N
S
Looking North
d)
W
E
e)
N
S
f)
NW
SE

Figure 3

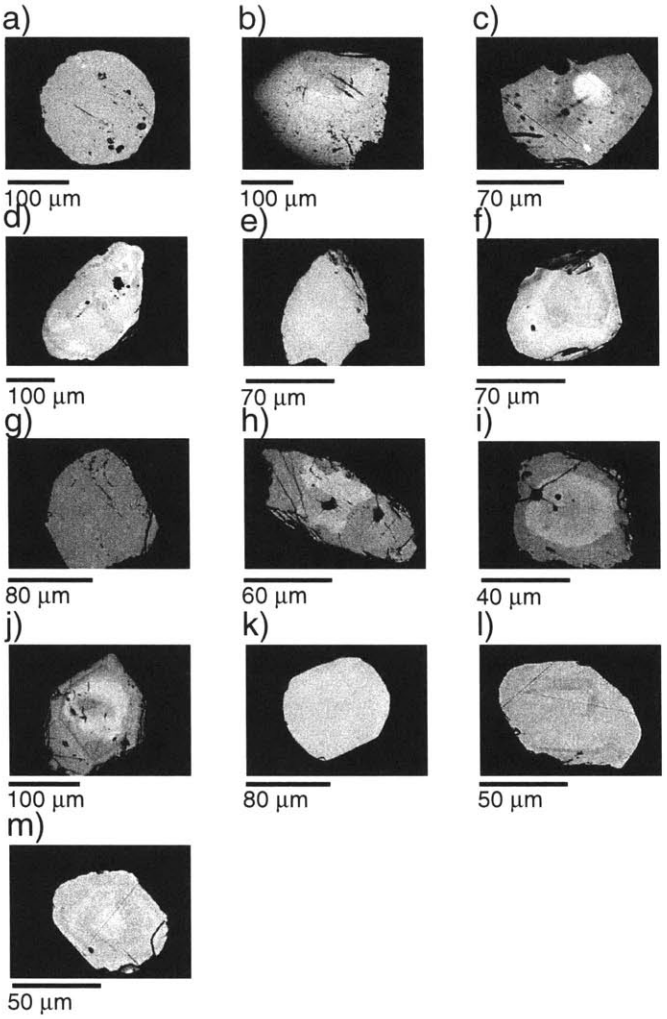
a)
100 µm
b)
100 µm
c)
70 µm
d)
100 µm
e)
70 µm
f)
70 µm
g)
80 µm
h)
60 µm
i)
40 µm
j)
100 µm
k)
80 µm
l)
50 µm
m)
50 µm

Figure 4

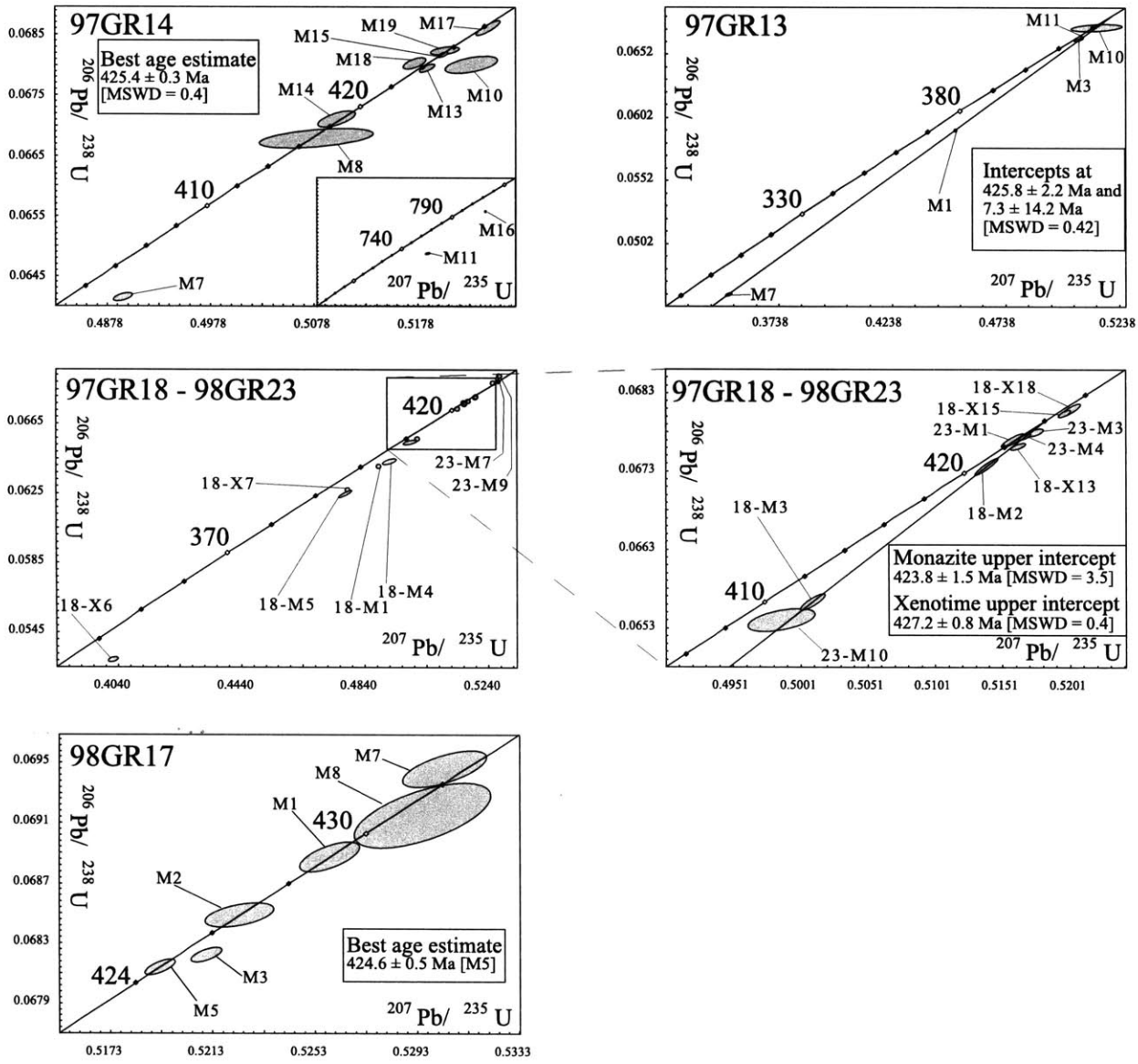
97GR14
Best age estimate
425.4 ± 0.3 Ma
[MSWD = 0.4]
M15
M19
M17
M18
M14
420
M13
M10
M8
410
790
740
M16
M11
M7
206 Pb/ 238 U
207 Pb/ 235 U
0.0685
0.0675
0.0665
0.0655
0.0645
0.4878
0.4978
0.5078
0.5178
97GR13
M11
M10
M3
380
330
M1
M7
Intercepts at
425.8 ± 2.2 Ma and
7.3 ± 14.2 Ma
[MSWD = 0.42]
0.0652
0.0602
0.0552
0.0502
0.3738
0.4238
0.4738
0.5238
97GR18 - 98GR23
420
23-M7
23-M9
18-X7
370
18-X6
18-M5
18-M1
18-M4
0.0665
0.0625
0.0585
0.0545
0.4040
0.4440
0.4840
0.5240
97GR18 - 98GR23
18-X18
18-X15
23-M1
23-M3
23-M4
420
18-X13
18-M3
18-M2
Monazite upper intercept
423.8 ± 1.5 Ma [MSWD = 3.5]
Xenotime upper intercept
427.2 ± 0.8 Ma [MSWD = 0.4]
410
23-M10
0.0683
0.0673
0.0663
0.0653
0.4951
0.5001
0.5051
0.5101
0.5151
0.5201
98GR17
M7
M8
M1
430
M2
M3
424
M5
Best age estimate
424.6 ± 0.5 Ma [M5]
0.0695
0.0691
0.0687
0.0683
0.0679
0.5173
0.5213
0.5253
0.5293
0.5333

Figure 5

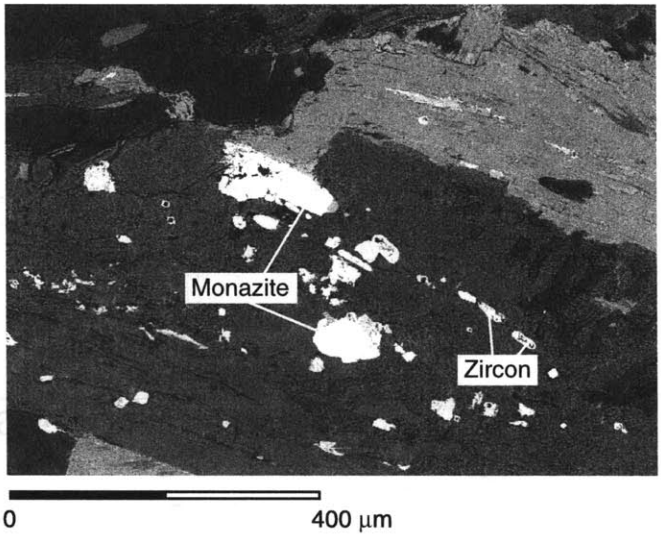

Figure 6

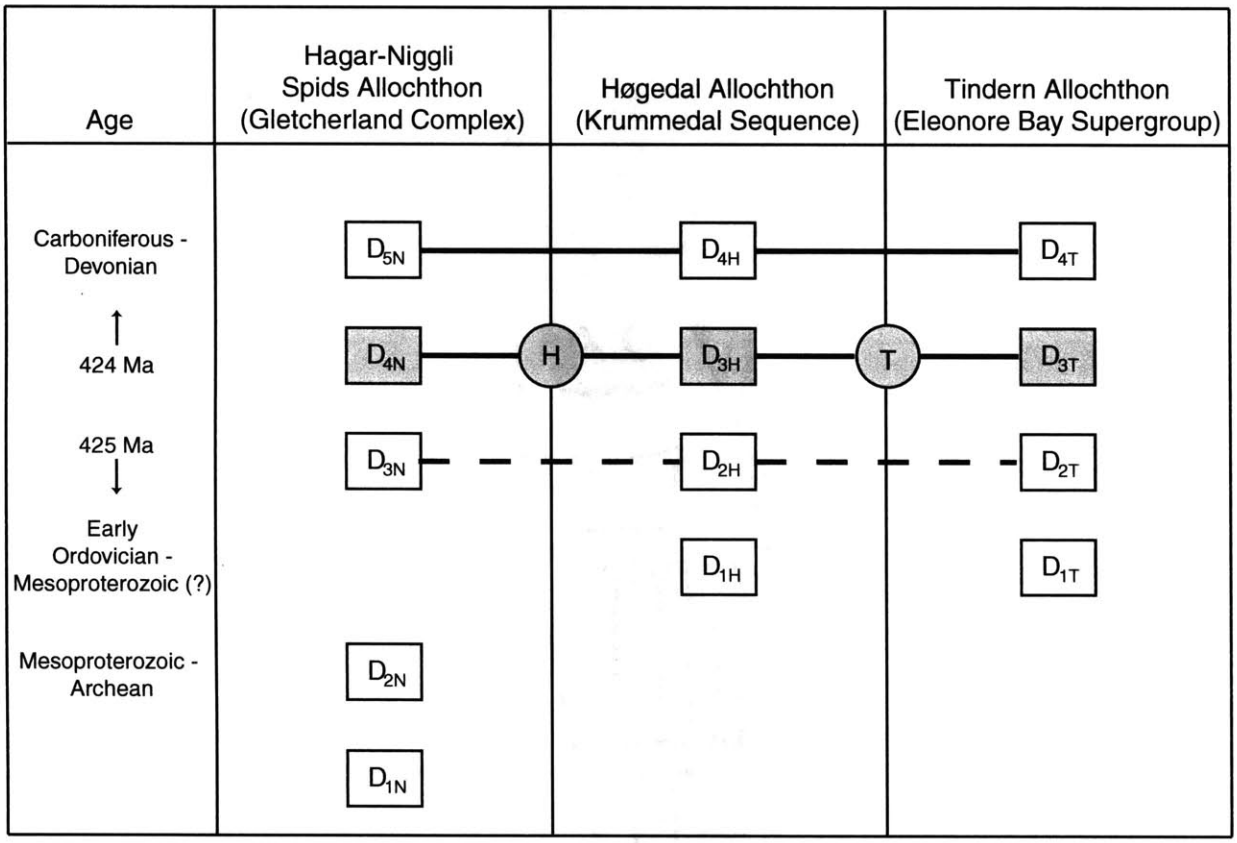
Age
Hagar-Niggli Spids Allochthon (Gletcherland Complex)
Høgedal Allochthon (Krummedal Sequence)
Tindern Allochthon (Eleonore Bay Supergroup)
Carboniferous - Devonian
424 Ma
425 Ma
Early Ordovician - Mesoproterozoic (?)
Mesoproterozoic - Archean
D5N
D4N
D3N
D2N
D1N
D4H
D3H
D2H
D1H
D4T
D3T
D2T
D1T
H
T

Figure 7

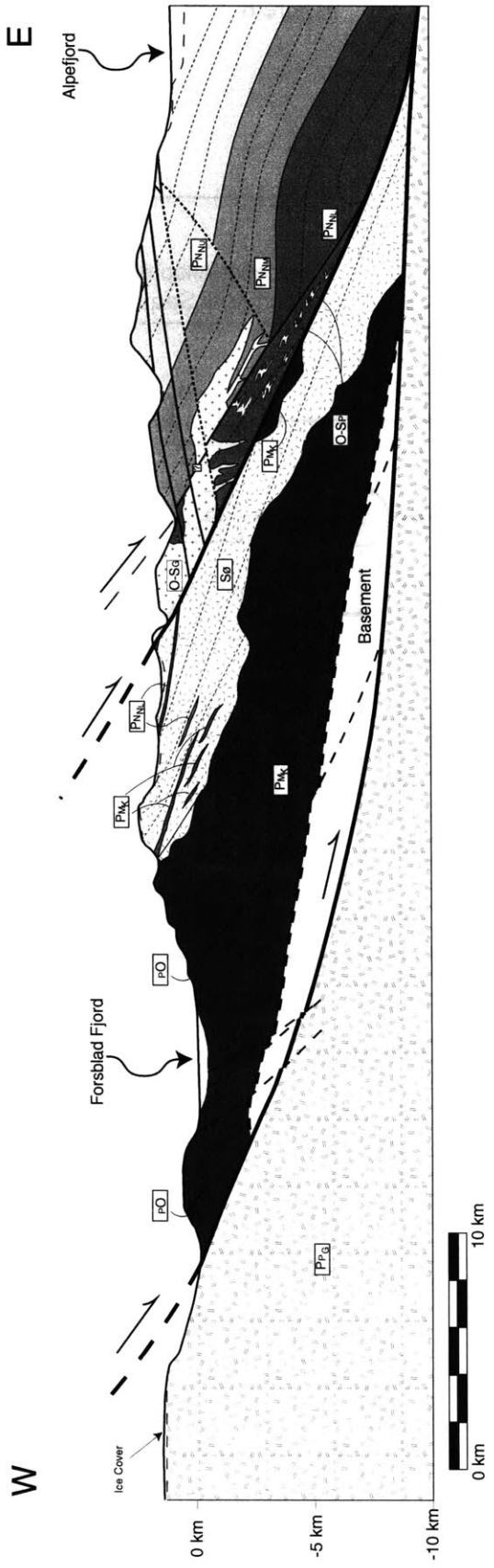
E
W
Alpefjord
Forsblad Fjord
Ice Cover
Basement
O-Sg
Sø
O-Sø
pO
pO
PNN
PNN
PNN
PNN
PMK
PMK
PMK
PPG
0 km
-5 km
-10 km
10 km
0 km

Figure 8

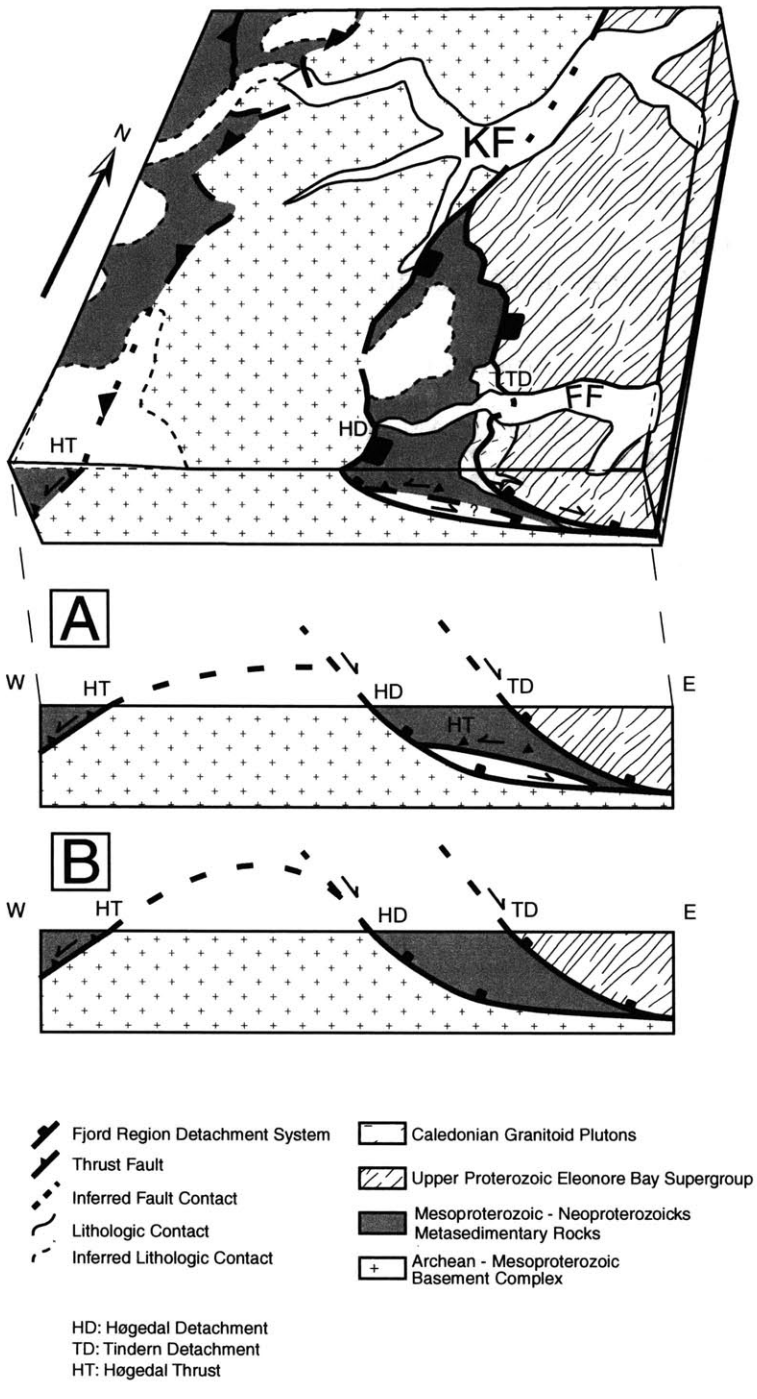
N
KF
TD
FF
HD
HT
A
W
HT
HD
TD
E
HT
B
W
HT
HD
TD
E
Fjord Region Detachment System
Thrust Fault
Inferred Fault Contact
Lithologic Contact
Inferred Lithologic Contact
Caledonian Granitoid Plutons
Upper Proterozoic Eleonore Bay Supergroup
Mesoproterozoic - Neoproterozoicks Metasedimentary Rocks
Archean - Mesoproterozoic Basement Complex
HD: Høgedal Detachment
TD: Tindern Detachment
HT: Høgedal Thrust

Figure 9

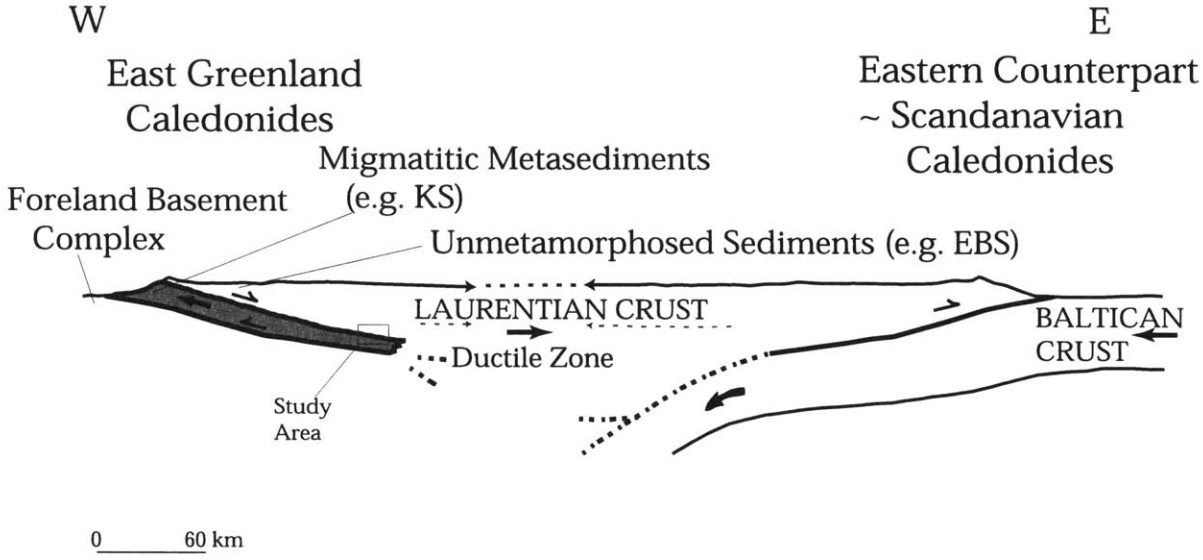
W
East Greenland
Caledonides
E
Eastern Counterpart
~ Scandanavian
Caledonides
Migmatitic Metasediments
(e.g. KS)
Foreland Basement
Complex
Unmetamorphosed Sediments (e.g. EBS)
LAURENTIAN CRUST
Ductile Zone
BALTICAN
CRUST
Study
Area
0
60 km

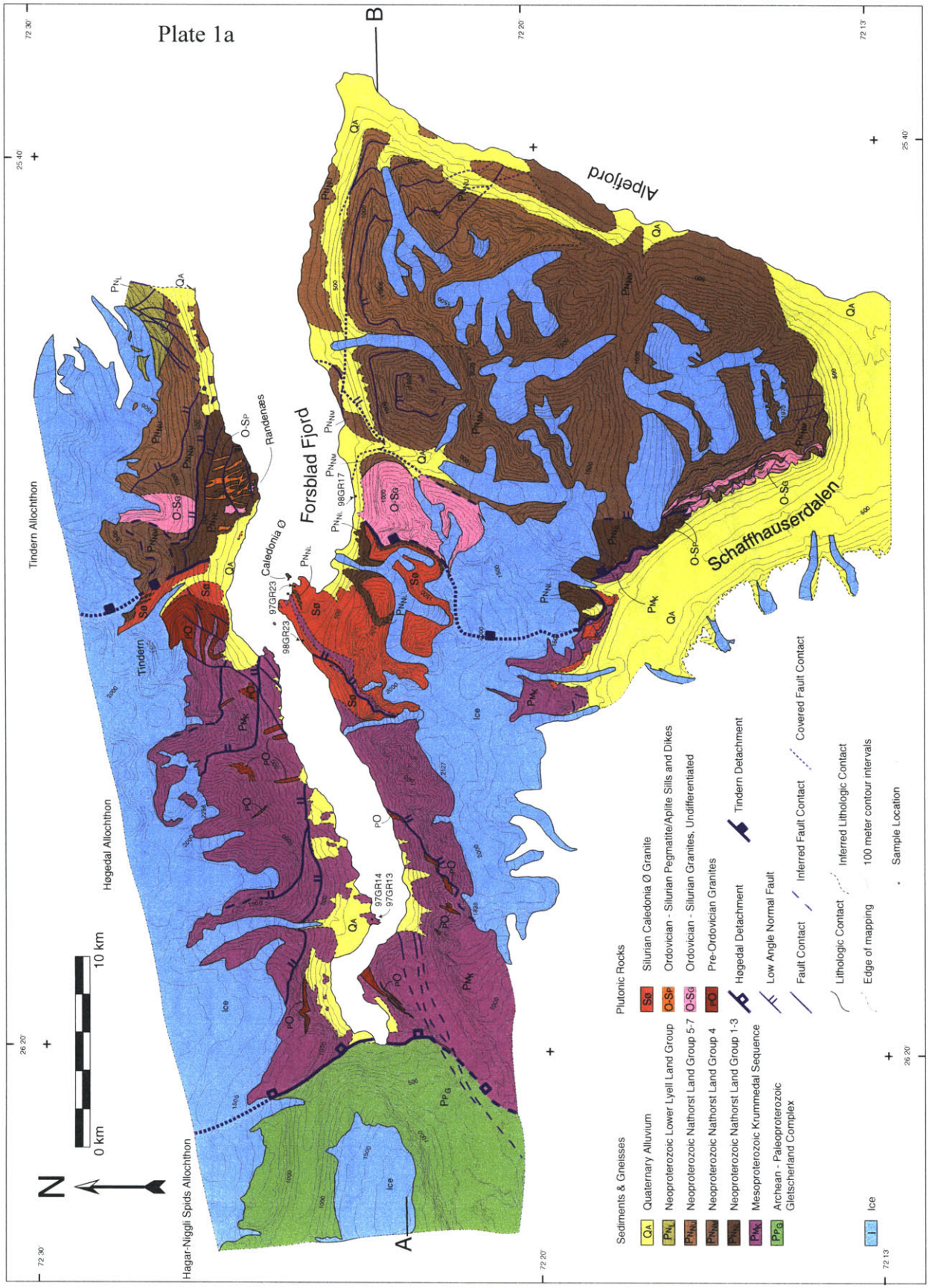
Plate 1a
Forsblad Fjord
Alpefjord
Schaffhauserdalen
Tindern Allochthon
Hagar-Niggli Spids Allochthon
Høgedal Allochthon
Randenæs
Caledonia Ø
Tindern
A
B
N
0 km
10 km
Ice
Sediments & Gneisses
Quaternary Alluvium
Neoproterozoic Lower Lyell Land Group
Neoproterozoic Nathorst Land Group 5-7
Neoproterozoic Nathorst Land Group 4
Neoproterozoic Nathorst Land Group 1-3
Mesoproterozoic Krummedal Sequence
Archean - Paleoproterozoic Gletscherland Complex
Plutonic Rocks
Silurian Caledonia Ø Granite
Ordovician - Silurian Pegmatite/Aplite Sills and Dikes
Ordovician - Silurian Granites, Undifferentiated
Pre-Ordovician Granites
Høgedal Detachment
Tindern Detachment
Low Angle Normal Fault
Fault Contact
Inferred Fault Contact
Covered Fault Contact
Lithologic Contact
Inferred Lithologic Contact
Edge of mapping
100 meter contour intervals
Sample Location
97GR14
97GR13
98GR23
97GR23
98GR17

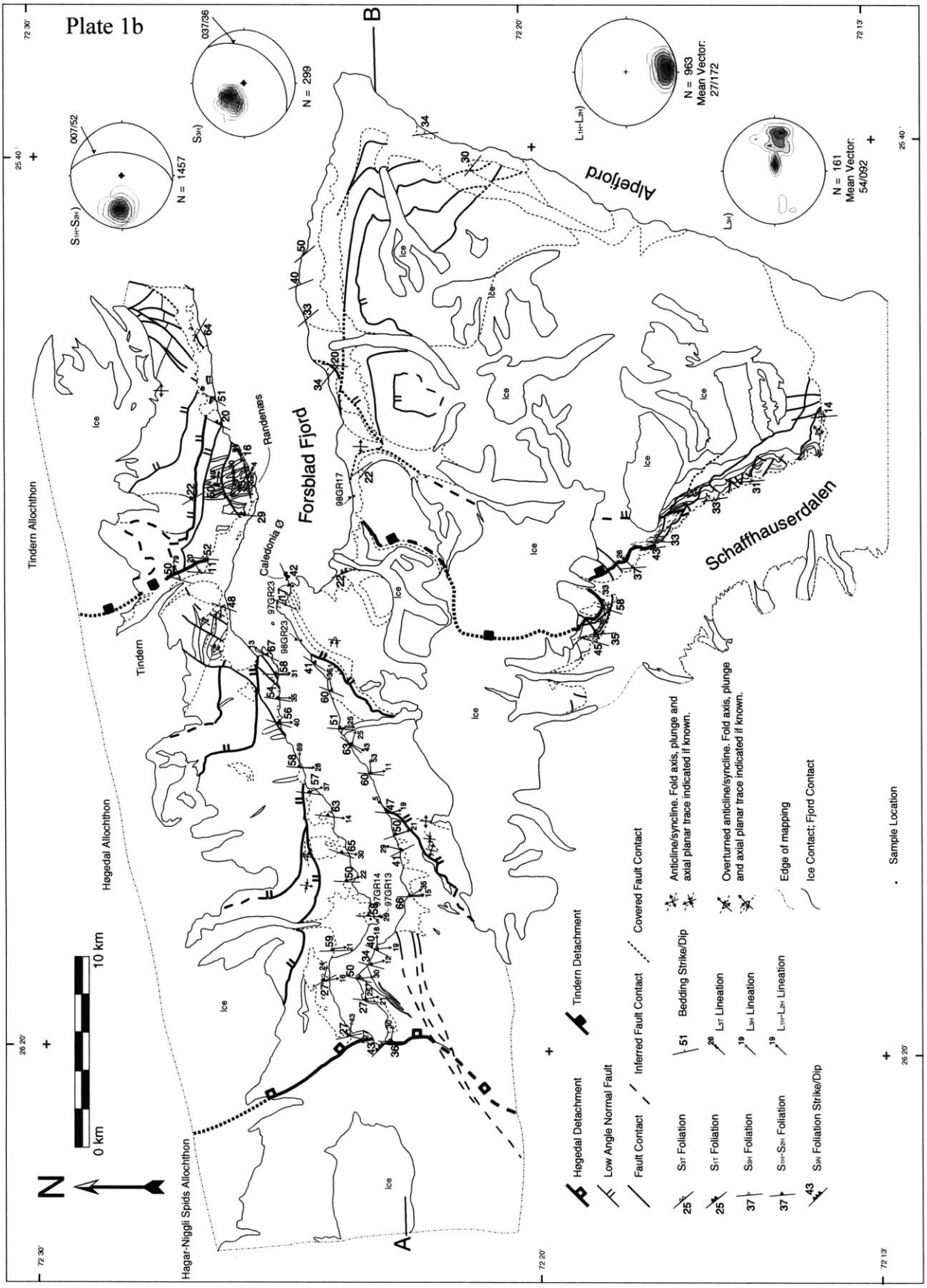
Plate 1b
Tindern Allochthon
Høgedal Allochthon
Hagar-Niggli Spids Allochthon
Forsblad Fjord
Randenæs
Caledonia Ø
Alpefjord
Schaffhauserdalen
Tindern
Ice
A
B
N
0 km
10 km
N = 1457
N = 299
N = 963
Mean Vector: 27/172
N = 161
Mean Vector: 54/092
Høgedal Detachment
Tindern Detachment
Low Angle Normal Fault
Fault Contact
Inferred Fault Contact
Covered Fault Contact
Bedding Strike/Dip
Anticline/syncline. Fold axis, plunge and axial planar trace indicated if known.
Overturned anticline/syncline. Fold axis, plunge and axial planar trace indicated if known.
Edge of mapping
Ice Contact; Fjord Contact
Sample Location
S1T Foliation
S1T Foliation
S2H Foliation
S1H-S2H Foliation
S2H Foliation Strike/Dip
L2T Lineation
L2H Lineation
L1H-L2H Lineation

Table 1. U-Pb isotopic data for monazite and xenotime, East Greenland.

Sample	Weight	Concentration					Error 2 Sigma %						Age, Ma			Corr.
Fractions[a]	µg[b]	U, ppm	Pb, ppm	Pb, pg[c]	$^{206}Pb/^{204}Pb$	$^{208}Pb/^{206}Pb$	$^{206}Pb/^{238}U$	Error	$^{207}Pb/^{235}U$	Error	$^{207}Pb/^{206}Pb$	Error	$^{206}Pb/^{238}U$	$^{207}Pb/^{235}U$	$^{207}Pb/^{206}Pb$	Coef.
97GR14, concordant leucosome [72• 23.4'N, 26• 10.4'W]																
M16	4.2	962.2	762.8	13.6	2422.9	5.853	0.13181	(.07)	1.24723	(.10)	0.06863	(.07)	**798.2**	**822.2**	**887.6**	0.74
M11	3 5	1831.2	2018.5	117.2	435.7	9.332	0.12035	(.21)	1.12651	(.45)	0.06789	(.38)	**732.6**	**766.1**	**865.1**	0 54
M17	13.0	496.5	433.4	12.9	2197.0	13 597	0.06861	(.17)	0.52456	(20)	0.05545	(.10)	**427.8**	**428.2**	**430.3**	0 85
M10	5.2	1786.8	935.7	77.9	522.7	7.691	0 06803	(.19)	0.52288	(50)	0.05575	(.44)	**424.3**	**427.1**	**442.3**	0.51
M19	25.6	790.2	537.7	129.5	687.1	10.343	0.06825	(.10)	0.52068	(.27)	0.05533	(.24)	**425.6**	**425.6**	**425.6**	0.48
M15	2.1	7183.5	1109.7	20.3	3136.6	1.547	0.06818	(.06)	0 52012	(.08)	0 05532	(.05)	**425.2**	**425.2**	**425.4**	0.76
M13	3.3	1100.9	774 3	16.2	978.0	10.826	0.06796	(.10)	0.51868	(.14)	0 05535	(.10)	**423.9**	**424.3**	**426.5**	0.70
M18	16.0	267.9	201.0	34 2	555.2	11.542	0.06804	(12)	0.51748	(.19)	0.05516	(.15)	**424.3**	**423.5**	**418.7**	0.66
M14	1.5	1167.8	720 9	35 5	231.6	9.253	0.06711	(.18)	0.50995	(.32)	0.05511	(.26)	**418.7**	**418.4**	**416.8**	0.60
M8	0.6	2358.2	1213.9	43.0	161.0	7.374	0.06679	(.24)	0.50789	####	0.05515	(.99)	**416.8**	**417.0**	**418.3**	0.46
M7	16.7	745.9	607.2	44.8	1136 1	13.522	0.06416	(.10)	0.48937	(16)	0.05532	(13)	**400.9**	**404.5**	**425.3**	0.60
97GR13, discordant leucosome [72• 23.4' N, 26• 10.4' W]																
M10	0.8	1533.5	755 2	73 3	88.8	6.415	0 06730	(.36)	0 51399	####	0.05539	####	**419.9**	**421.1**	**427.9**	0.45
M3	2.9	7737.5	1476.1	29.9	3156.9	2.239	0 06654	(13)	0.50744	(.17)	0 05531	(.11)	**415.3**	**416.7**	**424.8**	0.75
M11	3.4	3451.6	489.1	62.8	796.1	1 330	0.06633	(.18)	0.50630	(.30)	0 05536	(.22)	**414.0**	**416.0**	**426.9**	0.66
M1	2.9	2310.3	454.3	8.5	2941.1	2 770	0.05920	(.11)	0.45161	(.16)	0 05533	(.11)	**370.7**	**378.4**	**425.6**	0.71
M7	0.8	3059.3	422 4	4.0	1846.8	2.401	0.04612	(22)	0.35122	(.34)	0.05524	(.24)	**290.6**	**305.6**	**421.8**	0.70
97GR18, Caledonia Ø Granite [72• 25.0' N, 25• 51.0' W]																
X18	1.2	8022 7	509.4	5 4	7891.1	0.026	0.06811	(.11)	0.52001	(.14)	0.05537	(.09)	**424.8**	**425.2**	**427.2**	0 77
X15	2.5	7034.3	456.1	7.5	10122 7	0.049	0.06808	(.06)	0.51979	(.08)	0.05537	(.05)	**424.6**	**425.0**	**427.4**	0 80
X13	4.4	7930 2	522 1	101.2	1478.5	0 029	0.06765	(.06)	0.51627	(.08)	0 05535	(05)	**422.0**	**422.7**	**426.4**	0.74
M2	8.2	19717 9	1660.2	21 5	32364 8	0.393	0.06739	(15)	0.51393	(.16)	0.05531	(.04)	**420.4**	**421.1**	**424.6**	0.96
M3	1.6	10003 8	1219.7	12 1	5590 2	1.086	0.06567	(14)	0.50102	(.17)	0.05534	(.08)	**410.0**	**412.4**	**425.8**	0.87
M4	1.0	6302.7	998.9	28.1	907.7	1.723	0.06434	(.18)	0.49222	(.34)	0.05549	(.27)	**402.0**	**406.4**	**431.9**	0.59
M1	1 0	13763.1	1613 0	6 4	8796.4	1.059	0 06410	(.07)	0.48835	(.15)	0.05526	(.12)	**400.5**	**403.8**	**422.7**	0.52
X7	2.3	6445.6	381.5	8.7	6771.2	0.036	0 06273	(.11)	0.47839	(14)	0.05531	(.08)	**392.2**	**397.0**	**424.6**	0.82
M5	1.6	9359.4	546.4	13.8	4354.6	0.019	0 06247	(.32)	0.47770	(.34)	0.05546	(.09)	**390.6**	**396.5**	**431.0**	0.96
X6	0.7	9314.5	460.5	2.8	8036.8	0 032	0 05291	(.18)	0.40248	(.28)	0 05517	(.21)	**332.4**	**343.4**	**419.0**	0.65
98GR23, Caledonia Ø Granite [72• 24.2' N, 25• 55.8' W]																
M7	4.9	5461.1	1125.4	121.7	980.9	2.311	0.06928	(.07)	0.52766	(.11)	0.05524	(.08)	**431.8**	**430.3**	**421.8**	0.69
M9	1.1	13909.1	3114.5	48.5	1420.5	2.654	0.06888	(.09)	0.52565	(11)	0.05535	(.07)	**429.4**	**428.9**	**426.4**	0.80
M3	2.7	5816.9	1440.2	171.0	408 5	2.981	0.06783	(.07)	0.51753	(13)	0.05533	(.10)	**423.1**	**423.5**	**425.7**	0.57
M4	1.6	5505.0	1333.5	22.1	1714.3	3.039	0.06777	(.06)	0.51664	(09)	0 05529	(.06)	**422.7**	**422.9**	**424.1**	0.70
M1	1.6	9627.7	2169.6	92.7	724.3	2.691	0.06774	(.11)	0.51594	(.15)	0.05524	(.10)	**422.5**	**422.4**	**422.0**	0.77
M10	0.2	9774.5	2232.3	19 0	379.3	2.814	0.06545	(24)	0.49864	(.48)	0.05526	(.39)	**408.7**	**410.8**	**422.7**	0.57
98GR17, Klosterbjerg Granite [72• 23.6' N, 25• 42.1' W]																
M7	0 4	6311.2	2398.9	27.4	439.5	5.117	0.06941	(.18)	0.53033	(32)	0.05541	(.25)	**432.6**	**432.0**	**428.9**	0.62
M8	0.4	2776.3	1085.9	10.4	507.4	5.381	0 06910	(.29)	0.52944	(.50)	0.05557	(.38)	**430.7**	**431.4**	**435.2**	0.63
M1	4.1	2276.8	948.9	44.1	931.9	5.862	0.06883	(13)	0 52586	(.21)	0.05541	(17)	**429.1**	**429.1**	**428.8**	0 63
M2	0 6	7347.6	3180.6	25.7	754.8	6 161	0.06844	(.11)	0.52238	(.25)	0.05536	(.22)	**426.8**	**426.7**	**426.7**	0.50
M3	0.9	7600.0	2350.3	24.0	1241.0	4.133	0.06817	(.07)	0.52098	(.11)	0.05543	(.08)	**425.1**	**425.8**	**429.5**	0.67
M5	1.3	6745.6	2056.9	25.5	1489.4	4.075	0.06809	(.07)	0.51922	(.11)	0.05530	(.08)	**424.6**	**424.6**	**424.5**	0.70

Mass fractionation correction of 0.12% ±0 05%/amu and 0.15% ± 0.04%/amu was applied to dynamic faraday-daly analyses and single collector daly analyses, respectively
Total procedural blank for Pb ranged from 0.65 to 3.5 pg and < 1.0 pg for U. Age calculations are based on the decay constants of Steiger and Jager [1977]. Common-Pb

[a] Sample chemistry follows procedures outlined in Hawkins and Bowring, 1997

[b] Sample weights were estimated by using a videomonitor and are known to within 40%.

[c] Total common-Pb in analyses.

[d] Values are measured ratio corrected for spike and fractionation only.

[e] Values are corrected for fractionation, spike, blank, and initial common Pb.

3. Multi-stage Extensional Evolution of the Central East Greenland Caledonides

Arthur P. White*, Kip V. Hodges*

* Department of Earth, Atmospheric and Planetary Sciences, Massachusetts Institute of Technology, Cambridge, MA, 02139,USA. apwhite@mit.edu Tel (617)-253-8445 fax (617) 252-1800

Abstract:

The past decade of field investigations in the central East Greenland Caledonides (72°-74° N) have resulted in the identification of previously unrecognized orogen-scale extensional structures. In particular, several large N-S striking faults, once mapped as thrusts, have been subsequently reinterpreted as a system of normal faults called the Fjord Region Detachment system. Previous geochronologic constraints on the timing of their displacement indicated that these faults became active ca. 430-425 Ma, a time when the Baltica-Laurentia collision was thought to be occurring, and continued to be active for up to 80 million years. We present, new $^{40}Ar/^{39}Ar$ thermochronologic data from an E-W transect that cuts across two splays of this fault system. Our data constrain the structurally higher splay, called the Tindern detachment, to have been a short-lived fault that was active from ca. 425-423 Ma. Our data also indicate that the structurally lower splay (the Høgedal detachment) was active sometime between ~417 to 380 Ma during which time it partially reactivated the Tindern detachment at latitudes north of 72.5° N. Furthermore, we present *in situ* UV laser $^{40}Ar/^{39}Ar$ data for pseudotachylite collected along the Høgedal detachment that indicate this fault was active again as recently as ~357 Ma — a time that is comparable to the formation of the Devonian basins in East Greenland. These findings are important because they demonstrate that at least two

distinct episodes of faulting were responsible for extension in the East Greenland Caledonides: an earlier phase that was synorogenic and penetrated to middle-crustal levels, followed by a post-Caledonian phase of reactivation that affected even deeper structural levels. Furthermore, our results indicate that the Fjord Region Detachment system was not active continuously for 80 million years; but rather, there were multiple splays that were active for shorter intervals over discrete time periods separated by as much as 60 million years. Finally, our data provide evidence that young extensional deformation associated with post-orogenic collapse in East Greenland was not restricted to the young sedimentary basins in the far eastern part of the orogen, but also resulted in deformation of the Archean-Paleozoic crystalline basement.

Introduction:

The central East Greenland Caledonides (72° to 76° N) preserve spectacular three-dimensional exposures of middle-crustal rocks exhumed along detachments that strike parallel to the orogen. Recently, these faults have attracted much attention to the region as new structural, kinematic and geochronologic evidence has forced geologists to re-examine their interpretations of the orogen's evolution. Although revision has been ongoing since the 1970s, when the Greenland Geological Survey introduced Rb/Sr data along with new field interpretations [e.g. Rex et al., 1976; Henriksen and Higgins, 1976], we focus on the recent interest in syn- and post-orogenic normal faults that began with the mapping of extensional structures in central East Greenland by Caby (1976) and the documentation of post-orogenic collapse structures preserved up in NE Greenland by Strachan et al. (1989) and Holdsworth and Strachan (1991). Following this work, Hartz and Andresen (1995) remapped a prominent fault system, previously attributed to thrusting by Higgins et al. (1981), as a series of normal faults. This system was later called the Fjord Region Detachment (FRD) by Andresen et al. (1998). While these papers identified the FRD system as a post-orogenic collapse feature, subsequent U-Pb geochronologic data indicated that at least one splay of the FRD system developed at ca. 424 Ma, roughly contemporaneous with orogenic contraction at ca. 425 Ma [White et al., 1998]. Recently Hartz et al. (2000) published U-Pb and $^{40}Ar/^{39}Ar$ geochronologic data which they interpreted to suggest that syn-orogenic extension initiated sometime ca. 430 Ma; furthermore, they suggested that activity extended beyond the end of collisional orogenesis over a total period of greater than 80 million years.

The documentation of synorogenic extension in the East Greenland Caledonides adds to a growing pool of evidence that orogens undergo syn-collisional extension [e.g. Burchfiel et al., 1992; Burg et al., 1994]. Here we present new $^{40}Ar/^{39}Ar$ thermochronologic data that help constrain the thermal and tectonic evolution of the Forsblad Fjord region (72.5°N) of East Greenland (Figure 1) along an E-W transect that cuts exposures from the Archean-Paleoproterozoic basement complexes through to the post-Caledonian, Devonian basin sequences. Forsblad Fjord is an E-W-trending feature with shoreline outcrops that provide almost continuous exposures through most tectonostratigraphic elements of the East Greenland Caledonides. In particular, the Forsblad Fjord transect crosses two major splays of the FRD system: the Høgedal and the Tindern detachments (Figure 1) [White et al., 1998]. When the new data are combined with structural observations, U-Pb geochronologic constraints and field mapping [Koch and Haller, 1971; Hartz and Andresen, 1995; Andresen et al., 1998b; Greenland Geological Survey 1999; Hartz et al., 2000; White et al., in press], they imply that the FRD system has accommodated multiple episodes of synorogenic and post-orogenic extension. On the basis of our new findings, we propose a revised model of Caledonian orogenesis in East Greenland.

Geologic Background:

The Caledonides, a two-sided fold and thrust belt preserved in Scandinavia, Ireland, Scotland and East Greenland (Figure 1), was formed by continent-continent collision as Baltica subducted beneath Laurentia, during the Middle to Late Silurian [Gee, 1975; Sturt and Thon, 1978; Hodges et al., 1982; Henriksen, 1985; Andresen and Steltenpohl, 1994; Torsvik et al., 1996]. While numerous, west-vergent shortening structures were mapped during 1935-1958 geologic expeditions to East Greenland [Koch

and Haller, 1971], the regional E-dipping, N-S extensional structures that are the focus of this study were not recognized as such until this past decade [Hartz and Andresen, 1995; Andresen et al., 1998a]. Hartz and Andresen (1995) originally related these normal faults to post-orogenic extension of a similar nature to that documented in the Scandinavian Caledonides [e.g. Andersen and Jamtveit, 1990; Cashman, 1990; Fossen and Rykkelid, 1992; Northrup and Burchfiel, 1993; Gee et al., 1994; Rykkelid and Andresen, 1994; Fossen and Dunlap, 1998]. However, geochronologic constraints published since then have shown both contraction and extension to have been occurring ca. 425 Ma [White et al., 1998; Hartz, 2001; White et al., in press].

Recent fieldwork from 1997 and 1998, published by the Greenland Geological Survey, indicated that there are thrust-bounded tectonic windows exposing Archean to Neoproterozoic metamorphic gneiss complexes north of the study area (> 73° N) in Eleonore Sø, Målebjorg and Niggli Spids [Leslie and Higgins, 1999; Escher and Jones, 1999; Elvevold and Gilloti, 2000], as well as south of the study area (< 72°N) in Charcot Land and Gåseland [Christoffersen, 1984]. White et al. (in press) argued that thrusts in the north can be correlated to thrusts in the south in a straightforward way, These features can be projected west of the study area beneath the Greenland ice cap (Figure 1). To the east, these tectonic windows comprise the footwall of the E-dipping FRD system that truncated the window-bounding thrust faults. Newly published seismic refraction profiles suggest the presence of another potentially significant extensional feature, a W-dipping seismic reflector that is laterally extensive throughout the lower crust of the fjord region [Schlindwein and Jokat, 2000]. It has been suggested that this reflector may be the main extensional shear zone which accommodated post-orogenic collapse.

Previous quantitative estimates on the timing and amounts of displacement along these extensional faults are loosely constrained. There are no structurally-derived estimates of net-slip along either the FRD or the reflector described by Schlindwein and Jokat (2000). However, thermobarometry has been used to estimate tectonostratagraphic throw in a general sense. Vold (1997) suggested that the FRD footwall rocks exposed in Kempes Fjord, just north of the study area (73° N), were exhumed from 10-12 kilobars in near-isothermal conditions. Our own P-T data from the Forsblad Fjord region indicates that decompression by tectonic denudation was ca. 3-4.5 kilobars [White and Hodges, in preparation-b], suggesting a vertical component of displacement of roughly 10-16 kilometers. Thermochronologic data from Kajser Franz Josephs Fjord (Figure 1), further north of the location studied by Vold (1997), have been interpreted to suggest that movement along the FRD endured for ca. 80 My [Hartz et al., 2000], implying a time-averaged displacement rate of ca. 1/5 km per million years, although Hartz et al. (2000) do not address how slip might have been distributed over that period.

Just south of 73°N, the FRD separates into two splays (Figure 1). Although the intersection between the two faults is inaccessible in the field, the data discussed later in this paper suggest that the eastern splay developed first and is truncated by a younger western splay. Locally, the eastern splay is referred to as the Tindern detachment; the western, younger fault is the Høgedal detachment [White et al., in press]. These faults bound a wedge of amphibolite facies paragneisses that are interpreted to be the metamorphic equivalent of the Krummedal Supracrustal Sequence mapped in the Scoresby Sund region (~71.5° N) [Higgins, 1988]. These paragneisses preserve deformational structures indicative of ductile N-S flow in response to transpressional deformation that are, within the resolution of available U-Pb monazite geochronology, essentially coeval with displacement on the Tindern detachment [White et al., in press].

Geology of the Study Area

The best exposures of the Høgedal and Tindern detachments are found in the Forsblad-Fjord-region-transect from Tærskeldal to Forsblad Fjord and Segelsällskapets Fjord at 72.5°N (Figure 1, Figure 2). There, a continuous outcrop exposes three separate allochthons emplaced by movement along the two faults. Lying beneath and just to the east of the inland ice, are the Archean-Paleoproterozoic high-grade biotite-amphibolite gneisses of the Gletscherland Complex. These gneisses, which comprise the Hagar-Niggli Spids allochthon, were juxtaposed by the Høgedal detachment with the Mesoproterozoic-Neoproterozoic amphibolite facies biotite-garnet-sillimanite-kyanite metasedimentary rocks of the Krummedal Sequence in the Høgedal allochthon. Above the Krummedal Sequence, emplaced by movement along the Tindern detachment, are Neoproterozoic Eleonore Bay Supergroup sedimentary rocks of the Tindern allochthon (Figure 1).

Metamorphism and deformation of these rocks reflect multiple events ranging from Proterozoic to Middle Paleozoic age [e.g. Backlund, 1930; Wegmann, 1935; Haller, 1970; Henriksen and Higgins, 1976; Rex et al., 1976; Rex and Gledhill, 1981; White et al., in press]). Gneisses of unknown thickness from the Hagar-Niggli Spids allochthon preserve amphibolite facies metamorphic mineral assemblages. Undeformed pegmatite dikes cut across variably deformed lamprophyres that intruded these gneisses. Available Rb-Sr whole-rock and U-Pb zircon dates from the gneisses have been interpreted to suggest that high-temperature metamorphism extended from ca. 2450 Ma to 1700 Ma [Rex et al., 1976; Rex et al., 1977; Rex and Gledhill, 1981; Thrane et al., 1999]. Additional Rb-Sr dates, including a hornblende-biotite whole rock age of ~370 Ma and a biotite-muscovite age of ~410 Ma [Rex and Gledhill, 1981] record Caledonian ages. The combination of these data with a large array of K-Ar data has been interpreted

to indicate a low-temperature Caledonian thermal overprint ca. 430-370 Ma [Rex and Gledhill, 1981; Rex and Higgins, 1985].

Biotite-garnet-sillimanite gneisses of the Høgedal allochthon, representing a structural thickness of ca. 14 km, exhibit abundant evidence of *in situ* melting at amphibolite facies conditions. The ratio of leucosome to melanosome increases up-sequence to the point that melt appears to have mobilized ca. 1-2 km structurally beneath the Tindern detachment. The detachment itself was invaded by a large synkinematic granite orthogneiss referred to as the Caledonia Ø Granite. Recent U-Pb dates on metamorphic monazite and xenotime from this pluton and structurally deeper leucosomes imply that anatexis of the Krummedal Sequence occurred at ca. 425 Ma [White et al., in press] and intrusion of the Caledonia Ø Granite occurred ca. 424.5 Ma, implying that activity along the Tindern detachment began sometime between ca. 425-424.5 Ma.

The basal 3 km of the Tindern allochthon (Nathorst Land Group Formations 1-3 [Smith and Robertson, 1999]) contains chlorite-biotite-garnet schists and phyllites with intercalated garnet-amphibole calc-silicate rocks. Locally preserved sillimanite porphyroblasts are associated with contact metamorphism during intrusion of a large, undeformed granite pluton, the Klosterbjerg Granite, and an associated complex of interconnected feeder pegmatite/aplite dikes and sills. Metamorphic grade progressively decreases upwards through the remaining 6 km of the Nathorst Land Group. A recent U-Pb monazite age from the Klosterbjerg Granite suggests crystallization ca. 424.5 Ma [White et al., in press], implying that the genesis and intrusion of the Caledonia Ø and Klosterbjerg Granites may be related.

Structural Framework

From the original field investigations presented by White et al. (in press), we summarize here a simplified framework for Caledonian deformation in the Forsblad Fjord region (Figure 3). Note that $\mathbf{D_{1a}}$ corresponds to D_{1H} and D_{1T} in (White *et al.*, in press) while $\mathbf{D_{1b}}$ corresponds to D_{3N}, D_{2H} and D_{2T}, $\mathbf{D_2}$ corresponds to D_{3H} and D_{3T} and $\mathbf{D_3}$ corresponds to D_{4N}, and D_{3H}. $\mathbf{D_{3H}}$ has been subdivided into two events following thermochronologic investigations discussed below. $\mathbf{D_4}$ corresponds to D_{5N}, D_{4H} and D_{4T}.

The early stages of Caledonian crustal thickening, D_1, have been subdivided into two episodes: D_{1a}, a period of ~E-W shortening, and D_{1b} a period of orogen-parallel shear and E-W transpression. Although S_{1a}, typically defined by the alignment of biotite ± muscovite ± kyanite is almost entirely found transposed into parallelism with S_{1b}, intrafolial F_{1a} folds with axial planes parallel to S_{1a} provide structural evidence for shortening during this earliest deformation. The data necessary to constrain the absolute timing and duration of D_{1a} are not available. S_{1b} strikes N-S to NW-SE and dips ca. 50° eastward. It is typically defined by biotite ± muscovite. Prominent N-S trending mineral lineations (L_{1b}), along with kinematic shear-sense indicators such as asymmetric boudins, shear bands and asymmetric fold trains, show that material extruded both to the north and south, during E-W shortening. Open to tight, N-S trending F_{1b} folds deform S_{1a} fabrics (Figure 4a) and refold F_{1a} folds demonstrating the relative age relationships of these structures. Very broad, N-S trending F_{1b} folds deform S_{1a} cleavages preserved in the Eleonore Bay Supergroup sedimentary rocks of the Tindern allochthon (Figure 4b). Given that plate convergence between Baltica and Laurentia is thought to have been sinistrally oblique [Torsvik et al., 1996], it is likely that these features represent significant E-W transpressional deformation accompanied by orogen-parallel shear. The

absolute age of this deformation is constrained by a 425.3 ± 0.3 Ma [White et al., in press] U-Pb monazite date from a syn-D_{1b} leucosome sampled within the Høgedal allochthon. The geometric similarity between D_{1b} structures in all three allochthons led White et al. (in press) to infer that the structures were coeval.

The Tindern detachment, a low-angle normal fault, comprises the principle D_2 structure (Figure 4c, 4d). Fabrics related to ductile extension along the shear zone overprint S_{1b} schistosities and preserve top-to-the-east kinematic indicators. The abundance of shear-related fabric elements and the degree of apparent strain increases progressively upwards from about 2-3 km below the main metamorphic discontinuity. S_2, defined by the alignment of biotite and muscovite in the Caledonia Ø Granite, strikes SW-NE and dips ca. 35° SE. L_2, E-dipping stretching lineations overprint L_1 2-3 km below the detachment and become more intense upward in the metasedimentary rocks of the Krummedal Sequence. Situated directly above and subparallel to the Tindern detachment are a series of brittle fault splays that excised an unknown section of the Nathorst Land Group. Antithetic to these E-dipping brittle detachments are a series of high-angle, W-dipping normal faults with displacement on the order of tens of meters. These faults appear to be truncated by the E-dipping detachments.

While field observations were inadequate to distinguish the relative age relationship between the Tindern and the Høgedal detachments, our new thermochronologic data (discussed below) indicate that fabrics and structures formed during displacement along the Høgedal detachment (Figure 4e, 4f) represent a subsequent phase of deformation, D_3. At depths 1-2 km below the zone of maximum shear, D_3 strain is characterized by the progressive transposition of S_1 into parallelism with S_3 mylonitic fabrics that strike N-S and dip 30° - 50° eastward. There is a strong E- to ESE-plunging

lineation preserved on S_3. Overprinting the uppermost mylonites is an anastamosing decameter-thick cataclasite with discontinuous zones of pseudotachylite that formed during brittle deformation. Elongated boudin trains, SE-dipping slickensides, and chlorite-grade mylonitic fabrics, indicate that deformation was characterized by top-to-the-east sense-of-shear at lower-temperature conditions than those inferred from fabrics preserved within the Tindern detachment. Following the juxtaposition of allochthonous blocks within the study area by displacement along the Høgedal and Tindern detachments, a series of late to post-orogenic, D_4 brittle faults of varying orientation and displacement developed in the region.

$^{40}Ar/^{39}Ar$ Geochronology

Because the intersection of the Høgedal and Tindern detachments is underwater, field relationships alone do not permit determination of the relative ages of the two structures. This is an important issue to resolve because it has implications for the total duration of movement and episodicity of slip on the Fjord Region Detachment system. Based on geochronologic data from rocks principally collected north of the intersection of the two faults, Hartz et al. (2000) suggested an extremely long duration for Fjord Region Detachment slip. However, geologic relationships in Forsblad Fjord imply that deformation might have been partitioned into distinctive episodes. U-Pb geochronologic data for granitic rocks that are pre- and syn-kinematic with respect to ductile, high-temperature deformation on the Tindern detachment indicate that this structure became active ca. 425 Ma (White et al., in press). However, fault-rocks (e.g., greenschist facies S-C mylonites, pseudotachylites, etc.) along the structurally deeper Høgedal detachment suggest that most displacement on that structure took place under lower-temperature conditions, distinctive from the conditions of deformation on the Tindern detachment.

This implies that activity along the Høgedal detachment may have post-dated slip along the Tindern detachment. Furthermore, if the Høgedal detachment truncates the Tindern detachment beneath Kempes Fjord, then the Fjord Region Detachment from Kempes Fjord northward may display diachronous fabrics that could be misinterpreted to imply continuous, protracted slip rather than episodic slip. In order to better evaluate these alternative interpretations, we have applied a variety of $^{40}Ar/^{39}Ar$ thermochronometers to rocks from the Hagar-Niggli Spids, Høgedal and Tindern allochthons and the fault zones that separate them.

Sample characterization and methodology:

Samples were collected from granitic and metamorphic rocks spanning all three allochthons. Criteria for selection included relative age with respect to deformational fabrics, structural position with respect to the Høgedal and Tindern detachments, and availability of the K-rich minerals (e.g. Figure 4g). To maximize the breadth of cooling data recovered from each sample, we used the following minerals that display a natural range in nominal closure temperatures: e.g. muscovite ca. 415° - 350° C [Robbins, 1972; Hames and Bowring, 1994; Lister and Baldwin, 1996]; biotite ca. 350° - 300° C [Grove and Harrison, 1996a]; K-feldspar ca. 350° - 150° C [Lovera et al., 1989].

Granitic and gneissic samples were selected for their spatial distribution extending from below the Høgedal detachment to just above the Tindern detachment. This provides an orogen perpendicular, structural transect of ca. 20 kilometers. Although relationships observed in the field indicated whether or not granitic intrusives pre- or post-dated specific deformational episodes, both granite emplacement and metamorphism of the country rock occurred at temperatures above the closure temperature for $^{40}Ar/^{39}Ar$

diffusion in all analyzed minerals. Thus, the dates do not help constrain the timing of high-temperature deformation fabrics but can be used to evaluate the significance of low-temperature slip on the two detachments. For example significant slip on the Tindern detachment below ~350° C would be expected to disrupt the pattern of muscovite $^{40}Ar/^{39}Ar$ ages across the fault trace.

In addition, a sample of pseudotachylite was collected from the anastamosing cataclasite layer that forms the upper bound of the Høgedal Detachment. In the field, this decameter thick layer overprints the low-temperature mylonites that flatten the Gletscherland Complex. We infer that *in-situ* $^{40}Ar/^{39}Ar$ dates of this pseudotachylite represent ages for K-feldspar neoblasts of very fine grain size that crystallized shortly after melting related to fault-slip as discussed below.

Analytical Procedures

Analytical work was performed at the MIT Cambridge Laboratory for Argon Isotope Research. We used two methods to degas samples: 1) incremental heating of mineral separates in a double vacuum resistance furnace (VRF); 2) *in situ* ablation using the $^{40}Ar/^{39}Ar$ ultraviolet laser microprobe (ULA).

For furnace step heating, samples were crushed and minerals were separated by density and magnetic susceptibility using sodium polytungstate and a Frantz isodynamic separator, to isolate individual grains of muscovite, biotite and K-feldspar. Grain size varied from hundreds of microns to millimeters in diameter. In all cases, minerals were hand-picked to increase purity of the separates. Laser microprobe analyses were performed on polished thick sections of rock samples. Prior to irradiation, all samples and monitors were cleaned in an ultrasonic bath with acetone, distilled water, and ethanol.

Mineral separates and chips were irradiated in the McMaster University reactor in Ontario, Canada. The fast neutron flux was monitored using a combination of MMhb-1 (518.53 Ma) and GA1550 (98.56 Ma) standards (inter-calibrated against Fish Canyon tuff sanidine using the age of 28.02 Ma reported by Renne et al., 1998), and synthetic salts were used to correct for interfering nuclear reactions. We note that there is currently a discrepancy between the published U-Pb age (28.48 Ma) and $^{40}Ar/^{39}Ar$ age (28.02 Ma) for Fish Canyon sanidine [e.g. Renne et al., 1998; Schmitz and Bowring., 2001] which has been attributed both to unknown magma residence times and/or to potential uncertainties in the K decay constant. If we were to adopt the 28.48 Ma age for Fish Canyon sanidine and adjust the assumed ages of MMhb-1 and GA 1550 accordingly, the estimated fast neutron dosage for the Forsblad Fjord samples would change such that all muscovite ages reported here would be slightly older, in some cases older than the U-Pb monazite reported by White et al. (in press). While it is conceivable that the monazite could have grown at temperatures below the Ar closure temperatures for muscovites during cooling of the Forsblad Fjord granitic rocks, this phenomenon would be inconsistent with textural evidence that indicates monazite growth as a solidus phase [White et al., in press]. Thus, we provisionally adopt the Renne et al. (1998) age for Fish Canyon Sanidine.

Muscovite and biotite samples were degassed in the vacuum furnace using a monotonic step-heating schedule designed to maximize the distribution of gas released amongst the heating steps. Temperatures within the vacuum furnace were controlled to within 5° C. Heating schedules are included in the appendix.

The analytical procedure we used for running K-feldspar has been described in detail by Kirby (2001). The heating schedule was customized for the sample to optimize

the recovery of argon diffusion parameters and has been included in the appendix. We used duplicate isothermal heating steps at low temperatures to degas potential excess ^{40}Ar associated with the break-down of Cl-rich fluid inclusions [Harrison et al., 1994]. Additional isothermal steps of increasing duration were employed from 1075-1125°C to maximize the quantity of argon released via diffusion prior to K-feldspar incongruent melting. The diffusive loss of ^{39}Ar from the alkali feldspar crystals were used to develop model temperature-time histories based on multi-domain diffusion theory [Zeitler 1987; Lovera et al. 1989; Lovera et al. 1991; Lovera, 1992; Lovera et al. 1993].

It is important to note that one of the critical assumptions embodied in the multiple diffusion domain theory of Lovera et al. (1989), is that the feldspar cooled monotonically. U-Pb geochronologic data from the latest cross-cutting pegmatites in this region suggest a crystallization age older than ca. 413 Ma [White et al., in press], a date which precedes our $^{40}Ar/^{39}Ar$ K-feldspar data. Mafic dikes in other regions of the orogen have yielded Devonian ages and younger; however, since none of these more recent dikes have been found in our field area, it seems reasonable to accept that these feldspars cooled monotonically. The other important assumption made during our K-feldspar modeling was that the activation energy (E_a) and frequency factor (D_0) calculated from the diffusive loss of ^{39}Ar at low-temperatures are also appropriate to larger domain sizes.

Laser ablation experiments were conducted using a Mercantek frequency quadrupled Nd-YAG ultraviolet laser to mill out rectangular pits ranging from 50 to 150 microns along each side and 30 to 50 microns deep. Beam strength was set to 615 V and pulsed at a frequency of 20 Hz. Blank measurements during laser experiments were performed in-between every two to three analyses.

Gases were analyzed on an MAP 215-50 mass spectrometer using a combination of Faraday cup and electron multiplier detectors. Data were reduced using the constants recommended by Steiger and Jäger (1977); all analytical uncertainties, associated with both measured and blank data, were propagated through the calculations and are reported at 2σ.

All of the VRF experiments resulted in data that defined plateaux as described by Fleck et al. [1977]. We report a plateau date for each of these experiments as the ^{39}Ar-weighted mean of the dates for each step on the plateau (Table 1), and we assign an error to that date of twice the weighted standard error of the mean. On a $^{36}Ar/^{40}Ar$ vs. $^{39}Ar/^{40}Ar$ isotope correlation diagram [Roddick et al., 1980], a significant number of the steps for each VRF experiment (representing between 65.7 and 100% of the total ^{39}Ar released) defined a statistically significant isochron as defined by the mean squared weighted deviates or MSWD [Wendt and Carl, 1991]. In Table 1, we report the implied isochron dates, along with: 1) uncertainties as defined by a York [1969] regression analysis; 2) initial 40Ar/36Ar ratios and their errors as defined by the isochron analysis; and 3) the MSWD for each fit. For those experiments where the calculated initial ratios were within error of modern atmosphere (295.5), we took that plateau date and its uncertainty as the best estimate of the apparent cooling age of the sample. In other cases, we interpreted the isochron date and its larger error as the best estimate of the apparent age. For the ULA analyses of biotite and pseudotachylite (Table 2), we report a 39Ar-weighted mean date for all ablation pits, an inverse isochron date for the same data, initial ratios, and estimated errors at the 95% confidence level.

Muscovite $^{40}Ar/^{39}Ar$ Results:

We performed VRF experiments on seventeen samples collected from the Høgedal and Tindern allochthons (Figure 2): fifteen from granitic bodies such as leucosomes, dikes, sills and plutons and two from pelitic gneisses where the muscovite helped define the S_1 schistosity (Table 1; Figure 5). With the exception of one sample collected from a structurally deep level of the Høgedal allochthon (97GR36), muscovites from the transect yield generally decreasing $^{40}Ar/^{39}Ar$ apparent ages with increasing structural depth (Figure 6), maintaining a reasonable trend despite the apparent variation in closure temperature across the section. The lack of major discontinuities in this pattern implies that there has been little structural disruption of the section subsequent to the closure interval indicated by these samples (~423-416 Ma). Most disruptions from the trend can be attributed to analytical uncertainties and variations in grain size (ca. 315-3000 μm). The latter effect is the most likely explanation for the very young apparent age of the 97GR36 muscovite (411.0 ± 0.7 Ma) which is very fine grained (~150 μm).

Biotite $^{40}Ar/^{39}Ar$ Results:

The biotite dataset represents seven samples collected along a transect from the basal Tindern allochthon through the upper part of the Hagar-Niggli Spids allochthon. VRF experiments on biotites from above the Høgedal detachment yielded plateaux and statistically indistinguishable isochron dates (Table 1, Figure 7). The release spectra for three samples (97GR14, 98GR35, and 98GR23) displayed a common characteristic: although low-temperature steps defined a plateau, steps representing the last 20-40% of ^{39}Ar released had monotonically increasing apparent ages. We interpret this as a consequence of minor contamination of the biotite separates with an optically

indistinguishable second phase, such as chlorite, that preferentially incorporated ^{40}Ar not produced by *in situ* decay of ^{40}K ('excess" ^{40}Ar).

Despite this, examination of the data for all samples on isotope correlation diagrams suggests no significant contamination with excess ^{40}Ar. However, most steps for most samples had extremely high radiogenic yields, such that not-radiogenic reservoirs with high 40Ar/36Ar ratios would be difficult to detect and correct for using traditional inverse isochron methods (e.g. Roddick et al., 1980). This is an important factor for determining the significance of the data because conventional wisdom holds that the nominal closure temperature is lower for biotite (ca. 300° C) than for muscovite (ca. 350° C), yet the Forsblad Fjord biotites are consistently as old as or older than muscovites from the same structural level (Table 1). One possible explanation for this discrepancy between theory and observation is that the compositions of either the muscovites and the biotites are unusual enough that they have unusual Ar closure systematics. For example, Ar diffusion data for biotite suggest a dependency on Fe/Mg [e.g. Harrison et al., 1985; Grove and Harrison, 1996a]. In order to explore this possibility further, we performed wavelength-dispersive electron microprobe analyses on biotites from all VRF samples and estimated appropriate diffusion parameters for the measured mole fraction of annite by linear combination of the Harrison et al. (1985) and Grove and Harrison (1996) datasets (Tables 1, 2, and Figure 8).

For most of the samples, there is no significant difference to the interpretation of our results between using an invariant sub-grain diffusion domain of 150 μm as suggested by Harrison et al. (1985), versus the use of grain-size dependent diffusion domains consistent with the observations of Hodges et al. [1994]. However, we note that the calculation of closure temperature for biotite from 97GR36 was higher than that for

the coexisting, younger muscovite when the diffusion domains were assumed to be grain-size dependent. Unfortunately, the closure temperatures calculated for the other biotites for which we have comparable muscovite data are still too low for this explanation to be universally correct. These other cases might reflect contamination of the biotites with an excess ^{40}Ar component that was unresolved by isotope correlation analysis. Alternatively, the muscovites might have grown after biotite closure. We note that mineral textures in many of these samples imply that muscovite grew later than coexisting biotite. Although we infer that this occurred at temperatures above the closure temperatures for the coexisting biotites, we cannot rule out low-temperature growth from the data on hand.

These issues not withstanding, biotites from the hanging wall of the Høgedal detachment yield a pattern of increasing apparent age with decreasing structural depth (ranging from ~417 Ma to 424 Ma, Figure 9) that is similar to the pattern of muscovite ages in Figure (6). Although a paucity of biotite dates from the Tindern allochthon precludes the use of this pattern to evaluate the possibility of Tindern detachment slip at temperatures below ca. 356° C, the lack of major disruptions in the pattern through the Høgedal allochthon corroborates the implication of the muscovite data that this package is structurally intact.

We also performed ULA analyses of one biotite grain in a thin section of biotite-amphibolite gneiss from the upper part of the Hagar-Niggli Spids allochthon (98GR34). This biotite helps to define the S_{1B} fabric in the sample. Six ablation pits in this biotite produced a range of $^{40}Ar/^{39}Ar$ dates from ~392 - ~387 Ma, with no apparent within-grain variation. Analysis of these data on an inverse isotope correlation diagram indicated that the non-radiogenic Ar in the biotite has an essentially atmospheric $^{40}Ar/^{36}Ar$ ratio (296 ± 11), so we regard the weighted mean age of all ablation analyses (387.5±9.6 Ma) as the

best estimate of the timing of cooling of 98GR34 through ~369° C. This date is significantly younger than any of the biotite dates from the hanging wall of the Høgedal detachment, implying that the structure accommodated significant displacement after ca. 417 Ma. In order to better understand when this displacement might have occurred and what its influence on the cooling history of the footwall might have been, we also performed multidomain diffusion modeling on K-feldspar from the Hagar-Niggli Spids allochthon.

K-feldspar $^{40}Ar/^{39}Ar$ Results:

K-feldspar from sample 98GR32 was collected from a late-stage pegmatite dike located just beneath and truncated by the Høgedal detachment. VRF analysis of this feldspar produced a slightly saddle-shaped age-spectra (Figure 10a). Its form most likely reflects the degassing of excess ^{40}Ar from Cl-rich fluid inclusions at low temperatures [Harrison et al., 1994] and the high temperature release of excess ^{40}Ar trapped in anion vacancies [Zeitler, 1987]. Duplicate isothermal heating steps enabled us to correct for the low-temperature excess argon effects prior to the calculation of kinetic parameters used in multidomain modeling. Our modeling attempts were only partially successful, inasmuch as we could choose a range of time-temperature histories that would predict log r/r_0 and age spectrum patterns that matched the modeled data up to about 60% of the ^{39}Ar released during the VRF experiment. As a consequence, the modeled time-temperature path is robust for the 380-300 Ma time period but essentially unconstrained for earlier parts of the thermal history. Over the well-modeled time interval, the K-feldspar data suggest relatively slow cooling (ca. 10°C/my) from about 225 to 125° C. The tectonic implication of this is that any rapid cooling of the footwall that might be attributable to

denudation by slip on the Høgedal detachment [e.g. Ruppel et al., 1988] occurred before ca. 380 Ma.

Pseudotachylite $^{40}Ar/^{39}Ar$ Results:

Further constraints on the displacement history of the Høgedal detachment are provided by ULA data for a pseudotachylite sample (97GR06) from the breccia zone of the fault. The thin section we studied included a ~4 mm wide vein of pseudotachylite in sharp contact with a matrix of brecciated biotite gneiss (Figure 11). Numerous irregular enclaves of the matrix are preserved within the pseudotachylite. The glass itself has devitrified; both fine-grained and microcrystalline domains within the vein yield K-feldspar compositions upon wavelength dispersive analysis with an electron microprobe.

A focussed ultraviolet laser was used to mill twenty-one ablation pits in matrix-free domains for $^{40}Ar/^{39}Ar$ dating. Although the pit geometry was varied in order to avoid matrix enclaves, the typical pit size was 100 x 100 x 30 μm (Figure 11a). Collectively, the analyses define a linear relationship on an isotope correlation diagram (MSWD = 0.52) indicative of an age of 350 ± 20 Ma and an initial $^{40}Ar/^{36}Ar$ ratio indistinguishable from that of modern air (296 ± 11; Figure 12a). The relatively large uncertainty of this inverse isochron date principally reflects the relatively low radiogenic yield of the small ablation pits produced by the laser. We interpret the linearity of the data and similarity of the derived initial $^{40}Ar/^{36}Ar$ ratio to that of air as an indicator that the Ar in the pseudotachylite is a simple mixture of an atmospheric component and a single radiogenic component. Our most precise estimate of the age represented by the radiogenic component is the weighted mean ages of all ULA analyses (357 ± 11 Ma). Based on the probability that devitrification of this material occurred soon after shear-related melting,

we regard the data as indicative that the 97GR06 pseudotachylite developed just prior to 357 ± 7 Ma. Note that the K-feldspar-derived cooling path for 98GR32, collected nearby in the footwall of the Høgedal detachment, indicates ambient temperatures of about 150° C at this time, consistent with brittle conditions for deformation on the detachment and rapid quenching of any shear-related melts (Figure 10d).

Implication for the history of the Tindern detachment:

Previously determined U-Pb monazite data indicated that high-temperature (D_2) displacement along the Tindern detachment began between ~425 Ma and ~424.5 Ma [White et al., in press]. However, two important questions remain: 1) what was the duration of D_2 slip on the Tindern detachment; and 2) has the structure experienced significant reactivation since ca. 425 Ma? The pattern of cooling ages across the fault helps us address these issues.

Both muscovite and biotite $^{40}Ar/^{39}Ar$ dates decrease with structural depth across the Tindern detachment with no disruption in the vicinity of the shear zone, indicating that both the footwall and the hanging wall of the detachment share a similar thermal history over the 350 to 450° C temperature range. Thus, we infer that high-temperature deformation along the shear zone had ceased by ca. 423 Ma (the maximum closure age of muscovite collected in the transect). This is a critical constraint on Tindern detachment activity because field observations indicate that most of the displacement is coincident with high-temperature deformational fabrics developed in the synkinematic Caledonia Ø granite which has an age of ca. 425 Ma. [White et al., in press]. Thus, all available evidence is consistent with rapid slip (1-2 My duration) on the detachment at high temperatures. This time period coincides with the later-stages of crustal thickening in

central and northeast Greenland ca. 431-425 Ma [e.g. Hartz, 2001; Strachan et al., In Press; White et al., in press]

While the Tindern detachment is the most regionally significant structure that we associate with D_2 deformation in the study area, there is field evidence for additional lower-temperature, brittle faulting in the detachment's hanging wall that may be structurally related to the Tindern detachment. These low-angle E-dipping faults, that are coupled with antithetic high-angle W-dipping faults, do not appear to offset the Tindern detachment, but rather to root into the shear zone itself [White et al., in press]. Thus, while we interpret that these faults initiated around the same time as the Tindern detachment their duration of activity is unconstrained by the geochronology discussed above. An argument based on additional K-feldspar $^{40}Ar/^{39}Ar$ data suggests that this activity may have ceased ca. 400 Ma [White and Hodges, 2000].

Implications for the history of the Høgedal detachment

While structural and field observations were insufficient to determine the relative timing of the Tindern and Høgedal detachments the fact that most fabrics on the structurally deeper fault developed at low rather than high temperatures implies that the Høgedal detachment is the younger of the two [White et al., in press]. This hypothesis is born out by the $^{40}Ar/^{39}Ar$ data. In particular, the gap of ~30 My between the $^{40}Ar/^{39}Ar$ biotite cooling ages recorded in the footwall and hanging wall of the Høgedal detachment is a critical geochronologic constraint. The data indicate that cooling through the closure temperature of biotite (~381-323° C) in the hanging wall occurred millions of years prior to cooling in the footwall. In detail, the cooling history of the uppermost Hagar-Niggli Spids allochthon provides our best constraint on the timing of slip on the Høgedal

detachment. Although the thermal modeling results for the 98GR32 K-feldspar do not constrain the thermal structure prior to 380 Ma particularly well, the range of acceptable cooling curves passes through the temperature time coordinates of biotite 98GR34 (Figure 10d). Thus, the K-feldspar and biotite data for the uppermost Hagar-Niggli Spids allochthon imply that there was much more rapid cooling of the Høgedal footwall prior to 380 Ma than afterwards. We attribute the rapid cooling during the 388-380 Ma interval to tectonic denudation by slip on the detachment. Unfortunately, the data do not constrain the higher temperature history of the uppermost Hagar-Niggli Spids allochthon well enough to evaluate how long this phase of deformation might have gone on before 388 Ma; however, the distinctive biotite age pattern of the hanging wall suggests that the detachment did not accommodate significant slip before ~417 Ma.

Although the 417-380 Ma phase of movement may have been the most significant on the Høgedal detachment, evidence for subsequent activity exists in the form of the ~357 Ma pseudotachylite $^{40}Ar/^{39}Ar$ date. There is no reason to believe that the dated material is the youngest melt produced by slip on the detachment, or that the youngest slip on the detachment produced pseudotachylites; thus we have no constraints on how recently the detachment might have experienced deformational activity.

Our data demonstrate that the Høgedal detachment was active at least 60 million years after the cessation of movement on the Tindern detachment, at a time comparable to that at which the Devonian basins of East Greenland were forming. Previous work had suggested that young extensional deformation in East Greenland, related to post-orogenic collapse, was restricted to the far eastern part of the East Greenland Caledonides, the offshore Greenland Sea, and at deep structural levels beneath the continental margin [e.g. Schlindwein and Jokat, 2000]. Our geochronologic constraints on the Høgedal

detachment imply a broader distribution of post-orogenic deformation that took advantage of a least one and perhaps several older, syn-orogenic structural discontinuities.

Implications for extensional deformation during and after Caledonian Orogenesis:

Despite a recent resurgence of interest in the geology of the central East Greenland Caledonides, there has been considerable debate about the timing of extensional and contractional events and their relationship with one another. One particularly contentious issue has been the significance of the Fjord Region Detachment system to Caledonian Orogenesis. As previously mapped, this system truncates major tectonic windows bounded by the Hagar and Niggli Spids thrusts [Escher and Jones, 1999] and juxtaposes a variety of allochthonous terrains of differing metamorphic grade [Hartz and Andresen, 1995; Vold, 1997; Andresen et al., 1998a]. Previous interpretations were unable to determine whether one or both of the faults discussed above (Høgedal and Tindern detachments) comprise the southern extension of the FRD system. Given that the data presented here are strong evidence that the Høgedal detachment is younger than the Tindern detachment, the zone of convergence of these faults is either a point of truncation or a merger whereby the Høgedal detachment reactivated the Tindern detachment.

To clarify the structural relationship between the two faults, we compare field observations and temporal constraints from the Tindern and Høgedal detachments with other sections of the FRD system. The syn- and post-kinematic granite plutons found intruding amphibolite facies metasedimentary rocks coincident with the Tindern detachment at the base of the Eleonore Bay Supergroup in Forsblad Fjord form a distinctive feature that we also observed at the southern extension of the shear zone to the

Schaffhauserdalen and Alpefjord area shown in Figure 2 [White et al., in press]. This same relationship appears on maps by Koch and Haller (1971), Hartz and Andresen (1995), Andresen et al. (1998a), and the current compilation of the 1997-1998 mapping conducted by the Greenland Geological Survey. Dates published from one of these synkinematic granites sampled east of Junctiondal along Keiser Franz Joseph Fjord (just north of 73°N) yielded a U-Pb monazite age of 426 ± 2 Ma (*sic*), a muscovite $^{40}Ar/^{39}Ar$ age of 403 ± 8 Ma (*sic*) and a K-feldspar total gas age of 349 ± 8 Ma (*sic*) [Hartz et al., 2000]. Additionally, a monazite age of 422 ± 1 Ma (*sic*) has been reported from another such granite further north (just above 74°N) at Vogts Bjerg [Hartz, 2001]. There is remarkable similarity between these structural relationships and associated U-Pb geochronologic constraints with the Caledonia Ø Granite pluton and the Tindern detachment in Forsblad Fjord [White et al., in press], from which we infer that emplacement of these granites was roughly contemporaneous with emplacement of the Caledonia Ø Granite and movement along the Tindern detachment.

Hartz et al. (2000) also described a "late brittle detachment fault" defined by continuous cataclasite zones up to 0.5 m thick as truncating the top of the mylonites associated with the FRD and the synkinematic granite discussed above. This same brittle detachment is described by Leslie and Higgins (1999) who reported the presence of pseudotachylite along it. These descriptions are similar to those of the pseudotachylite-bearing cataclasite layers along the Høgedal detachment [Rasmussen and Andresen, 1998; White et al., in press]. Furthermore, the $^{40}Ar/^{39}Ar$ K-feldspar age reported by Hartz et al. (2000) for the "synkinematic" granite in Keiser Franz Joseph Fjord is equivalent to the age of the pseudotachylite presented in this paper.

There is excellent agreement between our data and a large set of K-Ar dates (207 samples) published by Rex and Higgins (1985). Those authors indicate a 405 Ma age-contour on their map, which roughly parallels the location where we map the Høgedal detachment. Ages from samples east of this contour, corresponding to where we have mapped the Krummedal Sequence (sampled in Forsblad Fjord, Keiser Franz Josephs Fjord and Western Lyell Land) range from 423 Ma to 414 Ma. Ages directly west of this contour range from 399 Ma to 377 Ma, including several biotite ages (389 Ma to 383 Ma) in the immediate footwall of the Høgedal detachment. We note that Rex and Higgins (1985) also published a few older K-Ar ages for rocks from sample localities that nominally lie in the footwall of the Høgedal detachment at the head of Forsblad Fjord. While mapping in this region, we observed that the valley floor of Tærskeldal (Figure 2) roughly paralleled the dip-plane of the detachment. Because of this, we suggest that these anomalous data may have come from scattered klippe of hanging wall material.

All these relationships suggest that the "late brittle detachment fault" of Hartz et al. (2000) is the northern extension of the Høgedal detachment, and that this fault reactivated the Tindern detachment north of Kempes Fjord. The evidence indicates that the Fjord Region Detachment was not a single fault active over 80 My, but at the least, two separate faults that were predominantly active at different times.

Revised model for the evolution of extension in East Greenland

Given the age constraints presented in this paper (Figure 3), we argue that there were at least two separate stages of crustal thinning: 1) synorogenic extension which initiated and endured for a few million years during plate convergence; and 2) post-orogenic extension which continued long after Caledonian orogenesis. Our data adds to

the mounting evidence for syn-contractional extension [e.g. Hartz, 2001; Strachan et al., in press; White et al., in press] during the Early Silurian. We propose the following model for the evolution of extensional structures in East Greenland after the onset of Ordovician-Silurian crustal thickening due to continent-continent collision (Figure 13). First, during the Early Silurian (likely ca. 445-430 Ma) crustal thickening was accompanied by rapid exhumation of high-grade metamorphic gneisses wedged beneath the Tindern detachment and above basal thrust faults [White and Hodges, 1999; Hartz, 2001] such as the Hagar or Niggli Spids thrusts [White et al., in press]. We note that while the Late Silurian marked an end to rapid exhumation along the Tindern detachment, tectonic denudation of the overlying Eleonore Bay Supergroup may have continued on structurally higher faults [White and Hodges, in preparation-a]. Second, during the Late Silurian to Devonian, extension began anew along the regionally extensive Høgedal detachment at relatively deeper structural levels. This event included partial reactivation of the Tindern detachment and marked the onset of post-orogenic extensional disruption of the East Greenland Caledonides. Movement along this fault appears to have been accompanied by a significant isostatic flexural response which caused domal upwelling in the footwall of the Høgedal detachment where some foliations and bedding now dip to the west. This extension was accompanied by additional crustal thinning along brittle structures in the overlying blocks that led to formation of the Devonian Basins and deposition of the Old Red Sandstone.

Conclusion:

Previous investigations into extensional processes in the East Greenland Caledonides have revealed significant structural evidence for regional detachments. Although temporal constraints on these faults have improved during the last few years,

their relative and absolute ages have been a source of constant debate and confusion. $^{40}Ar/^{39}Ar$ data presented in this paper clarifies the existence of two distinct episodes of normal faulting along the Fjord Region Detachment: one contemporaneous with orogenesis, and one post-dating orogenesis that partially reactivated the existing, synorogenic shear zone.

Based on our data, we propose a revised model for the evolution of extension in the central fjord region of East Greenland. During the Early Silurian, our thermochronologic constraints demonstrate that there was rapid and potentially short-lived exhumation of high-grade metamorphic rocks along the Tindern detachment (~425-423 Ma) at a time when collision must still have been occurring. Subsequently, activity along the Tindern detachment ceased while tectonic denudation in the overlying units may have continued. The Late Silurian was characterized by exhumation along the Høgedal detachment, a fault which partially reactivated the Tindern detachment. Our $^{40}Ar/^{39}Ar$ data suggest that the fault was active between ~417 to 380 Ma and again as recently as the Late Devonian (~357 Ma). This suggests contemporaneity between late slip on the Høgedal detachment and opening of the Devonian Basins.

Our data highlights the complexities that arise when multiple large-scale detachments rupture in close spatial proximity, overprinting and excising critical structural sections. In this situation, large data coverage is ideal; however, careful application of a range of thermochronometers to constrain both regional and local structural relationships remains invaluable.

Acknowledgements

This research was part of a collaborative effort between the Department of Earth, Atmospheric and Planetary Sciences at MIT and the University of Oslo in Norway. Funding for this study was provided by National Science Foundation grant EAR 930072 (to K.V. H.). We wish to thank the Greenland Geological Survey, Danish Polar Center, Sirius Patrol, A. Andresen, E. Hartz, N. Henriksen, J. Hurtado, L. Schoenbohm and N. Chatterjee for logistical assistance in and out of the field. We would particularly like to thank W. Olszewski and E. Kirby for advice at all different times of the day in the laboratory.

References:

Andersen, T.B., and B. Jamtveit, Uplift of deep crust during orogenic extensional collapse: A model based on field studies in the Sogn-Sunnfjord region, W. Norway, *Tectonics, 9*, 1097-1111, 1990.

Andresen, A., E.H. Hartz, and J. Vold, A late orogenic extensional origin for the infracrustal gneiss domes of the East Greenland Caledonides (72-74 N), *Tectonophysics, 285*, 353-369, 1998a.

Andresen, A., and M.G. Steltenpohl, A reevaluation of nappe sequences in the Ofoten-Troms region, north Norwegian Caledonides: Implications for terrane accretion, ophiolite obduction, and polyorogenic evolution, *Tectonophysics, 231*, 59-70, 1994.

Andresen, A., N. Walker, and E. Hartz, U-Pb and $^{40}Ar/^{39}Ar$ isotope constraints on Caledonian and Grenvillian orogenesis in the Kong Oscar Fjord region, in *Symposium on Caledonian geology in East Greenland: Abstract Volume*, vol. 46, edited by K.S. Frederiksen and K. Thrane, pp. 55, Danmarks og Grønlands Geologiske Undersøgelse Rapport, Denmark, 1998b.

Arnaud, N.O., M. Brunel, J.M. Cantagrel, and P. Tapponnier, High Cooling and Denudation Rates at Kongur-Shan, Eastern Pamir (Xinjiang, China) Revealed by Ar-40/Ar-39 Alkali Feldspar Thermochronology, *Tectonics, 12*, 1335-1346, 1993.

Backlund, H.G., Contributions to the geology of Northeast Greenland, *Meddelser om Grønland, 74*, 207-296, 1930.

Caby, R., Investigations on the lower Eleonore Bay group in the Alpefjord region, central East Greenland, *Rapport Grønlands geologiske Undersøgelse, 80*, 102-106, 1976.

Cashman, P.H., Evidence for extensional deformation during a collisional orogeny, Rombak window, North Norway, *Tectonics, 9*, 859-886, 1990.

Christoffersen, M., Scoresby Sund, Grønlands Geologiske Undersøgelse, Denmark, 1984.

Escher, J.C., and K.A. Jones, Caledonian geology of Frænkel Land and adjacent areas (73°00'-73°30'N), East Greenland, in *Geology of East Greenland 72°-75°, mainly Caledonian: preliminary reports from the 1998 expedition*, edited by A.k. Higgins and K.S. Frederiksen, Danmarks og Grønlands Geologiske Undersøgelse Rapport, Denmark, 1999.

Fossen, H., and W.J. Dunlap, Timing and kinematics of Caledonian thrusting and extension collapse, southern Norway; evidence from (super 40) Ar/ (super 39) Ar thermochronology, *Journal of Structural Geology, 20*, 765-781, 1998.

Fossen, H., and E. Rykkelid, Postcollisional extension of the Caledonide Orogen in Scandinavia; structural expressions and tectonic significance, *Geology (Boulder), 20*, 737-740, 1992.

Gee, D.G., A tectonic model for the central part of the Scandinavian Caledonides, *American Journal of Science, 275A*, 468-515, 1975.

Gee, D.G., M. Lobkowicz, and S. Singh, Late Caledonian extension in the Scandinavian Caledonides; the Roragen detachment revisited, *Tectonophysics, 231*, 139-155, 1994.

Giletti, B.J., Studies in diffusion I: Argon in phlogopite mica, in *Geochemical Transport and Kinetics*, vol. 634, edited by A.W. Hofmann, B.J. Giletti, H.S. Yoder and R.A. Yund, pp. 107-115, Carnegie Institute of Washington Publication, Washington, 1974.

Grove, M., and T.M. Harrison, 40Ar* diffusion in Fe-rich biotite, *American Mineralogist, 81*, 940-951, 1996.

Haller, J., Tectonic map of East Greenland (1:500,000). An account of tectonism, plutonism, and volcanism in East Greenland, *Meddelelser om Grønland, 171*, 1-286, 1970.

Haller, J., *Geology of the East Greenland Caledonides*, 413 pp., Interscience Publishers, New York, 1971.

Hames, W.E., and S.A. Bowring, An empirical evaluation of the argon diffusion geometry in muscovite, *Earth and Planetary Science Letters, 124*, 161-167, 1994.

Harrison, T.M., I. Duncan, and I. McDougall, Diffusion of ^{40}Ar in biotite: Temperature, pressure, and compositional effects, *Geochimica et Cosmochimica Acta, 49*, 2461-2468, 1985.

Harrison, T.M., M.T. Heizler, O.M. Lovera, W. Chen, and M. Grove, A chlorine disinfectant for excess argon released from K-feldspar during step heating, *Earth and Planetary Science Letters, 123*, 95-104, 1994.

Hartz, E., Late Orogenic Evolution of the East Greenland and Scandinavian Caledonides, Dissertation for the degree Doctor Scientiarum thesis, University of Oslo, Oslo, 1998.

Hartz, E., Syncontractional extension and exhumation of deep crustal rocks in the east Greenland Caledonides, *Tectonics, 20*, 58-77, 2001.

Hartz, E., and A. Andresen, Caledonian sole thrust of central East Greenland: A crustal-scale Devonian extensional detachment?, *Geology, 23*, 637-640, 1995.

Hartz, E.H., A. Andresen, M.W. Martin, and K.V. Hodges, U-Pb and (super 40) Ar/ (super 39) Ar constraints on the Fjord region detachment zone; a long-lived extensional fault in the central East Greenland Caledonides, *Journal of the Geological Society of London, 157, Part 4*, 795-809, 2000.

Henriksen, N., The Caledonides of central East Greenland 70 degrees -76 degrees N, in *The Caledonide Orogen — Scandinavia and Related Areas*, vol. 2, edited by D.G. Gee and B.A. Sturt, pp. 1095-1113, John Wiley & Sons, Chichester, U.K., 1985.

Henriksen, N., and A.K. Higgins, East Greenland Caledonian fold belt, in *Geology of Greenland*, edited by A. Escher and W.S. Watt, pp. 183-246, The Geological Survey of Greenland, Copenhagen, DK, 1976.

Higgins, A.K., The Krummedal supracrustal sequence in East Greenland, in *Winchester, J. A. Later Proterozoic stratigraphy of the northern Atlantic regions. Univ. Keele, Keele, United Kingdom. p.*, 1988.

Higgins, A.K., J.D. Friderichsen, and T. Thyrsted, Precambrian metamorphic complexes on the East Greenland Caledonides (72° -74° N) - their relationships to the Eleonore Bay Group, and Caledonian orogenesis, *Rapport Grønlands geologiske Undersøgelse, 104*, 1-82, 1981.

Hodges, K.V., J.M. Bartley, and B.C. Burchfiel, Structural evolution of an A-type subduction zone, Lofoten-Rombak area, northern Scandinavian Caledonides, *Tectonics, 1*, 441-462, 1982.

Holdsworth, R.E., and R.A. Strachan, Interlinked system of ductile strike slip and thrusting formed by Caledonian sinistral transpression in northeastern Greenland, *Geology (Boulder), 19*, 510-513, 1991.

Kirby, E., Structural, Thermal, and Geomorphic Evolution of the Eastern Margin of the Tibetan Plateau, PhD thesis, 211 pp., Massachusetts Institute of Technology, Cambridge, 2001.

Koch, L., and J. Haller, Geologic map of East Greenland 72°-76° N. Lat. (1:250,000)., *Meddelelser om Grønland, 183*, 1-26, 1971.

Krol, M.A., P.K. Zeitler, G. Poupeau, and A. Pêcher, Temporal variations in the cooling and denudation history of the Hunza plutonic complex, Karakoram Batholith, revealed by $^{40}Ar/^{39}Ar$ thermochronology, *Tectonics, 15*, 403-415, 1996.

Leloup, P.H., T.M. Harrison, F.J. Ryerson, C. Wenji, L. Qi, P. Tapponier, and R. Lacassin, Structural, petrological and thermal evolution of a Tertiary ductile strike-slip shear zone, Diancang Shan, Yunnan, *Journal of Geophysical Research, 98*, 6715-6743, 1993.

Leslie, A.G., and A.K. Higgins, On the Caledonian (and Grenvillian) geology of Bartholin Land, Ole Rømer Land and adjacent nunataks, East Greenland, in *Geology of East Greenland 72°-75°, mainly Caledonian: preliminary reports from the 1998 expedition*, edited by A.k. Higgins and K.S. Frederiksen, pp. 220, Danmarks og Grønlands Geologiske Undersøgelse Rapport, Denmark, 1999.

Lister, G.S., and S.L. Baldwin, Modeling the effect of arbitrary P-T-t histories on argon diffusion in minerals using the MacArgon program for the Apple Macintosh, *Tectonophysics, 253*, 83-109, 1996.

Lovera, O.M., Computer programs to model (super 40) Ar/ (super 39) Ar diffusion data from multidomain samples, *Computers & Geosciences, 18*, 789-813, 1992.

Lovera, O.M., M.T. Heizler, and T.M. Harrison, Argon diffusion domains in K-feldspar II: kinetic properties of MH-10, *Contributions In Mineralogy and Petrology, 113*, 381-393, 1993.

Lovera, O.M., F.M. Richter, and T.M. Harrison, $^{40}Ar/^{39}Ar$ geochronometry for slowly cooled samples having a distribution of diffusion domain size, *Journal of Geophysical Research, 94*, 17917-17936, 1989.

Lovera, O.M., F.M. Richter, and T.M. Harrison, Diffusion domains determined by ^{39}Ar released during step heating, *Journal of Geophysical Research, 96*, 2057-2069, 1991.

Northrup, C.J., and B.C. Burchfiel, Emplacement of the Scandinavian allochthon, Scandinavian Caledonides: A-type subduction, syn-collisional extension, or both?, *Geological Society of America Abstracts with Programs, 25*, A-340, 1993.

Parsons, I., W.L. Brown, and J.V. Smith, (super 40) Ar/ (super 39) Ar thermochronology using alkali feldspars; real thermal history or mathematical mirage of microtexture?, *Contributions to Mineralogy and Petrology, 136*, 92-110, 1999.

Peucat, J.J., D. Tisserant, R. Caby, and N. Clauer, Resistance of zircons to U-Pb resetting in a prograde metamorphic sequence of Caledonian age in East Greenland, *Canadian Journal of Earth Sciences, 22*, 330-338, 1985.

Rasmussen, T.V., and A. Andresen, Kinematic indicators in Høgedal related to the "Fjord Region Detachment", in *Symposium on Caledonian geology in East Greenland: Abstract Volume*, vol. 46, edited by K.S. Frederiksen and K. Thrane, pp. 55, Danmarks og Grønlands Geologiske Undersøgelse Rapport, Denmark, 1998.

Renne, P.R., C.C. Swisher, A.L. Deino, D.B. Karner, T.L. Owens, and D.J. DePaolo, Intercalibration of standards, absolute ages and uncertainties in (super 40) Ar/ (super 39) Ar dating, *Chemical Geology, 145*, 117-152, 1998.

Rex, D.C., A. Gledhill, and A.K. Higgins, Precambrian Rb-Sr isochron ages from the crystalline complexes of inner Forsblads Fjord, East Greenland fold belt, *Rapport Grønlands geologiske Undersøgelse, 85*, 122-126, 1977.

Rex, D.C., and A.R. Gledhill, Isotopic studies in the East Greenland Caledonides (72°-74°N) — Precambrian and Caledonian ages, *Rapport Grønlands geologiske Undersøgelse, 104*, 47-72, 1981.

Rex, D.C., A.R. Gledhill, and A.K. Higgins, Progress report on geochronological investigations in the crystalline complexes of the East Greenland Caledonian fold belt between 72°N and 76°N, *Rapport Grønlands geologiske Undersøgelse, 80*, 127-133, 1976.

Rex, D.C., and A.K. Higgins, Potassium-argon mineral ages from the East Greenland Caledonides between 72 degrees and 74 degrees N, in *The Caledonide Orogen — Scandinavia and Related Areas*, vol. 2, edited by D.G. Gee and B.A. Sturt, pp. 1115-1124, John Wiley & Sons, Chichester, U.K., 1985.

Robbins, G.A., Radiogenic argon diffusion in muscovite under hydrothermal conditions, M.S. thesis, Brown University, 1972.

Rykkelid, E., and A. Andresen, Late Caledonian extension in the Ofoten area, northern Norway, *Tectonophysics, 231*, 157-169, 1994.

Samson, S.D., and E.C. Alexander, Calibration of the interlaboratory $^{40}Ar/^{39}Ar$ dating standard, MMhb-1, *Chemical Geology, 66*, 27-34, 1987.

Schlindwein, V., and W. Jokat, Post-collisional extension of the East Greenland Caledonides; a geophysical perspective, *Geophysical Journal International, 140*, 559-567, 2000.

Schmitz, M.D., and S.A. Bowring, U-Pb zircon and titanite systematics of the Fish Canyon Tuff: an assessment of high-precision U-Pb geochronology and its application to young volcanic rocks, *Geochimica et Cosmochimica Acta, 65*, 2571-2587, 2001.

Smith, M.P., and S. Robertson, The Nathorst Land Group (Neoproterozoic) of East Greenland - lithostratigraphy, basin geometry and tectonic history, in *Geology of East Greenland 72°-75°, mainly Caledonian: preliminary reports from the 1998 expedition*, edited by A.k. Higgins and K.S. Frederiksen, pp. 220, Danmarks og Grønlands Geologiske Undersøgelse Rapport, Denmark, 1999.

Steiger, R.H., and E. Jäger, Subcommission on geochronology: convention on the use of decay constants in geo- and cosmochronology, *Earth and Planetary Science Letters, 36*, 359-362, 1977.

Strachan, R.A., A.K. Higgins, N.J. Soper, and J.D. Friederichsen, Late Precambrian-early Paleozoic extensional tectonics and basin inversion, NE Greenland, *Dymek, Robert F., Shelton, Kevin L. Geological Society of America, 21*, 1989.

Strachan, R.A., M.W. Martin, and J.D. Friderichsen, Evidence for contemporaneous yet contrasting styles of granite magmatism during extensional collapse of the northeast Greenland Caledonides, *Tectonics*, In Press.

Sturt, B.A., and A. Thon, An ophiolite complex of probable early Caledonian age discovered on Karmoy, *Nature (London), 275*, 538-539, 1978.

Thrane, K., F. Kalsbeek, and G.R. Watt, Evidence for a Grenvillian event in the East Greenland Caledonian fold belt, in *Second symposium on East Greenland geology, mainly Caledonian: Abstract volume*, vol. 21, edited by K.S. Frederiksen and K. Thrane, pp. 64, Danmarks og Grønlands Geologiske Undersøgelse Rapport, Denmark, 1999.

Torsvik, T.H., M.A. Smethurst, J.G. Meert, R. Van der Voo, W.S. McKerrow, M.D. Brasier, B.A. Sturt, and H.J. Walderhaug, Continental break-up and collision in the Neoproterozoic and Palaeozoic; a tale of Baltica and Laurentia, *Earth-Science Reviews, 40*, 229-258, 1996.

Vold, J., Et studie av den tectonomatemorphe utviklingen av gneisserne i liggblokken til "The Fjord Region Detachment Zone" på Kap hedlund, sentrale Øst Grønland, Cand. Scient Thesis, 122 pp., University of Oslo, Oslo, 1997.

Wegmann, C.E., Preliminary report on the Caledonian orogeny in Christian X's Land (North-East Greenland), *Meddelelser om Grønland, 128*, 145-156, 1935.

White, A.P., and K.V. Hodges, Dynamic compensation in the East Greenland Caledonides, in *Second symposium on East Greenland geology, mainly Caledonian*, vol.

46, edited by F. K.S. and K. Thrane, pp. 64, Danmarks og Grønlands Geologiske Undersøgelse Rapport, Denmark, 1999.

White, A.P., K.V. Hodges, and K. Davidek, U-Pb constraints on the age of deformation of the Krummedal Supracrustal Sequence in Forsblad Fjord, East Greenland, in *Symposium on Caledonian geology in East Greenland*, vol. 46, edited by K.S. Frederiksen and K. Thrane, pp. 55, Danmarks og Grønlands Geologiske Undersøgelse Rapport, Denmark, 1998.

White, A.P., K.V. Hodges, M.V. Martin, and A. Andresen, Geologic constraints on middle-crustal behavior during synorogenic extension in the East Greenland Caledonides, *International Journal of Earth Science*, in press.

Zeitler, P.K., Argon diffusion in partially outgassed alkali feldspars: Insights from $^{40}Ar/^{39}Ar$ analysis, *Isotope Geosci., 65*, 167-181, 1987.

Figure Captions:

Figure 1: Simplified tectonic map of the central fjord region of the East Greenland Caledonides interpreted after Koch and Haller (1971), Henriksen and Higgins [1976], Peucat et al. (1985), Andresen et al. (1998a), White et al. (1998), Smith and Robertson (1999), Leslie and Higgins (1999), Escher and Jones (1999), White and Hodges (1999). The following abbreviations have been used: Forsblad Fjord (FF); Alpefjord (AF); Kaiser Franz Joseph's Fjord (KFJF); Kong Oscar's Fjord (KOF); Furesø (F); Eleonore Sø (ES); Målebjorg (M); Niggli Spids (NS); Charcot Land (CL). *N.B.* Gåseland lies south to the south from this map. Box indicates study area. Question marks indicate unknown or enigmatic contacts, unexplained by past work in the region. We have interpreted the above thrust geometries based on correlations between the preliminary age relationships and fault contacts reported by the Greenland Geological Survey in 1999 and the earlier work of L. Koch, J. Haller and others as referenced above.

Figure 2: Simplified geologic map of the study area with sample names and locations used in this study. For further geologic and structural details, see White et al. [in press].

Figure 3: Structural and temporal correlations between allochthons in the Forsblad Fjord region. Labeled rectangles indicate deformational events within a given allochthon. Rounded boxes indicate mapped tectonic structures that separate allochthons. H – Høgedal detachment, T – Tindern detachment. Shaded fields indicate deformational events and fabrics which are interpreted to be extensional. Open rectangles indicate deformational events which are interpreted to be related to crustal thickening. Solid horizontal lines indicate correlative deformational events in different allochthons. Age assignments are based on U-Pb geochronologic data from [White et al., in press] and $^{40}Ar/^{39}Ar$ data presented in this paper.

Figure 4: a) Photo of tightly folded S_{1a} cleavage and compositional layering in gneisses of the Krummedal Sequence during D1 deformation. b) Photo of broad, overturned F1b fold that deforms sedimentary rocks of the Eleonore Bay Supergroup. Note, the island with the fold stands about 150 meters tall. c) Photo showing the Tindern Detachment where it crops out just west of Randenæs peninsula on the north shore of Forsblad Fjord. A white line has been added to indicate the trace of the fault against the cliff because it is extremely difficult to see. Note the talus-cone fanning outwards from the high glacial valley beneath the fault stands ca. 750 meters tall. d) Photo showing schlieren of footwall gneisses entrained in the Caledonia Ø granite deformed by movement along the Tindern Detachment. Note the boudin-train with top-to-the-E sense-of-shear. Camera-case included for scale. e) Photo of the Høgedal Detachment. Note the prominent brittle fault plane denoted by the arrows. f) Photo of boudin-train in the

immediate footwall of the Høgedal Detachment and associated with deformation due to movement along that same fault. Note the top-to-E sense-of-shear. g) Photo of dike (sample 98GR41) which crosscuts sedimentary rocks of the Lower Nathorst Land Group. This dike exhibits a flattening cleavage similar to that of the surrounding sediments indicating that it too was deformed by the same early phase of deformation that affected the country rock. The clear structural relationship between this dike, the country rock and local deformation are the characteristics that we looked for in order to pick each of the samples used for geochronology.

Figure 5: $^{40}Ar/^{39}Ar$ data for muscovite presented on plateau diagrams.

Figure 6: Plot of $^{40}Ar/^{39}Ar$ muscovite age versus structural distance from the Tindern Detachment. Note the simple trend of the data which is continuously distributed across the position of the Tindern Detachment, apparently undisturbed by movement along the fault. The labels reflect estimated closure temperatures assuming constant cooling at the rate of 25° C/My. The dashed curve represents a linear regression through the dataset.

Figure 7: $^{40}Ar/^{39}Ar$ data for biotite presented on plateau diagrams. Note, the $^{40}Ar/^{39}Ar$ data for 98GR34 is presented on an isotope correlation diagram because this dataset represents 6 laser ablation analyses which do not yield cumulative diffusion information.

Figure 8: This plot shows mole fraction phlogopite versus nominal grain size radius measured in microns. The curves represent lines of constant closure temperature as a function of a constant cooling rate of 25° C per million years. The dashed portions of the curves represent regions calculated from parameters that were extrapolated from

outside the region of available empirical data [Harrison et al., 1985; Grove and Harrison, 1996b].

Figure 9: Plot of $^{40}Ar/^{39}Ar$ biotite age versus structural distance from the Tindern Detachment. Note the simple trend of the data across the structural horizon corresponding to the Tindern Detachment. This pattern corroborates the pattern observed in the muscovite dataset. However, the pattern formed by the biotite data is disrupted at the position of the Høgedal Detachment. The labels reflect estimated closure temperatures assuming constant cooling at the rate of 25° C/My. Note that the estimated closure temperatures decrease with decreasing depth. The dashed curve represents a linear regression through the dataset above the Høgedal detachment.

Figure 10: a) Release spectra showing both measured and modeled results. Note the disagreement between actual and modeled spectra only appears at temperature steps above the incongruent melting temperature for K-feldspar; thus this section of the curve should be dismissed. b) Arrhenius plot showing measured and modeled results. c) Log (r/r_0) plot showing measured versus modeled results. Note the close agreement between measured and modeled curves on both the Arrhenius and the log (r/r_0) plots. d) Plot showing the range of cooling path trajectories that are output from our K-feldspar model in temperature-time space. Included on the plot are the biotite (98GR34) and pseudotachylite (97GR06) $^{40}Ar/^{39}Ar$ ages and approximate cooling temperatures. Note that the pseudotachylite plots in the region of the lowest temperature segment of the K-feldspar model Tt path. This is consistent with the notion that an age from the pseudotachylite represents the age of very small K-feldspar crystals that formed immediately after the pseudotachylite was quenched.

Figure 11: a) Close-up of a backscattered electron image of the polished section containing pseudotachylite from 97GR06 showing uv laser-ablation pits. Note the pit diameters average 150 microns. b) Back-scattered electron image of the entire section. Note the pseudotachylite is partially devitrified and consists mainly of K-feldspar. The darker areas are quartz while the light regions have been identified as plagioclase, sphene and several other accessory minerals.

Figure 12: Isotope correlation diagram showing 21 uv-laser ablation analyses of the pseudotachylite from 97GR06. Note the excellent linear correlation between the data points. This best-fit curve projects to an initial $^{40}Ar/^{36}Ar$ value that is very close to that of present day air.

Figure 13: Simplified series of 3D block diagrams depicting the schematic evolution of deformational structures in the Forsblad Fjord region and surrounding areas. Note, the first diagram depicts two thrust-fault splays. This is inferred from faults mapped north of the study area. The second diagram depicts a time during which the Tindern detachment was active. Note that in addition to exhumation along the Tindern detachment, material in the wedge beneath the detachment was flowing to both the north and the south. While it is not known whether there was simultaneous movement along the basal thrust fault, U-Pb geochronologic constraints suggest that the wedge was being compressed at the same time as movement along the Tindern detachment within our geochronologic resolution [White et al., in press]. The third diagram depicts a time when the Høgedal detachment was active and thrusting had ceased. In addition, isostatic upwelling in the footwall of the Høgedal detachment had initiated a flexural response. The fourth diagram represents the mapped and inferred geometries of structures in their present relationships. This diagram includes the conglomerates deposited during

Devonian basin formation. Note, there is a significant domal structure preserved in the footwall of the Høgedal detachment.

Figure 1

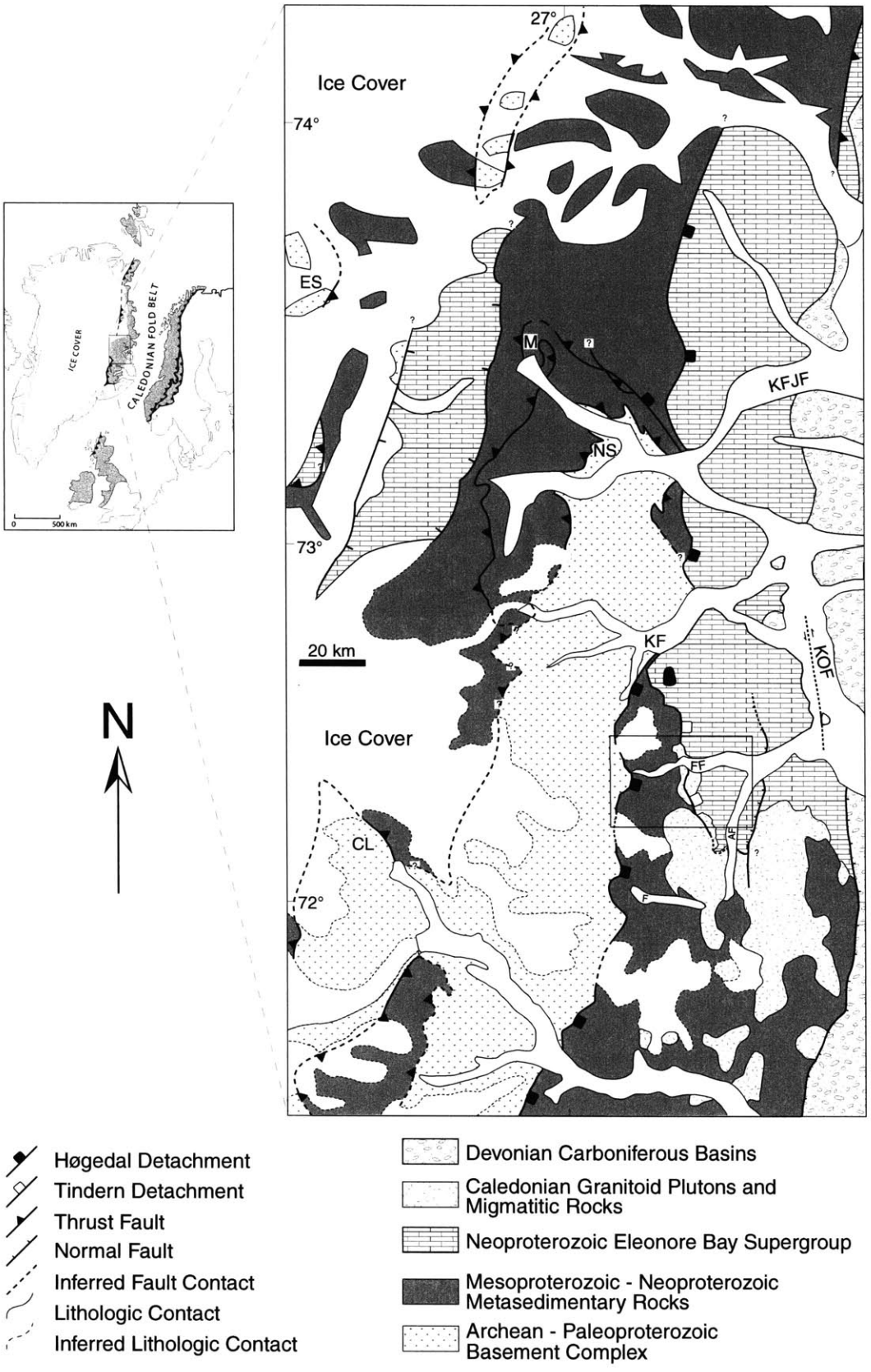
27°
Ice Cover
74°
ES
M
KFJF
NS
73°
20 km
KF
KOF
Ice Cover
FF
CL
72°
ICE COVER
CALEDONIAN FOLD BELT
0
500 km
N
Høgedal Detachment
Tindern Detachment
Thrust Fault
Normal Fault
Inferred Fault Contact
Lithologic Contact
Inferred Lithologic Contact
Devonian Carboniferous Basins
Caledonian Granitoid Plutons and Migmatitic Rocks
Neoproterozoic Eleonore Bay Supergroup
Mesoproterozoic - Neoproterozoic Metasedimentary Rocks
Archean - Paleoproterozoic Basement Complex

Figure 2

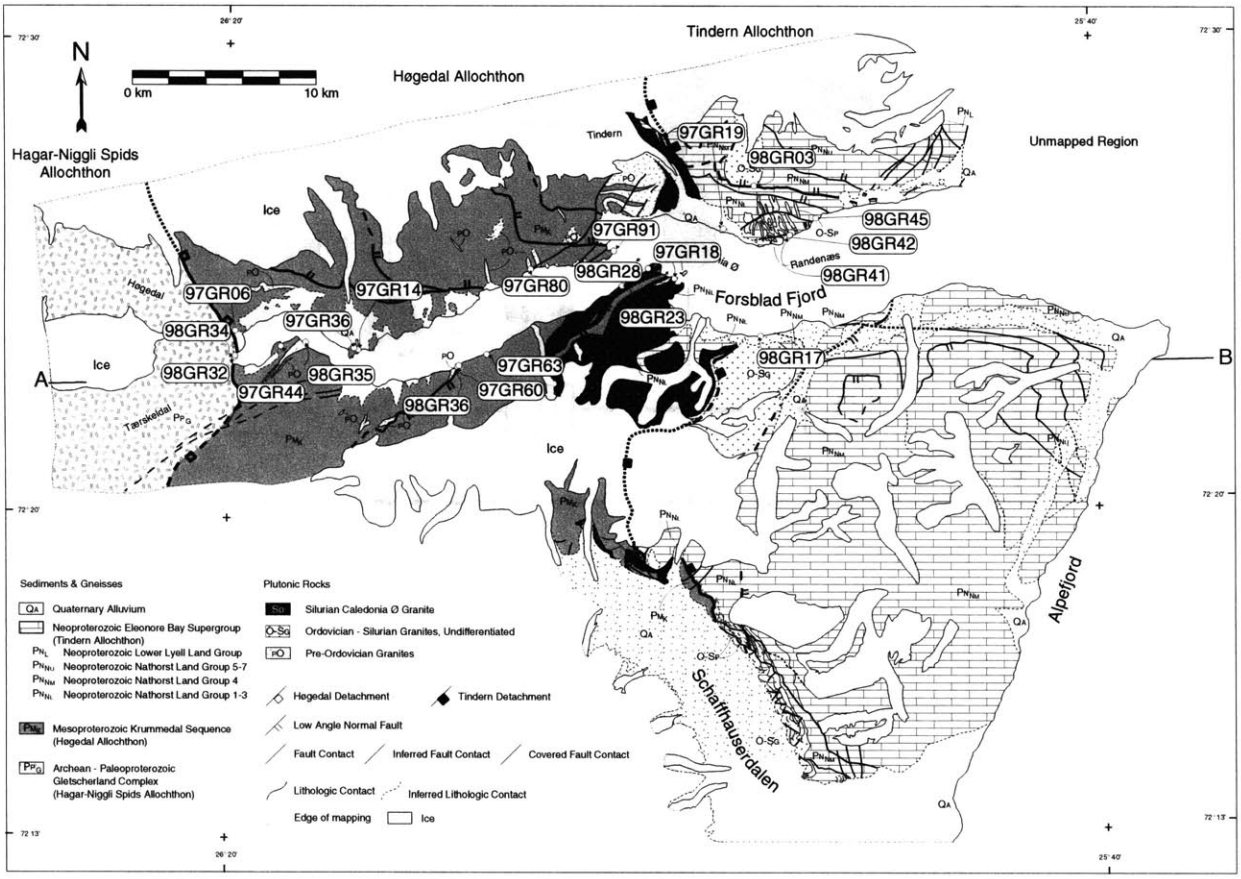
Tindern Allochthon
Høgedal Allochthon
Hagar-Niggli Spids Allochthon
Unmapped Region
N
0 km
10 km
Tindern
Ice
Høgedal
Forsblad Fjord
Randenæs
Tærskeldal
Alpefjord
Schaffhauserdalen
A
B
97GR19
98GR03
97GR91
98GR45
98GR42
97GR18
98GR28
98GR41
97GR06
97GR14
97GR80
98GR34
97GR36
98GR23
98GR17
98GR32
98GR35
97GR63
97GR44
97GR60
98GR36
Sediments & Gneisses
Quaternary Alluvium
Neoproterozoic Eleonore Bay Supergroup (Tindern Allochthon)
Neoproterozoic Lower Lyell Land Group
Neoproterozoic Nathorst Land Group 5-7
Neoproterozoic Nathorst Land Group 4
Neoproterozoic Nathorst Land Group 1-3
Mesoproterozoic Krummedal Sequence (Høgedal Allochthon)
Archean - Paleoproterozoic Gletscherland Complex (Hagar-Niggli Spids Allochthon)
Plutonic Rocks
Silurian Caledonia Ø Granite
Ordovician - Silurian Granites, Undifferentiated
Pre-Ordovician Granites
Hegedal Detachment
Tindern Detachment
Low Angle Normal Fault
Fault Contact
Inferred Fault Contact
Covered Fault Contact
Lithologic Contact
Inferred Lithologic Contact
Edge of mapping
Ice

Figure 3

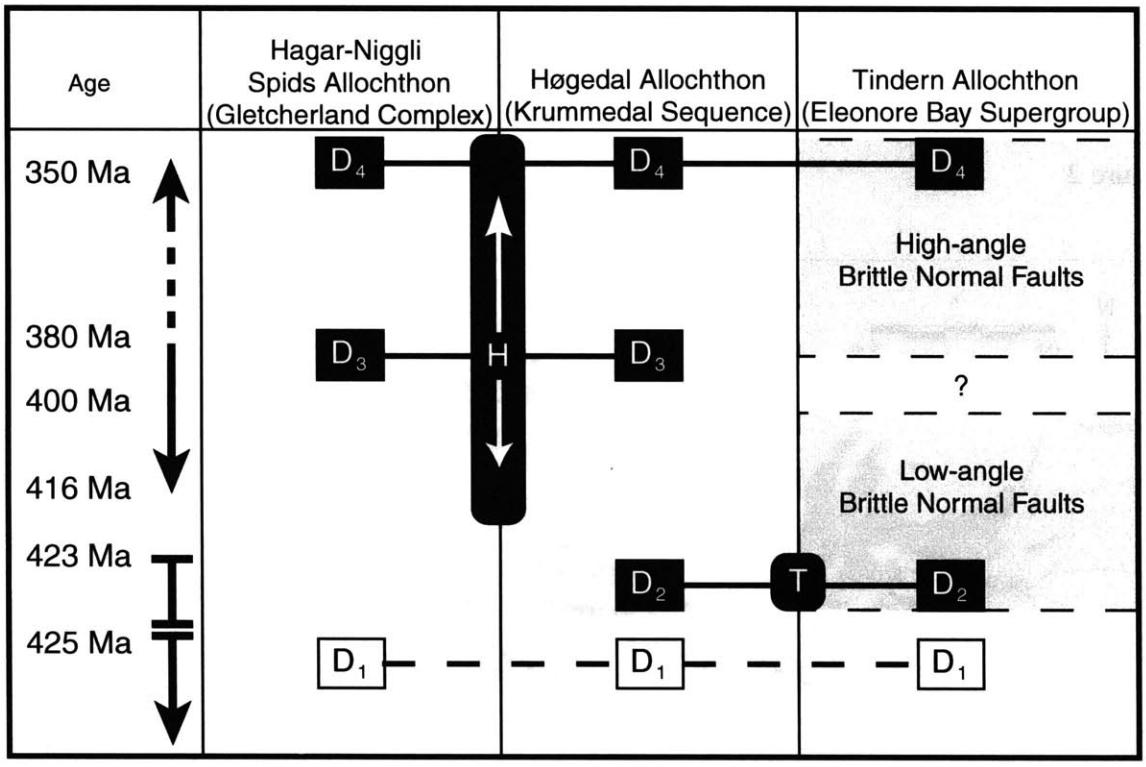
Age
Hagar-Niggli
Spids Allochthon
(Gletcherland Complex)
Høgedal Allochthon
(Krummedal Sequence)
Tindern Allochthon
(Eleonore Bay Supergroup)
350 Ma
380 Ma
400 Ma
416 Ma
423 Ma
425 Ma
D4
D3
D2
D1
H
T
High-angle
Brittle Normal Faults
?
Low-angle
Brittle Normal Faults

Figure 4

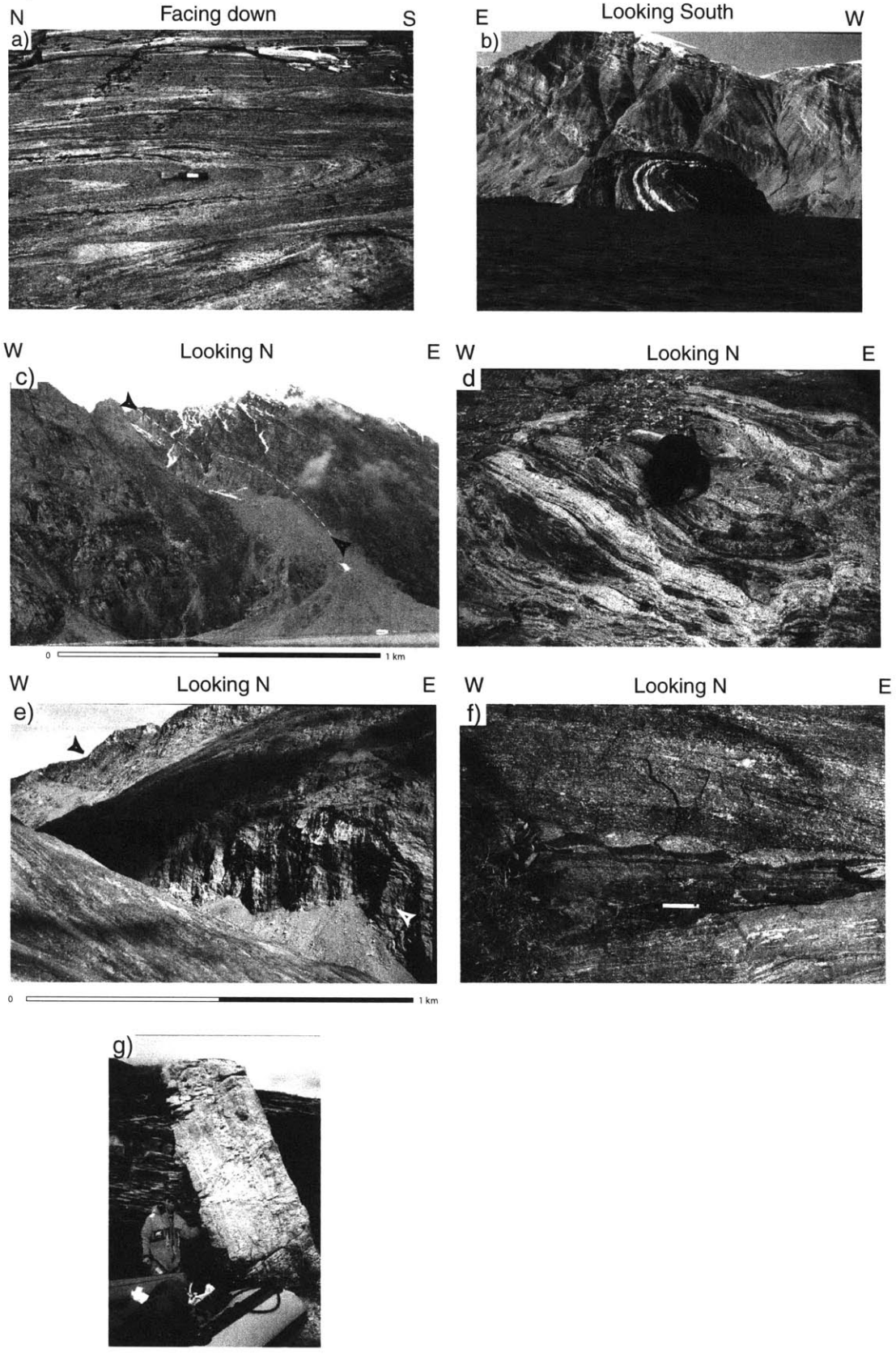
N
Facing down
S
a)
E
Looking South
W
b)
W
Looking N
E
c)
0
1 km
W
Looking N
E
d)
W
Looking N
E
e)
0
1 km
W
Looking N
E
f)
g)

Figure 5

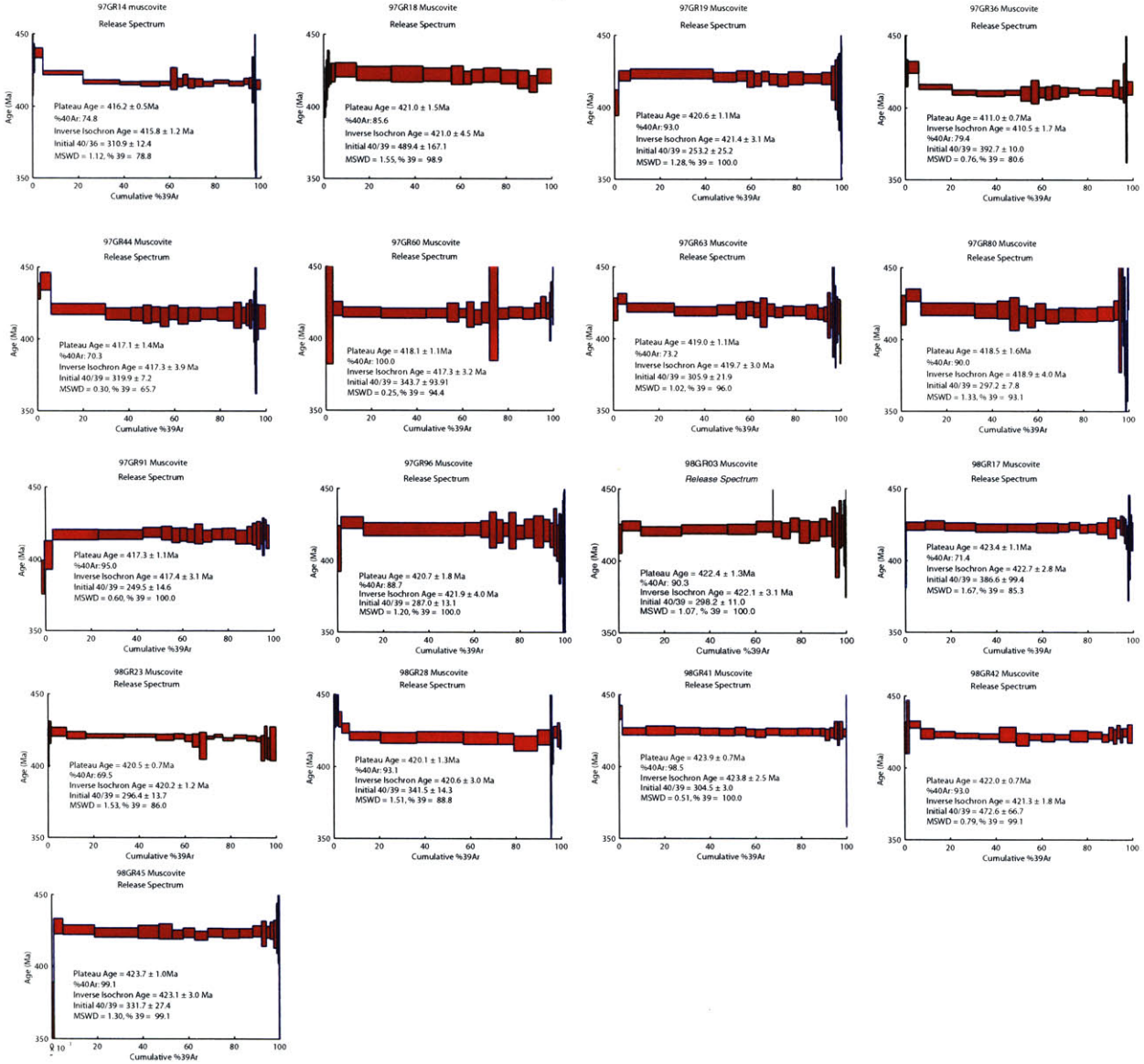
97GR14 muscovite
Release Spectrum
Plateau Age = 416.2 ± 0.5Ma
%40Ar: 74.8
Inverse Isochron Age = 415.8 ± 1.2 Ma
Initial 40/36 = 310.9 ± 12.4
MSWD = 1.12, % 39 = 78.8
97GR18 Muscovite
Release Spectrum
Plateau Age = 421.0 ± 1.5Ma
%40Ar: 85.6
Inverse Isochron Age = 421.0 ± 4.5 Ma
Initial 40/39 = 489.4 ± 167.1
MSWD = 1.55, % 39 = 98.9
97GR19 Muscovite
Release Spectrum
Plateau Age = 420.6 ± 1.1Ma
%40Ar: 93.0
Inverse Isochron Age = 421.4 ± 3.1 Ma
Initial 40/39 = 253.2 ± 25.2
MSWD = 1.28, % 39 = 100.0
97GR36 Muscovite
Release Spectrum
Plateau Age = 411.0 ± 0.7Ma
Inverse Isochron Age = 410.5 ± 1.7 Ma
%40Ar: 79.4
Initial 40/39 = 392.7 ± 10.0
MSWD = 0.76, % 39 = 80.6
97GR44 Muscovite
Release Spectrum
Plateau Age = 417.1 ± 1.4Ma
%40Ar: 70.3
Inverse Isochron Age = 417.3 ± 3.9 Ma
Initial 40/39 = 319.9 ± 7.2
MSWD = 0.30, % 39 = 65.7
97GR60 Muscovite
Release Spectrum
Plateau Age = 418.1 ± 1.1Ma
%40Ar: 100.0
Inverse Isochron Age = 417.3 ± 3.2 Ma
Initial 40/39 = 343.7 ± 93.91
MSWD = 0.25, % 39 = 94.4
97GR63 Muscovite
Release Spectrum
Plateau Age = 419.0 ± 1.1Ma
%40Ar: 73.2
Inverse Isochron Age = 419.7 ± 3.0 Ma
Initial 40/39 = 305.9 ± 21.9
MSWD = 1.02, % 39 = 96.0
97GR80 Muscovite
Release Spectrum
Plateau Age = 418.5 ± 1.6Ma
%40Ar: 90.0
Inverse Isochron Age = 418.9 ± 4.0 Ma
Initial 40/39 = 297.2 ± 7.8
MSWD = 1.33, % 39 = 93.1
97GR91 Muscovite
Release Spectrum
Plateau Age = 417.3 ± 1.1Ma
%40Ar: 95.0
Inverse Isochron Age = 417.4 ± 3.1 Ma
Initial 40/39 = 249.5 ± 14.6
MSWD = 0.60, % 39 = 100.0
97GR96 Muscovite
Release Spectrum
Plateau Age = 420.7 ± 1.8 Ma
%40Ar: 88.7
Inverse Isochron Age = 421.9 ± 4.0 Ma
Initial 40/39 = 287.0 ± 13.1
MSWD = 1.20, % 39 = 100.0
98GR03 Muscovite
Release Spectrum
Plateau Age = 422.4 ± 1.3Ma
%40Ar: 90.3
Inverse Isochron Age = 422.1 ± 3.1 Ma
Initial 40/39 = 298.2 ± 11.0
MSWD = 1.07, % 39 = 100.0
98GR17 Muscovite
Release Spectrum
Plateau Age = 423.4 ± 1.1Ma
%40Ar: 71.4
Inverse Isochron Age = 422.7 ± 2.8 Ma
Initial 40/39 = 386.6 ± 99.4
MSWD = 1.67, % 39 = 85.3
98GR23 Muscovite
Release Spectrum
Plateau Age = 420.5 ± 0.7Ma
%40Ar: 69.5
Inverse Isochron Age = 420.2 ± 1.2 Ma
Initial 40/39 = 296.4 ± 13.7
MSWD = 1.53, % 39 = 86.0
98GR28 Muscovite
Release Spectrum
Plateau Age = 420.1 ± 1.3Ma
%40Ar: 93.1
Inverse Isochron Age = 420.6 ± 3.0 Ma
Initial 40/39 = 341.5 ± 14.3
MSWD = 1.51, % 39 = 88.8
98GR41 Muscovite
Release Spectrum
Plateau Age = 423.9 ± 0.7Ma
%40Ar: 98.5
Inverse Isochron Age = 423.8 ± 2.5 Ma
Initial 40/39 = 304.5 ± 3.0
MSWD = 0.51, % 39 = 100.0
98GR42 Muscovite
Release Spectrum
Plateau Age = 422.0 ± 0.7Ma
%40Ar: 93.0
Inverse Isochron Age = 421.3 ± 1.8 Ma
Initial 40/39 = 472.6 ± 66.7
MSWD = 0.79, % 39 = 99.1
98GR45 Muscovite
Release Spectrum
Plateau Age = 423.7 ± 1.0Ma
%40Ar: 99.1
Inverse Isochron Age = 423.1 ± 3.0 Ma
Initial 40/39 = 331.7 ± 27.4
MSWD = 1.30, % 39 = 99.1
Age (Ma)
Cumulative %39Ar

Figure 6

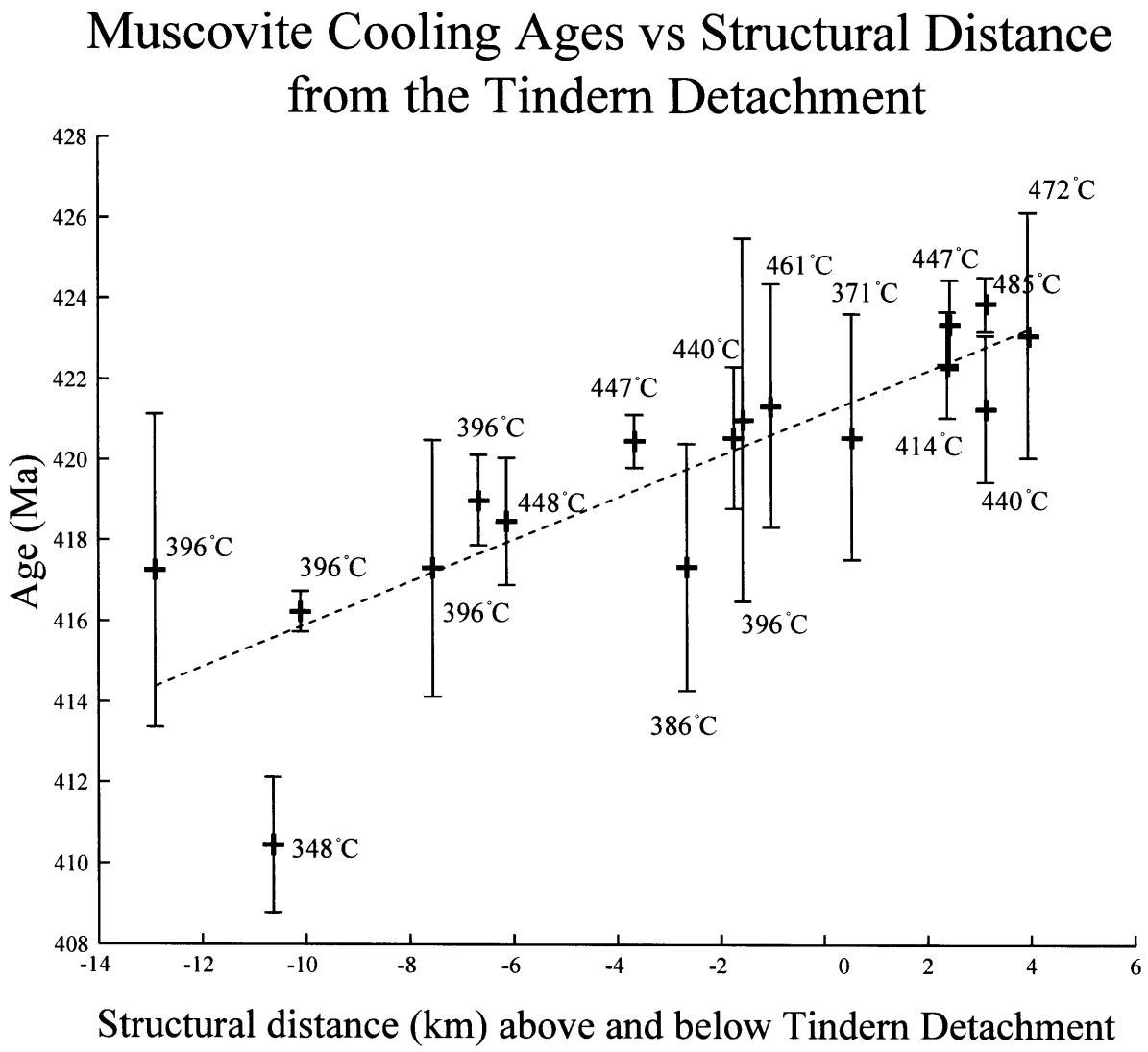
Muscovite Cooling Ages vs Structural Distance from the Tindern Detachment
Age (Ma)
428
426
424
422
420
418
416
414
412
410
408
-14
-12
-10
-8
-6
-4
-2
0
2
4
6
396˚C
396˚C
348˚C
396˚C
396˚C
448˚C
447˚C
386˚C
440˚C
461˚C
396˚C
371˚C
447˚C
414˚C
485˚C
440˚C
472˚C
Structural distance (km) above and below Tindern Detachment

Figure 7

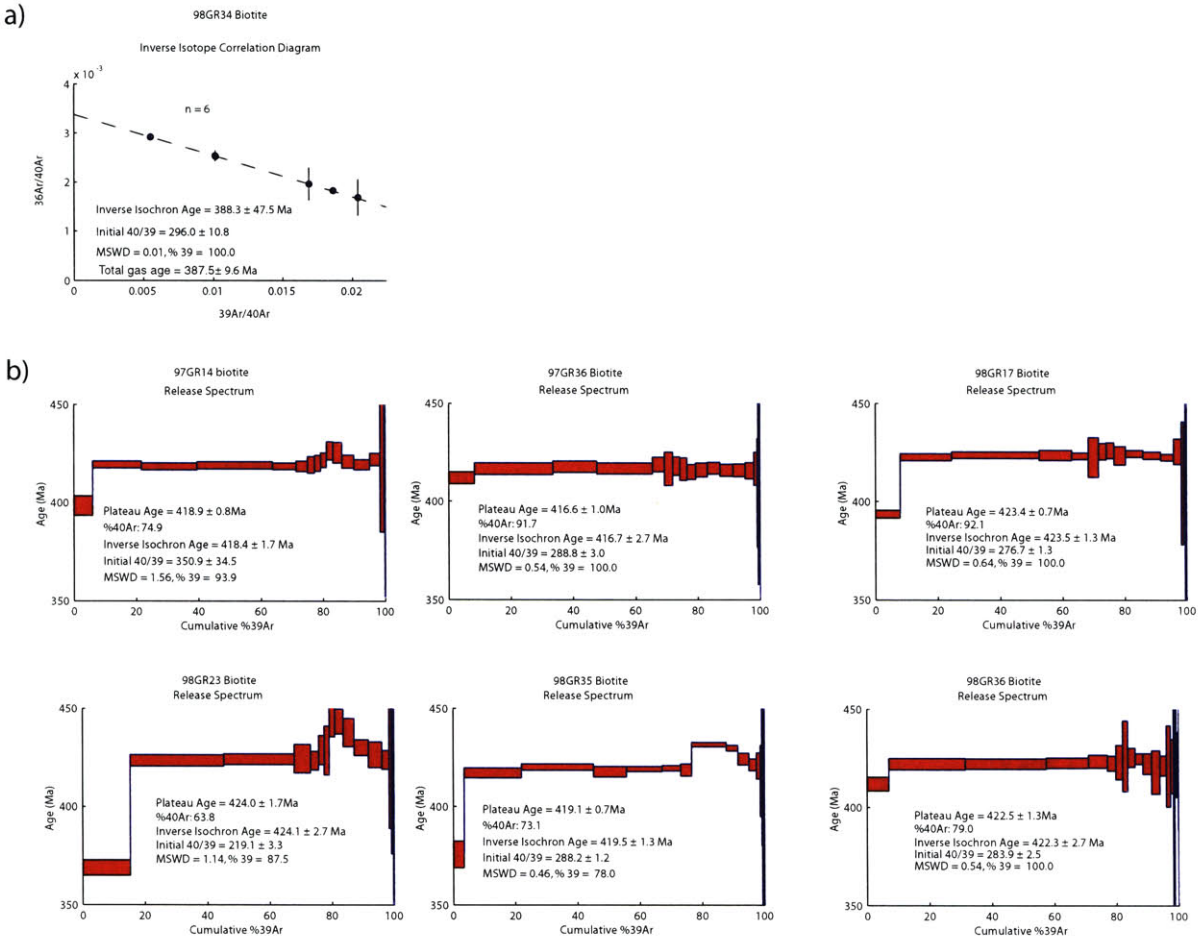
a)
98GR34 Biotite
Inverse Isotope Correlation Diagram
x 10^-3
n = 6
36Ar/40Ar
Inverse Isochron Age = 388.3 ± 47.5 Ma
Initial 40/39 = 296.0 ± 10.8
MSWD = 0.01, % 39 = 100.0
Total gas age = 387.5± 9.6 Ma
39Ar/40Ar
b)
97GR14 biotite
Release Spectrum
Plateau Age = 418.9 ± 0.8Ma
%40Ar: 74.9
Inverse Isochron Age = 418.4 ± 1.7 Ma
Initial 40/39 = 350.9 ± 34.5
MSWD = 1.56, % 39 = 93.9
97GR36 Biotite
Release Spectrum
Plateau Age = 416.6 ± 1.0Ma
%40Ar: 91.7
Inverse Isochron Age = 416.7 ± 2.7 Ma
Initial 40/39 = 288.8 ± 3.0
MSWD = 0.54, % 39 = 100.0
98GR17 Biotite
Release Spectrum
Plateau Age = 423.4 ± 0.7Ma
%40Ar: 92.1
Inverse Isochron Age = 423.5 ± 1.3 Ma
Initial 40/39 = 276.7 ± 1.3
MSWD = 0.64, % 39 = 100.0
98GR23 Biotite
Release Spectrum
Plateau Age = 424.0 ± 1.7Ma
%40Ar: 63.8
Inverse Isochron Age = 424.1 ± 2.7 Ma
Initial 40/39 = 219.1 ± 3.3
MSWD = 1.14, % 39 = 87.5
98GR35 Biotite
Release Spectrum
Plateau Age = 419.1 ± 0.7Ma
%40Ar: 73.1
Inverse Isochron Age = 419.5 ± 1.3 Ma
Initial 40/39 = 288.2 ± 1.2
MSWD = 0.46, % 39 = 78.0
98GR36 Biotite
Release Spectrum
Plateau Age = 422.5 ± 1.3Ma
%40Ar: 79.0
Inverse Isochron Age = 422.3 ± 2.7 Ma
Initial 40/39 = 283.9 ± 2.5
MSWD = 0.54, % 39 = 100.0
Age (Ma)
Cumulative %39Ar

Figure 8

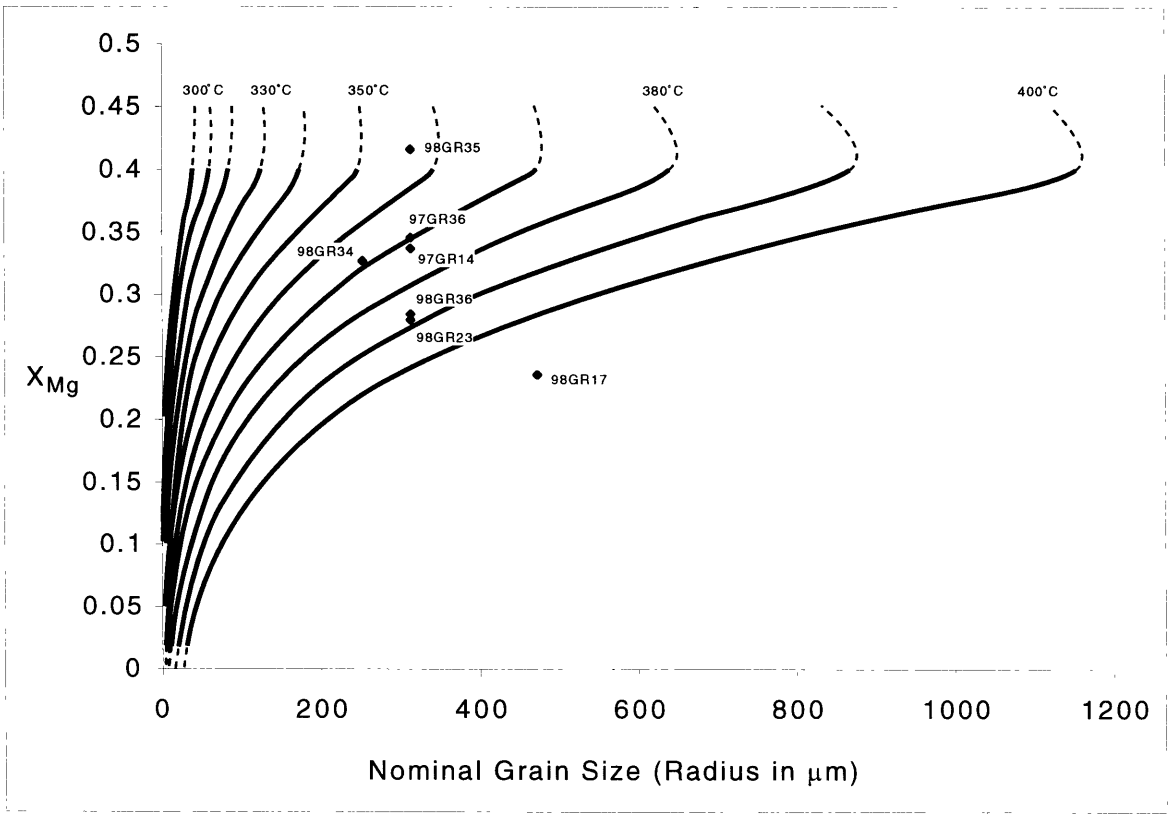
0.5
0.45
0.4
0.35
0.3
0.25
0.2
0.15
0.1
0.05
0
X_{Mg}
300°C
330°C
350°C
380°C
400°C
98GR35
97GR36
98GR34
97GR14
98GR36
98GR23
98GR17
0
200
400
600
800
1000
1200
Nominal Grain Size (Radius in μm)

Figure 9

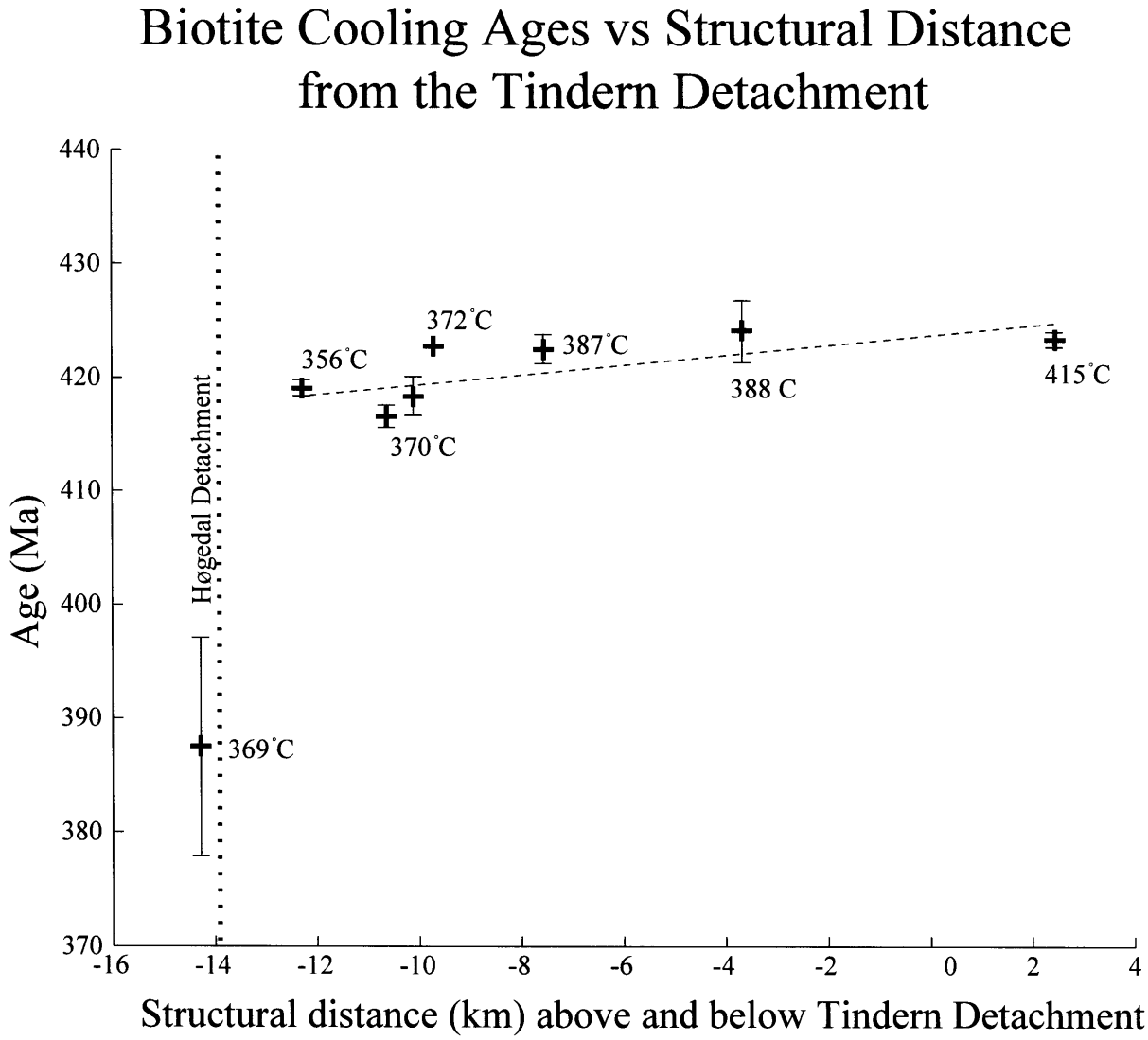
Biotite Cooling Ages vs Structural Distance from the Tindern Detachment
Age (Ma)
440
430
420
410
400
390
380
370
-16
-14
-12
-10
-8
-6
-4
-2
0
2
4
Høgedal Detachment
356˚C
372˚C
370˚C
387˚C
388 C
415˚C
369˚C
Structural distance (km) above and below Tindern Detachment

Figure 10

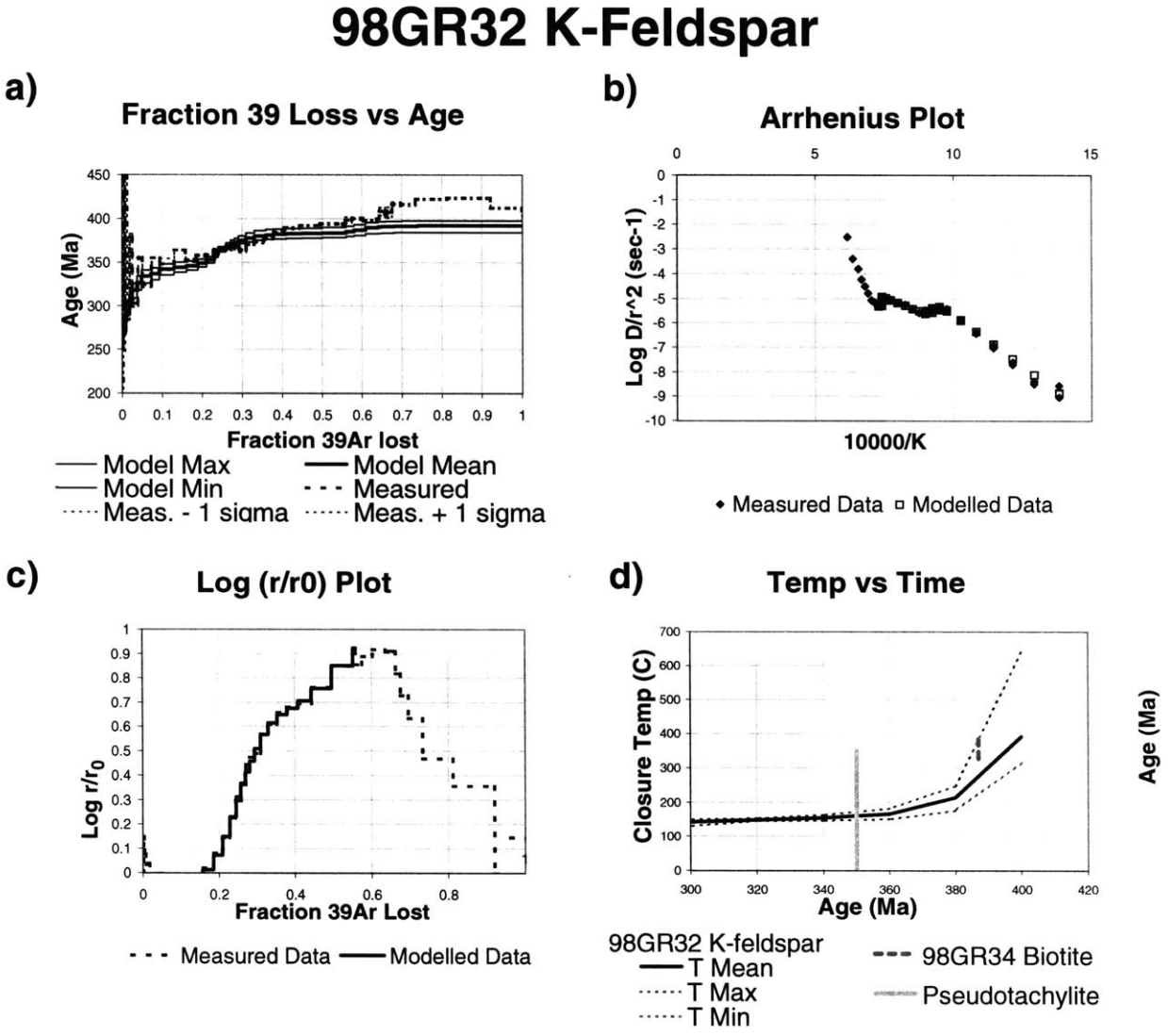
98GR32 K-Feldspar
a)
Fraction 39 Loss vs Age
Age (Ma)
Fraction 39Ar lost
Model Max
Model Mean
Model Min
Measured
Meas. - 1 sigma
Meas. + 1 sigma
b)
Arrhenius Plot
Log D/r^2 (sec-1)
10000/K
Measured Data
Modelled Data
c)
Log (r/r0) Plot
Log r/r0
Fraction 39Ar Lost
Measured Data
Modelled Data
d)
Temp vs Time
Closure Temp (C)
Age (Ma)
98GR32 K-feldspar
T Mean
T Max
T Min
98GR34 Biotite
Pseudotachylite

Figure 11

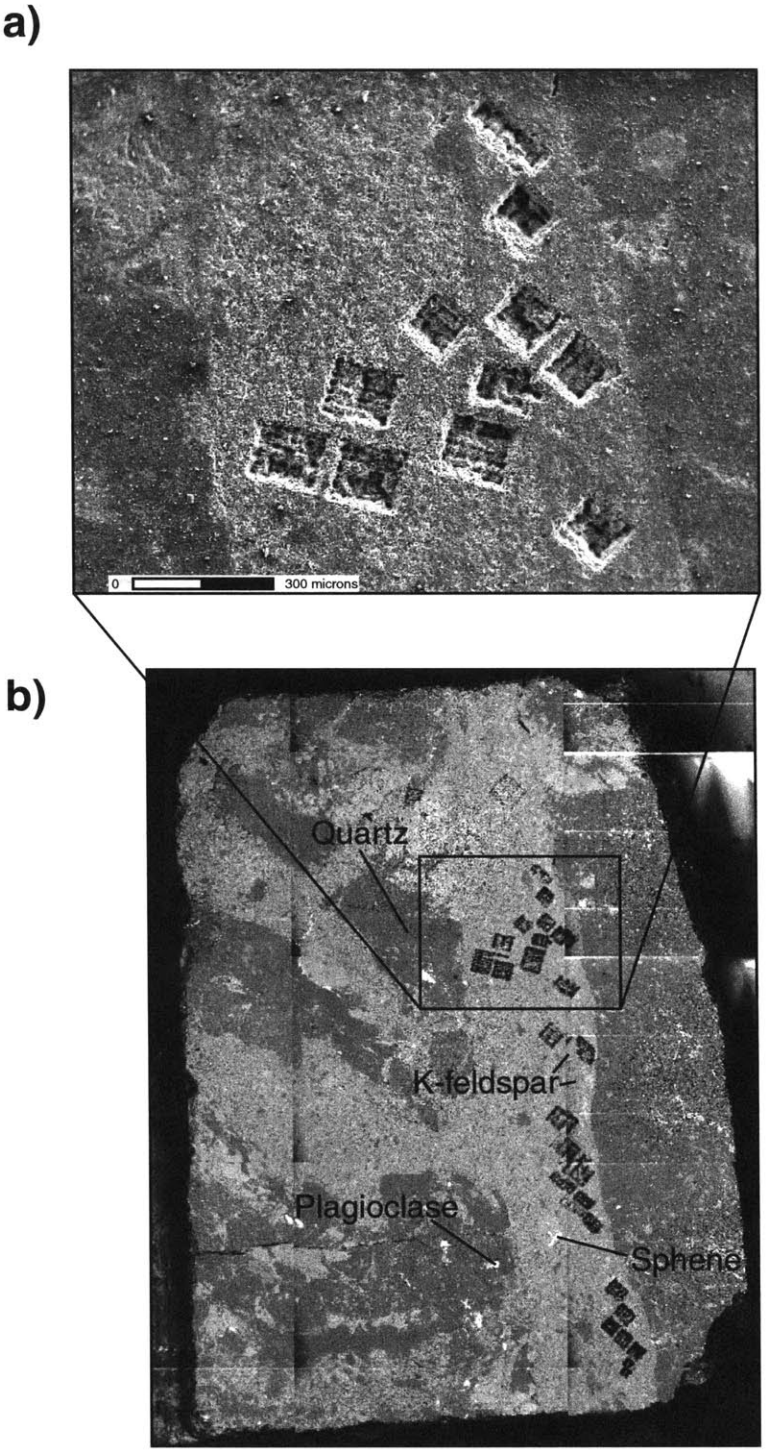

Figure 12

97GR06 Pseudotachylite
Isotope Correlation Diagram

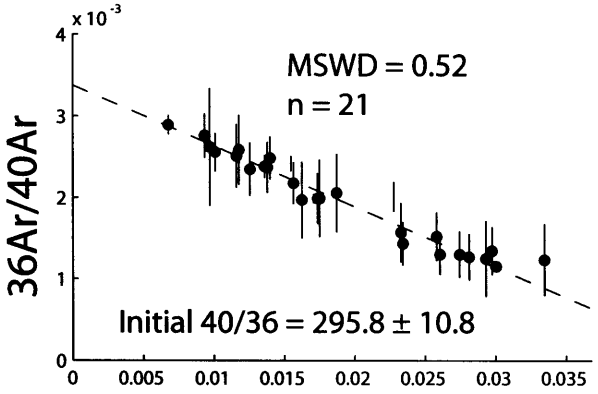

Inverse Isochron Age = 349.8 ± 20.1 Ma
Total Gas Age = 356.8 ± 10.8 Ma

Figure 13

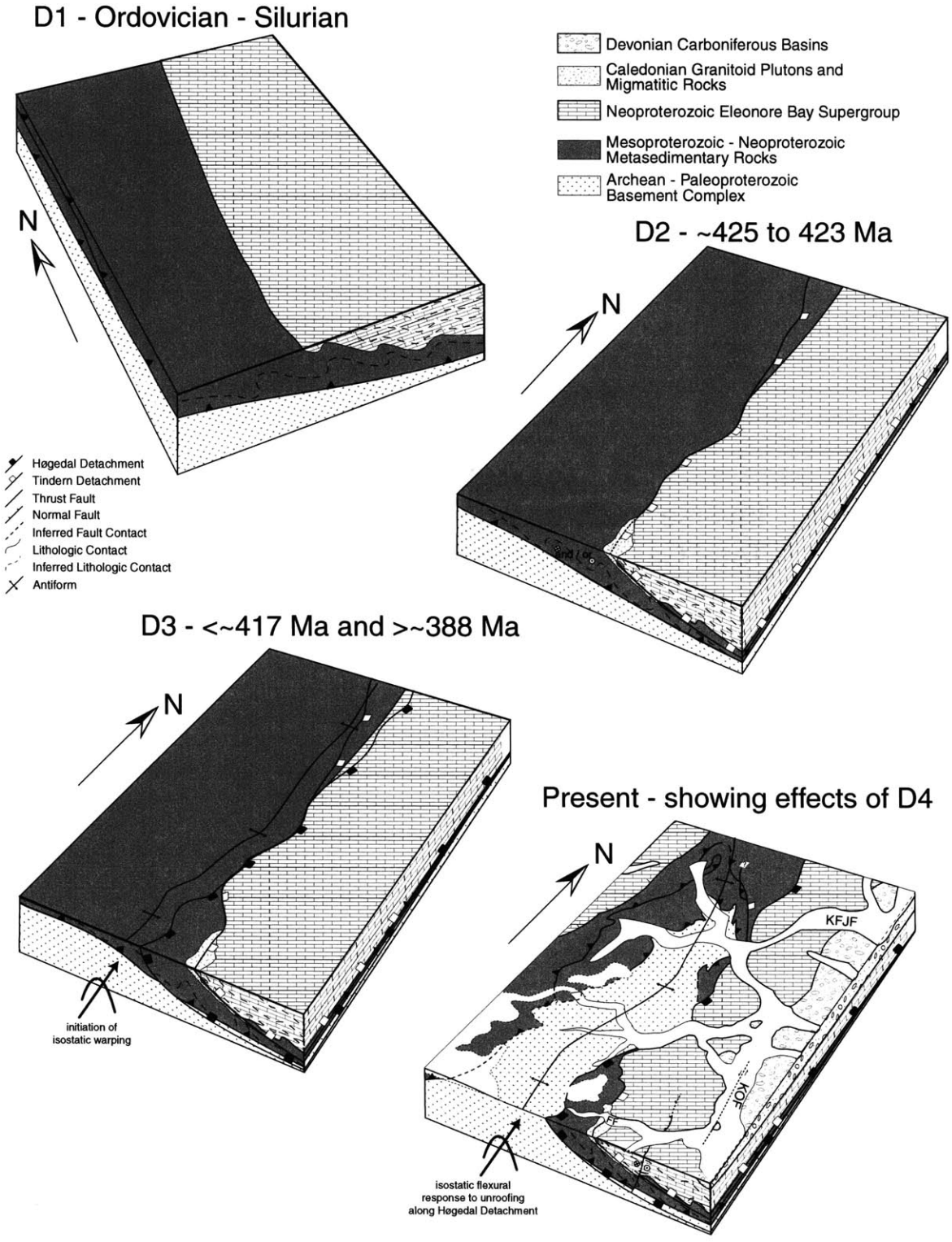
D1 - Ordovician - Silurian
N
Devonian Carboniferous Basins
Caledonian Granitoid Plutons and Migmatitic Rocks
Neoproterozoic Eleonore Bay Supergroup
Mesoproterozoic - Neoproterozoic Metasedimentary Rocks
Archean - Paleoproterozoic Basement Complex
Høgedal Detachment
Tindern Detachment
Thrust Fault
Normal Fault
Inferred Fault Contact
Lithologic Contact
Inferred Lithologic Contact
Antiform
D2 - ~425 to 423 Ma
N
D3 - <~417 Ma and >~388 Ma
N
initiation of isostatic warping
Present - showing effects of D4
N
KFJF
KOF
isostatic flexural response to unroofing along Høgedal Detachment

Table 1 VRF analyses

Sample Name	Mineral	Plateau Age	Error	%40Ar	Inverse Isochron Age	Error	%39Ar	Initial 40/39	Error	MSWD	Lat	Long.	Average Grain Radius (μm	Average Comp X_{Ann}	Grain-size Dependent Estimated Closure Temp *	Grain-size Independent Estimated Closure Temp **
97GR14	muscovite	**416.2**	± **0.5**	74 8	415 8	± 1 2	78.8	311	± 12	1 12	72′ 23.431	26′ 10.366	315	-	396	369
97GR18	muscovite	421.0	± 1.5	85.6	**421.0**	± **4.5**	98 9	489	± 167	1 55	72′ 24.967	25′ 51.028	315	-	396	369
97GR19	muscovite	420 6	± 1 1	93 0	**421.4**	± **3.1**	100.0	253	± 25	1 28	72′ 25.882	25′ 46 190	158	-	371	369
97GR36	muscovite	411.0	± 0 7	79.4	**410.5**	± **1.7**	80.6	393	± 10	0.76	72′ 23.413	26′ 11 562	79	-	348	369
97GR44	muscovite	417.1	± 1.4	70.3	**417.3**	± **3.9**	65.7	319 9	± 7 2	0.30	72′ 23.203	26′ 16 708	1260	-	453	369
97GR60	muscovite	418.1	± 1.1	100.0	**417.3**	± **3.2**	94.4	344	± 94	0 25	72′ 23.866	26′ 8 764	315	-	396	369
97GR63	muscovite	**419.0**	± **1.1**	73 2	419 7	± 3 0	96.0	306	± 22	1 02	72′ 23.185	26′ 2.640	315	-	396	369
97GR80	muscovite	**418.5**	± **1.6**	90.0	418 9	± 4 0	93 1	297 2	± 7 8	1 33	72′ 24 640	26′ 1.359	1125	-	448	369
97GR91	muscovite	417 3	± 1 1	95 0	**417.4**	± **3.1**	100 0	250	± 15	0.60	72′ 25 350	25′ 53.457	1103	-	447	369
97GR96	muscovite	**420.7**	± **1.8**	88 7	421 9	± 4 0	100.0	287	± 13	1 20	72′ 26 108	25′ 51 332	930	-	440	369
98GR03	muscovite	**422.4**	± **1.3**	90 3	422 1	± 3 1	100 0	298	± 11	1.07	72′ 26 185	25′ 41.992	788	-	414	369
98GR17	muscovite	**423.4**	± **1.1**	71 4	422.7	± 2.8	99 4	387	± 99	1.67	72′ 23 637	25′ 42 055	1103	-	447	369
98GR23	muscovite	**420.5**	± **0.7**	69 5	420 2	± 1 2	86 0	296	± 14	1 53	72′ 24 191	25′ 55 806	236	-	386	369
98GR28	muscovite	420.1	± 1 3	93 1	**420.6**	± **3.0**	88.8	341	± 14	1 51	72′ 24 902	25′ 49.780	1500	-	461	369
98GR41	muscovite	**423.9**	± **0.7**	98.5	423.8	± 2 5	100.0	304 5	± 3.0	0.51	72′ 25 762	25′ 40.353	2500	-	485	369
98GR42	muscovite	422.0	± 0.7	93 0	**421.3**	± **1.8**	99.1	473	± 67	0.79	72′ 25 762	25′ 40 353	930	-	440	369
98GR45	muscovite	423.7	± 1 0	99 1	**423.1**	± **3.0**	99 1	332	± 27	1.30	72′ 26 083	25′ 38 471	1890	-	472	369
97GR14	biotite	418 9	± 0 8	74 9	**418.4**	± **1.7**	93 9	351	± 34	1 56	72′ 23 431	26′ 10 366	315	0 66	372	350
97GR36	biotite	**416.6**	± **1.0**	91 7	416 7	± 2.7	100.0	288.8	± 3 0	0 54	72′ 23.413	26′ 11.562	315	0 65	370	335
98GR17	biotite	**423.4**	± **0.7**	92 1	423 5	± 1.3	100.0	276 7	± 1 3	0 64	72′ 23.637	25′ 42 055	473	0 76	415	379
98GR23	biotite	424 0	± 1 7	63 8	**424.1**	± **2.7**	87.5	219 1	± 3.3	1 14	72′ 24.191	25′ 55.806	315	0 72	388	366
98GR35	biotite	**419.1**	± **0.7**	73 1	419.5	± 1.3	78 0	288 2	± 1.2	0 46	72′ 23.668	26′ 15 291	315	0 58	356	334
98GR36	biotite	422 5	± 1 3	79 0	**422.3**	± **2.7**	100 0	283 9	± 2.5	0 54	72′ 22.981	26′ 4 656	315	0.72	387	364

Bold indicates preferred age All samples irradiated with a monitor, either GA1550 or MMHB-1

Uncertainties are reported at 2s and include uncertainty in the J-value

* Assuming a nominal cooling rate of 25-C/million years

** Assuming a sub-grain diffusion domain of 150μm and a nominal cooling rate of 25-C/million years

Table 2 ULA analyses

Sample Name	Mineral	Total Gas Age***	Error	%40Ar	Inverse Isochron Age	Error	Initial 40/39	Error	MSWD	Lat	Long	Average Grain Radius (μm	Average Comp X_{Ann}	Grain-size Dependent Estimated Closure Temp.*	Grain-size Independent Estimated Closure Temp **
97GR06	pseudotachylite	**357**	± **11**	NA	349 8	± 20 1	295.8	± 10.8	0 52	72′ 23.736	26′ 20 051	-	-	-	-
98GR34	biotite	**387.5**	± **9.6**	NA	388.3	± 47 5	296 0	± 10 8	0.01	72′ 23.147	26′ 19.800	250	0 32	369	353

Bold indicates preferred age All samples irradiated with a monitor, either GA1550 or MMHB-1

Uncertainties are reported at 2s and include uncertainty in the J-value

* Assuming a nominal cooling rate of 25-C/million years

** Assuming a sub-grain diffusion domain of 150 μm and a nominal cooling rate of 25-C/million years

*** Represents the average total gas age for ULA analyses - 21 spot analyses for 97GR06 and 6 spot analyses for 98GR34

Appendix

Heating Schedules

Muscovite 97GR14	(min)	Muscovite 97GR18		Muscovite 97GR19		Muscovite 97GR36		Muscovite 97GR44		Muscovite 97GR60		Muscovite 97GR63	
Temperature	Duration	Temperature	Duration	Temperature	Duration	Temperature	Duration	Temperature	Duration	Temperature	Duration	Temperature	Duration
600 (C)	10	600 (C)	10	600 (C)	10	600 (C)	10	600 (C)	10	600 (C)	10	600 (C)	10
700 (C)	10	700 (C)	10	700 (C)	10	700 (C)	10	700 (C)	10	700 (C)	10	700 (C)	10
800 (C)	10	800 (C)	10	800 (C)	10	800 (C)	10	800 (C)	10	800 (C)	10	800 (C)	10
825 (C)	10	825 (C)	10	825 (C)	10	825 (C)	10	825 (C)	10	825 (C)	10	825 (C)	10
850 (C)	10	850 (C)	10	850 (C)	10	850 (C)	10	850 (C)	10	850 (C)	10	850 (C)	10
875 (C)	10	875 (C)	10	875 (C)	10	875 (C)	10	875 (C)	10	875 (C)	10	875 (C)	10
900 (C)	10	900 (C)	10	900 (C)	10	900 (C)	10	900 (C)	10	900 (C)	10	900 (C)	10
925 (C)	10	925 (C)	10	925 (C)	10	925 (C)	10	925 (C)	10	925 (C)	10	925 (C)	10
950 (C)	10	950 (C)	10	950 (C)	10	950 (C)	10	950 (C)	10	950 (C)	10	950 (C)	10
975 (C)	10	975 (C)	10	975 (C)	10	975 (C)	10	975 (C)	10	975 (C)	10	975 (C)	10
1000 (C)	10	1000 (C)	10	1000 (C)	10	1000 (C)	10	1000 (C)	10	1000 (C)	10	1000 (C)	10
1025 (C)	10	1050 (C)	10	1025 (C)	10	1025 (C)	10	1025 (C)	10	1025 (C)	10	1025 (C)	10
1050 (C)	10	1075 (C)	10	1050 (C)	10	1050 (C)	10	1050 (C)	10	1050 (C)	10	1050 (C)	10
1075 (C)	10	1100 (C)	10	1075 (C)	10	1075 (C)	10	1075 (C)	10	1075 (C)	10	1075 (C)	10
1100 (C)	10	1150 (C)	10	1100 (C)	10	1100 (C)	10	1100 (C)	10	1100 (C)	10	1100 (C)	10
1125 (C)	10	1200 (C)	10	1125 (C)	10	1125 (C)	10	1125 (C)	10	1125 (C)	10	1125 (C)	10
1150 (C)	10	1225 (C)	10	1150 (C)	10	1150 (C)	10	1150 (C)	10	1150 (C)	10	1150 (C)	10
1200 (C)	10	1250 (C)	10	1200 (C)	10	1200 (C)	10	1200 (C)	10	1200 (C)	10	1200 (C)	10
1225 (C)	10	1300 (C)	10	1250 (C)	10	1250 (C)	10	1250 (C)	10	1250 (C)	10	1250 (C)	10
1250 (C)	10	1350 (C)	10	1350 (C)	10	1350 (C)	10	1350 (C)	10	1350 (C)	10	1350 (C)	10
1300 (C)	10	1550 (C)	10	1550 (C)	10	1550 (C)	10	1550 (C)	10	1550 (C)	10	1550 (C)	10
1350 (C)	10												
1550 (C)	10												

Muscovite 97GR80		Muscovite 97GR91		Muscovite 97GR96		Muscovite 98GR03		Muscovite 98GR17		Muscovite 98GR23		Muscovite 98GR28	
Temperature	Duration	Temperature	Duration	Temperature	Duration	Temperature	Duration	Temperature	Duration	Temperature	Duration	Temperature	Duration
600 (C)	10	600 (C)	10	600 (C)	10	600 (C)	10	600 (C)	10	600 (C)	10	600 (C)	10
700 (C)	10	700 (C)	10	700 (C)	10	700 (C)	10	700 (C)	10	700 (C)	10	700 (C)	10
800 (C)	10	800 (C)	10	800 (C)	10	800 (C)	10	800 (C)	10	800 (C)	10	800 (C)	10
825 (C)	10	825 (C)	10	825 (C)	10	825 (C)	10	825 (C)	10	825 (C)	10	825 (C)	10
850 (C)	10	850 (C)	10	850 (C)	10	850 (C)	10	850 (C)	10	850 (C)	10	850 (C)	10
875 (C)	10	875 (C)	10	875 (C)	10	875 (C)	10	875 (C)	10	875 (C)	10	875 (C)	10
900 (C)	10	900 (C)	10	900 (C)	10	900 (C)	10	900 (C)	10	900 (C)	10	900 (C)	10
925 (C)	10	925 (C)	10	925 (C)	10	925 (C)	10	925 (C)	10	925 (C)	10	925 (C)	10
950 (C)	10	950 (C)	10	950 (C)	10	950 (C)	10	950 (C)	10	950 (C)	10	950 (C)	10
975 (C)	10	975 (C)	10	975 (C)	10	975 (C)	10	975 (C)	10	975 (C)	10	975 (C)	10
1000 (C)	10	1000 (C)	10	1000 (C)	10	1000 (C)	10	1000 (C)	10	1000 (C)	10	1000 (C)	10
1025 (C)	10	1025 (C)	10	1025 (C)	10	1025 (C)	10	1025 (C)	10	1025 (C)	10	1025 (C)	10

1050 (C)	10	1050 (C)	10	1050 (C)	10	1050 (C)	10	1050 (C)	10	1050 (C)	10	1050 (C)	10
1075 (C)	10	1075 (C)	10	1075 (C)	10	1075 (C)	10	1075 (C)	10	1075 (C)	10	1075 (C)	10
1100 (C)	10	1100 (C)	10	1100 (C)	10	1100 (C)	10	1100 (C)	10	1100 (C)	10	1125 (C)	10
1125 (C)	10	1125 (C)	10	1125 (C)	10	1125 (C)	10	1125 (C)	10	1125 (C)	10	1150 (C)	10
1150 (C)	10	1150 (C)	10	1150 (C)	10	1150 (C)	10	1150 (C)	10	1150 (C)	10	1200 (C)	10
1200 (C)	10	1200 (C)	10	1200 (C)	10	1200 (C)	10	1200 (C)	10	1200 (C)	10	1225 (C)	10
1250 (C)	10	1250 (C)	10	1250 (C)	10	1250 (C)	10	1225 (C)	10	1250 (C)	10	1250 (C)	10
1350 (C)	10	1350 (C)	10	1350 (C)	10	1350 (C)	10	1250 (C)	10	1350 (C)	10	1300 (C)	10
1550 (C)	10	1550 (C)	10	1550 (C)	10	1550 (C)	10	1300 (C)	10	1550 (C)	10	1350 (C)	10
								1350 (C)	10			1550 (C)	10
								1550 (C)	10				

Muscovite 98GR41		Muscovite 98GR42		Muscovite 98GR45	
Temperature	Duration	Temperature	Duration	Temperature	Duration
600 (C)	10	600 (C)	10	600 (C)	10
700 (C)	10	700 (C)	10	700 (C)	10
800 (C)	10	800 (C)	10	800 (C)	10
825 (C)	10	825 (C)	10	825 (C)	10
850 (C)	10	850 (C)	10	850 (C)	10
875 (C)	10	875 (C)	10	875 (C)	10
900 (C)	10	900 (C)	10	900 (C)	10
925 (C)	10	925 (C)	10	925 (C)	10
950 (C)	10	950 (C)	10	950 (C)	10
975 (C)	10	975 (C)	10	975 (C)	10
1000 (C)	10	1000 (C)	10	1000 (C)	10
1025 (C)	10	1025 (C)	10	1025 (C)	10
1050 (C)	10	1050 (C)	10	1050 (C)	10
1075 (C)	10	1075 (C)	10	1075 (C)	10
1100 (C)	10	1100 (C)	10	1100 (C)	10
1125 (C)	10	1125 (C)	10	1125 (C)	10
1150 (C)	10	1150 (C)	10	1150 (C)	10
1200 (C)	10	1200 (C)	10	1200 (C)	10
1250 (C)	10	1250 (C)	10	1250 (C)	10
1350 (C)	10	1350 (C)	10	1350 (C)	10
1550 (C)	10	1550 (C)	10	1550 (C)	10

Biotite 97GR14		Biotite 97GR36		Biotite 98GR17		Biotite 98GR23		Biotite 98GR35		Biotite 98GR36	
Temperature	Duration	Temperature	Duration	Temperature	Duration	Temperature	Duration	Temperature	Duration	Temperature	Duration
600 (C)	10	600 (C)	10	600 (C)	10	600 (C)	10	600 (C)	10	600 (C)	10
700 (C)	10	700 (C)	10	700 (C)	10	700 (C)	10	700 (C)	10	973 (C)	10
800 (C)	10	800 (C)	10	800 (C)	10	800 (C)	10	800 (C)	10	1073 (C)	10
825 (C)	10	825 (C)	10	825 (C)	10	825 (C)	10	825 (C)	10	1098 (C)	10
850 (C)	10	850 (C)	10	850 (C)	10	850 (C)	10	850 (C)	10	1123 (C)	10

875 (C)	10	875 (C)	10	875 (C)	10	875 (C)	10	875 (C)	10	1148 (C)	10
900 (C)	10	900 (C)	10	900 (C)	10	900 (C)	10	900 (C)	10	1173 (C)	10
925 (C)	10	925 (C)	10	925 (C)	10	925 (C)	10	925 (C)	10	1198 (C)	10
950 (C)	10	950 (C)	10	950 (C)	10	950 (C)	10	950 (C)	10	1223 (C)	10
975 (C)	10	975 (C)	10	975 (C)	10	975 (C)	10	975 (C)	10	1248 (C)	10
1000 (C)	10	1000 (C)	10	1000 (C)	10	1000 (C)	10	1000 (C)	10	1273 (C)	10
1025 (C)	10	1025 (C)	10	1025 (C)	10	1025 (C)	10	1025 (C)	10	1298 (C)	10
1050 (C)	10	1050 (C)	10	1050 (C)	10	1050 (C)	10	1050 (C)	10	1323 (C)	10
1075 (C)	10	1075 (C)	10	1075 (C)	10	1075 (C)	10	1075 (C)	10	1348 (C)	10
1100 (C)	10	1100 (C)	10	1100 (C)	10	1100 (C)	10	1100 (C)	10	1373 (C)	10
1125 (C)	10	1125 (C)	10	1125 (C)	10	1125 (C)	10	1125 (C)	10	1398 (C)	10
1150 (C)	10	1150 (C)	10	1150 (C)	10	1150 (C)	10	1150 (C)	10	1423 (C)	10
1200 (C)	10	1200 (C)	10	1200 (C)	10	1200 (C)	10	1200 (C)	10	1473 (C)	10
1250 (C)	10	1250 (C)	10	1250 (C)	10	1250 (C)	10	1250 (C)	10	1523 (C)	10
1350 (C)	10	1350 (C)	10	1350 (C)	10	1350 (C)	10	1350 (C)	10	1623 (C)	10
1550 (C)	10	1550 (C)	10	1550 (C)	10	1550 (C)	10	1550 (C)	10	1823 (C)	10

K-feldspar
98GR32

Temperature	Duration	Temperature	Duration
400 (C)	20	900 (C)	25
400 (C)	36	940 (C)	25
450 (C)	20	980 (C)	25
450 (C)	36	1020 (C)	25
500 (C)	28	1050 (C)	25
500 (C)	36	1075 (C)	25
550 (C)	28	1075 (C)	40
550 (C)	36	1075 (C)	80
600 (C)	28	1075 (C)	150
600 (C)	36	1100 (C)	20
650 (C)	28	1100 (C)	40
650 (C)	36	1100 (C)	80
700 (C)	28	1100 (C)	120
700 (C)	36	1125 (C)	20
750 (C)	28	1125 (C)	40
750 (C)	36	1150 (C)	15
780 (C)	28	1175 (C)	15
780 (C)	36	1200 (C)	15
810 (C)	28	1225 (C)	15
810 (C)	36	1250 (C)	15
840 (C)	28	1300 (C)	15
840 (C)	36	1350 (C)	15
870 (C)	28		

4. Pressure-temperature-time evolution of the Central East Greenland Caledonides: quantitative constraints on crustal thickening and synorogenic extension

Arthur P. White*, Kip V. Hodges*

** Department of Earth, Atmospheric and Planetary Sciences, Massachusetts Institute of Technology, Cambridge, MA, 02139,USA. apwhite@mit.edu Tel (617)-253-8445 fax (617) 252-1800*

Abstract:

While geologists have known for three-quarters of a century that there was significant crustal thickening in the central East Greenland Caledonides, the crucial role of extensional faulting during Caledonian orogenesis has only been recognized during the past decade. In this paper, we present new petrographic and thermobarometric observations from migmatitic metasedimentary gneisses of the Krummedal Sequence in the footwall of the upper of two significant splays of the main extensional fault system, the Fjord Region Detachment (FRD), that enable us to establish a relative sequence of metamorphism in the Forsblad Fjord region (~72.5° N). Our pressure temperature results indicate that the data follow a clockwise loop in P-T space, with a net increase of ~4 kb and 250° C (peak conditions of ~10.5 kb at 785°C) followed by near isothermal decompression of ~4.5 kb. From this we estimate a minimum amount of burial of ca. 16 km, and an approximate tectonostratigraphic throw along the upper splay of the FRD of ~18 km. Combining our data with the data published by Vold (1997), we estimate that the approximate tectonostratigraphic throw along the lower splay of the FRD was ~16 km.

Our preliminary U-Pb-monazite chemical ages, determined with an electron microprobe, indicate that the earliest phase of metamorphism recorded in the Krummedal Sequence gneisses occurred during the Caledonian orogeny. Furthermore, the combination of our new data with previous geochronologic data imply that movement along the uppermost splay of the FRD (ca. 425-423 Ma) occurred at maximum time-averaged slip-rates of ~9 mm-of-vertical displacement-per-year, and that the final stages of metamorphism occurred prior to ca. 411 Ma; however, part of this denudation was likely accommodated on overlying extensional structures that may have been active more recently. The close agreement between our data and rocks from the Krummedal Sequence north of our field area (72.25°-74° N), and rocks of the Smallefjord Sequence (75°-76° N) that we suggest correlate with the Krummedal Sequence, leads us to infer that the events recorded in the Forsblad Fjord region are of orogen-scale significance.

Introduction:

Recent structural and geochronologic investigations in the central East Greenland Caledonides (72° to 74° N) have revealed a multi-stage extensional history along a system of faults called the Fjord Region Detachment (FRD), with splays that were active both during and after collisional orogenesis (e.g. Andresen *et al.*, 1998; Caby, 1976; Hartz, 2001; Hartz & Andresen, 1995; Hartz *et al.*, 2000; White & Hodges, in preparation; White *et al.*, in press). The spectacular middle-crustal structural exposure and preservation of syn- and post-orogenic normal faults in this transpressive orogen presents a valuable opportunity to improve our understanding of the spatial and temporal relationships between orogen-parallel shear, contraction and extension over the course of the orogen's evolution. At present, there is very little in the way of published thermobarometric data to compliment the growing base of structural and geochronologic

data (e.g. Andresen *et al.*, 1998; Hartz, 2001; Hartz *et al.*, 2000; Higgins & Leslie, 2000; Strachan *et al.*, In Press; White *et al.*, in press). In this paper, we present the results of qualitative petrographic and quantitative thermobarometric studies of amphibolite facies metamorphic rocks from the Forsblad Fjord area of East Greenland (~72.5° N; Figure 1). When these data are interpreted in conjunction with our new geochronologic results for monazite inclusions in metamorphic garnet, they suggest that there were at least 4 stages of metamorphism in this region, all Caledonian in age, associated with crustal thickening and thinning during orogenesis. The combination of thermobarometric data with P-T constraints derived from the petrogenetic grid indicate that there was a substantial amount of burial (~16 km) proceeded by a nearly equal amount of tectonic exhumation (~18 km) along the uppermost splay of the FRD system.

Geological Background:

Oblique convergence led to the subduction of Baltica beneath Laurentia during the Middle to Late Silurian and the formation of the Caledonian orogen (Torsvik *et al.*, 1996; Andresen & Steltenpohl, 1994; Gee, 1975; Henriksen, 1985; Hodges *et al.*, 1982; Sturt & Thon, 1978). Remnants of this collision are found in Scandinavia, Ireland, Scotland and East Greenland (Figure 1, subset). Evidence for west-directed translation of material is preserved in thrust-bounded tectonic windows that expose Archean to Neoproterozoic metamorphic gneiss complexes that lie north of the study area (>73° N) in Eleonore Sø, Målebjorg and Niggli Spids (Elvevold *et al.*, 2000; Escher & Jones, 1999; Leslie & Higgins, 1999) and south of the study area (< 72°N) in Charcot Land and Gåseland (Christoffersen, 1984). A prominent system of N-S striking, E-dipping normal faults truncated the eastern margin of these tectonic windows. Originally mapped as

thrusts, they were reinterpreted as extensional shear zones by Hartz & Andresen (1995) and later named the Fjord Region Detachment (FRD) by Andresen *et al.* (1998).

The faults that comprise the FRD system diverge south of 73° N into two splays (Figure 1) locally referred to as the Høgedal and Tindern detachments (White *et al.*, in press). A range of U-Pb and $^{40}Ar/^{39}Ar$ thermochronologic constraints on the timing of these faults suggests that rapid slip at high temperature (> 450° C) occurred along the Tindern detachment between ca. 425 to 423 Ma, while activity along the Høgedal detachment occurred at lower temperatures (< 400°-350 ° C) between ca. 417-380 Ma with subsequent activity as recent as ca. 357 Ma (White *et al.*, 1998; White *et al.*, in press; White & Hodges, in preparation-a). Bounded between these faults lies a ~14 km thick wedge of amphibolite facies migmatitic paragneisses interpreted to be the metamorphic equivalent of the Krummedal Supracrustal Sequence mapped in the Scoresby Sund region (71.5° N; Higgins, 1988). These gneisses are particularly interesting because they preserve E-W contractional and synkinematic N-S orogen-parallel flow fabrics, deformation associated with the oblique Laurentia-Baltica convergence, that are essentially coeval with E-W extension along the Tindern detachment (White *et al.*, in press).

The Forsblad Fjord Transect (~72.5° N)

Spectacular 3-dimensional exposures of the structures described above are found in the Forsblad Fjord Transect (Figures 1 and 2). There, the E-dipping Høgedal and Tindern detachments juxtapose three separate allochthons from structurally lowest to highest and west to east, the Hagar-Niggli Spids, Høgedal and Tindern allochthons (White *et al.*, in press). Lying primarily beneath the Inland Ice, the Hagar-Niggli Spids

allochthon is comprised of granulite and amphibolite facies Archean and Paleoproterozoic orthogneisses of the Gletscherland Complex. These rocks preserve metamorphism and deformation ranging from Proterozoic to Middle Paleozoic in age (e.g. (Backlund, 1930; Haller, 1970; Henriksen & Higgins, 1976; Rex & Gledhill, 1981; Rex *et al.*, 1976; Wegmann, 1935; White *et al.*, in press). To the east and structurally above these orthogneisses lie the migmatitic amphibolite-facies metasedimentary gneisses of the Krummedal Sequence that comprise the Høgedal allochthon. These Caledonian-aged kyanite/sillimanite + biotite + garnet paragneisses preserve a structural thickness of ~14 km, along the Forsblad Fjord section, that is rapidly thinned north of the Fjord between the merging Høgedal and Tindern detachments (Figure 1). Further to the east are low-grade chlorite + biotite + garnet Caledonian-aged schists and phyllites that comprise the basal 3 km of the Tindern allochthon (White *et al.*, in press; White & Hodges, in preparation-a), also referred to as Nathorst Land Group Formations 1-3 (Smith & Robertson, 1999) — the lowermost of 4 groups that comprise the Eleonore Bay Supergroup.

The focus of our work has been upon the Krummedal Sequence aluminous schists and gneisses of the Høgedal allochthon that are particularly well suited for quantitative thermobarometric study. Previous metamorphic studies of nearby units correlative to these rocks have suggested that an early phase of high-temperature/high-pressure ($T > 700^\circ$ C and $< 850^\circ$ C, $P > 8$ kb) garnet growth in the kyanite stability field was followed by a second phase of garnet growth in the sillimanite stability field (Elvevold & Gilotti, 1998). Vold (1997) has suggested that maximum P-T conditions may have reached 10-12 kb at 700-850° C followed by subsequent garnet growth at ~3.5 kb at 650° C.

Rocks of the Høgedal allochthon were affected by four important deformational phases that have been described in detail by White *et al.* (in press). Note that in this paper, $\mathbf{D_1}$ corresponds to D_{1H} from White *et al.* (in press), while $\mathbf{D_2}$ corresponds to D_{2H}, and $\mathbf{D_3}$ to D_{3H}, $\mathbf{D_4}$ represents an additional event not defined in the earlier paper, and $\mathbf{D_5}$ to D_{3N}. The dominant metamorphic mineral assemblages grew during the first two phases of deformation. While evidence for the geometry of strain during D_1 has been largely obscured during later deformation, a penetrative schistosity (S_1, defined by alignment of biotite ± muscovite ± kyanite) has been preserved. The timing of this deformation has remained largely unconstrained; however, it has been suggested previously that the age of metamorphism deformed by D_1 is "Grenvillian" (~1 Ga), and pre-dates the Caledonian orogeny (e.g. Kalsbeek *et al.*, 1998; Thrane *et al.*, 1999; Watt & Thrane, 1999); later in this paper, we present new geochronologic data that instead indicate a Caledonian age for D_1.

D_2 also preserves a penetrative schistosity (S_2, defined by biotite ± muscovite ± kyanite ± ribboned quartz) that strikes N-S to NW-SE and dips ~50° E. The earlier S_1 foliation is frequently transposed into parallelism with S_2 making it difficult to distinguish between the two. Both prismatic and fibrolitic sillimanite define a N-S trending mineral lineation (L_2). Kinematic indicators suggest that material flowed to the north and south, parallel to these lineations. N-S trending F_2 folds deform S_1 fabrics and refold F_1 folds. The age of this deformation is constrained by a syn-D_2 leucosome that has yielded a U-Pb monazite age of 425.3 ± 0.3 Ma (White *et al.*, in press).

The D_3 event corresponds to syn-orogenic ductile E-W extension and crustal thinning along the E-dipping Tindern detachment. High-temperature deformation along this shear zone juxtaposed amphibolite facies metasedimentary rocks of the Krummedal

Sequence against the greenschist facies Lower Eleonore Bay Supergroup at a time that was coeval with D_2 (ca. 425-423 Ma) within the resolution of the published geochronology (White *et al.*, in press).

Following movement along the Tindern detachment, evidence presented in this paper indicates that there was subsequent growth and deformation of retrograde muscovite and chlorite in the Krummedal Sequence gneisses. This D_4 deformation is associated with continued crustal thickening along an inferred D_4 thrust fault (White et al., in press) that placed the Høgedal allochthon on top of the Hagar Niggli-Spids allochthon in-between movement along the Tindern and Høgedal detachments.

The final episode of deformation (D_5) corresponds to activity along the E-dipping Høgedal detachment. Low-temperature shear along this fault, between ca. 417-380 Ma (White & Hodges, in preparation-a), led to the truncation of Krummedal Sequence base and thus provides a minimum age constraint on the latest retrograde growth of muscovite and chlorite within the Krummedal Sequence at ca. 380 Ma. Given the need for a reasonable amount of time for displacement along the inferred D_4 thrust fault mentioned above, we argue that movement along the Høgedal detachment most likely began during the later portion of the bracketed time-period presented by White & Hodges (in preparation-a). Detailed descriptions of FRD shear-zones may be found in White *et al.* (in press).

Because D_2-D_5 are well constrained within a short period of time yet previous investigators have regarded D_1 as a possible "Grenvillian"-aged event, one of our aspirations has been to evaluate the possibility that the earliest stages of metamorphism in the Krummedal Sequence pre-date the Caledonian orogeny using *in situ* electron microprobe U-Pb dates on monazite. This work builds upon our primary goal which is to

explore the PT evolution of these pelitic assemblages and thus to weave their metamorphic and deformational histories into a tectonic context.

Pelitic Schists of the Krummedal Sequence

In outcrop, the Krummedal Sequence is typically banded with a stromatic layering between one to ten centimeters in thickness. Anatexites are scattered throughout the sequence, increasing in abundance up-section to the point that melt appears to have mobilized at ~1-2 km structurally beneath the Tindern detachment. Both concordant leucosomes and cross-cutting granites are common. The strike and dip of the schistosity is remarkably consistent everywhere (White *et al.*, in press). This fact — in conjunction with the lack of significant, obvious structural discontinuities between the Høgedal and Tindern detachments — implies that the Krummedal Sequence in Forsblad Fjord represents a continuous tilted section ~14 km thick.

Petrography

In order to maximize our understanding of the events recorded in Forsblad Fjord, a suite of samples was collected, from a variety of structural horizons that span from the Tindern detachment to the base of the Høgedal allochthon. Given that high-temperature metamorphism preserved in the Høgedal detachment footwall was indisputably pre-Caledonian (Rex *et al.*, 1977; Rex & Gledhill, 1981), samples from the Hagar-Niggli Spids allochthon were not analyzed.

The primary metamorphic mineral assemblage preserved in the migmatitic metasedimentary rocks of the Krummedal Sequence consists of biotite + garnet + plagioclase + quartz ± K-feldspar ± muscovite ± kyanite/sillimanite ± cordierite (Table

1). Concordant (syn-S_2) leucosomes typically contain K-feldspar + plagioclase + quartz ± sillimanite ± biotite. Cross-cutting, post-D_2 leucosomes are also present; they typically contain K-feldspar + plagioclase + quartz ± sillimanite ± biotite. Secondary muscovite and chlorite occur in some samples. Biotite is ubiquitous, while primary muscovite disappears at ~7.5 kilometers beneath the Tindern detachment; neoblastic, idiomorphic, post-D_2 muscovite is found overprinting the primary metamorphic mineral assemblages that crystallized pre- to syn-D_1-D_2. The ratio of kyanite/sillimanite decreases up-section; however, the two minerals are frequently seen in the same thin-section or hand-sample. The kyanite isograd lies ~7 km beneath the Tindern detachment, and the cordierite isograd lies ~4.5 km beneath the detachment.

Quartz (20-50%)

Subhedral quartz is the most abundant mineral found in pelitic rocks of the Krummedal Sequence. Aggregates of quartz form ribbons that help define S_2. Dynamically recrystallized rods of quartz near the Tindern detachment define L_3. Quartz crystals frequently display undulose extinction and well developed subgrain domains, and range up to 2 mm in size. Subhedral quartz inclusions (<0.5 mm in size) are abundant in Phase 1 garnet (see below).

Plagioclase (5-30%)

After quartz, plagioclase is the second most abundant mineral in Krummedal Sequence metapelites. Subhedral laths of plagioclase that grew pre- to syn-kinematically with respect to D_2 are common with long dimensions that range from < 0.5 - 3 millimeters. Anhedral plagioclase inclusions (< 0.5 mm in size) are found included in garnet that grew pre- to syn-D_1 as described below. Matrix plagioclase is found in D_2

pressure shadows around garnets. Some subhedral crystals also overprint S_2 fabrics in the matrix indicating that they grew post-kinematically with respect to D_2. Myrmekitic intergrowths of quartz and plagioclase are abundant in the upper part of the section, near the Tindern detachment, where plagioclase crystals that grew pre- to syn-kinematically with respect to D_3 fabrics replace garnet porphyroblasts (Figure 3b, 3c, 3d). Many plagioclase grains include subhedral quartz and biotite and display albite twinning.

Biotite (5-20%)

Subhedral biotite laths are ubiquitous within the matrix. Dark brown in color with long-axis dimensions of ~0.5-3 millimeters, it helps to define both the S_1 and S_2 schistosities. Minor amounts of subhedral porphyroblastic biotite overgrow the syn-S_2 generation of crystals. Armored relics of biotite found included in Phase 1 garnet (< .25 mm in size) are almost always subhedral to anhedral, while biotite found included in Phase 2 garnet is euhedral in some instances.

K-feldspar (<1-15%)

At depths less than ~9 km beneath the Tindern detachment (97GR70) K-feldspar comprises a significant component of the Krummedal Sequence metamorphic mineral assemblage. Crystals form subhedral to euhedral laths that range from < 0.5 - 2 mm. The Caledonia Ø granite contains schlieren of Krummedal Sequence gneisses in which K-feldspar augen are as large as ~2.5 centimeters. For the most part, K-feldspar crystals are deformed by D_2 deformation, displaying undulose extinction and definite subgrain formation. Asymmetric tails on rotated K-feldspar porphyroblasts help to define the sense-of-shear along the Tindern detachment. These K-feldspars are often fractured into a series of separate, small grain fragments during D_3 deformation.

Garnet (<1-15%)

Fabrics observed in the Forsblad Fjord samples provide evidence for two stages of garnet growth. The first generation of garnets (Phase 1) are characteristically subhedral and range widely in size from 1 mm to 10 cm in diameter (Figure 3a). They typically include anhedral quartz and subhedral biotite, plagioclase, and K-feldspar, as well as accessory minerals such as monazite and zircon. At structural levels beneath the kyanite isograd, subhedral kyanite is also a common inclusion. Most inclusions in the garnets are randomly oriented; however, some garnets contain well-defined, sigmoidal inclusion trails (Figure 4a) or straight inclusion trails that are not parallel to the matrix S_2 schistosity. This indicates that Phase 1 garnet grew syn- to post-kinematically with respect to D_1 and pre-kinematically with respect to D_2. Most of these garnets are flanked by symmetric or asymmetric pressure shadows containing sillimanite. Many Phase 1 garnets are embayed, suggesting some degree of resorbtion after crystallization. With increasing structural depth, garnet morphologies change progressively from predominantly spheroidal to predominantly ellipsoidal, with the intermediate and long axes of the ellipsoidal garnets lying within the S_2 plane.

The second generation of garnets (Phase 2) includes anhedral and frequently oblate porphyroblasts (Figure 3f). They range in size from 1 - 10 mm in length. Their long axes lie within S_2. They include quartz, biotite and sillimanite that define an internal foliation in most samples that is parallel to the matrix S_2 schistosity, indicating that Phase 2 garnets grew syn- or post- kinematically with respect to D_2. The quantity of inclusions found in these garnets is much less than that found in Phase 1 garnet.

Frequently, garnets encountered in the Krummedal Sequence are composite Phase1-2 porphyroblasts. These grains have well-defined inclusion rich, Phase 1 cores

surrounded by inclusion-poor Phase 2 rims. Based on our observations, Phase 1 and Phase 1-2 garnets are substantially more common than monogenetic Phase 2 garnets. All the garnets contain late-stage brittle fractures that were filled with hypidioblastic biotite and muscovite.

Sillimanite (<0.1-10%)

Sillimanite was found at all structural horizons. Euhedral, prismatic grains up to 1 mm in length form in parallel clusters and help define the L_2 lineation. Fibrolitic mats of sillimanite, intergrown with biotite ± muscovite, occur in garnet pressure shadows. Small prismatic sillimanite crystals, less than 0.1 mm in length, are found included in syn-D_2 garnet and help define an intracrystalline S_2 fabrics.

Muscovite (0-5%)

Unlike biotite, muscovite is not ubiquitous. Primary subhedral laths of muscovite help define the S_2 schistosity at structural levels less than ~6.5 km beneath the Tindern detachment. These crystals are typically less than 0.25 mm in length, and represent 1-5% of the modal abundance of the pelitic schists in which they occur. Secondary, retrograde muscovite is variably present throughout the entire Krummedal Sequence. These moderately deformed, neoblastic crystals range in size from 1-5 mm.

Kyanite (<1-3%)

Anhedral grains of kyanite, less than 0.25 mm in size, are found included in pre- to syn-D_1 garnet at structural levels below the kyanite isograd. Also at these structural horizons are subhedral relict blades of kyanite in the matrix that lie oriented parallel to

the S_2 cleavage. These blades are seen being replaced by epitaxial overgrowths of fibrolitic sillimanite and decussate biotite (Figure 3e). Kyanite grains are typically deformed and may contain subhedral biotite and quartz. Their edges are often embayed with intrusions of syn-D_2 biotite.

Cordierite (0-<1%)

Subhedral grains of cordierite up to 0.5 mm in size were found near the Tindern detachment. In the vicinity of the cordierite isograd, there is sub-idioblastic, undeformed cordierite that grew post-kinematically with respect to D_2 fabrics. Closer to and within the zone of maximum shear, cordierite (bearing evidence for alteration to pinite), K-feldspar and myrmekite of plagioclase and quartz are seen to replace garnet. In particular, sample 97GR17, an enclave of Krummedal Sequence gneiss in the highly deformed (D_3) region of the Caledonia Ø granite pluton, contains remnants of garnets that have been almost completely replaced in this manner (Figure 3c). Their euhedral crystal shapes are outlined by the distribution of muscovite, biotite and sillimanite crystals which rim cordierite-feldspar-quartz simplectites that surround the garnet remnants. F_3 kink-folding of the S_2 biotite-sillimanite fabrics around the pseudomorph simplectite after garnet indicate that D_3 began prior to the initial growth of the cordierite; subcrystal domains and fractures filled with cordierite in the feldspar component of the simplectite suggest that D_3 deformation continued during synkinematic cordierite growth.

Chlorite (0-<1%)

Chlorite occurs as a secondary phase in a few of the samples. The most prominent occurrence is in the zone of deformation associated with the Høgedal detachment at the base of the Krummedal Sequence. These crystals are moderately deformed.

Accessory phases

Accessory phases include apatite, zircon, monazite, xenotime, rutile and ilmenite. Monazite, which is important for the geochronology discussed later, is found both along the edges of mica in the matrix and included in both Phase 1 and Phase 2 garnets.

Sample Selection

Samples were collected from a variety of structural horizons that span the Krummedal Sequence from the base of the Høgedal allochthon to the zone of shear associated with the Tindern detachment (Figure 2). For the most part, we sampled the biotite-garnet metapelitic gneisses and schists that typically comprise the Krummedal Sequence. Although these rocks contain abundant anatectic leucosomes, we restricted our sampling to the mesosomic material. There were two exceptions within our suite of samples: 97GR14 represents the pelitic enclave in a syn-D_2 leucosome that was dated by White et al. (in press); 97GR17 represents a highly deformed, xenolith of Krummedal Sequence gneiss entrained in the syn-D_3 Caledonia Ø granite also dated by White et al. (in press).

Major Element Zoning of Garnets

In order to examine the chemical variability within different phases of garnet, we made backscattered electron (BSE) and X-ray compositional (XRC) maps (e.g. Figure 4) of the major elements (Ca, Mg, Mn) in 1 or 2 garnets from each structural horizon represented in our suite of samples (see appendix for analytical methods).

Phase 1 garnets are characteristically zoned in Ca from highest concentrations in the core to lowest concentrations in the rim (Figure 4b). Although zonation in Mg is not as dramatic, the images show that Mg is inversely zoned with respect to Ca such that the lowest concentrations are in the garnet core. Mn is essentially uniform across these garnets, with a sharp enrichment near the outer rim which supports petrographic evidence for partial resorbtion.

Composite Phase 1-2 garnets yield spectacular XRC maps. For example, two phases of garnet may be distinguished in Figure 4a: a syn-D_1 Phase 1 garnet core that was flattened during D_2 deformation, and a neoblastic Phase 2 garnet rim. Figure 4c depicts a Phase 1 garnet core (note the high density of inclusions) and a well-defined Phase 2 garnet rim; while there is a slight increase in the grossular mole-fraction from core to rim, there is no distinguishable difference in the other major element concentrations despite textural evidence for two generations of garnet growth. Figure 4d depicts a Phase 2 garnet from 97GR47. The XRC maps of this garnet indicate that Ca increases from core to rim while Mg decreases. This pattern is the reverse of the typical zonation found in Phase 1 garnet and provides strong chemical evidence for a second generation of garnet growth.

In addition to major element zoning in garnet, our XRC maps show compositional differences between inclusions in the garnet and their matrix counterparts. For example, biotite included in the garnet display significantly higher concentrations of Mg than biotite in the matrix. Plagioclase included in the garnet display significantly higher concentrations of Ca than plagioclase in the matrix. XRC maps reveal major element zoning within individual biotite and plagioclase grains as well. While matrix plagioclase

crystals are sometimes depleted from core to rim in Ca, we did not observe such a simple zonation of Mg in matrix biotite.

Metamorphic Sequence in the Forsblad Fjord Area

Altogether, our petrographic observations indicate that there were four phases of metamorphism that affected the Krummedal Sequence in Forsblad Fjord which can be placed into a relative chronologic order based on the relationship between the growth of metamorphic mineral assemblages and the development of deformational fabrics.

M_1 corresponds to the earliest growth of Phase 1 garnet along with quartz + plagioclase + biotite ± kyanite/sillimanite ± muscovite. Fabric relationships indicate that these garnets grew pre- to syn-kinematically with respect to D_1 deformation.

M_2 included the growth of Phase 2 garnet and equilibration of most matrix phases with Phase 1 and 2 garnet rims. The pre- to synkinematic relationship between Phase 2 garnet growth and D_2 fabrics indicates that M_2 ranged over a time period that extended from post-D_1 to syn-D_2. Textural evidence from leucosomes such as 97GR14 indicate that the Krummedal Sequence underwent partial melting during M_2 as well .

M_3 corresponds to the growth of cordierite near the Tindern detachment with coexisting plagioclase + quartz + K-feldspar + biotite + sillimanite (e.g. sample 97GR17). The textural relationship between D_3 fabrics and the cordierite/feldspar/quartz simplectite that replaced the garnet in that sample indicate that M_3 occurred synkinematically with respect to D_3 activity along the Tindern detachment.

M_4: the latest stages of metamorphism are represented by the retrograde growth of neoblastic muscovite and chlorite that overprint all fabrics associated with D_1-D_3. The

fact that these retrograde mica are moderately deformed indicates that M_4 metamorphism was pre- to syn-kinematic with respect to D_4 deformation.

While the relative age relationships between M_1 - M_4 are self-evident, the absolute timing of metamorphism is not completely bracketed by its relationship to the deformational events as discussed above. However, we know that retrograde muscovite (M_4) could not have grown more recently than the ca. 411 Ma cooling age indicated by $^{40}Ar/^{39}Ar$ data from muscovite along the Forsblad Fjord transect (White & Hodges, in preparation-a). Furthermore, the available geochronology indicates that M_3 must have been ongoing between ca. 425-423 Ma, and that M_2 occurred ca. 425 Ma. However, there is no published geochronology that constrains the absolute timing of D_1. Previous investigators, working at slightly different latitudes, have argued that the dominant deformation and metamorphism in migmatitic metasedimentary gneisses that correlate with the Krummedal Sequence in Forsblad Fjord, was significantly pre-Caledonian or "Grenvillian" in age (e.g. Higgins & Leslie, 2000; Kalsbeek *et al.*, 1998; Thrane *et al.*, 1999; Watt & Thrane, 1999). This seems inconsistent with the ages of M_2-M_4. For this reason, we used the chemical dating technique outlined by Williams *et al.* (1999) to obtain a preliminary age for monazite inclusions in an M_1 garnet in order to place a maximum age constraint on M_1.

Chemical Dating of Monazite

We selected 97GR53 for this work primarily because this sample contained euhedral M_1 garnet with relatively abundant inclusions of monazite. Reconnaissance XRC mapping for Y, Th, Pb and U concentrations reveals distinct chemical zonation within the matrix monazite (Figure 5). To characterize this zonation, we note that

subhedral, single-phase cores display relatively high concentrations of Y and low concentrations of Th and U. These cores are mantled by a relatively low-Y phase that has high concentrations of Th and U. In circumstances where the monazite is euhedral, this mantle is overgrown by a single-phase, high Y component. In contrast, monazite found included in both the core and rim regions of Phase 1-2 garnet (Figure 5), appears to consist of either a homogeneous single-phase or a metamict, two-phase mixture.

Average monazite ages and uncertainties are presented in Table 2 along with the three population average ages. The first observation is that the oldest, monazite age was 439 ± 3 Ma and this was a monazite included in the core of a M_1 garnet; monazite ages ranged to as young as 398 ± 5 Ma in the matrix. The average population age for armored monazite in garnet cores was 414 ± 3 Ma, while monazite from garnet rims (409 ± 9 Ma) was the same age as monazite from the matrix (409 ± 2 Ma). Although monazite population ages are consistent with textural relationships, all the monazite population average ages are the same within uncertainty. However, it is important to note there is a discrepancy between these ages and previously published conventional U-Pb monazite ages from leucosomes and gneisses of the Krummedal Sequence in Forsblad Fjord (e.g. Hartz, 1998; White *et al.*, in press) of ~10-15 My. The electron microprobe data are internally consistent, however, which leads us to believe that there may be a minor systematic error in our calibration that is responsible for the difference between the two datasets. At the present, we do not have a conventional U-Pb monazite age from this sample to test this hypothesis. However, the microprobe data leave no doubt that all phases of garnet growth in these rocks occurred during Caledonian orogenesis.

These results conflict with the notion that D_1 deformation and M_1 metamorphism was "Grenvillian" in age. The original arguments on which that notion was built were

based on U-Pb zircon SHRIMP analyses that indicate there was thermal activity ~1 Ga that resulted in the growth of zircon rims on even older zircon cores (e.g. Higgins & Leslie, 2000; Kalsbeek *et al.*, 1998; Thrane *et al.*, 1999; Watt & Thrane, 1999). We suggest that those arguments are highly susceptible to issues of inheritance and do not constrain the metamorphism and deformation as effectively as the *in situ* electron microprobe data presented here.

Estimates of Metamorphic Conditions from the Petrogenetic Grid

Having established that the metamorphic sequence, M_1 - M_4, is entirely Caledonian, our goal is to use the mineral assemblages preserved from each phase of metamorphism to reconstruct a "qualitative" P-T path with pressure-temperature constraints derived from the petrogenetic grid. The ubiquitous presence of M_1 almandine sets a lower constraint on the temperature of early prograde metamorphism at ~500° C (Spear, 1993). The inclusion of kyanite in M_1 garnet from 97GR66 implies that this garnet grew in the kyanite stability field and thus sets a lower constraint on the pressure conditions of metamorphism (at ~7 km beneath the Tindern detachment) of ~4 kb (marked by a boxed **1** in Figure 6). Given that M_1 garnet above this structural horizon includes sillimanite and no kyanite, we suspect that pressure-temperature conditions during M_1 metamorphism did not reach the kyanite stability field for the shallowest rocks.

The dominant metamorphic mineral assemblage of the matrix grew during M_2. The presence of concordant anatectic M_2 leucosomes indicate that the Krummedal Sequence underwent partial melting as well. The fact that these pelitic rocks are devoid of prograde M_2 muscovite at depths greater than ~7 km beneath the Tindern detachment

suggests that melting may have occurred according to the reaction (labeled **b** in Figure 6; Spear, 1993; Thompson, 1982; Thompson & Tracy, 1979):

$$Ms + Pl + Qtz \rightarrow Kfs + Ky/Sil + melt \qquad (1)$$

(mineral abbreviations are after Kretz, 1983). The observation that an anatexite collected ~10 km beneath the Tindern detachment (beneath the kyanite isograd), preserves an enclave of pelitic schist that contains M_2 sillimanite, M_1 garnet and no M_1 kyanite (97GR14), leads us to suggest that melting at this particular structural horizon transpired in the sillimanite stability field. The relative order of these events indicates that the maximum temperature and pressure conditions for the path along which this structural horizon passed from the kyanite stability field into the sillimanite stability field are constrained by the intersection between the kyanite-sillimanite curve and the muscovite dehydration reaction curve at ~725° C and ~8 to 8.5 kb.

The overall maximum temperatures reached during M_2 are constrained by the fact that M_2 biotite is ubiquitous at all structural levels indicating that it was stable throughout this phase of metamorphism. This observation implies that temperatures did not rise enough to drive the biotite dehydration reaction (labeled **c** in Figure 6; Clemens & Wall, 1981; Spear, 1993; Vielzeuf & Holloway, 1988):

$$Bt + Ky/Sil + Pl + Qtz \rightarrow Grt + Kfs + melt \quad (2)$$

to completion. Therefore, at structural depths comparable to the location of 97GR14 where the stable aluminum silicate pseudomorph during M_2 was sillimanite, peak pressures and temperatures could not have greatly exceeded the intersection between reaction (2) and the kyanite-sillimanite phase transition at ~9 kb and ~765°C. We suggest that extrapolation of this constraint to the bottom of the Krummedal Sequence (~14 km

beneath the Tindern detachment assuming a lithostatic gradient of 250 b/km) constrains approximate peak pressure and temperature conditions at ~10 kb and ~770° C.

The pressure-temperature path during M_3 is difficult to constrain. A xenolith of Krummedal Sequence gneiss (97GR17) trapped within the Caledonia Ø granite footwall of the Tindern detachment contains garnets that were almost completely consumed by the growth of M_3 biotite, sillimanite and myrmekite of plagioclase and quartz. This suggests that decreasing pressure and/or temperature conditions drove the following reaction:

$$\text{Grt} + \text{Kfs} + \text{melt} \rightarrow \text{Bt} + \text{Sil} + \text{Pl} + \text{Qtz} \quad (3)$$

Anhedral K-feldspar rimmed by plagioclase, quartz and biotite provide additional evidence to support reaction (3). Furthermore, the fact that cordierite is part of this replacement assemblage suggests that decreasing pressure drove the reaction:

$$\text{Bt} + \text{Sil} \rightarrow \text{Grt} + \text{Crd} \quad (4)$$

The coexistence of sillimanite and cordierite places a minimum temperature constraint at ~650°C, and the fact that biotite appears to be a stable component of the M_3 mineral assemblage provides a narrow range of maximum temperature constraints along the biotite dehydration reaction curve (2). Thus the intersection between that curve and reaction (4) places a maximum pressure and temperature constraint on samples with the M_3 cordierite-sillimanite subassemblage (found as deep as 4.5 km beneath the Tindern detachment — e.g. 97GR73) of ~4 kb and ~750° C (marked by a boxed **3** in Figure 6). A simple extrapolation of the maximum pressure during M_2 metamorphism of 97GR14 to the structural horizon of 97GR73 (~7.5-8 kb), implies that pressure conditions decreased significantly prior to crystallization of M_3 mineral assemblages.

Following M_3, cooling was most likely responsible for the growth of neoblastic M_4 muscovite observed throughout the section as decreasing temperature conditions triggered the reaction:

$$Kfs + Sil + Melt \rightarrow Ms + Pl + Qtz \quad (5)$$

Further cooling probably led to retrograde growth of M_4 chlorite as the pelites passed into the chlorite stability field.

Estimating M_2 Conditions by Near-Rim Thermobarometry

To further resolve and constrain the pressure-temperature history preserved in rocks from the Høgedal allochthon, we exploit the common assemblage Grt + Bt + Pl + Qtz + Ky/Sil using a pair of well calibrated thermobarometers. The Fe-Mg exchange between garnet and biotite (GARB thermometer; Ferry & Spear, 1978) and the garnet-plagioclase-aluminum silicate-quartz net transfer reaction (GASP barometer; Ghent, 1976) enable us to estimate P-T conditions of presumed chemical equilibrium between mineral rims in direct contact. Because of the high probability of some resorbtion around garnet rims, we analyzed near-rim loci just inside the zone of Mn enrichment seen on the XRC maps.

GARB-GASP Thermobarometry

Data presented in this paper are based on the thermobarometric calibrations of Hodges and McKenna (1987) for GARB and McKenna and Hodges (1988) for GASP. Non-ideal solution behavior was modeled using the approaches of Berman (1990) for garnet, Patiño Douce *et al.* (1993) for biotite, and Elkins and Grove (1990) for plagioclase. Aluminum silicate and quartz were treated as pure phases.

Samples were chosen to maximize the breadth of structural coverage across the Høgedal Allochthon. In addition, samples had to satisfy the following criteria: 1) apparent textural equilibrium between mineral assemblages used for thermobarometric calculations; and 2) a lack of evidence for secondary, low-temperature retrograde metamorphism. The mineral assemblages preserved in the samples (as described earlier) that we analyzed are listed in Table 3. In addition to the above criteria, we used Mg, Ca and Mn x-ray, elemental abundance maps to examine chemical zonation patterns in our samples and determine which regions of the sample were most likely in chemical equilibrium (e.g. Figure 4).

Uncertainties in the oxide measurements were propagated following the approach outlined by Hodges and McKenna (1987) and Hodges *et al.* (1993). With a few exceptions (Table 4) cited oxide abundances typically reflect averages of 3-6 spot measurements for each domain. In cases where the number of analyses was to low to justify calculating uncertainties as standard deviations from the mean, we assumed a conservative 2% 1σ uncertainty.

While many researchers attempt to use thermobarometry to estimate peak metamorphic pressures and temperatures, we note that the variable kinetics of the metamorphic reactions involved make this task very difficult to accomplish. For example, two garnets from the same horizon may preserve information from different segments of the pressure-temperature path encountered by that horizon and may not even record the peak pressure and temperature encountered by the sample. Furthermore, the kinetics of the GARB thermometer and GASP barometer may vary independently at different temperatures. Thus significant disparity between the timing of temperatures and pressures recorded by these reactions can arise during slow cooling. However, we note that

available thermochronologic data from these rocks indicate that they cooled relatively rapidly, especially in the footwall of the Tindern detachment (White & Hodges, in preparation), limiting kinetic effects on calculated pressures and temperatures.

Results

We present results from 8 structural horizons that span the Krummedal Sequence (Figure 7). Oxide data and 1σ uncertainties for mineral rim analyses are presented in Table 4. P-T results with nominal calculated 2σ uncertainties are presented in Table 5. Sample 97GR57 contained no aluminum silicate, precluding the use of GASP; however, we have plotted the GARB reaction curve and included a hypothetical GASP curve assuming the presence of kyanite for comparative purposes.

The first observation from the complete dataset is that rim equilibration of the thermobarometric assemblages along the Forsblad Fjord transect was not isochronous. This is demonstrated by a simple plot of pressure versus structural depth beneath the Tindern detachment (Figure 8) on which the data define a non-linear array. The data are also non-linear in temperature-depth space. On the other hand, there is a slight tendency towards higher pressures at deeper structural horizons, which is consistent with the expectation that pressures increased with depth.

In addition, rim thermobarometry for all samples indicate that P-T conditions exceeded the water-saturated minimum melt curve for pelitic compositions (curve **a** in Figures 6, 7, 9; Thompson, 1982) within analytical uncertainty throughout the Høgedal allochthon. For the majority of samples, the P-T conditions exceeded the muscovite dehydration reaction curve. Samples 97GR70, 97GR04a and 97GR47 record P-T conditions of chemical equilibrium that exceed the biotite dehydration reaction curve;

however, we note that these results overlap the biotite dehydration reaction curve within analytical uncertainty.

A third important observation is that garnet rim equilibration pressures and temperatures plot in the sillimanite stability field for samples from the shallowest structural horizons, and the kyanite stability field for deeper samples (within analytical uncertainty). Because the deeper samples contain matrix sillimanite, it appears that chemical equilibrium between mineral rims was last achieved prior to the late-stage growth of M_2 sillimanite. One analysis from sample 97GR47 is an exception, plotting entirely within the sillimanite stability field despite its deep structural position. The most probable explanation for this consistent with textural evidence is that the garnet used in this analysis grew synkinematically with respect to D_2 while sillimanite was the stable Al_2SiO_5 polymorph.

The shallowest sample with mineral assemblages suitable for rim thermobarometry was 97GR73, located ~4.5 km structurally beneath the Tindern detachment. GARB and GASP results from two sets of analyses suggest that rim equilibration occurred at 7.0 ± 1.1 kb at 687 ± 80° C and 8.4 ± 0.7 kb at 756 ± 37° C. The high pressure of these statistically indistinguishable results implies that the GARB and GASP thermobarometric subassemblages in 97GR73 equilibrated for the final time prior to the growth of M_3 cordierite, a hypothesis supported by the textural observations.

Results from the next three deeper structural horizons (97GR02, 97GR66 and 97GR53) suggest that the pressures of rim equilibration for the P-T assemblages were lower than those recorded in 97GR73. Given that pressure is expected to increase with structural depth, a likely explanation is that the rim equilibration in 97GR73 post-dated

that of the P-T assemblages in the other samples. Thus, the combination of data from these 4 samples imply that ambient pressures were increasing over time during M_2.

The thermobarometric data for 97GR47 are particularly interesting because they pertain to two different generations of garnet, one that grew prekinematically with respect to D_2, and one that grew synkinematically with respect to D_2 The Phase 1 garnet and its thermobarometric assemblage yielded a pressure of 11.8 ± 1.2 kb at 851 ± 66° C. Although these conditions are nominally inconsistent with P-T estimates based on the petrogenetic grid (discussed earlier), the uncertainty ellipse for this domain is large and overlaps the appropriate stability fields. Combining the two methods, we estimate P and T during final equilibration of the Phase 1 garnet at about 10.5 kb and 785° C. The Phase 2 garnet domain yielded a contrasting GARB-GASP P-T estimate of 8.1 ± 0.5 kb at 746 ± 31° C. Together, this data suggest a net decrease in pressure of about 2.5 kb and no significant change in temperature of the pre-to syn-D_2 interval (Figure 9a).

Estimating Earlier (M_1) Conditions by Inclusion Thermobarometry

In addition to our near-rim thermobarometry, we used the presence of inclusions in garnet to calculate the P-T conditions of chemical equilibrium preserved at the point of contact between these inclusions and their garnet hosts as described and demonstrated by St-Onge (1987). This technique enables us to explore the pressure-temperature conditions during M_1 garnet growth assuming that there was chemical equilibrium between all the inclusions necessary for GARB and GASP thermobarometry, and the adjacent region of their garnet hosts. All samples on which we performed inclusion thermobarometry contained garnet with inclusions of biotite, plagioclase and quartz. In the event that the aluminum silicate pseudomorph was not included, we only performed the analysis if

aluminum silicate was in the matrix assemblage; and then we assumed that an aluminum silicate polymorph was present throughout the entire phase of garnet growth. The GARB-GASP calibrations, analytical procedure and error propagation are the same as described above.

Oxide data and 1σ uncertainties for mineral analyses are presented in Table 6. P-T results with calculated 2σ uncertainties are presented in Table 7. For each sample, the results indicate lower pressures and temperatures than the near-rim results for the sample, suggesting a prograde P-T path. In addition, the inclusion data indicate that chemical equilibrium during M_1 garnet growth was reached almost entirely at P-T conditions below the water-saturated minimum melt curve for pelitic compositions. Only data from 97GR70 (the deepest sample on which we performed inclusion thermobarometry) are exceptional. However, we note that these results fall short of the muscovite dehydration reaction curve.

Despite the paucity of data, there is a tendency for the pressures indicated by the inclusion assemblages to increase with increasing structural depth of the samples. However, it is clear that equilibration was not isochronous (Figure 8b). Inclusion thermobarometry from 97GR73 (~4.5 km beneath the Tindern detachment) yields a pressure of 4.1 ± 0.5 kb while inclusion barometry from 97GR70 (~8.5 km beneath the Tindern detachment) yields a pressure of 8.5 ± 0.7 kb. Taking into account the difference in structural position between the two samples, there still remains an unexplained discrepancy of ~3.5 kb. We interpret this number as a minimum estimate for the pressure increase during M_1 metamorphism.

The differences between inclusion and rim equilibration conditions for these samples gives some indication of how pressure and temperature changed over the M_1-M_2

interval (Figures 9b-9e). The greatest variation is recorded by 97GR73, which contained an inclusion suite indicative of equilibration at 250° C lower temperature and 4 kb lower pressure than the garnet rim (Figure 9b). Thus, subtracting the ~3.5 kb of compression recorded during M_1 from the minimum estimate for pressure change during M_1-M_2 (4 kb), implies that pressures continued to increase a minimum of ~0.5 kb during M_2.

Pressure-Temperature-Time Reconstructions in Tectonic Context

By combining the total geochronologic and metamorphic results presented earlier with previously reported structural, and U-Pb and $^{40}Ar/^{39}Ar$ geochronologic data (White *et al.*, in press; White & Hodges, in preparation-a), we can derive the following PTt history for the Forsblad Fjord area. A representative PTt path based on this reconstruction is depicted in Figure 10 for a structural horizon equivalent to sample 97GR73, ~4.5 km beneath the Tindern detachment.

The earliest stage of metamorphism observed in the Krummedal Sequence, M_1, occurred pre- to syn-kinematically with respect to D_1. Pressure-temperature conditions of rocks at the deepest structural levels were in the garnet-kyanite stability field (minimum of 4 kb and 500° C at depths 7 km beneath the Tindern detachment) whereas the shallowest structural levels were in the garnet-sillimanite stability field. Our thermobarometry indicates that this was probably the period over which pressure increased the most (minimum estimate ~3.5 kb). Meanwhile, our geochronology indicates that the age of this metamorphism was Caledonian. Therefore, we interpret M_1 as occurring during a period of crustal thickening related to the Baltica-Laurentia collision.

As deformation continued, D_1 fabrics gave way to orogen-parallel shear and E-W contraction (D_2), coincident with the second phase of metamorphism (M_2). Our data suggest that M_2 involved significant temperature increases, but only limited (~0.5 kb) pressure increases. This is evidenced by the thermobarometry discussed above, and the replacement of M_1 kyanite by M_2 sillimanite as well as the production of melt as P-T conditions exceeded the muscovite dehydration reaction curve. Maximum temperatures are constrained by the fact that samples did not reach M_2 temperatures in excess of that of the biotite dehydration reaction curve at 10-10.5 kb, the maximum M_2 pressure recorded by a sample 14 km below the Tindern detachment, or 770-785° C, consistent with normal geotherms. U-Pb geochronologic constraints indicate that the syn-M_2 crystallization of this melt was occurring ca. 425 Ma (White *et al.*, in press). Therefore, we interpret M_2 as having occurred during a period of crustal thickening accompanied by significant orogen-parallel shear and thermal re-equilibration upon burial.

Sometime thereafter — and synkinematic with respect to D_2 — pressures and temperatures peaked and near-isothermal decompression of at least ~2.5 kb heralded the onset of M_3. This is indicated by the rim-thermobarometry of 97GR47. Meanwhile D_3 extension along the Tindern detachment began ca. 425 Ma to 424.5 Ma (White *et al.*, in press). Reaction textures and equilibrium constraints from reactions on the petrogenetic grid indicate that enclaves of the footwall (e.g. 97GR17), entrained in the zone of maximum D_3 shear also underwent considerable decompression allowing both sillimanite and cordierite to coexist. Thus we infer that the syn-D_2 and D_3 decompression events and emplacement of the Caledonia Ø granite were related to unroofing along the Tindern detachment and that relatively little heat was lost during this activity as evidenced by the anomalously high-temperature, low-pressure M_3 metamorphism that accompanied this deformation. These observations are further supported by previous U-Pb geochronology

that indicates a syn-D_2 leucosome and the syn-D_3 Caledonia Ø granite crystallized at the same time within analytical uncertainty (White *et al.*, in press).

Field observations indicate that the majority of deformation along the Tindern detachment was at high-temperature (White *et al.*, in press). This is important to note because $^{40}Ar/^{39}Ar$ muscovite and biotite ages can thus be used to constrain most of the displacement to have occurred over a very short time-period of ca. 2 My (White & Hodges, in preparation). Thus, the appearance of moderately deformed retrograde M_4 muscovite in the Krummedal sequence, dated by $^{40}Ar/^{39}Ar$ to no younger than ca. 411 Ma (White & Hodges, in preparation), indicates that these gneisses cooled at a slower rate for the next 12 My after decompression while continuing to experience moderate deformation most likely related to continued movement along an underlying, unexposed D_4 thrust fault. Cooling during M_4 metamorphism is further characterized by the retrograde growth of chlorite.

Implications

The constraints in PTt space discussed above can be used to make rough estimations of vertical movement of specific structural horizons within the crust during various stages of the Caledonian orogeny. Considering the lack of published data that constrain the amount of crustal thickening and thinning in the East Greenland Caledonides, these first-order estimations yield valuable insights into the tectonic evolution of the region.

Crustal Position of the Høgedal Allochthon During the early stages of M_1

First, we note that the shallowest structural horizon for which we have P-T data lies ~4.5 km beneath the Tindern detachment and yields an M_1 P-T estimate from inclusion thermobarometry of 4.5 ± 0.5 kb. Assuming a simple lithostatic gradient of 250 bar/kilometer, this implies a structural depth of ~18 kilometers, comparable to the potential overburden provided by the overlying Krummedal Sequence (~4.5 km) and the Eleonore Bay Supergroup (~14 km; Smith & Robertson, 1999; Sønderholm & Tirsgaard, 1993)

Crustal Position of the Høgedal Allochthon During M_2 Final Equilibration

We can estimate the minimum amount of burial during M_1 and M_2 garnet growth, based on the sample (97GR73) with the largest net increase in pressure from inclusion to rim thermobarometry (~4 kb), to be an additional ~16 km. This implies that rocks near the base of the sequence (~8km structurally deeper than 97GR73) were buried to depths of at least ~40 km, implying maximum M_2 pressures of ~10 kb. This is remarkably close to the peak pressure constrained by the petrogenetic grid and rim-thermobarometry for 97GR47 (~10.5 kb), which was collected near the base of the section.

Limits on the Thermal Significance and Tectonostratigraphic Throw on the Fjord Region Detachment System

As mentioned above, normal-sense movement along the Tindern detachment is the most likely mechanism for near-isothermal decompression over the M_2-M_3 transition (e.g. Hodges *et al.*, 1993; Ruppel *et al.*, 1988). Thus, we can perform simple calculations based on the amount of decompression to estimate tectonostratigraphic throw on the

Fjord Region Detachment System. The thermobarometric data from 97GR47 imply that there was a minimum of ~2.5 kb of near-isothermal decompression during M_3. The fact that cordierite appears in textural equilibrium with sillimanite in 97GR17 is consistent with this conclusion and implies that the maximum pressure of cordierite-sillimanite co-existence in the Tindern detachment's immediate footwall at the highest temperatures recorded in the entire Krummedal Sequence (~790° C) was ~5 kb. Since temperatures probably didn't greatly exceed 750° C (maximum temperature recorded in the thermobarometry from the uppermost structural horizon analyzed — 97GR73), 4 kb is a more realistic estimation for the maximum pressure at which cordierite and sillimanite could have coexisted. Given that the previously discussed burial estimations imply that a structural horizon comparable to that of 97GR17 (4.5 km structurally above 97GR73) would have reached depths of ~28 km or pressures of ~7 kb, we argue from the combination of constraints that 97GR17 underwent decompression of at least ~3 kb. Sample 97GR73 records the greatest total decompression of all the samples: 4.5 kb.

If we assume that all of this decompression was related to tectonic denudation by movement on the Tindern detachment, then we can estimate the approximate tectonostratigraphic throw on that structure of nearly 18 kilometers. Assuming a constant rate of exhumation, this estimate implies an unroofing rate of 9 mm/yr. In reality, this is a maximum estimate because at least some of the denudation must be attributable to shallower structures which may have been active more recently than the Tindern detachment.

Regional Stratigraphic Correlations

The clockwise pressure-temperature-time path that we present here is consistent with the pressure-temperature conditions of chemical equilibrium preserved in rocks of the Krummedal Sequence north of the study area (Elvevold & Gilotti, 1998; Vold, 1997). Investigations that focused on the footwall of the FRD in Keiser Franz Joseph's Fjord (~72.75° N) estimated peak metamorphic conditions at ~10-12 kb and 700-850° C, followed by decompression and metamorphism at ~3.5 kb and 650°C (Vold 1997). This PT path was interpreted by Vold (1997) as related to exhumation along the FRD. Elvevold & Gilotti (1998), who worked nearby this area (73-74° N), reported that there was no single detachment but rather a series of splays. The $^{40}Ar/^{39}Ar$ data presented by White & Hodges (in preparation-a) that indicated the Høgedal detachment reactivated the Tindern detachment is consistent with the observations of multiple fault splays by Elvevold & Gilotti (1998). Thus, while it is unclear whether Vold (1997) performed his research in the footwall or the hanging wall of the Høgedal detachment, it is clear that his study area was in the footwall of the Tindern detachment. The fact that he reported slightly higher pressures and temperatures than presented in this paper may indicate that his data reflect additional tectonic denudation due to activity along the Høgedal detachment.

Therefore, if we assume that the metamorphic investigations of Vold (1997) were performed in the footwall of both the Tindern and the Høgedal detachments, we can roughly estimate tectonostratigraphic throw on the Høgedal detachment by subtracting the amount of decompression indicated by our thermobarometry data from his estimates of decompression (maximum of ~8.5 kb — discussed below). This yields an apparent estimate of ~4 kb of decompression in excess of the figure that we associate with the

Tindern detachment. This simplified calculation implies that there was ~16 kilometers of tectonostratigraphic throw on the Høgedal detachment. Furthermore, as already mentioned, arguments presented by White *et al.* (in press) indicate that an unexposed (post-M_3) thrust underlying the Krummedal Sequence gneisses must have been excised by the Høgedal detachment. This implies that most movement on the Høgedal detachment must be of M_4 age or later.

Our results are also consistent with the observations and data from metasedimentary rocks of the Smallefjord Sequence even further north (75°-76°N; Jones & Strachan, 2000). Furthermore, there are remarkable similarities between the Smallefjord Sequence and the Krummedal Sequence of Forsblad Fjord in terms of lithology, texture, metamorphism and migmatization. For example, Jones and Strachan (2000) reported that the dominant metamorphic mineral assemblage of the Smallefjord Sequence is Grt + Kfs + Ky/Sil + Bt + Pl + Rt + Qtz. Those authors also recorded two phases of garnet growth — an earlier generation that includes kyanite and a later generation that includes sillimanite. Pervasive migmatization is described as having formed discontinuous, concordant layers and augen of granitic neosome prior to extensional deformation that is crosscut by migmatization discordant to the regional foliation interpreted to be syn-extensional (Friderichsen *et al.*, 1994; Jones & Strachan, 2000). These are relationships that mirror the migmatization in the Krummedal Sequence of Forsblad Fjord. Furthermore, the Smallefjord Sequence lies in the same structural position as the Krummedal Sequence, juxtaposed by normal faults between Archean-Paleozoic basement rocks and the Eleonore Bay Supergroup. Most importantly, the Smallefjord sequence records a clockwise P-T path with peak metamorphic conditions of ~9-10 kb at 790-850° C followed by exhumation (Jones & Strachan, 2000). With such strong similarities, we think it is likely that the Smallefjord Sequence correlates with the

Krummedal Sequence in Forsblad Fjord. We infer from the continuity of structural position, metamorphism, migmatization and thermobarometry of the metasedimentary rocks that crop out beneath the Fjord Region Detachment for the length of the central East Greenland Caledonides that our interpretation of the events which affected the Krummedal Sequence of Forsblad Fjord are of general applicability to the central East Greenland Caledonides.

Conclusions

Given the recent explosion of structural and geochronologic evidence that demonstrate the East Greenland Caledonides preserve a significant component of extensional deformation, there has been a growing need for quantitative pressure-temperature estimates. In this paper, we integrate our new P-T and geochronologic data with our previous structural and geochronologic investigations from the Forsblad Fjord region along a transect of the orogen at 72.5° N. We address several important questions that have been outstanding: how much thickening, how much exhumation, how fast, and when?

Using an electron microprobe to perform reconnaissance, *in situ*, U-Pb dating of monazite included in pre-D_1 garnet, our new data indicate that the oldest metamorphism and deformation of the Krummedal Sequence was Caledonian in age. Given that it has been argued from U-Pb zircon SHRIMP ages that this early metamorphism and deformation occurred ~1 Ga, we suggest that such arguments are plagued with issues of inheritance and that our data provide a more robust constraint on these events, even though inconsistencies among conventional U-Pb and chemical Pb dates suggest that the latter slightly underestimate actual crystallization ages.

Estimates of equilibrium pressures and temperatures made semi-quantitatively by comparison with petrogenetic grids are consistent with those made quantitatively with GARB-GASP thermobarometry. The data indicate a clock-wise loop in P-T space, which is to be expected for orogens that have undergone crustal thickening followed by tectonic denudation. Thermobarometric constraints indicate a minimum net increase in pressure and temperature of ~4 kb and 250°C (peak conditions of ~10.5 kb at 785° C) over the preserved portion of the PT path, followed by near-isothermal decompression of ~4.5 kb with minimal cooling. There is good agreement between our data from the Forsblad Fjord region (72° N) and previously published data from metasedimentary rocks immediately north of the study area (73°-74°N) and from the Smallefjord Sequence (75°-76°N). Additional comparison of the lithology, structural position, migmatization and metamorphism between the Smallefjord Sequence and the Krummedal Sequence suggests that the two are probably correlative. In any case, the continuity of the observations from metasedimentary rocks in the footwall of the Fjord Region Detachment system, leads us to infer that events recorded in the Krummedal Sequence of Forsblad Fjord are of orogen-scale significance.

Therefore, we propose the following tectonic model of the central East Greenland Caledonides. Early crustal thickening buried the Krummedal Sequence by at least 16 km to a minimum depth of ~28 km. Prograde metamorphism continued as orogen-parallel shear accompanied by E-W transpression formed the prominent N-S trending lineations and folds that are preserved today. Peak pressures and temperatures were disturbed ca. 425 Ma with the initiation of syn-orogenic activity along the Tindern detachment splay of the Fjord Region Detachment system. Displacement along this and structurally higher extensional faults was responsible for ~18 km of vertical exhumation. Given that the Tindern detachment was active over a 2 million year period, this implies that the time-

averaged unroofing rate due to detachment slip may have been as high as ~9 millimeters per year; however, some of the tectonic denudation may have occurred at a later time, accomplished by slip on extensional structures that lie in the hanging wall of the Tindern detachment.

Acknowledgements

This research was part of a collaborative effort between the Department of Earth, Atmospheric and Planetary Sciences at MIT and the University of Oslo in Norway. Funding for this study was provided by National Science Foundation grant EAR 930072 (to K.V. H.). We wish to thank the Greenland Geological Survey, Danish Polar Center, Sirius Patrol, A. Andresen, E. Hartz, N. Henriksen, J. Hurtado, and L. Schoenbohm for logistical assistance. We especially wish to thank N. Chatterjee for his generous assistance and patience with regards to our use of the electron microprobe facility at MIT, and M. Jercinovic and M. Williams for their generous assistance and the use of their lab at UMass Amherst.

References:

Anderson, G. M., 1976. Error propagation by the Monte Carlo method in geochemical calculations. *Geochimica et Cosmochimica Acta*, **40**, 1533-1538.

Andresen, A., Hartz, E. H. & Vold, J., 1998. A late orogenic extensional origin for the infracrustal gneiss domes of the East Greenland Caledonides (72-74 N). *Tectonophysics*, **285**(3-4), 353-369.

Andresen, A. & Steltenpohl, M. G., 1994. A reevaluation of nappe sequences in the Ofoten-Troms region, north Norwegian Caledonides: Implications for terrane accretion, ophiolite obduction, and polyorogenic evolution. *Tectonophysics*, **231**, 59-70.

Backlund, H. G., 1930. Contributions to the geology of Northeast Greenland. *Meddelser om Grønland*, **74**(11), 207-296.

Berman, R. G., 1990. Mixing properties of Ca-Mg-Fe-Mn garnets. *American Mineralogist*, **75**, 328-344.

Caby, R., 1976. Tension structures related to gliding tectonics in the Caledonian superstructure of Canning Land and Wegener Halvø, central East Greenland. *Rapport Grønlands geologiske Undersøgelse*, **72**, 1-24.

Christoffersen, M., 1984. Scoresby Sund, Grønlands Geologiske Undersøgelse, Denmark.

Clemens, J. D. & Wall, V. J., 1981. Origin and crystallization of some peraluminous (S-type) granitic magmas. *Canadian Mineralogist*, **19**, 111-131.

Cocherie, A., Legendre, O., Peucat, J. J. & Kouamelan, A., 1998. Geochronology of polygenic monazites constrained by in situ electron microprobe Th-U-total-Pb determination: Implications for Pb behavior in monazite. *Geochemica et Cosmochimica Acta*, **62**, 2475-2497.

Elkins, L. T. & Grove, T. L., 1990. Ternary feldspar experiments and thermodynamic models. *American Mineralogist*, **75**, 544-559.

Elvevold, S., Escher, J. C., Frederiksen, K. S., Friderichsen, J. D., Gilotti, J. A., Henriksen, N., Higgins, A. K., Jepsen, H. F., Jones, K. A., Kalsbeek, F., Kinny, P. D., Leslie, A. G., Robertson, S., Smith, M. P., Thrane, K. & Watt, G. R., 2000. Tectonic architecture of teh East Greenland Caledonides 72° - 74°30' N. In: *Danmarks og Grønlands Gelogiske Undersøgelse Rapport*, pp. 34, Geological Survey of Denmark and Greenland, Denmark.

Elvevold, S. & Gilotti, J. A., 1998. Metamorphic and structural studies in the Caledonian fold belt of East Greenland (72°30'-73°N). In: *Caledonian geology of East Greenland 72°-74°N: preliminary reports from the 1997 expedition* (eds Higgins, A. K. & Frederiksen, K. S.), pp. 146, Danmarks og Grønlands Geologiske Undersøgelse Rapport, Denmark.

Escher, J. C. & Jones, K. A., 1999. Caledonian geology of Frænkel Land and adjacent areas (73°00'-73°30'N), East Greenland. In: *Geology of East Greenland 72°-75°, mainly Caledonian: preliminary reports from the 1998 expedition* (eds Higgins,

A. k. & Frederiksen, K. S.), Danmarks og Grønlands Geologiske Undersøgelse Rapport, Denmark.

Ferry, J. M. & Spear, F. S., 1978. Experimental calibration of the partitioning of Fe and Mg between biotite and garnet. *Contrib. Mineral. Petrol.*, **66**, 113-117.

Friderichsen, J. D., Strachan, R. A. & Henriksen, N., 1994. Basement-cover relationships and regional structure in the Grandjean Fjord-Bessel Fjord region 72°-76° N, North-East Greenland. *Rapport Grønlands geologiske Undersøgelse*, **162**, 17-33.

Gee, D. G., 1975. A tectonic model for the central part of the Scandinavian Caledonides. *American Journal of Science*, **275A**, 468-515.

Ghent, E. D., 1976. Plagioclase-garnet-Al2SiO5-quartz: a potential geobarometer-geothermometer. *Am. Min.*, **61**, 710-714.

Haller, J., 1970. Tectonic map of East Greenland (1:500,000). An account of tectonism, plutonism, and volcanism in East Greenland. *Meddelelser om Grønland*, **171**, 1-286.

Haller, J., 1971. *Geology of the East Greenland Caledonides*. Interscience Publishers, New York.

Hartz, E., 1998. Late Orogenic Evolution of the East Greenland and Scandinavian Caledonides. *Unpub. Dissertation for the degree Doctor Scientiarum Thesis, University of Oslo, Oslo.*

Hartz, E., 2001. Syncontractional extension and exhumation of deep crustal rocks in the east Greeland Caledonides. *Tectonics*, **20**(1), 58-77.

Hartz, E. & Andresen, A., 1995. Caledonian sole thrust of central East Greenland: A crustal-scale Devonian extensional detachment? *Geology*, **23**, 637-640.

Hartz, E. H., Andresen, A., Martin, M. W. & Hodges, K. V., 2000. U-Pb and (super 40) Ar/ (super 39) Ar constraints on the Fjord region detachment zone; a long-lived extensional fault in the central East Greenland Caledonides. *Journal of the Geological Society of London*, **157, Part 4**, 795-809.

Henriksen, N., 1985. The Caledonides of central East Greenland 70 degrees -76 degrees N. In: *The Caledonide Orogen — Scandinavia and Related Areas* (eds Gee, D. G. & Sturt, B. A.), pp. 1095-1113, John Wiley & Sons, Chichester, U.K.

Henriksen, N. & Higgins, A. K., 1976. East Greenland Caledonian fold belt. In: *Geology of Greenland* (eds Escher, A. & Watt, W. S.), pp. 183-246, The Geological Survey of Greenland, Copenhagen, DK.

Higgins, A. K., 1988. The Krummedal supracrustal sequence in East Greenland. In: *Winchester, J. A. Later Proterozoic stratigraphy of the northern Atlantic regions. Univ. Keele, Keele, United Kingdom. p.*

Higgins, A. K. & Leslie, A. G., 2000. Restoring thrusting in the East Greenland Caledonides. *Geology*, **28**(11), 1019-1022.

Hodges, K. V., Bartley, J. M. & Burchfiel, B. C., 1982. Structural evolution of an A-type subduction zone, Lofoten-Rombak area, northern Scandinavian Caledonides. *Tectonics*, **1**(5), 441-462.

Hodges, K. V., Burchfiel, B. C., Royden, L. H., Chen, Z. & Liu, Y., 1993. The metamorphic signature of contemporaneous extension and shortening in the central Himalayan orogen: Data from the Nyalam transect, southern Tibet. *Journal of Metamorphic Geology*, **11**, 721-737.

Hodges, K. V. & McKenna, L. W., 1987. Realistic propagation of uncertainties in geologic thermobarometry. *American Mineralogist*, **72**, 671-680.

Jones, K. A. & Strachan, R. A., 2000. Crustal thickening and ductile extension in the NE Greenland Caledonides: a metamorphic record from anatectic pelites. *Journal of Metamorphic Geology*, **18**(6), 719-735.

Kalsbeek, F., Nutman, A. P. & Jepsen, H. F., 1998. Granites in the Caledonian fold belt, East Greenland. In: *Symposium on Caledonian geology - abstract volume* (eds Frederiksen, K. S. & Thrane, K.), pp. 43-44, Danmarks og Grønlands Geologiske Undersøgelse Rapport, Denmark.

Kretz, R., 1983. Symbols for rock-forming minerals. *American Mineralogist*, **68**, 277-279.

Leslie, A. G. & Higgins, A. K., 1999. On the Caledonian (and Grenvillian) geology of Bartholin Land, Ole Rømer Land and adjacent nunataks, East Greenland. In: *Geology of East Greenland 72°-75°, mainly Caledonian: preliminary reports from the 1998 expedition* (eds Higgins, A. k. & Frederiksen, K. S.), pp. 220, Danmarks og Grønlands Geologiske Undersøgelse Rapport, Denmark.

McKenna, L. W. & Hodges, K. V., 1988. Accuracy versus precision in locating reaction boundaries: Implications for the garnet-plagioclase-aluminum silicate-quartz geobarometer. *Am. Mineral.*, **73**, 1205-1208.

Montel, J., Foret, S., Veschambre, M., Nicollet, C. & Provost, A., 1996. Electron microprobe dating of monazite. *Chemical Geology*, **131**, 37-53.

Patiño Douce, A. E., Johnston, A. D. & Rice, J. M., 1993. Octahedral excess mixing properties in biotite: a working model with applications to geobarometry and geothermometry. *American Mineralogist*, **78**, 113-131.

Peucat, J. J., Tisserant, D., Caby, R. & Clauer, N., 1985. Resistance of zircons to U-Pb resetting in a prograde metamorphic sequence of Caledonian age in East Greenland. *Canadian Journal of Earth Sciences*, **22**, 330-338.

Rex, D. C., Gledhill, A. & Higgins, A. K., 1977. Precambrian Rb-Sr isochron ages from the crystalline complexes of inner Forsblads Fjord, East Greenland fold belt. *Rapport Grønlands geologiske Undersøgelse*, **85**, 122-126.

Rex, D. C. & Gledhill, A. R., 1981. Isotopic studies in the East Greenland Caledonides (72°-74°N) — Precambrian and Caledonian ages. *Rapport Grønlands geologiske Undersøgelse*, **104**, 47-72.

Rex, D. C., Gledhill, A. R. & Higgins, A. K., 1976. Progress report on geochronological investigations in the crystalline complexes of the East Greenland Caledonian fold belt between 72°N and 76°N. *Rapport Grønlands geologiske Undersøgelse*, **80**, 127-133.

Ruppel, C., Royden, L. & Hodges, K. V., 1988. Thermal modeling of extensional tectonics: application to pressure-temperature-time histories of metamorphic rocks. *Tectonics*, **7**, 947-957.

Smith, M. P. & Robertson, S., 1999. The Nathorst Land Group (Neoproterozoic) of East Greenland - lithostratigraphy, basin geometry and tectonic history. In: *Geology of East Greenland 72°-75°, mainly Caledonian: preliminary reports from the 1998 expedition* (eds Higgins, A. k. & Frederiksen, K. S.), pp. 220, Danmarks og Grønlands Geologiske Undersøgelse Rapport, Denmark.

Sønderholm, M. & Tirsgaard, H., 1993. Lithostratigraphic framework of the Upper Proterozoic Eleonore Bay Supergroup of East and North-East Greenland. *Grønlands Geologiske Undersøgelse*, **167**.

Spear, F. S., 1993. *Metamorphic Phase Equilibria and Pressure-Temperature-Time Paths*. Mineralogical Society of America, Washington, D.C.

St-Onge, M. R., 1987. Zoned poikiloblastic garnets: P-T paths and synmetamorphic uplift through 30km of structural depth, Wopmay Orogen, Canada. *J. Petrol.*, **28**, 1-27.

Strachan, R. A., Martin, M. W. & Friderichsen, J. D., In Press. Evidence for contemporaneous yet contrasting styles of granite magmatism during extensional collapse of the northeast Greenland Caledonides. *Tectonics*.

Sturt, B. A. & Thon, A., 1978. An ophiolite complex of probable early Caledonian age discovered on Karmoy. *Nature (London)*, **275**(5680), 538-539.

Thompson, A. B., 1982. Dehydration melting of pelitic rocks and the generation of H_2O-undersaturated granitic liquids. *Am. J. Sci.*, **282**, 1567-1595.

Thompson, A. B. & Tracy, R. J., 1979. Model systems for anatexis of pelitic rocks: II. Facies series melting and reactions in the system CaO-$KAlO_2$-$NaAlO_2$-Al_2O_3-SiO_2-H_2O. *Contributions In Mineralogy and Petrology*, **70**, 429-438.

Thrane, K., Kalsbeek, F. & Watt, G. R., 1999. Evidence for a Grenvillian event in the East Greenland Caledonian fold belt. In: *Second symposium on East Greenland geology, mainly Caledonian: Abstract volume* (eds Frederiksen, K. S. & Thrane, K.), pp. 64, Danmarks og Grønlands Geologiske Undersøgelse Rapport, Denmark.

Torsvik, T. H., Smethurst, M. A., Meert, J. G., Van der Voo, R., McKerrow, W. S., Brasier, M. D., Sturt, B. A. & Walderhaug, H. J., 1996. Continental break-up and collision in the Neoproterozoic and Palaeozoic; a tale of Baltica and Laurentia. *Earth-Science Reviews*, **40**(3-4), 229-258.

Vielzeuf, D. & Holloway, J. R., 1988. Experimental determination of the fluid-absent melting relations in the pelitic system. Consequences for crustal differentiation. *Contrib. Mineral. Petrol.*, **98**, 257-276.

Vold, J., 1997. Et studie av den tectonomatemorphe utviklingen av gneisserne i liggblokken til "The Fjord Region Detachment Zone" på Kap hedlund, sentrale Øst Grønland. *Unpub. Cand. Scient Thesis Thesis, University of Oslo, Oslo.*

Watt, G. R. & Thrane, K., 1999. The nature of the Grenvillian orogeny in central East Greenland. In: *Second symposium on East Greenland geology, mainly Caledonian: Abstract volume* (eds Frederiksen, K. S. & Thrane, K.), pp. 64, Danmarks og Grønlands Geologiske Undersøgelse Rapport, Denmark.

Wegmann, C. E., 1935. Preliminary report on the Caledonian orogeny in Christian X's Land (North-East Greenland). *Meddelelser om Grønland*, **128**, 145-156.

White, A. & Hodges, K., in preparation. Multi-stage dxtensional evolution of the central East Greenland Caledonides. .

White, A. P., Hodges, K. V. & Davidek, K., 1998. U-Pb constraints on the age of deformation of the Krummedal Supracrustal Sequence in Forsblad Fjord, East Greenland. In: *Symposium on Caledonian geology in East Greenland* (eds Frederiksen, K. S. & Thrane, K.), pp. 55, Danmarks og Grønlands Geologiske Undersøgelse Rapport, Denmark.

White, A. P., Hodges, K. V., Martin, M. V. & Andresen, A., in press. Geologic constraints on middle-crustal behaviour during synorogenic extension in the East Greenland Caledonides. *International Journal of Earth Science.*

Williams, M. L., Jercinovic, M. J. & Terry, M. P., 1999. Age mapping and dating of monazite on the electron microprobe: Deconvoluting multistage tectonic histories. *Geology*, **27**(11), 1023-1026.

Figure Captions:

Figure 1: Simplified tectonic map of the central fjord region of the East Greenland Caledonides interpreted after Koch and Haller (1971), Henriksen and Higgins (1976), Peucat *et al.* (1985), Andresen *et al.* (1998a), White *et al.* (1998), Smith and Robertson (1999), Leslie and Higgins (1999), Escher and Jones (1999), White and Hodges (1999). The following abbreviations have been used: Forsblad Fjord (FF); Alpefjord (AF); Kaiser

Franz Joseph's Fjord (KFJF); Kong Oscar's Fjord (KOF); Furesø (F); Eleonore Sø (ES); Målebjorg (M); Niggli Spids (NS); Charcot Land (CL). *N.B.* Gåseland lies south to the south from this map. Box indicates study area. Question marks indicate unknown or enigmatic contacts, unexplained by past work in the region. We have interpreted the above thrust geometries based on correlations between the preliminary age relationships and fault contacts reported by the Greenland Geological Survey in 1999 and the earlier work of L. Koch, J. Haller and others as referenced above.

Figure 2: Simplified geologic map of the study area with sample names and locations used in this study. For further geologic and structural details, see White *et al.* [in press].

Figure 3: Mineral abbreviations after Kretz (1983). a) Photograph of M_1-M_2 garnet that grew prekinematically with respect to D_2. Note the symmetric pressure shadows. While plagioclase is not shown in the picture, it is an important member of the mineral assemblage in this sample (97GR53). b) Photo showing a garnet that was almost entirely replaced by Quartz+Plagioclase+K-feldspar simplectite (97GR17). c) Photo showing a quartz+plagioclase+Crd simplectite that completely replaced a garnet during M_3 metamorphism (97GR17). d) This is a close-up of the right side of the simplectite in c) to show the myrmekitic intergrowths of plagioclase and quartz that are difficult to see at lower magnification. e) Photo of kyanite crystal being replaced by sillimanite. f) Photo of M_2 garnet that grew synkinematically with respect to D_2. Note that the long axis of the garnet lies parallel to S^2.

Figure 4: XRC maps showing Ca, Mg, and Mn. Note the relative intensity scale bars are different for each map. To help clarify the elemental abundance for absolute comparison from one map to another, we have marked several spots on the garnets with

their known oxide weight percents. a) 97GR57, M_1 garnet that grew synkinematically with respect to D_1. c) 97GR70 - M1 garnet showing strong zonation in Ca from core to rim and sharp, near-rim enrichment of Mn. c) 97GR53 - showing M_1 garnet core surrounded by a well defined M_2 garnet overgrowth. d) 97GR47 - showing M_2 garnet. Note the zonation in Ca and Mg is the reverse pattern from that characteristically displayed in M_1 garnet such as seen in Figure 4b.

Figure 5: Representative XRC maps of monazite for Y, Th, Pb and U. a) Monazite from matrix, 97GR53. Note the 2-phase metamict core most easily seen in the Th map, surrounded by a 2-phase, metamict mantle rimmed by a single-phase overgrowth that is most easily seen in the Y map. b) Monazite included in garnet core, 97GR53. Note that the entire monazite is essentially a single phase.

Figure 6: Petrogenetic grid constructed with equilibrium reactions determined from petrographic observations. Note the curve labeled **a** is the granite minimum-melt curve (Thompson, 1982), **b** is the muscovite dehydration reaction curve described by equation (1) in the text (Spear, 1993; Thompson, 1982; Thompson & Tracy, 1979), **c** is the biotite dehydration reaction curve described by equation (2) in the text (Clemens & Wall, 1981; Spear, 1993; Vielzeuf & Holloway, 1988). The hatched fields represent reasonably constrained regions of P-T space in which metamorphism occurred. The boxed numbers represent points in P-T space that are constrained by reactions explained in the text. The curvature of the arrows qualitatively suggests the shape of the P-T path that we interpret based on our petrographic observations. The rest of the curves have been drawn after Spear (1993).

Figure 7: a) The reaction curves are the same as found on Figure 6. The equilibrium curves are drawn for all thermobarometric analyses. The shaded field

represents the region of P-T space occupied by the dataset as a whole. The black arrows are drawn from the results of inclusion thermobarometry to the results of rim thermobarometry for a given garnet and reflect the change in pressure and temperature over time. The white arrow is drawn between two rim analyses from separate garnets from sample 97GR47 — one equilibrated during M_2 and the other during M_3. The arrow is drawn from the lower bound of the error ellipse for reasons explained in the text. b) Arrows showing change in P-T over time for given structural horizons as determined from the thermobarometry are plotted on the petrogenetic grid from Figure 5. Note the close consistency between the two sets of constraints.

Figure 8: a) Plot of pressure versus structural depth from all samples analyzed with the results from our rim thermobarometry. b) This is a similar plot to a), depicting the results of our inclusion thermobarometry. Note, while both datasets roughly indicate that pressures increased with structural depth, neither the rim nor the inclusion thermobarometry plots along a straight line. Given the consistency of the foliations in the Krummedal Sequence with the lack of any significant structural disruption along the exposed section, the spread of the data on these plot implies that the equilibration of the thermobarometry assemblages was not isochronous.

Figure 9: All curves as described in Figure 6. Arrows as described in Figure 7. Data are plotted with error ellipses. a) This plot shows the results of rim thermobarometry from two different generations of garnet from the same sample. Thus the arrow shows the change in P-T conditions over time.

The plots in b)-e) show samples for which we have both rim and inclusion thermobarometry. Thus, the arrows also show the change in pressure temperature

conditions over time. These samples were all collected from different structural horizons as shown in Figure 8. b) 97GR73; c) 97GR02; d) 97GR53; e) 97GR70.

Figure 10: Summary of the pressure-temperature-time reconstruction from a structural horizon 4.5 km beneath the Tindern detachment (97GR73). Prograde metamorphism and burial associated with crustal thickening prior to ca. 425 Ma (M_1-M_2) was followed by near-isothermal decompression (M_3) associated with exhumation due to slip along the Tindern detachment over 2 million years. This was followed by cooling during M_4. Absolute ages are depicted next to the positions that they constrain in P-T space. The events and ages are discussed in more detail in the text.

Appendix:

Analytical Techniques For Petrography And Thermobarometry

Thin-sections (30 micron width) were made of all samples for petrographic analysis. Sections for probing were polished and coated with a thin layer of carbon. Wavelength-dispersive spectroscopy (WDS) was performed both on the Cameca SX50 Electron Microprobe at the UMASS Amherst Electron Microprobe Laboratory and the JEOL Superprobe 733 using software by Frank Spear and Geller Inc. at the MIT Electron Microprobe Laboratory. Backscattered electron (BSE) and X-ray composition (XRC) maps showing elemental abundance of Ca, Mg and Mn, were produced of all samples to be used for quantitative thermobarometry. These maps were made using an accelerating voltage of 15 kV, a beam current of 100 nA, and a dwell time of 0.1 seconds/pixel. Sometimes the XRC images contain artifacts due to a hysteresis effect in the stage controller.

Analytical Techniques for Electron Microprobe Dating

XRC maps of Ce were collected from a thin section of 97GR53 (100 micron width) at the UMASS Amherst Electron Microprobe Laboratory using an accelerating voltage of 15 kV, a beam current of 250 nA, and a dwell time of 0.01 seconds/pixel. The XRC map was used to locate monazite *in situ* within garnet cores, rims and the surrounding gneissic matrix. After selection of the monazites for analysis, individual XRC maps of U, Th, Pb and Y were made to look for chemical zonation. Assuming that there was negligible common lead and that mass transfer had not significantly altered the elemental concentrations in the monazite (Cocherie *et al.*, 1998; Montel *et al.*, 1996), an age estimate was determined by measuring concentrations of U, Th and Pb and solving the age equation of Montel *et al.* (1996) by iteration. Because of the spectral overlap between X-ray peaks associated with Pb and Y, total Pb counts were adjusted to remove the overestimated amount of Pb using a Y correction factor determined for each spot analysis. A minimum Pb/Y criteria was applied to the raw data to determine whether the Pb values would be reasonable after this Y-correction. Data that failed this test were dropped. Five spot analyses were performed on each monazite, though some of these data had to be dropped because of the Pb/Y test. The monazite were selected from three populations: four were from pre-D_1 garnet cores; two were from pre-D_1 garnet mantles; six were from the surrounding matrix dominated by D_2 fabrics.

Minimum uncertainties were estimated using a standard Monte-Carlo approach (Anderson, 1976). First, we calculated the average and standard deviation of the valid spot analyses for U, Th, Pb and Y that were measured at each monazite. Then we generated four numerical arrays, with 1000 elements each that were assigned to hold U, Th, Pb and Y values. The arrays were generated such that each was normally distributed

around the assigned element's average measured values and standard deviation. Following this, a value from each of these numerical arrays was randomly selected to make an age determination. The Y correction was performed and the age equation was iteratively solved. This procedure was repeated 1000 times, yielding an array of 1000 ages. Thus, twice the standard deviation of these 1000 ages was taken to be the 2σ uncertainty for the age of a given monazite. A similar procedure was used to estimate the uncertainty on the average age of the three populations of monazite described above. It must be emphasized that these uncertainties are minimum estimates and do not take into account the geologic uncertainty built into the assumptions mentioned above. Thus, it is important that the reader not be mislead by our estimated uncertainties to believe that events separated by a few million years are distinguishable by this technique with confidence; however, we may be confident that events separated by several hundred million years are distinguishable — which renders this technique ideal for reconnaissance geochronology.

Figure 1

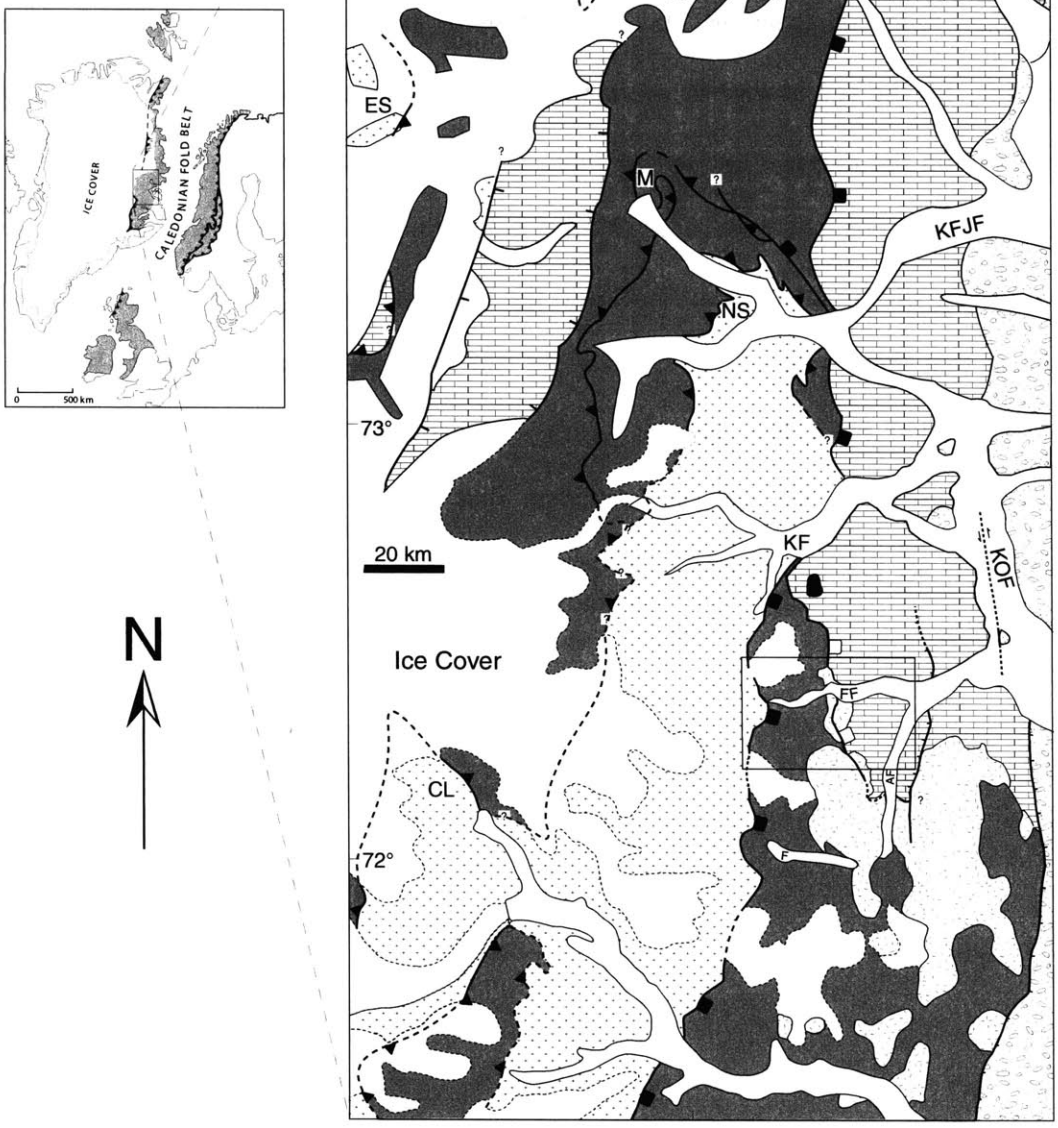
27°
Ice Cover
74°
ES
M
KFJF
NS
73°
20 km
KF
KOF
Ice Cover
FF
CL
72°
ICE COVER
CALEDONIAN FOLD BELT
0
500 km
N
Høgedal Detachment
Tindern Detachment
Thrust Fault
Normal Fault
Inferred Fault Contact
Lithologic Contact
Inferred Lithologic Contact
Devonian Carboniferous Basins
Caledonian Granitoid Plutons and Migmatitic Rocks
Neoproterozoic Eleonore Bay Supergroup
Mesoproterozoic - Neoproterozoic Metasedimentary Rocks
Archean - Paleoproterozoic Basement Complex

Figure 2

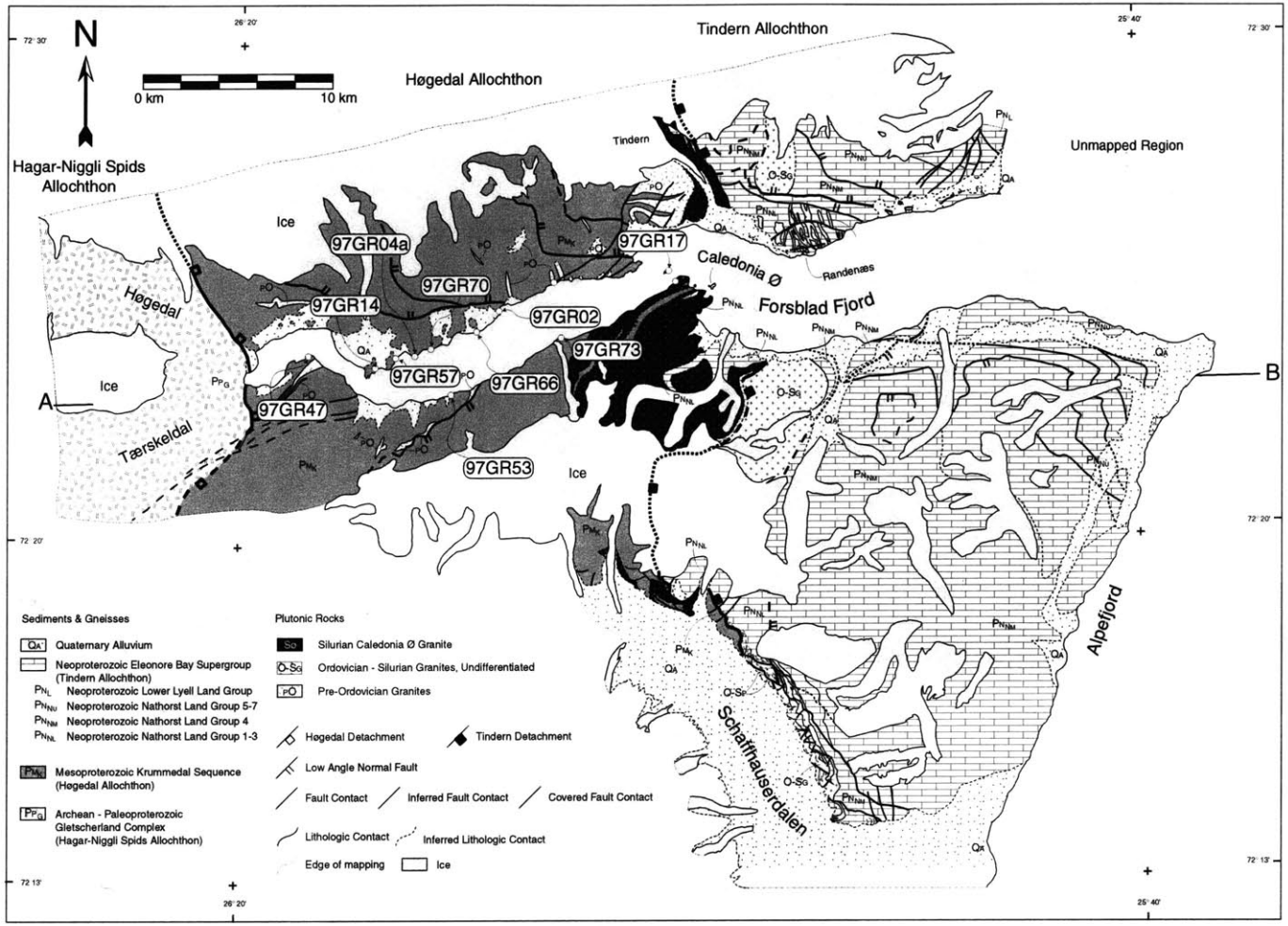
N
0 km
10 km
Tindern Allochthon
Høgedal Allochthon
Hagar-Niggli Spids Allochthon
Tindern
Unmapped Region
Ice
97GR04a
97GR17
Caledonia Ø
Randenæs
Høgedal
97GR14
97GR70
97GR02
Forsblad Fjord
97GR73
97GR57
97GR66
A
B
Ice
97GR47
Tærskeldal
97GR53
Ice
Alpefjord
Schaffhauserdalen
Sediments & Gneisses
Quaternary Alluvium
Neoproterozoic Eleonore Bay Supergroup (Tindern Allochthon)
Neoproterozoic Lower Lyell Land Group
Neoproterozoic Nathorst Land Group 5-7
Neoproterozoic Nathorst Land Group 4
Neoproterozoic Nathorst Land Group 1-3
Mesoproterozoic Krummedal Sequence (Høgedal Allochthon)
Archean - Paleoproterozoic Gletscherland Complex (Hagar-Niggli Spids Allochthon)
Plutonic Rocks
Silurian Caledonia Ø Granite
Ordovician - Silurian Granites, Undifferentiated
Pre-Ordovician Granites
Høgedal Detachment
Tindern Detachment
Low Angle Normal Fault
Fault Contact
Inferred Fault Contact
Covered Fault Contact
Lithologic Contact
Inferred Lithologic Contact
Edge of mapping
Ice

Figure 3

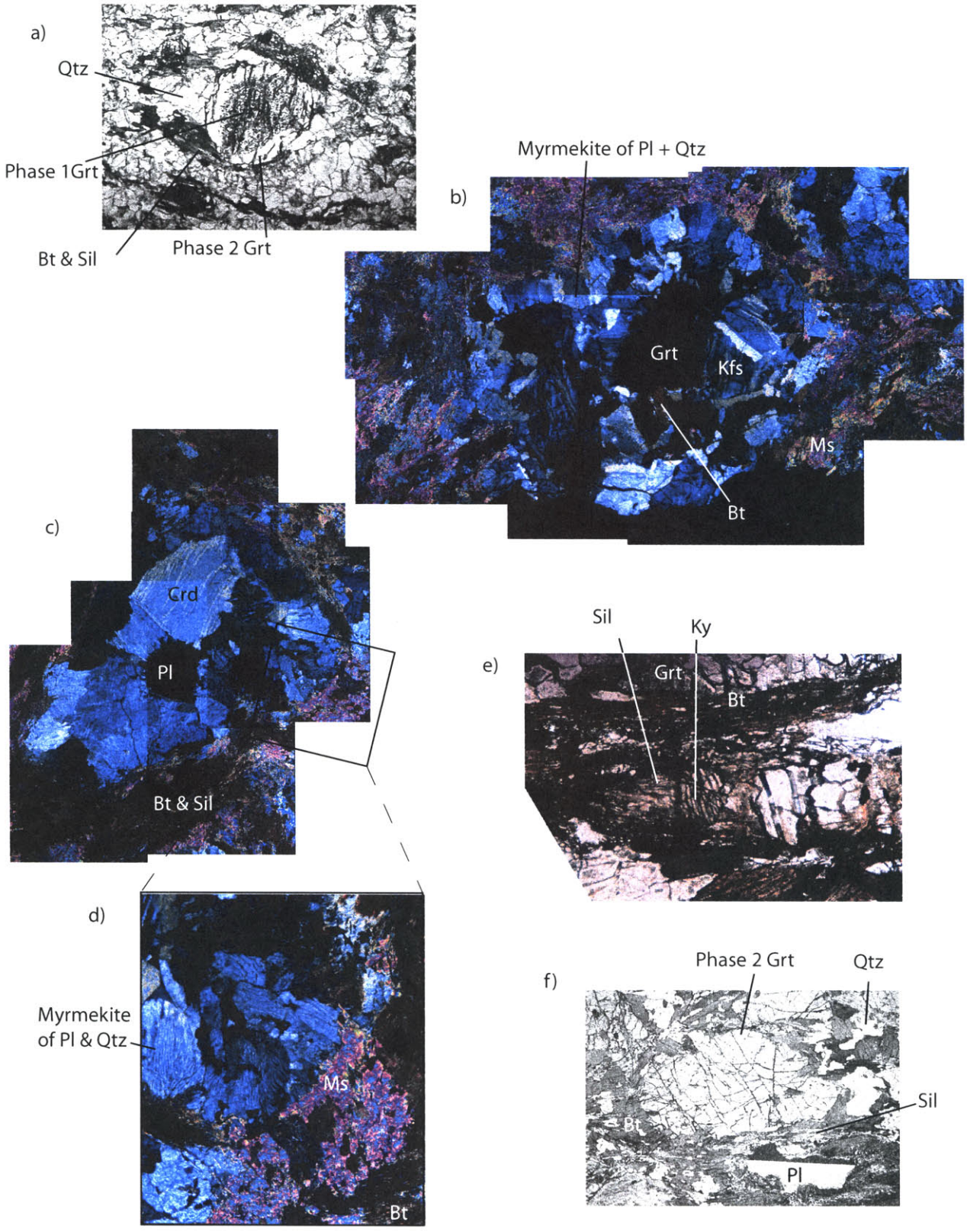
a)
Qtz
Phase 1Grt
Bt & Sil
Phase 2 Grt
b)
Myrmekite of Pl + Qtz
Grt
Kfs
Ms
Bt
c)
Crd
Pl
Bt & Sil
d)
Myrmekite
of Pl & Qtz
Ms
Bt
e)
Sil
Ky
Grt
Bt
f)
Phase 2 Grt
Qtz
Sil
Bt
Pl

Figure 4

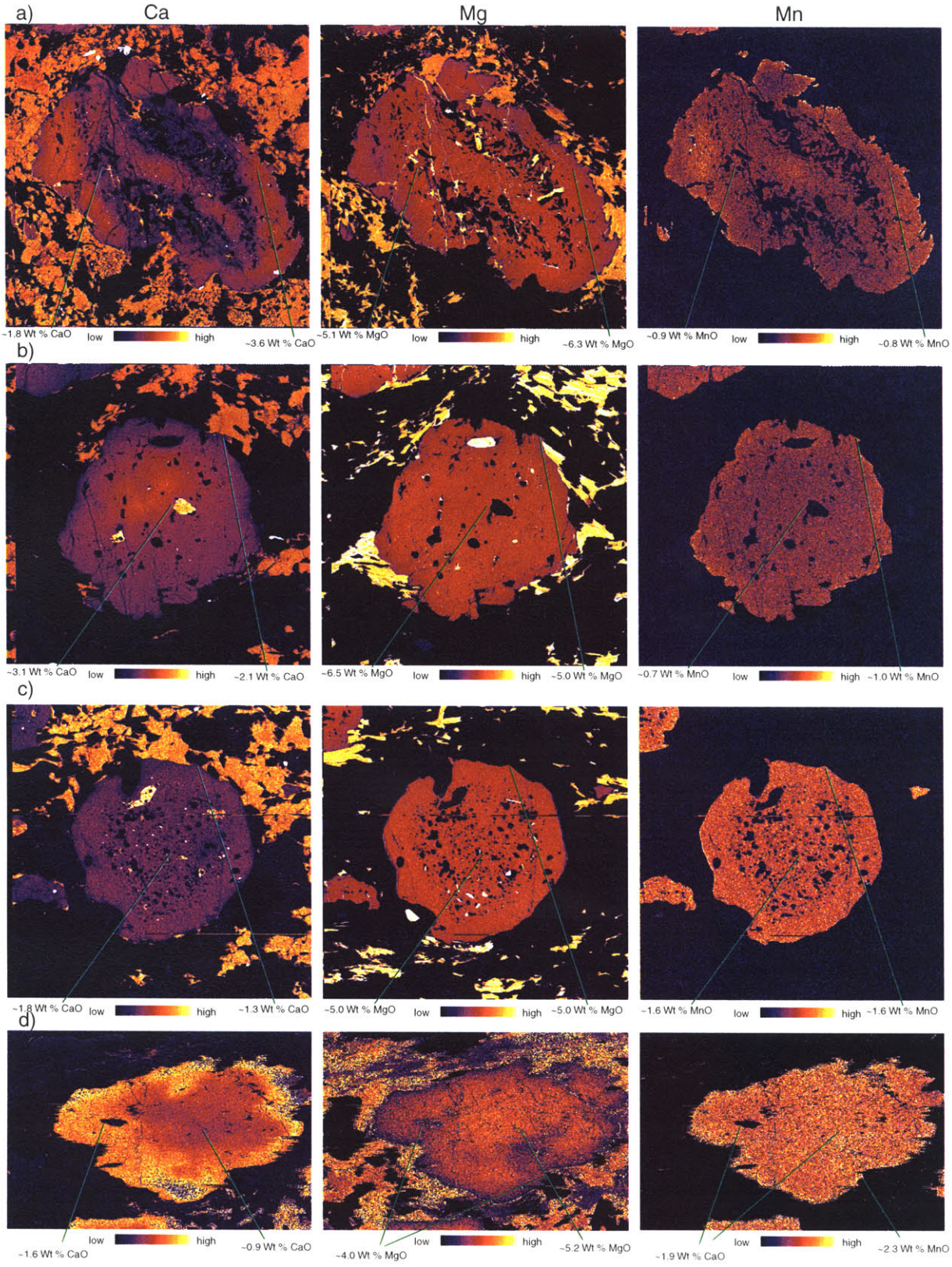
a)
Ca
Mg
Mn
~1.8 Wt % CaO
low
high
~3.6 Wt % CaO
~5.1 Wt % MgO
low
high
~6.3 Wt % MgO
~0.9 Wt % MnO
low
high
~0.8 Wt % MnO
b)
~3.1 Wt % CaO
low
high
~2.1 Wt % CaO
~6.5 Wt % MgO
low
high
~5.0 Wt % MgO
~0.7 Wt % MnO
low
high
~1.0 Wt % MnO
c)
~1.8 Wt % CaO
low
high
~1.3 Wt % CaO
~5.0 Wt % MgO
low
high
~5.0 Wt % MgO
~1.6 Wt % MnO
low
high
~1.6 Wt % MnO
d)
low
high
~1.6 Wt % CaO
~0.9 Wt % CaO
low
high
~4.0 Wt % MgO
~5.2 Wt % MgO
low
high
~1.9 Wt % CaO
~2.3 Wt % MnO

Figure 5

Monazite from matrix, 97GR53

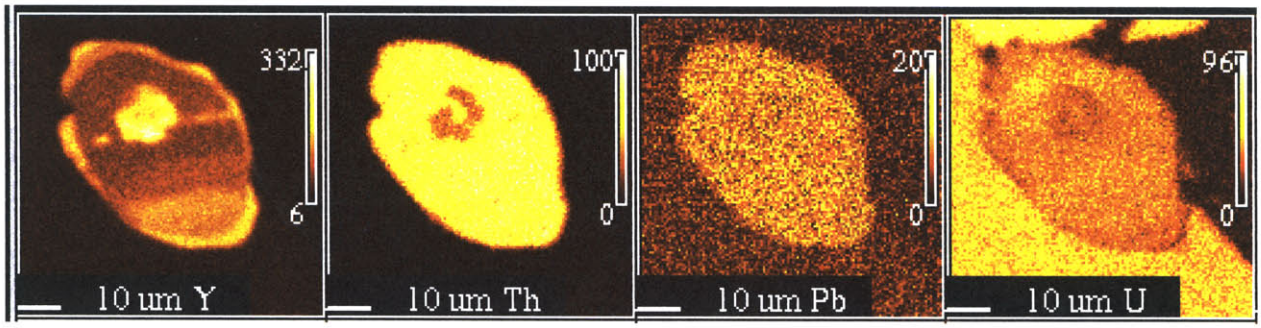

Monazite included in garnet core, 97GR53

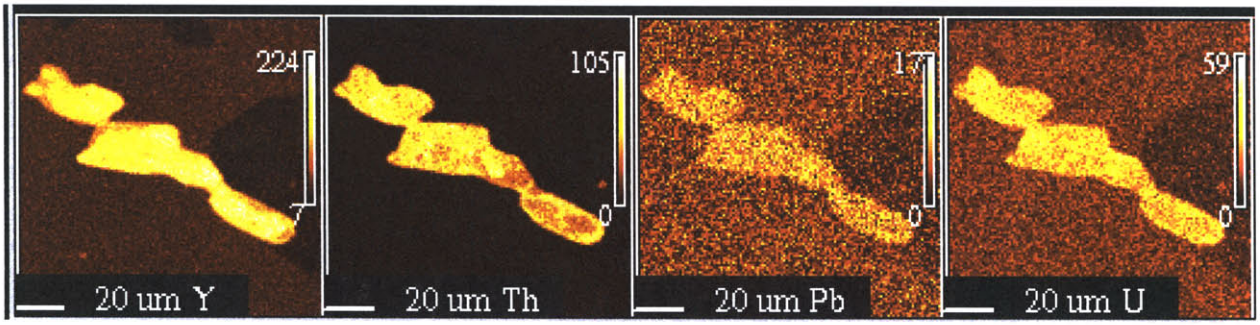

Figure 6

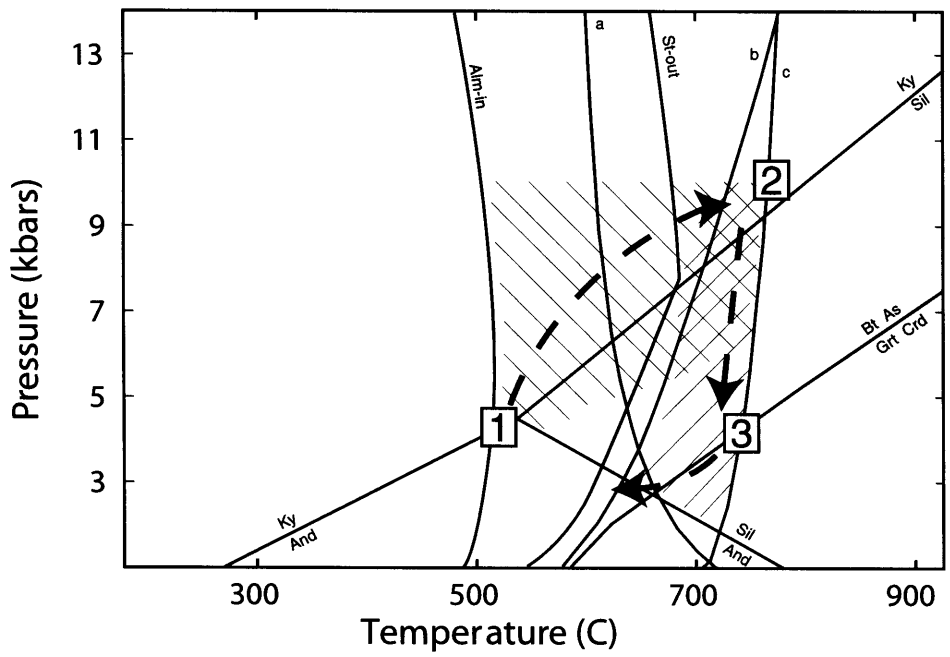
Pressure (kbars)
13
11
9
7
5
3
300
500
700
900
Temperature (C)
Alm-in
a
St-out
b
c
Ky
Sil
Bt As
Grt Crd
Ky
And
Sil
And
1
2
3

Figure 7

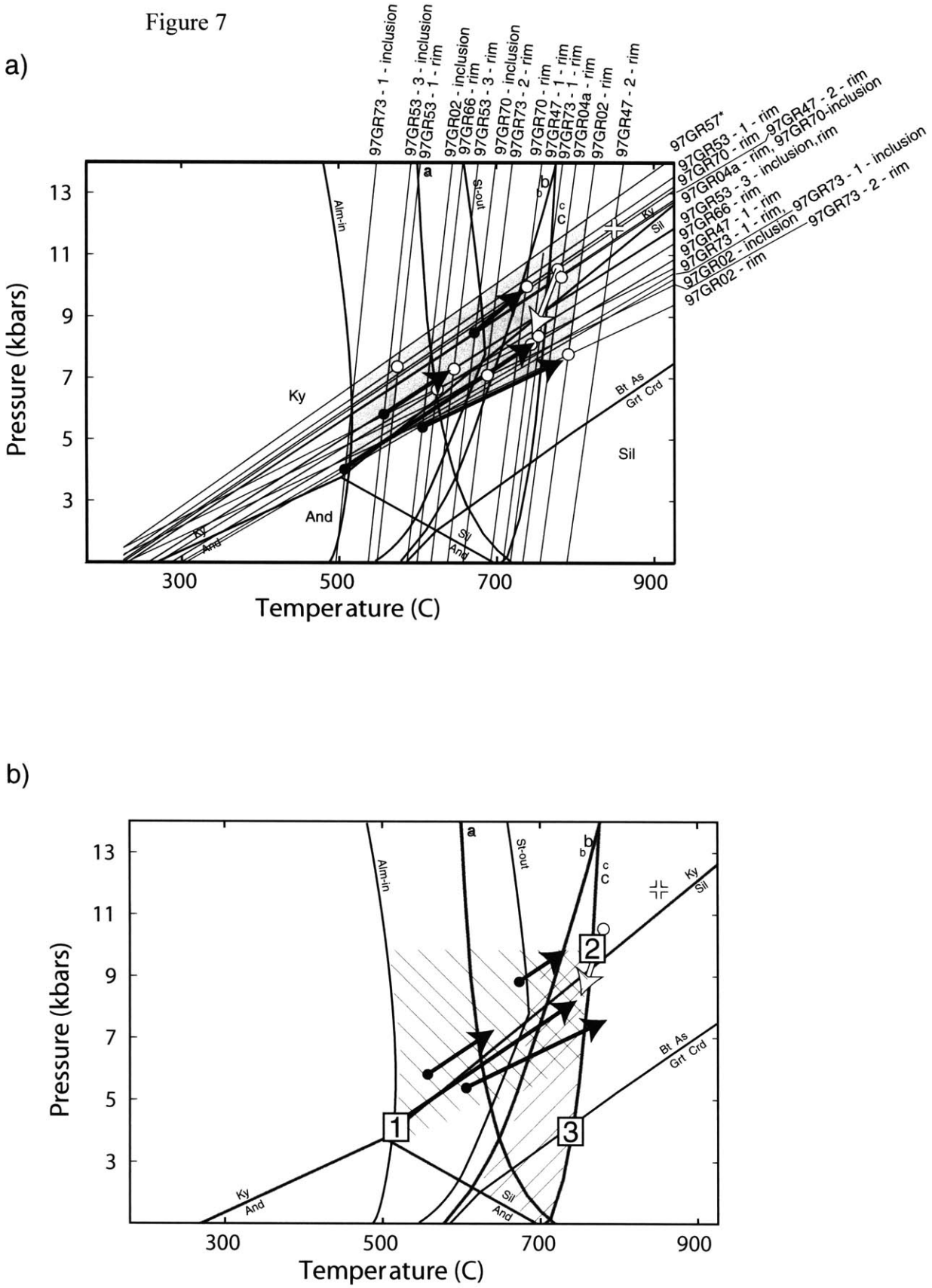
a)
97GR73 - 1 - inclusion
97GR53 - 3 - inclusion
97GR53 - 1 - rim
97GR02 - inclusion
97GR66 - rim
97GR53 - 3 - rim
97GR70 - inclusion
97GR73 - 2 - rim
97GR70 - rim
97GR47 - 1 - rim
97GR73 - 1 - rim
97GR04a - rim
97GR02 - rim
97GR47 - 2 - rim
97GR57*
97GR53 - 1 - rim
97GR70 - rim, 97GR47 - 2 - rim
97GR04a - rim, 97GR70-inclusion
97GR53 - 3 - inclusion, rim
97GR66 - rim
97GR47 - 1 - rim
97GR73 - 1 - rim, 97GR73 - 1 - inclusion
97GR02 - inclusion, 97GR73 - 2 - rim
97GR02 - rim
Alm-in
St-out
Ky
Sil
Ky
And
Bt As
Grt Crd
Sil
And
Ky
And
Sil
And
Pressure (kbars)
Temperature (C)
b)
Alm-in
St-out
Ky
Sil
1
2
3
Bt As
Grt Crd
Ky
And
Sil
And
Pressure (kbars)
Temperature (C)

Figure 8

a) Rim Thermobarometry

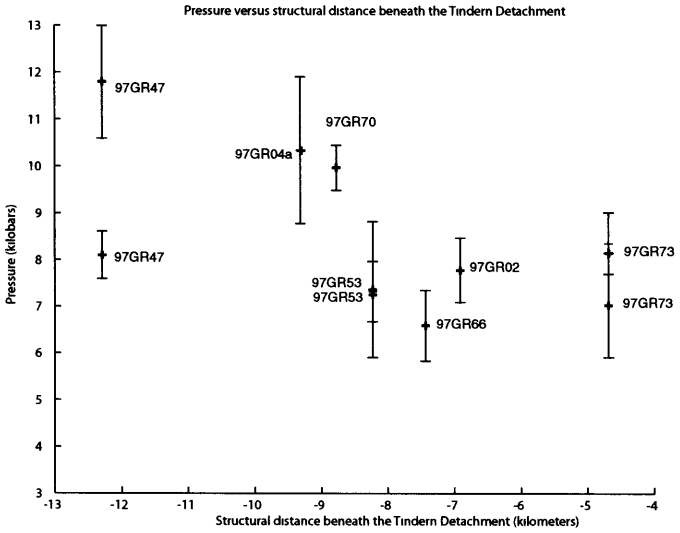

b) Inclusion Thermobarometry

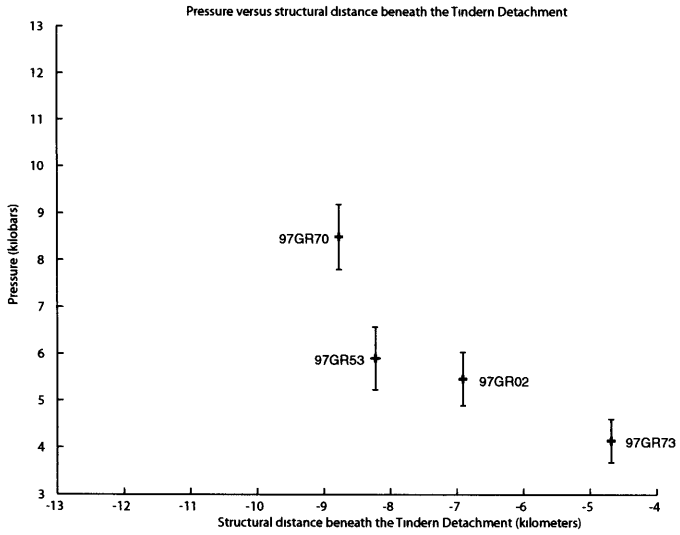

Figure 9

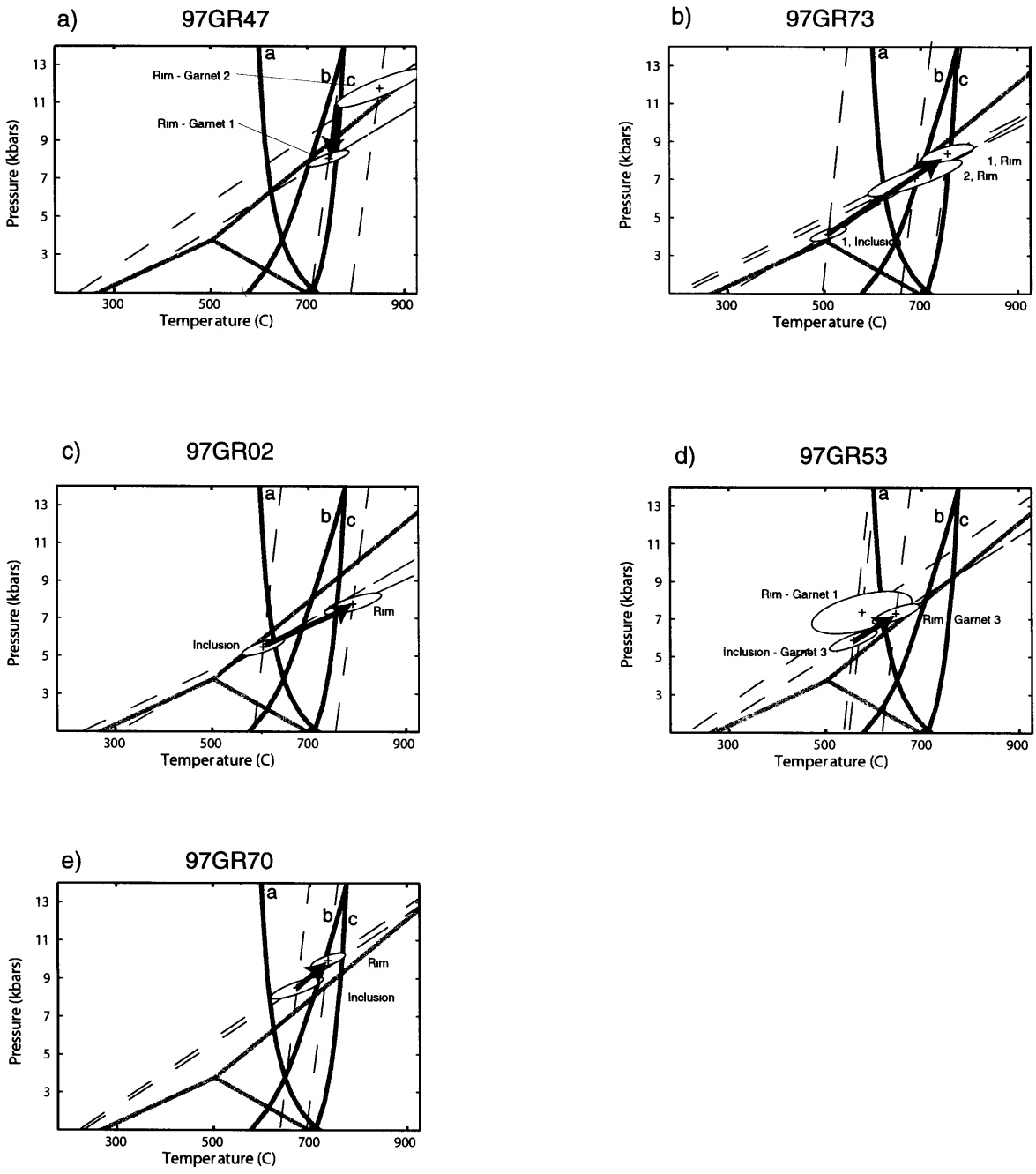
a)
97GR47
Rim - Garnet 2
Rim - Garnet 1
a
b
c
Pressure (kbars)
Temperature (C)
b)
97GR73
1, Rim
2, Rim
1, Inclusion
c)
97GR02
Inclusion
Rim
d)
97GR53
Rim - Garnet 1
Rim - Garnet 3
Inclusion - Garnet 3
e)
97GR70
Rim
Inclusion

Figure 10

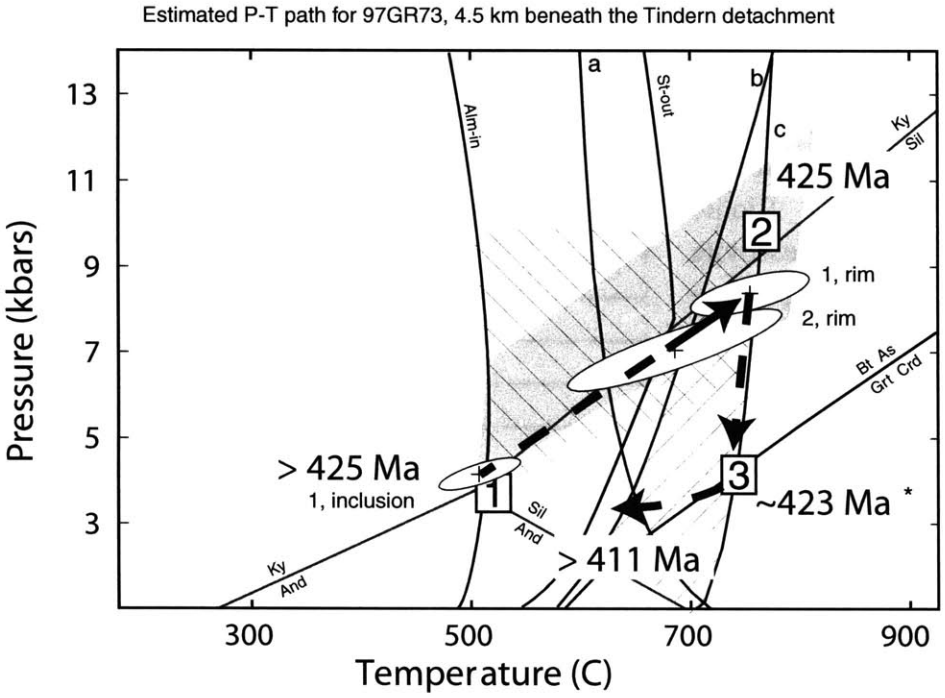
Estimated P-T path for 97GR73, 4.5 km beneath the Tindern detachment
Pressure (kbars)
Temperature (C)
13
11
9
7
5
3
300
500
700
900
Alm-in
a
St-out
b
c
Ky
Sil
425 Ma
2
1, rim
2, rim
Bt As
Grt Crd
> 425 Ma
1, inclusion
1
Sil
And
Ky
And
3
~423 Ma *
> 411 Ma

Table 1

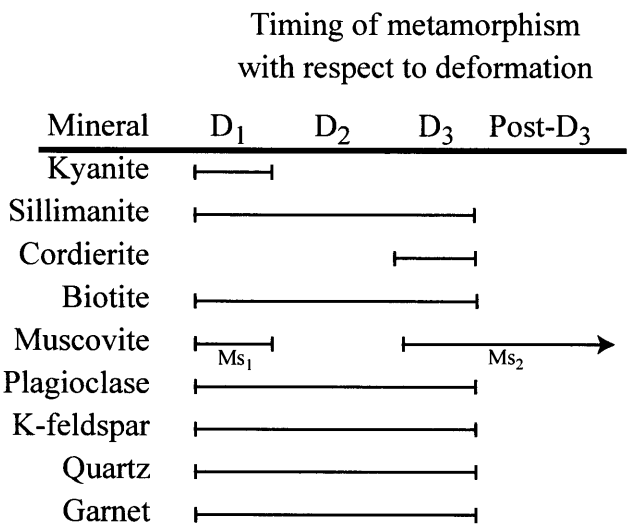
Timing of metamorphism
with respect to deformation
Mineral
D1
D2
D3
Post-D3
Kyanite
Sillimanite
Cordierite
Biotite
Muscovite
Ms1
Ms2
Plagioclase
K-feldspar
Quartz
Garnet

Table 2

Monazite from 97GR53		averages Age		2σ
Matrix	M1	410	±	10
Matrix	M3	412	±	12
Matrix	M5	405	±	10
Matrix	M7	398	±	10
Matrix	M8	422	±	10
Matrix	M6	409	±	11
Included in garnet mantle	M9	409	±	17
Included in garnet core	M4	400	±	9
Included in garnet core	M10	439	±	6
Included in garnet core	M11	416	±	13
Average age of monazite in the matrix		**409**	**±**	**4**
Average age of monazite included in garnet mantles		**409**	**±**	**17**
Average age of monazite included in garnet cores		**414**	**±**	**6**

Table 3

Sample	Rock Type	Primary Metamorphic Mineral Subassemblage								Grt inclusion suite				
		Ky	Sil	Crd	Bt	Ms	Pl	Kfs	Qtz	Grt	Ky	Sil	Bt	Pl	Qtz
97GR73	Gar-Bt Gneiss		●	●	●	●	●	●	●	●			●	●	●
97GR66	Gar-Bt Gneiss	●	●		●	●	●	●	●	●	●		●	●	●
97GR70	Gar-Bt Gneiss	●	●		●	●	●	●	●	●			●	●	●
97GR53	Gar-Bt Gneiss	●	●		●		●	●	●	●			●	●	●
97GR04a	Gar-Bt Gneiss	●	●		●	●	●	●	●	●	●		●	●	●
97GR57	Gar-Bt Gneiss				●		●	●	●	●			●		●
97GR47	Gar-Bt Gneiss	●	●		●		●	●	●	●		●	●		●

Table 4:

Garnet near-rim compositions (12 O basis)

Sample	97GR73 - 1	97GR73 - 2	97GR02-2*	97GR66	97GR53-1	97GR53-3*	97GR70-1	97GR04a-2*	97GR57-1	97GR47 - 1	97GR47 - 2*
Sio2	36.89 (0.08)	36.80 (0.10)	36.74 (0.73)	37.89 (0.08)	36.22 (0.26)	38.20 (0.76)	38.07 (0.12)	36.91 (0.74)	37.56 (0.09)	36.83 (0.12)	38.34 (0.77)
Tio2	0.00 (0.00)	0.02 (0.02)	0.00 (0.00)	0.01 (0.02)	0.07 (0 02)	0.03 (0.00)	0.02 (0.03)	0.07 (0.00)	0.00 (0.00)	0.02 (0.01)	0.00 (0.00)
Al2o3	21.58 (0.06)	21.83 (0.22)	21.46 (0.43)	22.11 (0.24)	21.01 (0.19)	21.59 (0.43)	22.20 (0.20)	21.39 (0.43)	21.92 (0.09)	21.66 (0.19)	21 62 (0.43)
Cr2o3	0.05 (0.01)	0.00 (0.00)	0.01 (0.00)	0.00 (0.00)	0.01 (0.02)	0.03 (0.00)	0.03 (0.01)	0.02 (0.00)	0.01 (0.01)	0.02 (0.02)	0 04 (0.00)
Feo	35.29 (0.13)	35.75 (0.24)	33.94 (0.68)	33.09 (0.43)	35.14 (0.29)	34.28 (0.69)	31.63 (0.31)	35.05 (0.70)	31 49 (0.22)	34.61 (0.06)	33.20 (0.66)
Mno	3.89 (0.12)	3.76 (0.16)	1.00 (0.02)	1.04 (0.04)	2.25 (0.12)	1.81 (0.04)	0.84 (0.01)	2.36 (0.05)	1.25 (0.12)	2.37 (0.08)	1.83 (0.04)
Mgo	2.86 (0.02)	2.73 (0.25)	4.38 (0.09)	5.81 (0.38)	3.03 (0.20)	3.93 (0.08)	6.33 (0.07)	1.57 (0.03)	4 87 (0.38)	3.97 (0.09)	4.26 (0.09)
Cao	0.89 (0.01)	0.89 (0.03)	1.10 (0.02)	1 45 (0.05)	1.90 (0.09)	1.35 (0.03)	2.23 (0.07)	3.81 (0.08)	3.24 (0.13)	1.45 (0 02)	2.14 (0.04)
Na2o	0.02 (0.01)	0.03 (0.01)	0.00 (0.00)	0.03 (0.03)	0 02 (0.01)	0.00 (0 00)	0.01 (0 01)	0.00 (0.00)	0 01 (0.01)	0.01 (0.01)	0.00 (0.00)
Total	101.46	101.798	98.590	101.428	99 623	101.220	101.342	101.180	100.354	100.93	101.430
Si	2.951	2.937	2.972	2.959	2 946	3.013	2.958	2.963	2.965	2 94	3.009
Ti	0.000	0 001	0 000	0.001	0 004	0.002	0.001	0.004	0 000	0 00	0.000
Al	2.034	2.053	2.046	2.035	2.014	2.007	2.033	2.024	2.039	2.04	1.999
Cr	0.003	0.000	0 001	0.000	0.001	0.002	0.002	0.001	0.001	0.00	0.003
Fe	2.361	2.386	2.296	2.161	2.390	2.261	2.055	2.353	2.079	2.31	2.179
Mn	0.264	0.254	0.068	0.069	0.155	0.121	0.055	0.160	0.084	0.16	0.122
Mg	0.341	0.324	0.527	0.676	0.367	0.462	0.733	0.188	0.573	0.47	0.498
Ca	0.076	0.076	0.095	0.121	0.165	0.114	0.185	0.328	0 275	0.12	0.180
Na	0.003	0.004	0.000	0.004	0.002	0.000	0.001	0.000	0.001	0 00	0.000
Total	8.032	8.037	8.005	8.025	8.044	7.981	8.024	8.021	8.016	8.04	7.990
Numbers in parentheses denote 1σ uncertainties in composition established using the approach of Hodges and McKenna (1987)											
* Data represents less than 3 spot analyses. Uncertainty estimated to be 2% of measured values											
n =	6	5	2	4	5	1	5	1	5	3	2

Biotite rim compositions (11 O basis)

Sample	97GR73 - 1	97GR73 - 2	97GR02-2*	97GR66	97GR53-1	97GR53-3*	97GR70-1	97GR04a-2	97GR57-1	97GR47 - 1	97GR47 - 2
Sio2	35.05 (0.15)	34.36 (0 29)	35.53 (0.71)	36.64 (0.20)	35 46 (0.36)	35.57 (0.71)	36.22 (0.33)	34.54 (0.35)	35.58 (0.59)	35.52 (0.36)	34.97 (0.34)
Tio2	2.02 (0.04)	2.28 (0.36)	4.66 (0.09)	2.81 (0.04)	4 72 (0.11)	4.30 (0.09)	3.03 (0.06)	3 99 (0.28)	1.88 (0.72)	2.81 (0.12)	1.65 (0.44)
Al2o3	21.09 (0.17)	20.41 (0.26)	20 04 (0.40)	19.60 (0.17)	18.19 (0.29)	17.98 (0.36)	18.87 (0.23)	18 63 (0.39)	19.40 (0.60)	19.27 (0.09)	19.69 (0.28)
Cr2o3	0.07 (0.01)	0.02 (0.02)	0 05 (0.00)	0.04 (0.02)	0.06 (0.01)	0.03 (0.00)	0.06 (0.02)	0.06 (0.01)	0.01 (0.01)	0.01 (0.01)	0.03 (0.02)
Feo	21.68 (0.11)	20.84 (0.63)	17.25 (0.35)	13.95 (0.23)	17.26 (0.43)	17.70 (0.35)	14.73 (0.17)	25.31 (0.60)	16.28 (0.36)	19.63 (0.43)	20.24 (0.87)
Mno	0.20 (0.02)	0.12 (0.02)	0 03 (0.00)	0.04 (0.02)	0.02 (0.02)	0.00 (0.00)	0.03 (0.01)	0 11 (0.03)	0.04 (0 01)	0.15 (0.04)	0.13 (0.03)
Mgo	7.10 (0.09)	7.41 (0.06)	8 26 (0.17)	13.22 (0 30)	9 84 (0.16)	10.56 (0.21)	12.77 (0.18)	4.95 (0.39)	12.58 (0 60)	9.37 (0.06)	9.29 (0.22)
Cao	0.00 (0 00)	0.00 (0.00)	0 03 (0.00)	0.02 (0.01)	0 03 (0.01)	0.01 (0.00)	0.04 (0.03)	0.04 (0.03)	0.03 (0.02)	0.01 (0.01)	0.08 (0.04)
Na2o	0.16 (0 01)	0.12 (0.03)	0 22 (0.00)	0.08 (0 03)	0 13 (0.02)	0.09 (0.00)	0.13 (0.02)	0.07 (0.02)	0.38 (0 08)	0.19 (0.02)	0.15 (0.03)
K2o	9.12 (0.03)	9.49 (0.50)	9 41 (0.19)	9.46 (0.15)	9 71 (0.03)	9.76 (0.20)	9.25 (0.31)	9.27 (0.11)	8.12 (0.83)	8.52 (0.58)	8.68 (0.24)
Total	96 47	95.05	95.47	95.88	95.43	96.01	95.13	96.97	94.32	95.48	94.91

Table 4 (continued)

Biotite rim compositions (continued)

Sample	97GR73 - 1	97GR73 - 2	97GR02-2*	97GR66	97GR53-1	97GR53-3*	97GR70-1	97GR04a-2	97GR57-1	97GR47 - 1	97GR47 - 2
Si	2.653	2.643	2.667	2.691	2.676	2.674	2.694	2.662	2 675	2 685	2.673
Ti	0.115	0.132	0.263	0.155	0.268	0.243	0 170	0 231	0.106	0 160	0.095
Al	1.881	1.851	1 772	1.697	1.619	1.593	1.655	1.692	1.720	1 718	1.773
Cr	0.004	0.001	0 003	0.002	0.004	0.002	0 004	0.004	0.001	0 001	0.002
Fe	1.372	1.341	1 083	0.857	1.090	1.113	0.916	1.631	1.024	1.241	1 294
Mn	0.013	0.008	0.002	0.003	0.001	0.000	0.002	0.007	0.003	0.010	0.009
Mg	0.800	0 850	0.924	1.447	1.107	1.183	1.415	0.568	1.411	1.056	1.058
Ca	0 000	0.000	0.002	0.002	0.002	0.001	0.003	0.004	0.002	0.001	0.006
Na	0.024	0.017	0.032	0.011	0 020	0.014	0.019	0.010	0.055	0.028	0.022
K	0.880	0.931	0.901	0 887	0 935	0.936	0.878	0.911	0.779	0.822	0 847
Total	7.742	7 773	7.649	7.752	7.722	7.760	7.756	7.720	7.775	7.721	7.779

Numbers in parentheses denote 1σ uncertainties in composition established using the approach of Hodges and McKenna (1987)

* Data represents less than 3 spot analyses. Uncertainty estimated to be 2% of measured values

n = 4 5 1 5 5 2 5 5 5 3 3

Plagioclase rim compositions (8 O basis)

Sample	97GR73 - 1	97GR73 - 2	97GR02-2*	97GR66	97GR53-1	97GR53-3	97GR70-1	97GR04a-2	97GR57-1	97GR47 - 1*	97GR47 - 2*
Sio2	64.19 (0.01)	63.30 (0.25)	64.28 (1.29)	61.63 (0.38)	63.89 (0.91)	62.03 (0.93)	61.95 (0.29)	58.10 (0 40)	60.26 (0 32)	61.85 (1.24)	59.63 (1.19)
Al2O3	23.63 (0 10)	23.75 (0.15)	24.27 (0.49)	24.88 (0.20)	23.42 (0.60)	24.24 (0.34)	24.94 (0.11)	27.65 (0.27)	25.28 (0 19)	24.95 (0.50)	24.81 (0.50)
FeO	0.03 (0.01)	0.26 (0.15)	0.29 (0.01)	0.10 (0.04)	0 46 (0.10)	0.38 (0.21)	0.08 (0.10)	0.13 (0.07)	0.23 (0.06)	0.36 (0.01)	1.44 (0.03)
MgO	0.00 (0.00)	0.00 (0.01)	0.00 (0.00)	0.01 (0 01)	0 01 (0.01)	0 01 (0.01)	0.00 (0.00)	0.01 (0.01)	0.01 (0.00)	0.00 (0.00)	0.04 (0.00)
CaO	4.02 (0.06)	4.42 (0.14)	4.76 (0.10)	5.95 (0.12)	4.02 (0.61)	4 35 (0.07)	5.81 (0.06)	9.05 (0.32)	6.63 (0.08)	5.52 (0.11)	4.52 (0.09)
Na2O	9.86 (0.06)	9.73 (0.11)	6.14 (0.12)	8.70 (0.02)	8.86 (0.27)	8 86 (0.28)	8.70 (0.11)	6.61 (0.18)	8.16 (0.08)	8.35 (0.17)	7.93 (0 16)
K2O	0 19 (0.03)	0.15 (0.04)	0.03 (0.00)	0.14 (0 03)	0.18 (0.11)	0.18 (0.04)	0.20 (0.05)	0.18 (0.02)	0 12 (0 01)	0.06 (0.00)	0.69 (0.01)
Total	101 91	101 60	99 77	101.39	100.83	100.04	101 67	101.71	100.70	101.07	99.07
Si	2.788	2.766	2.813	2.706	2.799	2.748	2.711	2.562	2.671	2.717	2.690
Al	1.210	1 223	1 252	1.287	1.209	1.265	1.286	1.437	1.321	1.291	1.319
Fe	0.001	0.009	0.011	0.004	0.017	0.014	0.003	0.005	0.009	0.013	0.055
Mg	0.000	0 000	0.000	0.000	0.001	0.001	0.000	0.001	0.001	0.000	0.003
Ca	0.187	0 207	0 223	0.280	0.189	0.206	0.272	0.428	0.315	0.260	0 219
Na	0.831	0.824	0.521	0.740	0.753	0.761	0.738	0.565	0.701	0.710	0 693
K	0.010	0.008	0 002	0 008	0.010	0.010	0.011	0.010	0.007	0.003	0.040
Total	5.027	5.039	4.822	5.025	4.977	5.005	5.021	5.007	5.023	4.994	5.017

Numbers in parentheses denote 1σ uncertainties in composition established using the approach of Hodges and McKenna (1987)

* Data represents less than 3 spot analyses. Uncertainty estimated to be 2% of measured values.

n = 3 6 1 3 5 3 6 4 4 2 1

Table :
Rim Thermobarometric Data

	GARB -GASP	
Sample	T (C)	P (kbar)
97GR73 - 1	756 (37)	8.4 (0.7)
97GR73 - 2	687 (80)	7.0 (1.1)
97GR02 - 2	791 (44)	7.8 (0.7)
97GR66 - 1	624 (42)	6.6 (0.8)
97GR53 - 1	577 (48)	7.4 (1.5)
97GR53 - 3	647 (32)	7.3 (0.7)
97GR70 - 1	739 (22)	10.0 (0.5)
97GR04a - 1	783 (89)	10.3 (1.6)
97GR57 - 1	701 (81)	10.1 (1.5)
97GR47 - 1	746 (31)	8.1 (0.5)
97GR47 - 2	851 (66)	11.8 (1.2)

Numbers in parentheses denote 2σ uncertainties. See text for explanation.

Table 6·

Garnet compositions for inclusion thermobarometry(12 O basis)

Sample	97GR73 - 1	97GR02-2*	97GR53-3	97GR70-1
Sio2	37.01 (0.20)	36.81 (0.74)	38.70 (0.48)	37.70 (0.40)
Tio2	0.00 (0.00)	0.00 (0.00)	0.01 (0.02)	0.05 (0.02)
Al2o3	21.63 (0.14)	21.14 (0.42)	21.69 (0.03)	22.26 (0.09)
Cr2o3	0.00 (0.00)	0 04 (0 00)	0.01 (0.01)	0.03 (0.01)
Feo	35 70 (0.12)	36.36 (0.73)	32.93 (0.84)	30.35 (0.14)
Mno	2 77 (0.07)	0.96 (0.02)	1.62 (0.05)	0.71 (0 02)
Mgo	2.96 (0.08)	3.92 (0 08)	4.72 (0.16)	6.40 (0.21)
Cao	0.87 (0.02)	1.10 (0.02)	1.66 (0.04)	2.81 (0 03)
Na2o	0.00 (0.00)	0.00 (0 00)	0.00 (0.00)	0 03 (0.02)
Total	100.933	100.320	101.340	100.336
Sı	2.965	2.959	3 025	2.949
Ti	0.000	0.000	0 001	0.003
Al	2.042	2.003	1 999	2.052
Cr	0.000	0 003	0.001	0.002
Fe	2.391	2 444	2.153	1.985
Mn	0.188	0 066	0.107	0.047
Mg	0.354	0 470	0.550	0.746
Ca	0.075	0.095	0 139	0.236
Na	0.000	0.000	0.000	0.005
Total	8.014	8.038	7.975	8.024

Numbers ın parentheses denote 1σ uncertaınties ın composition established using the approach of Hodges and McKenna (1987)

* Data represents less than 3 spot analyses. Uncertainty estımated to be 2% of measured values.

n = 4 1 3 4

Biotite rim compositions from both matrix and inclusion suites (11 O basis)

Sample	97GR73 - 1	97GR02-2*	97GR53-3	97GR70-1
Sio2	35.41 (0.46)	35 85 (0.72)	36.17 (0.72)	36.49 (0.47)
Tio2	1.03 (0.05)	3.69 (0.07)	4.04 (0.08)	4.44 (0.23)
Al2o3	21 19 (0.33)	19.33 (0.39)	17 99 (0 36)	17.51 (0.09)
Cr2o3	0 00 (0.00)	0.02 (0.00)	0 02 (0.00)	0.01 (0.01)
Feo	17.05 (0.55)	16.99 (0.34)	14.04 (0.28)	13.63 (0.48)
Mno	0.05 (0.02)	0.00 (0.00)	0 02 (0.00)	0.04 (0.02)
Mgo	10.68 (0.21)	10.35 (0.21)	13 40 (0.27)	14.67 (0.18)
Cao	0.00 (0.01)	0.03 (0.00)	0.00 (0.00)	0.04 (0.03)
Na2o	0.22 (0.02)	0.31 (0 01)	0.23 (0.00)	0.38 (0 03)
K2o	9.21 (0 23)	8.43 (0.17)	9 25 (0.18)	7.80 (0.20)
Total	94 84	95.00	95 14	95.00
Sı	2.665	2.687	2.687	2.688
Tı	0 059	0.208	0.226	0.246
Al	1.880	1 707	1 575	1.521
Cr	0.000	0 001	0.001	0.000
Fe	1 073	1 065	0.872	0 840
Mn	0.003	0 000	0.001	0.003
Mg	1.199	1 156	1 484	1.611
Ca	0 000	0.002	0.000	0.003
Na	0.032	0.046	0 033	0 055
K	0.884	0.806	0.876	0.733
Total	7.795	7.677	7 754	7.699

Numbers in parentheses denote 1σ uncertainties in composition established usıng the approach of Hodges and McKenna (1987)

* Data represents less than 3 spot analyses Uncertaınty estimated to be 2% of measured values.

n = 10 1 2 4

Table 6 (continued)

Plagioclase rim compositions from both matrix and inclusion suites (8 O basis)

Sample	97GR73 - 1*	97GR02-2*	97GR53-3*	97GR70-1
Sio2	63.57 (1.27)	60.54 (1.21)	60.78 (1.22)	58.40 (0.73)
Al2O3	23.16 (0.46)	23.77 (0.48)	25 17 (0.50)	26.57 (0.36)
FeO	0.48 (0.01)	0.28 (0.01)	0.59 (0.01)	0.18 (0.03)
MgO	0 01 (0.00)	0.00 (0.00)	0.02 (0.00)	0.01 (0.01)
CaO	3.90 (0.08)	5.14 (0 10)	5 46 (0.11)	7.92 (0.38)
Na2O	9.55 (0.19)	9.02 (0.18)	8.06 (0.16)	6.92 (0.25)
K2O	0.08 (0.00)	0.08 (0.00)	0.09 (0.00)	0.33 (0.04)
Total	100.74	98 84	100.17	100.33
Si	2.794	2.726	2 697	2.605
Al	1.200	1.262	1.317	1.397
Fe	0.018	0 011	0.022	0.007
Mg	0.000	0 000	0.001	0.000
Ca	0.184	0 248	0.260	0.379
Na	0.814	0 788	0.693	0.599
K	0.004	0 005	0 005	0.019
Total	5.015	5.039	4.994	5.005

Numbers in parentheses denote 1σ uncertainties in composition established using the approach of Hodges and McKenna (1987)

* Data represents less than 3 spot analyses. Uncertainty estimated to be 2% of measured values.

n = 2 1 1 5

Table :
Inclusion Thermobarometric Data

	GARB -GASP	
Sample	T (C)	P (kbar)
97GR73 - 1	509 (66)	4.1 (0.5)
97GR02 - 2	606 (30)	5.5 (0.6)
97GR53 - 3	558 (33)	5.9 (0.7)
97GR70 - 1	673 (39)	8.5 (0.7)

Numbers in parentheses denote 2σ uncertainties. See text for explanation.

5. The role of upper crustal extension in the evolution of the central East Greenland Caledonides

Arthur P. White*, Kip V. Hodges*

** Department of Earth, Atmospheric and Planetary Sciences, Massachusetts Institute of Technology, Cambridge, MA, 02139,USA. apwhite@mit.edu Tel (617)-253-8445 fax (617) 252-1800*

Abstract:

Recent geologic investigations in the central East Greenland Caledonides have revealed two spatially overlapping, yet temporally distinct, splays of a large orogen-perpendicular extensional fault system known as the Fjord Region Detachment (FRD). Activity on the structurally shallowest splay was synkinematic with respect to the Baltica-Laurentia collision, while slip on the deeper fault extended through to the period traditionally associated with post-collisional gravitational collapse. In this paper, we attempt to quantify the relative importance of additional pre-Devonian upper-crustal extensional structures in the region with respect to the FRD. We present new structural and $^{40}Ar/^{39}Ar$ geochronologic data that enable us to define and constrain the absolute timing of the sequence of deformation in the Eleonore Bay Supergroup sedimentary rocks that comprise the hanging-wall of the uppermost of these two splays, the Tindern detachment. These structures are important because they are the principal products of deformation that occurred after the initial stages of movement on the FRD and prior to the opening of the Devonian basins in central East Greenland.

A reconstructed cross-section of this segment of the upper crust indicates that these rocks were horizontally extended a minimum of ~22%, accounting for roughly 5 km of crustal thinning. Temporal constraints yielded from models of ^{39}Ar loss from K-feldspar suggest that tectonic denudation was associated with steady cooling from ca. 420 to ca. 400 Ma. This implies a slow rate of upper crustal extension relative to the rapid slip inferred for the underlying Tindern detachment (several millimeters per year) from other data. Furthermore, this implies that upper crustal extension was roughly coeval with middle crustal thickening which must have been occurring sometime between ca. 425 Ma and the initiation of movement along the Høgedal detachment (ca. 417-380 Ma). Collectively, the data suggest that extension in the central East Greenland Caledonides, prior to the opening of the Devonian basins, was largely accommodated by brief episodes of slip on the FRD, and was not uniformly distributed through the crust or over the orogenic period.

Introduction

Since McClay *et al.* (1986) first proposed that deposition of the Old Red Sandstone and formation of the Devonian basins resulted from gravitational collapse of the overthickened crustal welt in the central East Greenland Caledonides, field investigations have revealed a substantial amount of additional evidence to support their hypothesis. Of particular importance was the identification of an orogen-scale extensional fault system, known as the Fjord Region Detachment (FRD, 72-74°N), that is located westward and structurally beneath the Devonian basins, deforming the Archean-Paleozoic crystalline basement (e.g. Andresen et al., 1998; Hartz and Andresen, 1995; White et al., in press). Our previous structural, geochronologic, and metamorphic investigations have indicated that the FRD system consists of multiple splays that were

active both synkinematically with respect to orogen-parallel shear and E-W contraction during the Baltica-Laurentia collision, and post-kinematically during the period traditionally associated with orogenic collapse (White et al., in press; White and Hodges, submitted). In this paper, we examine the extensional structures that were active during the time between major episodes of syn- and post-orogenic slip along the FRD system. We present structural observations from the hanging wall of the FRD in the Forsblad Fjord Region (~72.5° N) which indicate that crustal thinning was also accommodated by movement along antithetic normal faults that sole into the upper splay of the FRD system and lie beneath the Devonian basins. While our new $^{40}Ar/^{39}Ar$ data suggest that these structures were active during the period between episodes of significant syn- and post-orogenic slip along the FRD system, the total quantity of extension that can be attributed to them was small compared to the overall amount of crustal thinning accomplished by displacement along the Fjord Region Detachment system.

Geologic Background:

The Caledonides formed as a two-sided fold and thrust belt during the sinistrally oblique plate collision between Baltica and Laurentia during the Middle to Late Silurian (Andresen and Steltenpohl, 1994; Gee, 1975; Henriksen, 1985; Hodges et al., 1982; Sturt and Thon, 1978). Remnants that preserve evidence of east-directed translation of material are found today in Scandinavia, Ireland and Scotland, and structures with opposing vergence are common in East Greenland (Figure 1, subset). Thrust-bounded Archean to Neoproterozoic metamorphic gneiss complexes are found in the Eleonore Sø, Målebjorg and Niggli Spids tectonic windows that lie north of the study area (>73° N; Elvevold et al., 2000; Escher and Jones, 1999; Leslie and Higgins, 1999), and the Charcot Land and Gåseland windows that lie south of the study area (< 72°N) in (Christoffersen, 1984). The

thrust faults that surround these windows were truncated by a prominent system of N-S striking, E-dipping normal faults called the Fjord Region Detachment (FRD) (Hartz and Andresen, 1995).

Just south of 73° N, the FRD system separates into two splays: the structurally deeper is called the Høgedal detachment, and the shallower is the Tindern detachment (White et al., in press). Previous metamorphic and U-Pb and $^{40}Ar/^{39}Ar$ geochronologic investigations suggest that the Tindern detachment was active from ca. 425-423 Ma with as much as ~18 km of tectonostratigraphic throw, synkinematic with ongoing orogen-parallel shear and E-W contraction (White and Hodges, submitted; White and Hodges, in preparation; White et al., in press). Activity along the Høgedal detachment occurred sometime between ca. 417 and 380 Ma, and again as recently as ca. 357 Ma (White and Hodges, submitted) — essentially coeval with Devonian basin formation in East Greenland. The amount of tectonostratigraphic throw on this fault has been estimated at ~16 kilometers (White and Hodges, in preparation).

These faults juxtaposed three separate and distinct allochthons. From west to east and structurally lowest to highest, they are comprised of the Archean-Paleoproterozoic granulite and amphibolite facies gneisses of the Gletscherland Complex (Hagar-Niggli Spids allochthon), the Neoproterozoic amphibolite facies migmatitic metasedimentary gneisses of the Krummedal Sequence (Høgedal Allochthon) and the low-grade schists to unmetamorphosed sedimentary rocks of the Eleonore Bay Supergroup (Tindern allochthon). While details of the lower two allochthons may be found in White *et al.* (in press), White and Hodges (submitted) and White and Hodges (in preparation), we focus here upon the upper allochthon where additional extensional structures are preserved.

The Forsblad-Segelsällskapets Fjords transect (~72.5° N)

Our field observations were taken in the Forsblad and Segelsällskapets Fjords transect (Figures 1 and 2) where fantastic exposures of the Tindern allochthon provide a near-complete section of the E- to NE-dipping sedimentary rocks that originally comprised the Tindern detachment's hanging-wall. The basal section of the allochthon consists of a 9 kilometer thick group of predominately post-Riphean-aged (Proterozoic) silici-clastic sand- and mudstone units called the Nathorst Land Group (Smith and Robertson, 1999; Sønderholm and Tirsgaard, 1993; Vidal, 1976; Vidal, 1979) – the lowermost group in the Eleonore Bay Supergroup (EBS). The true thickness of this section is unknown because the basal contact is truncated by the Tindern detachment. Rocks closest to the detachment are generally metamorphosed to greenschist facies. Locally, amphibolite facies were achieved in the near-vicinity of synorogenic granite plutons and their associated feeder dike complexes (White et al., in press). Nevertheless, these rocks are not strongly deformed and preserve primary sedimentary structures that are excellent facing indicators. The degree of metamorphism decreases up-section to the point where the sediments are essentially unmetamorphosed.

Above the Nathorst Land Group lie the three subgroups of the Upper EBS. From bottom to top, these consist of ~2 kilometers of brightly colored sand- and mudstone members of the Lyell Land Group, ~1 kilometer of further silici-clastic members of the Ymer Ø Group, and ~1.5 kilometers of carbonates that comprise the Andrée Land Group (Figure 3). Given that many outcrops in East Greenland are unreachable by foot, the wide variety of colors combined with the consistency of bedding thickness over large tracts of exposed section makes the Upper EBS particularly amenable for mapping stratigraphic units and small-scale faults from the fjord level (Figure 4).

Just north of the eastern margin of Segelsällskapets Fjord, there is a small outcrop of Vendian tillite within the Quaternary alluvium that appears to sit directly on top of the Andrée Land Group. However, within the Segelsällskapets Fjord transect, Devonian conglomerates sit on top of the Andrée Land Group, separated by an erosional unconformity. Further descriptions of the stratigraphy and lithology of these units may be found in Haller (1971), Sønderholm and Tirsgaard (Frederiksen et al., 1999; Smith and Robertson, 1999; Sønderholm and Tirsgaard, 1993).

Evidence for Polyphase Deformation in the Tindern Allochthon

The deformational history of the Tindern allochthon, as outlined by White et al. (in press), was primarily based on structural information from the Nathorst Land Group. Here we integrate that history with new observations from the Upper Eleonore Bay Supergroup to define a more complete deformational history and sequence of faulting. We note that we were unable to connect structures mapped on the south side of Segelsällskapets Fjord with structures on the north side. This implies that there may be additional structural complexity that lies hidden in the fjord.

The dominant S_1 cleavage defined by fine-grained white mica was formed during the first phase of deformation, $\mathbf{D_1}$ (corresponding to D_{1T} in White et al., in press). This cleavage does not always parallel the bedding. Mineral lineations are apparent near the base of the sequence; however, the fact that they are randomly oriented led White et al. (in press) to interpret this deformation as related to flattening. The preservation of D_1 fabrics is primarily restricted to the lowermost 3 km of the Nathorst Land Group. There are some additional E-W trending L_1 mineral lineations that we observed in a member of the Ymer Ø Group (~12 km structurally above the Tindern detachment). Although it

remains ambiguous whether these formed during D_1 or a subsequent phase of deformation, it is clear that they pre-date D_2.

Following initial flattening, bedding was transposed into parallelism with an S_2 schistosity defined by very fine-grained white-mica in mudstones from the Upper Nathorst Land, Lyell Land and Ymer Ø Groups. The approximate NW-SE strike and NE dip of this planar fabric is consistent throughout the Tindern allochthon (Figure 4). During this phase of deformation, E-W contraction formed broad (> 1-2 kilometer wavelength) open folds with N-S trending hinge lines. There is no evidence for the orogen-parallel shear that is so apparent in the D_2 strain fabrics found in the Høgedal allochthon. However, smaller-scale F_2 folds deform the S_1 cleavage. The L_1 lineation found in the Ymer Ø Group was seen to wrap around F_2 fold axes that deform the S_1 schistosity. Small-displacement, E-dipping reverse faults are occasionally found in the Upper Eleonore Bay Supergroup, We interpret these as D_2 structures.

D_2 structures were overprinted by synorogenic extension along the Tindern detachment. $\mathbf{D_3}$ (corresponding to D_{3T}) fabrics are related to activity along this low-angle, E-dipping fault. The development of D_3 lineations and schistosities are restricted to the zone of shear associated with the detachment itself. Several of the overlying brittle normal faults are similar in geometry to the Tindern detachment. These low-angle faults have been interpreted as an extensional fan complex associated with Tindern detachment activity (Figure 5; White et al., in press). It has not been possible to connect units across these faults. Antithetic, high-angle, D_3 west-dipping brittle faults sole into these shallower E-dipping low-angle structures at Randenæs. There is no evidence that these steep, W-dipping faults penetrate to deeper structural levels. At shallower structural

levels within the Eleonore Bay Supergroup, these high-angle, W-dipping faults truncate and displace the D_2 reverse faults.

The deformation that followed D_3 (corresponding to D_{4t}) can be subdivided into two stages of diachronous activity based on the relative sequence of faulting that we observed in the upper section of the Nathorst Land Group and Upper Eleonore Bay Supergroup. **D_4** is characterized by low-angle west-dipping faults that displace the high-angle D_3 west-dipping faults up to several hundred meters. These faults penetrate to the basal levels of the EBS (Figures 2 and 5). However, they do not appear to penetrate to deeper structural levels from which we interpret that they sole into the Tindern detachment. There are two significant D_4 structures. This first is called the Fangsthyttegletscher fault after Watt *et al.* (1999), and crops out near the top of the mountains on the east side of Alpefjord (Figures 2 and 6). We note that while Watt *et al.* (1999) drew the Fangsthyttegletscher fault as subvertical on their cross-section, the angle of the shear zone as we determined it using S-C fabric measurements from a mylonitized granite (average strike and dip of S planes = 244°, 22°NW; C planes = 236°, 38° NW) was consistent with other low-angle D_4 faults. This top-to-the-west fault juxtaposes the Lower Nathorst Land Group next to the Kap Alfred Formation of the Ymer Ø Group (nomenclature after Sønderholm and Tirsgaard, 1993, and Smith and Robertson, 1999). Estimating tectonostratigraphic throw on this fault is complicated by an additional, high angle, D_3, W-dipping fault and three low-angle, D_4, W-dipping faults that all intersect to affect the total apparent displacement across the Fangsthyttegletscher fault. The combined minimum tectonostratigraphic throw of these five faults at the present-day surface position of the Fangsthyttegletscher fault is ~6.5 km. However, based on reconstructing the cross-section shown in Figure 6, we estimate net slip along the Fangsthyttegletscher fault of ~4.5 km. The second significant D_4 fault crops out east of

the Fangsthyttegletscher fault, cutting the walls of the valley just north of the Skjoldungebræ Glestcher. We estimate net slip on this fault of ~5 km.

D_4 extension was overprinted by a complex system of multiple faults that we associate with **D_5** sinistral, strike-slip deformation. There are two major generations of brittle faults that comprise this system. The first are high-angle E-W striking, N- and S-dipping faults that displace all previous structures. In addition, there is a second set of faults that are subvertical and strike ~N-NW to S-SE. Kinematic indicators, such as slickensides, are preserved on the subvertical fault planes and indicate left-lateral strike-slip movement. These faults truncate Devonian conglomerate deposits that lie unconformably on top of the Andrée Land Group at Aakerbloms Ø, an island at the junction of Segelsällskapets and Kong Oscar's Fjord. Given that the Høgedal detachment is a large Devonian-aged tectonic structure that lies beneath these faults (White and Hodges, submitted), we suggest that the D_5 faults most likely sole into the Høgedal detachment at depth.

Reconstructing Extension in the Tindern Detachment Hanging-wall

Given the abundant evidence for small-scale brittle normal faults in the hanging-wall of the Tindern detachment, our goal was to determine the magnitude of this extension in order to determine its relative importance with respect extension along the underlying Tindern detachment. Figure 6a depicts a simplified cross-section of the Tindern allochthon from A-B on Figure 2. Because of the strike-slip nature of the D_5 faults, it is not possible to reconstruct a balanced cross-section; it is also not possible to estimate slip within the extensional fan complex just above the Tindern detachment because we could not match units across the faults. However, our cross-section is retro-

deformable above this structural level, allowing us to estimate an apparent horizontal extension across the allochthon of ~22%. Most of this extension was accommodated along a D_3 fault (net slip of ~1.5 km) and the D_4 Fangsthyttegletscher and Skjoldungebræ faults (net slip of ~4.5 and ~5 km respectively). However, in terms of vertical thinning above the Tindern detachment where it crops out in Forsblad Fjord, our retro-deformable cross-section indicates that the hanging-wall accommodated only about 5 km of crustal thinning. While our analysis indicates that the amount of thinning in the Eleonore Bay Supergroup at structural levels above the Tindern detachment was non-trivial, it is less than a third of the total estimated thinning related to slip on the Tindern detachment itself, and a sixth of the total estimated tectonostratigraphic throw on the FRD system (White and Hodges, in preparation).

$^{40}Ar/^{39}Ar$ Thermochronology

Given the complex polyphase deformational history experienced by the Tindern allochthon, absolute age constraints on the timing of these events are necessary in order to put the deformation into a tectonic context. Previous geochronologic data constrain the timing of high-temperature D_3 deformation along the Tindern detachment from ca. 425-423 Ma (White et al., in press), thus bracketing the minimum age of D_1 and D_2. Furthermore, the fact that D_5 faults cut-across Devonian conglomerates places a bracket on the maximum age of D_5 to the Devonian time-period. To investigate the timing of the additional brittle D_3 and D_4 structures, $^{40}Ar/^{39}Ar$ thermochronology on K-feldspar was used to explore the age and rate of cooling from 300° to 150° C (Lovera et al., 1991). Samples were collected from four leucogranites and a late-stage pegmatite dike, described by White *et al.* (in press) and White and Hodges (submitted) to maximize the structural breadth of our data (Figure 2). Because we found no granite intrusions above

the Nathorst Land Group, most of our data reflects cooling age information from structural levels that lie beneath the Tindern detachment and overlying D_3-D_4 faults. Within this limitation, our data are still able to provide some of the best absolute age constraints that are available to bracket the timing of deformation on the upper level structures.

Analytical Procedure

The crux of the $^{40}Ar/^{39}Ar$ geochronology that we present in this paper depends on the assumptions embodied in the multiple diffusion domain theory of Lovera et al. (Lovera et al., 1989). Essentially, we performed step heating experiments on K-feldspar using the analytical methods described by White and Hodges (submitted) to measure the diffusive loss of ^{39}Ar over a range of temperature increments. Heating schedules are included in the appendix. The data were then inverted to model a range of time-temperature histories with a variety of diffusion domain sizes and volumes in order to reproduce most accurately, the measured ^{39}Ar diffusive loss spectra. One important point to mention is that the multiple diffusion domain theory of Lovera et al. (1989) depends critically upon the assumption that the feldspar cooled monotonically. As discussed by White and Hodges (submitted), there are no late-stage intrusions near the granites that we sampled nor any other evidence to suggest a late thermal spike; thus, this seems like a reasonable assumption.

Minerals were separated using standard gravimetric and magnetic techniques, and hand-picked for purity and uniform grain size. Samples were irradiated in the McMaster University reactor in Ontario, Canada. The fast neutron flux was monitored using a combination of MMhb-1 (518.53 Ma) and GA1550 (98.56 Ma) standards (inter-

calibrated against Fish Canyon tuff sanidine using the age of 28.02 reported by Renne et al. (1998), and synthetic salts were used to correct for interfering nuclear reactions. All analytical work was performed at the MIT Cambridge Laboratory for Argon Isotope Research following methods reported in White and Hodges (submitted). Gases were analyzed on an MAP 215-50 Mass spectrometer using a Faraday cup. Data were reduced using the constants recommended by Steiger and Jäger (1977); all analytical uncertainties, associated with both measured and blank data, were propagated through the calculations and are reported at 2σ.

K-feldspar Results:

Sample **98GR36** came from a peraluminous granite sill ~4 kilometers above the Høgedal detachment and ~11 kilometers below the Tindern detachment. The age-spectra display a "double-saddle" geometry (Figure 7a) that might be attributable to degassing of excess ^{40}Ar from multiple Cl-rich fluid inclusions with different Ar retentivities (Harrison et al., 1994) and high-temperature degassing of excess ^{40}Ar trapped in anion vacancies (Zeitler, 1987). Our modeling attempts resulted in a range of time-temperature histories that reasonably reproduce the sample's kinetic parameters (E_a and D_O/r^2) as derived from an Arrhenius plot (Figure 7b), and predict $log\ r/r_0$ (a measure of relative diffusion domain size, Figures 7c) and age spectrum plots (Figure 7a) comparable to those exhibited by the sample during the experiment for temperatures beneath the incongruent melting point of K-feldspar. After inversion of the ^{39}Ar release data, the modeled time-temperature path is robust over a time period that extends from ca. 415 Ma to 330 Ma and a temperature range ~340° to 170° C (Figure 7d). Over this interval , the K-feldspar data suggest relatively slow, steady cooling at a rate of ~2° C/my. Backwards projection of this time-

temperature path is generally consistent with previously reported muscovite and biotite $^{40}Ar/^{39}Ar$ analyses from the same structural horizon (White and Hodges, submitted).

Our next two samples were collected ~10 kilometers structurally above **98GR36**, from the syn-D_3 Caledonia Ø Pluton (White et al., in press). This pluton is distinguished because of its synkinematic structural relationship with the Tindern detachment and its striking visual appearance defined by an abundance of biotite schlieren and feldspar augen, all having been subjected to varying degrees of deformation. The feldspar that we analyzed was selected from the least deformed portions of the granite.

Ages increased monotonically with increasing temperature in the release spectrum for K-feldspar from **98GR23** (the structurally lower of the two samples). On the other hand, **97GR18** yielded a saddle-shaped spectrum somewhat similar to that of **98GR36**, suggesting slight contamination with excess ^{40}Ar. In addition, diffusion parameters derived from this experiment suggest that 97GR18 feldspar is considerably more retentive of Ar than 98GR23 feldspar (E_a = 56.7 kCal/mol vs. E_a = 44.7 kCal/mol). This difference has ramifications on the range of temperatures selected in the time-temperature histories that were used for our inversion modeling (Figures 8a, 9a): the most robust time-temperature path for **97GR18** ranges from 410 Ma to 320 Ma and 450° to 200° C; **98GR23** ranges from 410 Ma to 250 Ma and 320° to 145° C. Figures 8d and 9d show these model time-temperature paths with previously obtained muscovite and biotite $^{40}Ar/^{39}Ar$ dates from the same respective structural horizons (White and Hodges, submitted). While a backwards projection of the K-feldspar data from **98GR23** is consistent with the older thermochronologic data, the path of **97GR18** appears to be shifted upwards relative to the position of the muscovite data, implying that the E_a may be overestimated. In spite of this unresolved complexity, both samples yielded time-

temperature paths with knickpoints at ca. 390 Ma. Thus, the K-feldspar data from **97GR18** suggest that rapid cooling at about 9° C/my was followed by slow cooling at ~1° C/my while the data from **98GR23** suggest that rapid cooling at ~6° C/my was followed by slow cooling at ~0.5° C/my.

In addition to the above samples, we analyzed K-feldspar from an undeformed pegmatite (**98GR28**) that cuts the Caledonia Ø pluton. The age spectrum (Figure 10a) indicates degassing of excess ^{40}Ar at low temperatures. Inversion of the ^{39}Ar release-data yielded a time-temperature history (Figure 10a) spanning 410 Ma to 310 Ma and 400° to 200° C. This model time-temperature path also has a knickpoint at ca. 390 Ma, indicating that rapid cooling (~6.5° C/my) was followed by slower cooling (~1°C/my). Furthermore, backward projections of this cooling path in time-temperature space intersect with previously obtained muscovite $^{40}Ar/^{39}Ar$ data for the same sample (White and Hodges, submitted).

The final feldspar (**98GR17**) was collected from the undeformed Klosterbjerg Granite (White et al., in press). The spectrum from this retentive sample (E_a = 57.9 kCal/mol) indicates that excess ^{40}Ar was degassed during the low temperature heating steps (Figure 11a). The time-temperature inversion model calculated from the kinetic parameters and ^{39}Ar release data yielded diffusion information spanning temperatures from 422° to 120° C and ages from 420 Ma to 280 Ma (Figure 11d). Again, we note the presence of a knickpoint in the modeled cooling path; however, the time associated with the change in cooling rate (from ~12°C/my to ~0.25° C/my) lies at ca. 400 Ma, about 10 My older than the knickpoints in model time-temperature paths for **97GR18**, **98GR23**, and **98GR28**. Projecting the early portions of this cooling trajectory backwards in Tt

space, it also intersects with previous muscovite and biotite $^{40}Ar/^{39}Ar$ data for 98GR17 (White and Hodges, submitted).

Interpretation of K-feldspar Data

Three characteristics of the multi-domain diffusion models for these K-feldspars provide important clues to the tectonic significance of the $^{40}Ar/^{39}Ar$ data presented here. First, all samples collected near the Tindern detachment yielded time-temperature paths characterized by an early phase of moderately fast cooling followed by an abrupt transition to cooling at a much slower rate. The timing of this transition migrates from older to younger ages with increasing structural depth. Moreover, the rate of cooling over the early segments of the cooling curves is higher for shallower structural levels and lower for deeper structural levels. The one sample collected far (~11 km) below the Tindern detachment (**98GR36**) exhibits no time-temperature knickpoint at all.

We infer that the knickpoints for the samples collected near the Tindern detachment imply a change in cooling rate related to tectonic processes. The migration of these knickpoints to younger ages with increasing depth implies a directional component to the mechanism responsible for this transition and a lag-time in the thermal response with distance from the source. The decrease in early cooling rates with increasing depth reinforces this interpretation. Following these arguments and the expected topology of time-temperature paths associated with tectonic denudation (Ruppel et al., 1988), we infer that the oldest (and structurally shallowest; **98GR17**) knickpoint of ca. 400 Ma represents the approximate end of the tectonic denudation by slip on overlying "Caledonian" extensional faults. In addition, we infer that the steady rate of cooling over

the 420-400 Ma interval reflects more-or-less continual denudation by slip on these structures.

Implications for extension in East Greenland

Although the high temperature (greater than ~356° C) deformation on the Tindern detachment has been well constrained to within 425-423 Ma (coeval with the Baltica-Laurentia collision), our new data indicate that the hanging wall continued to extend until roughly ca. 400 Ma, producing an additional ~22% extension. Based on our interpretation of the structural evidence, we suggest that the geometry of these normal faults was controlled by the Tindern detachment inasmuch as we can determine that they sole into it. If we subtract the 5 kilometers of vertical denudation due to thinning of the Eleonore Bay Supergroup from the total tectonostratigraphic throw implicated by thermobarometric data from the Tindern detachment footwall (White and Hodges, in preparation), the result implies that the remaining 13 kilometers of tectonostratigraphic throw occurred over a 2 million year time interval at a time-averaged rate of ~6.5 millimeters per year. Furthermore, if the 5 kilometers of thinning in the Eleonore Bay Supergroup occurred for a duration of ~20 to ~25 million years, then this implies time-averaged rates of ~0.25 to ~0.2 millimeters per year. This line of reasoning suggests that synorogenic activity on the Tindern detachment began ca. 425 Ma, removed a large amount of material over a brief (~ 2 my interval), but persisted at high structural levels at a much slower rate for an additional 20-25 million years.

At some time following deep-seated movement on the Tindern detachment and prior to the next major episode of crustal thinning that occurred along the Høgedal detachment (417 to 380 Ma; White and Hodges, submitted), White *et al.* (in press) argued

from the relative ages of metamorphism in adjacent allochthons that an underlying thrust fault with significant throw placed the Høgedal allochthon on top of the Hagar-Niggli Spids allochthon. This thrust fault was excised by slip on the Høgedal detachment, constraining its activity to between ca. 425 Ma and the inititation of slip of the Høgedal shear, which indicates that middle-crustal thickening was roughly coeval with upper-crustal extension in the Tindern allochthon as constrained by the $^{40}Ar/^{39}Ar$ data presented in this paper. Furthermore, to allow for this thrusting to occur at reasonable geologic rates, White and Hodges (in preparation) argued that the Høgedal detachment must have become active later rather than sooner within the loose geochronologic brackets that constrain its activity. Given that evidence from the Scandinavian Caledonides indicates the Baltica-Laurentia collision had stopped by ca. 402 Ma (Fossen and Dallmeyer, 1998), it is likely that most if not all deformation on the Høgedal detachment was post-kinematic with respect to the Baltica-Laurentia collision.

Conclusions

The past decade of structural and geochronologic investigations in central East Greenland has led to the identification of syn- and post-orogenic normal fault activity along the Fjord Region Detachment system. The timing and lateral extent of these structures demonstrate that crustal thinning was an active process throughout much of Caledonian orogenesis. In this paper, we have presented new structural observations and $^{40}Ar/^{39}Ar$ data from K-feldspar that outline the sequence of deformation in-between the major episodes of syn- and post-orogenic extension on the Fjord Region Detachment. Our reconstructions indicate that the Tindern detachment hanging-wall was extended by a minimum of ~ 22%. Based on our models of K-feldspar ^{39}Ar loss from a suite of samples that span ~12 kilometers of structural thickness, we have argued that this extension

(accounting for 5 kilometers of denudation above the present outcrop of the Tindern detachment) occurred from ca. 425 Ma to 400 Ma. Our results and previously reported data (White and Hodges, submitted; White and Hodges, in preparation; White et al., in press) imply that 13 kilometers of tectonostratigraphic throw on the Tindern detachment occurred rapidly at a minimum time-averaged rate of ~6.5 mm/yr, while the remaining 5 kilometers could have been removed as slowly as ~0.2 mm/yr as strain was partitioned in the hanging-wall along antithetic normal faults.

Collectively, the structural and geochronologic data imply that most of the extension in this section of the East Greenland Caledonides was accommodated by brief episodes of slip on the FRD system. The significant activity was partitioned into an episode of synorogenic activity on the Tindern detachment and post-orogenic activity on the Høgedal detachment. However, protracted upper crustal extension over a 25 million year period was roughly coeval with middle-crustal thickening. From this, we infer, that the simple collapse model proposed by McClay et al. (1986) is inadequate to explain the structures that we observed. However, we suggest that our observations are consistent with an overthickened Caledonian crustal welt that partially thinned during orogenesis, only to continue being rebuilt until its eventual collapse following the Baltica-Laurentia collision.

Acknowledgements

This research was part of a collaborative effort between the Department of Earth, Atmospheric and Planetary Sciences at MIT and the University of Oslo in Norway. Funding for this study was provided by National Science Foundation grant EAR 930072 (to K.V. H.). We wish to thank the Greenland Geological Survey, Danish Polar Center,

Sirius Patrol, A. Andresen, E. Hartz, N. Henriksen, J. Kaufman, J. Hurtado and L. Schoenbohm for logistical assistance. We would particularly like to thank W. Olszewski and E. Kirby for advice in the laboratory.

References:

Andresen, A., Hartz, E.H., and Vold, J., 1998, A late orogenic extensional origin for the infracrustal gneiss domes of the East Greenland Caledonides (72-74 N): Tectonophysics, v. 285, p. 353-369.

Andresen, A., and Steltenpohl, M.G., 1994, A reevaluation of nappe sequences in the Ofoten-Troms region, north Norwegian Caledonides: Implications for terrane accretion, ophiolite obduction, and polyorogenic evolution: Tectonophysics, v. 231, p. 59-70.

Christoffersen, M., 1984, Scoresby Sund: Denmark, Grønlands Geologiske Undersøgelse.

Elvevold, S., Escher, J.C., Frederiksen, K.S., Friderichsen, J.D., Gilotti, J.A., Henriksen, N., Higgins, A.K., Jepsen, H.F., Jones, K.A., Kalsbeek, F., Kinny, P.D., Leslie, A.G., Robertson, S., Smith, M.P., Thrane, K., and Watt, G.R., 2000, Tectonic architecture of the East Greenland Caledonides 72° - 74°30' N, Danmarks og Grønlands Gelogiske Undersøgelse Rapport, Volume 88: Denmark, Geological Survey of Denmark and Greenland, p. 34.

Escher, J.C., and Jones, K.A., 1999, Caledonian geology of Frænkel Land and adjacent areas (73°00'-73°30'N), East Greenland, *in* Higgins, A.k., and Frederiksen, K.S., eds., Geology of East Greenland 72°-75°, mainly Caledonian: preliminary reports from the 1998 expedition: Denmark, Danmarks og Grønlands Geologiske Undersøgelse Rapport.

Fossen, H., and Dallmeyer, R.D., 1998, (super 40) Ar/ (super 39) Ar muscovite dates from the nappe region of southwestern Norway; dating extensional deformation in the Scandinavian Caledonides: Tectonophysics, v. 285, p. 119-133.

Frederiksen, K.S., Craig, L.E., and Skipper, C.B., 1999, New observations of the stratigraphy and sedimentology of the Upper Proterozoic Andrée Land Group, East Greenland: supporting evidence for a drowned carbonate ramp, *in* Higgins,

A.K., and Frederiksen, K.S., eds., Geology of East Greenland 72°-75° N, mainly Caledonian: preliminary reports from the 1998 expedition, Volume 19: Denmark, Danmarks og Grønlands Geologiske Undersøgelse Rapport, p. 145-158.

Gee, D.G., 1975, A tectonic model for the central part of the Scandinavian Caledonides: American Journal of Science, v. 275A, p. 468-515.

Haller, J., 1971, Geology of the East Greenland Caledonides: New York, Interscience Publishers, 413 p.

Harrison, T.M., Heizler, M.T., Lovera, O.M., Chen, W., and Grove, M., 1994, A chlorine disinfectant for excess argon released from K-feldspar during step heating: Earth and Planetary Science Letters, v. 123, p. 95-104.

Hartz, E., and Andresen, A., 1995, Caledonian sole thrust of central East Greenland: A crustal-scale Devonian extensional detachment?: Geology, v. 23, p. 637-640.

Henriksen, N., 1985, The Caledonides of central East Greenland 70 degrees -76 degrees N, *in* Gee, D.G., and Sturt, B.A., eds., The Caledonide Orogen — Scandinavia and Related Areas, Volume 2: Chichester, U.K., John Wiley & Sons, p. 1095-1113.

Henriksen, N., and Higgins, A.K., 1976, East Greenland Caledonian fold belt, *in* Escher, A., and Watt, W.S., eds., Geology of Greenland: Copenhagen, DK, The Geological Survey of Greenland, p. 183-246.

Hodges, K.V., Bartley, J.M., and Burchfiel, B.C., 1982, Structural evolution of an A-type subduction zone, Lofoten-Rombak area, northern Scandinavian Caledonides: Tectonics, v. 1, p. 441-462.

Leslie, A.G., and Higgins, A.K., 1999, On the Caledonian (and Grenvillian) geology of Bartholin Land, Ole Rømer Land and adjacent nunataks, East Greenland, *in* Higgins, A.k., and Frederiksen, K.S., eds., Geology of East Greenland 72°-75°, mainly Caledonian: preliminary reports from the 1998 expedition: Denmark, Danmarks og Grønlands Geologiske Undersøgelse Rapport, p. 220.

Lovera, O.M., Richter, F.M., and Harrison, T.M., 1989, $^{40}Ar/^{39}Ar$ geochronometry for slowly cooled samples having a distribution of diffusion domain size: Journal of Geophysical Research, v. 94, p. 17917-17936.

Lovera, O.M., Richter, F.M., and Harrison, T.M., 1991, Diffusion domains determined by ^{39}Ar released during step heating: Journal of Geophysical Research, v. 96, p. 2057-2069.

McClay, K.R., Norton, M.G., Coney, P., and Davis, G.H., 1986, Collapse of the Caledonian orogen and the Old Red Sandstone: Nature, v. 323, p. 147-149.

Peucat, J.J., Tisserant, D., Caby, R., and Clauer, N., 1985, Resistance of zircons to U-Pb resetting in a prograde metamorphic sequence of Caledonian age in East Greenland: Canadian Journal of Earth Sciences, v. 22, p. 330-338.

Renne, P.R., Swisher, C.C., Deino, A.L., Karner, D.B., Owens, T.L., and DePaolo, D.J., 1998, Intercalibration of standards, absolute ages and uncertainties in (super 40) Ar/ (super 39) Ar dating: Chemical Geology, v. 145, p. 117-152.

Ruppel, C., Royden, L., and Hodges, K.V., 1988, Thermal modeling of extensional tectonics: application to pressure-temperature-time histories of metamorphic rocks.: Tectonics, v. 7, p. 947-957.

Smith, M.P., and Robertson, S., 1999, The Nathorst Land Group (Neoproterozoic) of East Greenland - lithostratigraphy, basin geometry and tectonic history, *in* Higgins, A.k., and Frederiksen, K.S., eds., Geology of East Greenland 72°-75°, mainly Caledonian: preliminary reports from the 1998 expedition: Denmark, Danmarks og Grønlands Geologiske Undersøgelse Rapport, p. 220.

Sønderholm, M., and Tirsgaard, H., 1993, Lithostratigraphic framework of the Upper Proterozoic Eleonore Bay Supergroup of East and North-East Greenland: Grønlands Geologiske Undersøgelse, v. 167.

Steiger, R.H., and Jäger, E., 1977, Subcommission on geochronology: convention on the use of decay constants in geo- and cosmochronology: Earth and Planetary Science Letters, v. 36, p. 359-362.

Sturt, B.A., and Thon, A., 1978, An ophiolite complex of probable early Caledonian age discovered on Karmoy: Nature (London), v. 275, p. 538-539.

Vidal, G., 1976, Late Precambrian acritarchs from the Eleonore Bay Group and Tillite Group in East Greenland; a preliminary report, Rapport - Groenlands Geologiske Undersoegelse, p. 19.

Vidal, G., 1979, Acritarchs from the upper Proterozoic and Lower Cambrian of East Greenland, Bulletin - Gronlands Geologiske Undersogelse, p. 37.

Watt, G.R., and Friderichsen, J.D., 1999, Further remarks on Caledonian anatexis in the Stauning Alper migmatite zone, East Greenland Caledonides, *in* Higgins, A.K., and Frederiksen, K.S., eds., Geology of East Greenland 72°-75° N, mainly Caledonian: preliminary reports from the 1998 expedition, Volume 19: Denmark, Danmarks og Grønlands Geologiske Undersøgelse Rapport, p. 59-69.

White, A., and Hodges, K., submitted, Multi-stage dxtensional evolution of the central East Greenland Caledonides: .

White, A.P., and Hodges, K.V., in preparation, Pressure-temperature-time evolution of the Central East Greenland Caledonides: quanitative constraints on crustal thickening and synorogenic extension: .

White, A.P., Hodges, K.V., Martin, M.V., and Andresen, A., in press, Geologic constraints on middle-crustal behaviour during synorogenic extension in the East Greenland Caledonides: International Journal of Earth Science.

Zeitler, P.K., 1987, Argon diffusion in partially outgassed alkali feldspars: Insights from 40Ar/39Ar analysis: Isotope Geosci., v. 65, p. 167-181.

Appendix:

Heating schedules for 39Ar diffusion experiments on K-Feldspar have been appended below.

Figure Captions:

Figure 1: Simplified tectonic map of the central fjord region of the East Greenland Caledonides interpreted after Koch and Haller (1971), Henriksen and Higgins (1976), Peucat *et al.* (1985), Andresen *et al.* (1998a), White *et al.* (1998), Smith and Robertson (1999), Leslie and Higgins (1999), Escher and Jones (1999), White and Hodges (1999). The following abbreviations have been used: Forsblad Fjord (FF); Segelsällskapets Fjord

(SF); Alpefjord (AF); Kaiser Franz Joseph's Fjord (KFJF); Kong Oscar's Fjord (KOF); Furesø (F); Eleonore Sø (ES); Målebjorg (M); Niggli Spids (NS); Charcot Land (CL). *N.B.* Gåseland lies south to the south from this map. Box indicates study area. Question marks indicate unknown or enigmatic contacts, unexplained by past work in the region. We have interpreted the above thrust geometries based on correlations between the preliminary age relationships and fault contacts reported by the Greenland Geological Survey in 1999 and the earlier work of L. Koch, J. Haller and others as referenced above.

Figure 2: Simplified geologic map of the Forsblad-Segelsällskapets Fjord Region, East Greenland. Data for the topographic base was provided by the Geological Survey of Denmark and Greenland (GEUS). Fault lines are drawn with varying weights to indicate inferred importance. Note that the Klosterbjerg granite is included with the undifferentiated, Ordovician-Silurian granites. Location of cross-section in Figure 6 depicted by dashed line between **A** to **B**. Note that $^{40}Ar/^{30}Ar$ geochronology samples are located on this map. Also, Fangsthyttegletscher and Skjoldungebræ Glestcher have been included and the Tindern and Høgedal detachments have been marked separately. Structural data from the Hagar Niggli-Spids allochthon has been indicated by a subscripted **N**, while structural data from the Høgedal allochthon has been indicated by a subscripted **H** and the Tindern allochthon with a subscripted **T** as defined in White et al. (in press). Structural data are statistical averages of 10 to 100 measurements for each symbol presented.

Figure 3: Stratigraphic column of the Eleonore Bay Supergroup after Smith and Robertson (1999) and Sønderholm and Tirsgaard (1993). We have included the additional subdivisions that we used on our map. *There have been a variety of Formation names

used to describe these units over the past 70 years. The Formation names that we use represent the nomenclature used in the above mentioned publications.

Figure 4: Photographic panorama showing the northern wall of Forsblad Fjord, just east of Randenæs. The image has been warped to create the panoramic effect. Included in the image are rocks from the middle and upper Nathorst Land Groups to the Lower Lyell Land Group. Note on the western edge of the image, the uppermost D_3 E-dipping fault that comprises part of the extensional fan complex above the Tindern detachment. Above this fault are two generations of W-dipping faults. The high-angle D_3 W-dipping faults do not appear beneath the low-angle D_3 E-dipping fault from which we infer that they sole into it. On the other hand, the low angle D_4 W-dipping faults clearly displace the high-angle D_3 W-dipping faults and appear to displace the low-angle D_3 E-dipping fault on the south side of the fjord. We have shown this on the geometries extrapolated beneath the photographic panorama.

Figure 5: Photographic panorama showing the Upper Eleonore Bay Supergroup from the lower Lyell Land Group to the Lower Andrée Land Group. Note the tremendous exposure and large number of easily-observable high-angle D_3 W-dipping normal faults. This collage shows the north side of Segelsällskapets Fjord, east of Pohlemsdal.

Figure 6: Retro-deformable cross-section from **A** to **B** on Figure 2. The first frame depicts the present-day geometries as measured in outcrop. Eroded units are projected above the current topography assuming constant bed thickness. The second frame depicts the cross-section prior to D_5. D_5 faults are drawn in pink to show where they will deform the section. Note that we have no control on the strike-slip component of displacement on these D_5 faults. The next frame depicts the section prior to D_4 deformation. The final frame depicts the section prior to antithetic D_3 deformation in the hanging-wall of the

Tindern allochthon. However, as we cannot match beds across the E-dipping faults that comprise the extensional fan complex just above the Tindern detachment, this frame depicts deformation subsequent to any movement on those faults. Thus, this represents a period synkinematic with D_3 activity.

Figure 7: $^{40}Ar/^{39}Ar$ data from 98GR36. a) Release spectra showing both measured and modeled results. Note the disagreement between actual and modeled spectra only appears at temperature steps above the incongruent melting temperature for K-feldspar; thus this section of the curve should be dismissed. b) Arrhenius plot showing measured and modeled results. c) Log (r/r_0) plot showing measured versus modeled results. Note the close agreement between measured and modeled curves on both the Arrhenius and the log (r/r_0) plots. d) Plot showing the range of cooling path trajectories that are output from our K-feldspar model in time-temperature space. Included on the plot are biotite (98GR36) and muscovite (97GR60) $^{40}Ar/^{39}Ar$ ages and approximate cooling temperatures from the same structural horizon as this K-feldspar. See White and Hodges (submitted) for a discussion of the biotite and muscovite ages and closure temperatures. Note the consistency between the three data and the steady, gradual cooling curve that they depict.

Figure 8: $^{40}Ar/^{39}Ar$ data from 97GR18 — collected from the synkinematic Caledonia Ø granite. a) Release spectra showing both measured and modeled results. b) Arrhenius plot showing measured and modeled results. Note the close agreement between modeled and measured data. This curve implies a high activation energy as discussed in the text. c) Log (r/r_0) plot showing measured versus modeled results. d) Plot showing the range of cooling path trajectories that are output from our K-feldspar model in time-temperature space. Included on the plot is a muscovite (97GR18) $^{40}Ar/^{39}Ar$ age and approximate cooling temperature from the same sample as this K-feldspar. See White and

Hodges (submitted) for a discussion of the muscovite data. Note the inconsistency between the K-feldspar cooling curve and the muscovite data. Also, note the knickpoint at ca. 390 Ma in the K-feldspar t-T path.

Figure 9: $^{40}Ar/^{39}Ar$ data from 98GR23 — collected from the synkinematic Caledonia Ø granite. a) Release spectra showing both measured and modeled results. b) Arrhenius plot showing measured and modeled results. Note that the E_a implied by this curve is lower than that from 97GR18 as discussed in the text. c) Log (r/r_0) plot showing measured versus modeled results. d) Plot showing the range of cooling path trajectories that are output from our K-feldspar model in time-temperature space. Included on the plot are biotite (98GR23) and muscovite (98GR23) $^{40}Ar/^{39}Ar$ ages and approximate cooling temperatures from the same sample as this K-feldspar. See White and Hodges (submitted) for a discussion of the additional $^{40}Ar/^{39}$ Ar data. Note the apparent consistency between the K-feldspar cooling curve and the muscovite data. Also, note the knickpoint at ca. 390 Ma in the K-feldspar t-T path, similar to that of 97GR18 despite the inconsistency in the temperature associated with that time.

Figure 10: $^{40}Ar/^{39}Ar$ data from 98GR28 – a pegmatite dike that cuts the Caledonia Ø granite. a) Release spectra showing both measured and modeled results. b) Arrhenius plot showing measured and modeled results. c) Log (r/r_0) plot showing measured versus modeled results. d) Plot showing the range of cooling path trajectories that are output from our K-feldspar model in time-temperature space. Included on the plot is a muscovite (98GR28) $^{40}Ar/^{39}Ar$ age and approximate cooling temperature from the same sample as this K-feldspar. See White and Hodges (submitted) for a discussion of the muscovite data. Note the apparent consistency between the K-feldspar cooling curve and the

muscovite data. Also, note the knickpoint at ca. 390 Ma in the K-feldspar t-T path, similar to that of 97GR18 and 98GR23.

Figure 11: $^{40}Ar/^{39}Ar$ data from 98GR17. a) Release spectra showing both measured and modeled results. b) Arrhenius plot showing measured and modeled results. c) Log (r/r_0) plot showing measured versus modeled results. d) Plot showing the range of cooling path trajectories that are output from our K-feldspar model in time-temperature space. Included on the plot are biotite (98GR17) and muscovite (98GR17) $^{40}Ar/^{39}Ar$ ages and approximate cooling temperatures from the same sample as this K-feldspar. See White and Hodges (submitted) for a discussion of the additional $^{40}Ar/^{39}$ Ar data. Note the consistent cooling gradient defined by the K-feldspar cooling curve and the biotite and muscovite data from ~423 Ma to ~400 Ma. Also, note the knickpoint at ca. 400 Ma in the K-feldspar t-T path, ~10 million years older than the previous knickpoints mentioned. Finally, note how the steep portion of the cooling curve is actually steeper than that of 98GR28 which is steeper than that of 98GR23 and 97GR18 and 98GR36.

Figure 1

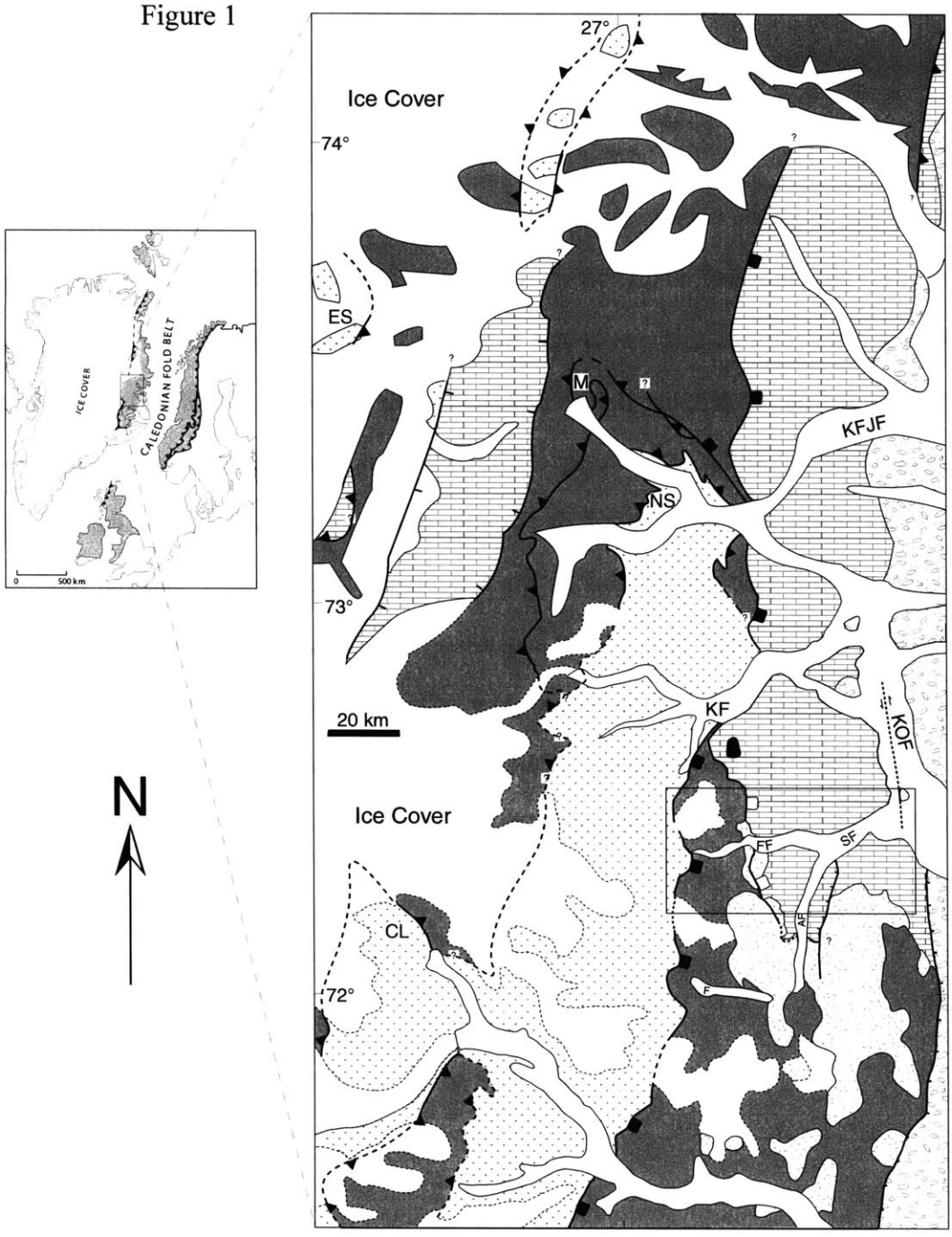
27°
Ice Cover
74°
ES
M
KFJF
NS
73°
20 km
KF
KOF
Ice Cover
FF
SF
AF
CL
72°
F
ICE COVER
CALEDONIAN FOLD BELT
0
500 km
N
Høgedal Detachment
Tindern Detachment
Thrust Fault
Normal Fault
Inferred Fault Contact
Lithologic Contact
Inferred Lithologic Contact
Devonian Carboniferous Basins
Caledonian Granitoid Plutons and Migmatitic Rocks
Neoproterozoic Eleonore Bay Supergroup
Mesoproterozoic - Neoproterozoic Metasedimentary Rocks
Archean - Paleoproterozoic Basement Complex

Figure 2

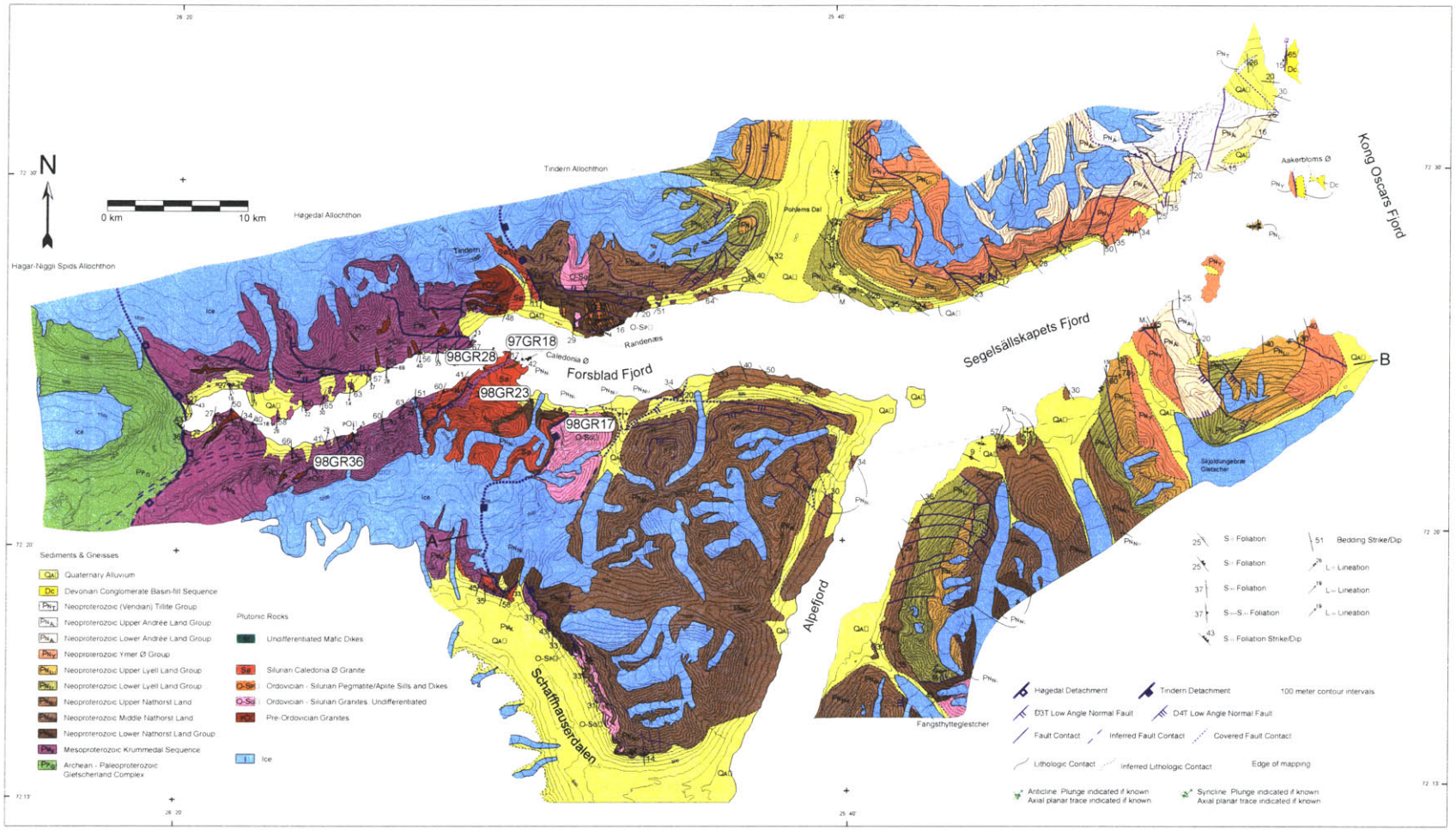

See CD attached to thesis.

Figure 3

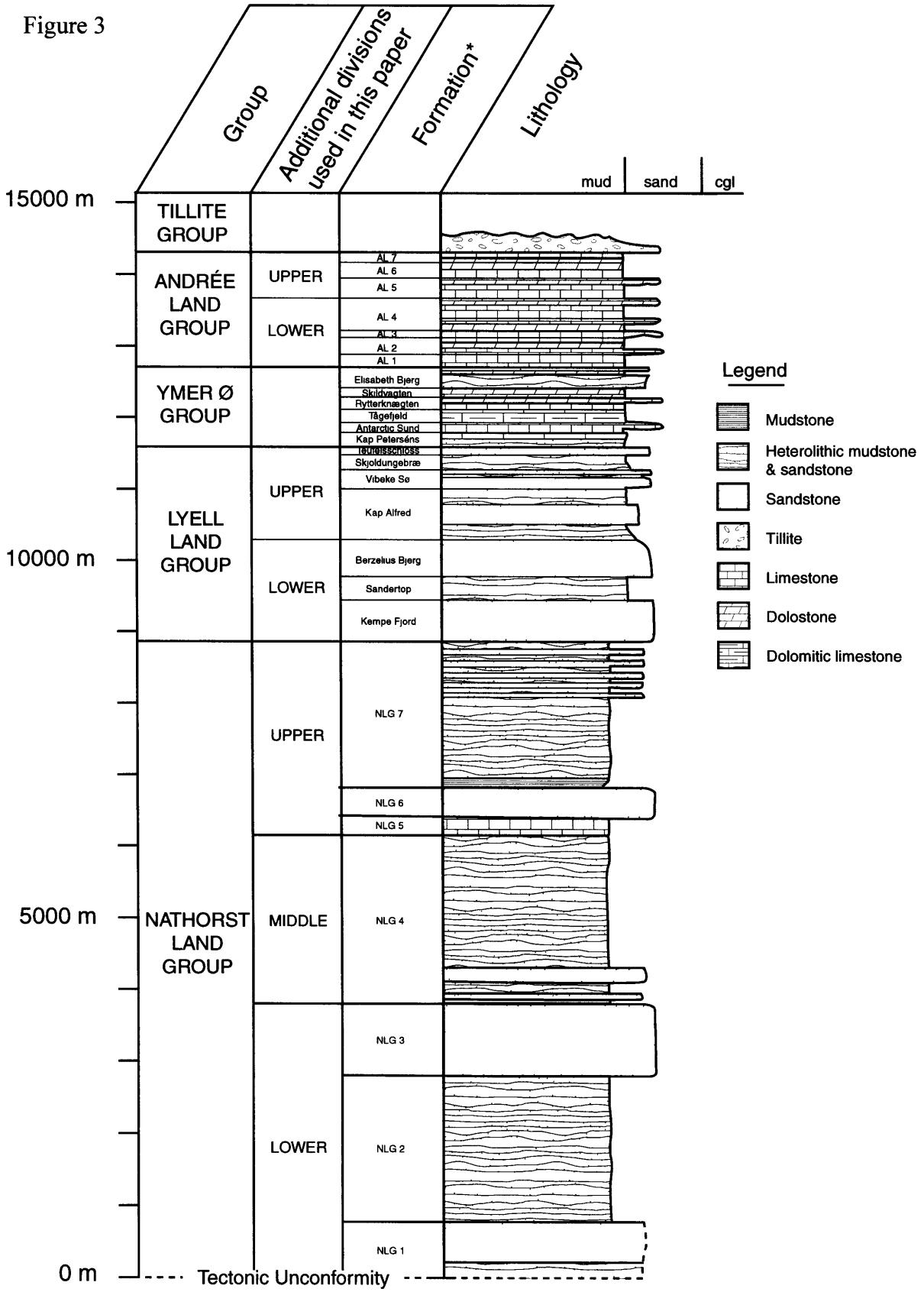
Group
Additional divisions used in this paper
Formation*
Lithology
mud
sand
cgl
15000 m
10000 m
5000 m
0 m
TILLITE GROUP
ANDRÉE LAND GROUP
UPPER
LOWER
AL 7
AL 6
AL 5
AL 4
AL 3
AL 2
AL 1
YMER Ø GROUP
Elisabeth Bjerg
Skildvagten
Rytterknægten
Tågefjeld
Antarctic Sund
Kap Peterséns
Teufelsschloss
LYELL LAND GROUP
UPPER
LOWER
Skjoldungebræ
Vibeke Sø
Kap Alfred
Berzelius Bjerg
Sandertop
Kempe Fjord
NATHORST LAND GROUP
UPPER
MIDDLE
LOWER
NLG 7
NLG 6
NLG 5
NLG 4
NLG 3
NLG 2
NLG 1
Tectonic Unconformity
Legend
Mudstone
Heterolithic mudstone & sandstone
Sandstone
Tillite
Limestone
Dolostone
Dolomitic limestone

Figure 4

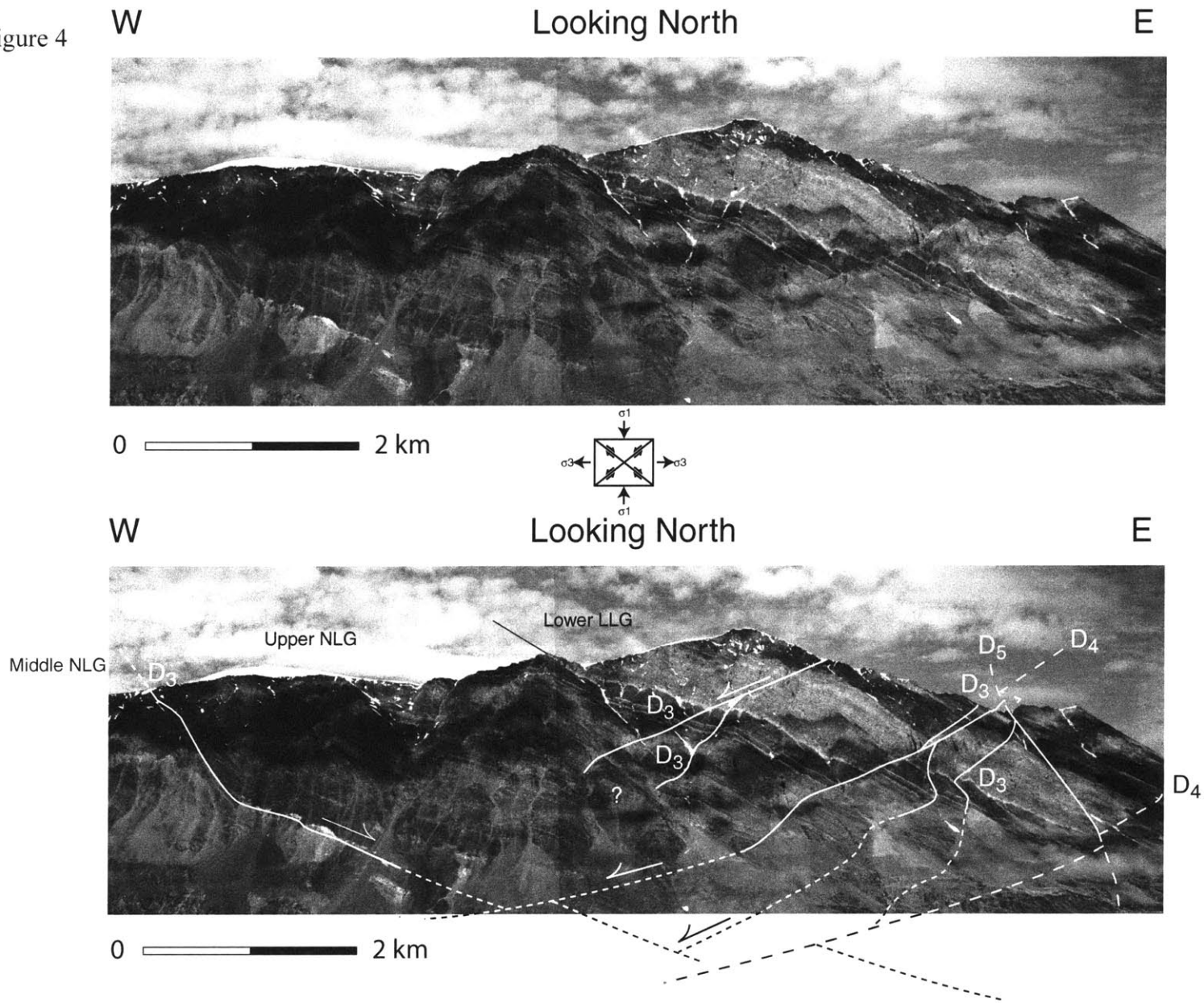
W
Looking North
E
0
2 km
σ1
σ3
σ3
σ1
W
Looking North
E
Middle NLG
Upper NLG
Lower LLG
D3
D3
D3
D3
D5
D3
D4
D4
?
0
2 km

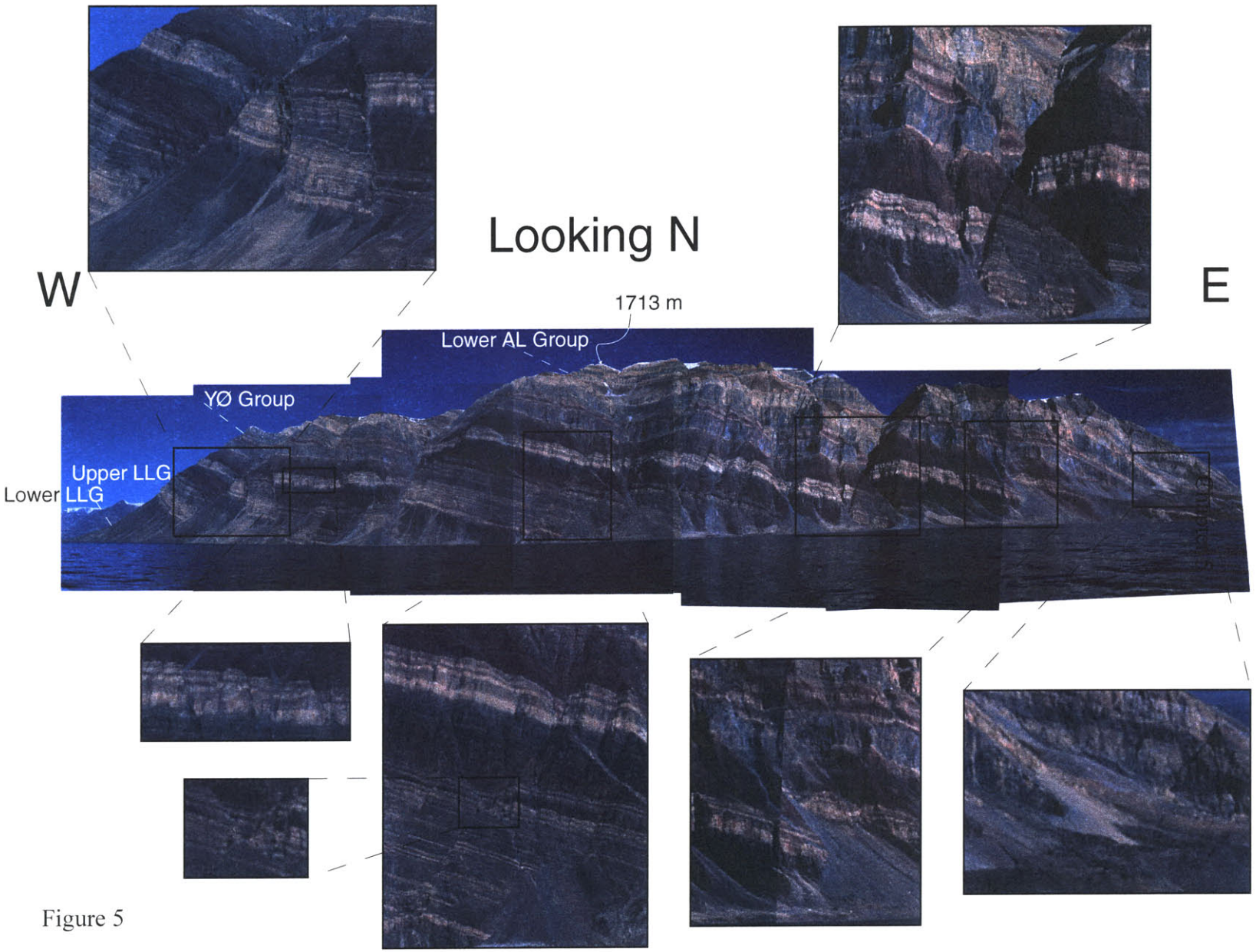
Looking N
W
E
1713 m
Lower AL Group
YØ Group
Upper LLG
Lower LLG

Figure 5

Figure 6

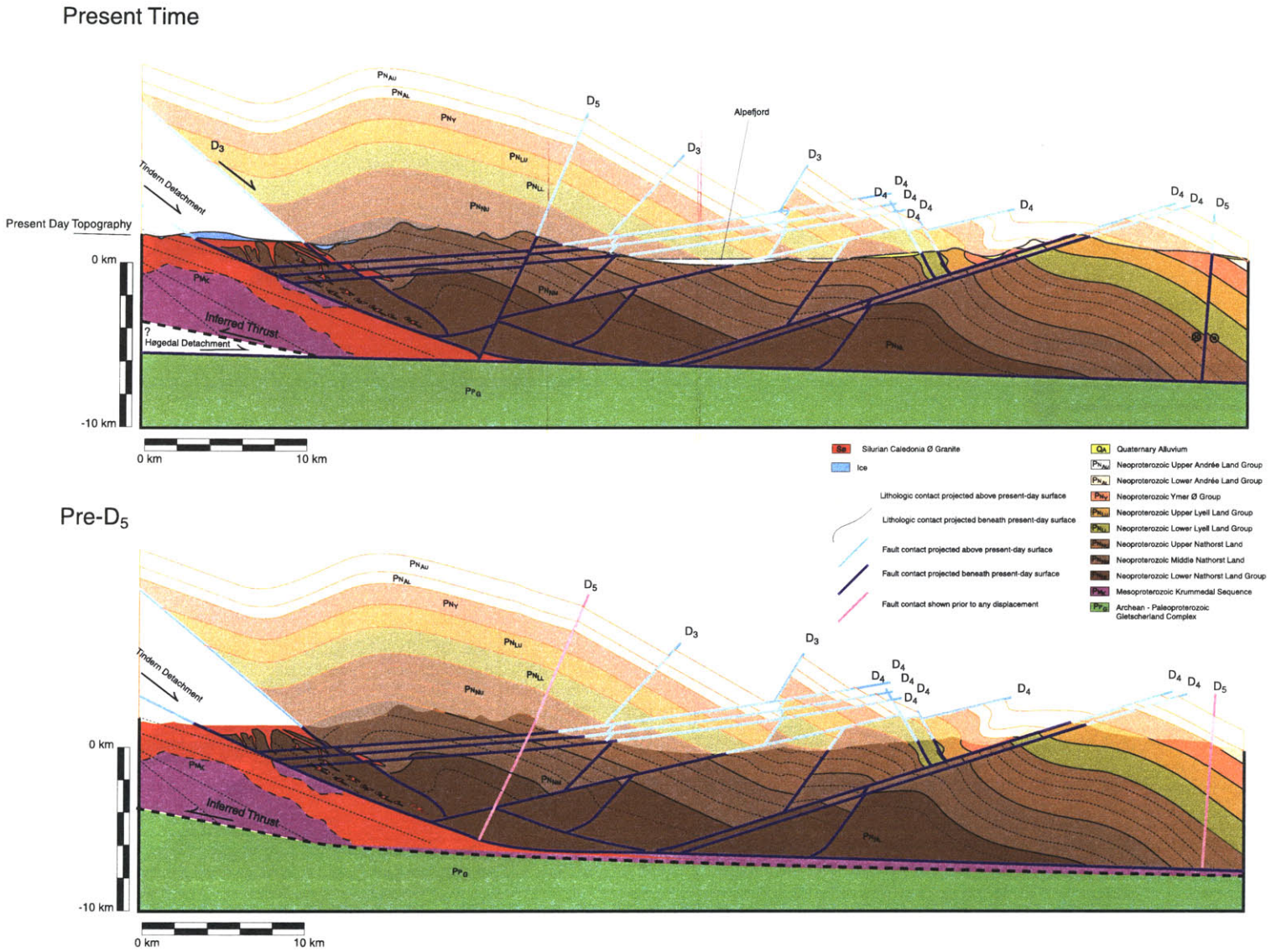
Present Time
Present Day Topography
0 km
-10 km
Tindern Detachment
Inferred Thrust
? Høgedal Detachment
Alpefjord
D3
D4
D5
0 km
10 km
Pre-D5
Tindern Detachment
Inferred Thrust
0 km
-10 km
0 km
10 km
Silurian Caledonia Ø Granite
Ice
Lithologic contact projected above present-day surface
Lithologic contact projected beneath present-day surface
Fault contact projected above present-day surface
Fault contact projected beneath present-day surface
Fault contact shown prior to any displacement
Quaternary Alluvium
Neoproterozoic Upper Andrée Land Group
Neoproterozoic Lower Andrée Land Group
Neoproterozoic Ymer Ø Group
Neoproterozoic Upper Lyell Land Group
Neoproterozoic Lower Lyell Land Group
Neoproterozoic Upper Nathorst Land
Neoproterozoic Middle Nathorst Land
Neoproterozoic Lower Nathorst Land Group
Mesoproterozoic Krummedal Sequence
Archean - Paleoproterozoic Gletscherland Complex

Figure 6 (continued)

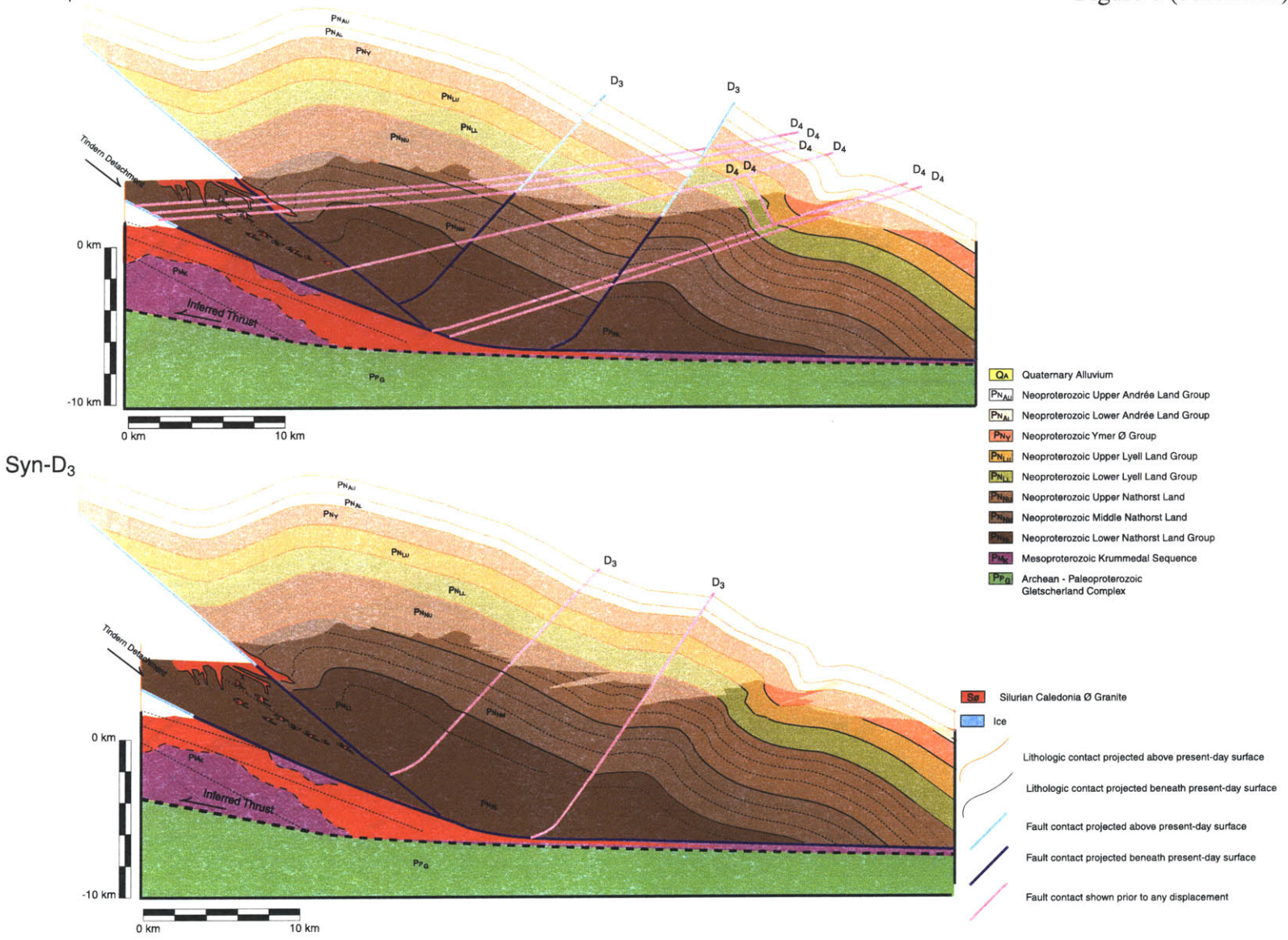

Figure 7

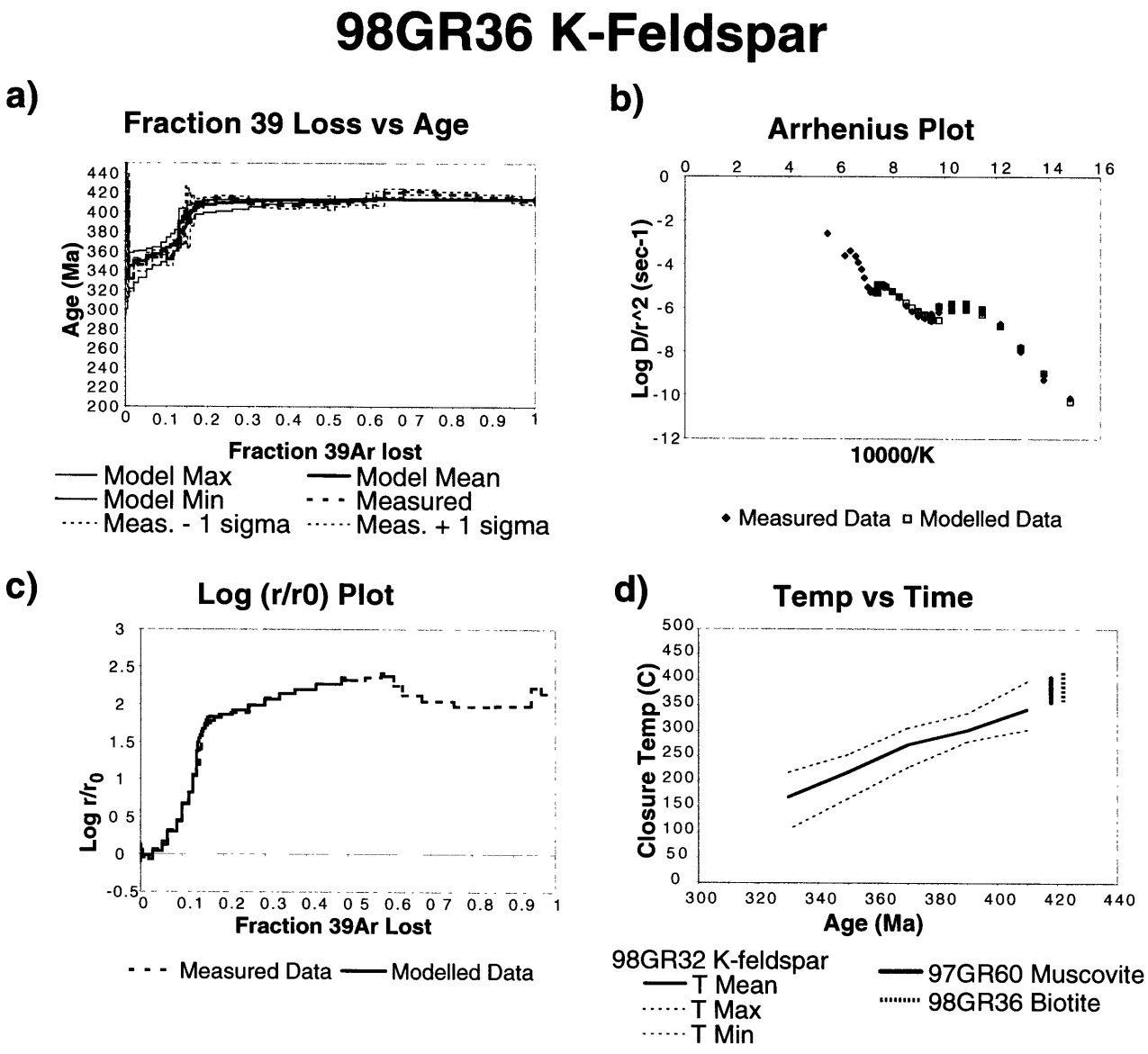
98GR36 K-Feldspar
a)
Fraction 39 Loss vs Age
Age (Ma)
Fraction 39Ar lost
Model Max
Model Mean
Model Min
Measured
Meas. - 1 sigma
Meas. + 1 sigma
b)
Arrhenius Plot
Log D/r^2 (sec-1)
10000/K
Measured Data
Modelled Data
c)
Log (r/r0) Plot
Log r/r0
Fraction 39Ar Lost
Measured Data
Modelled Data
d)
Temp vs Time
Closure Temp (C)
Age (Ma)
98GR32 K-feldspar
T Mean
T Max
T Min
97GR60 Muscovite
98GR36 Biotite

Figure 8

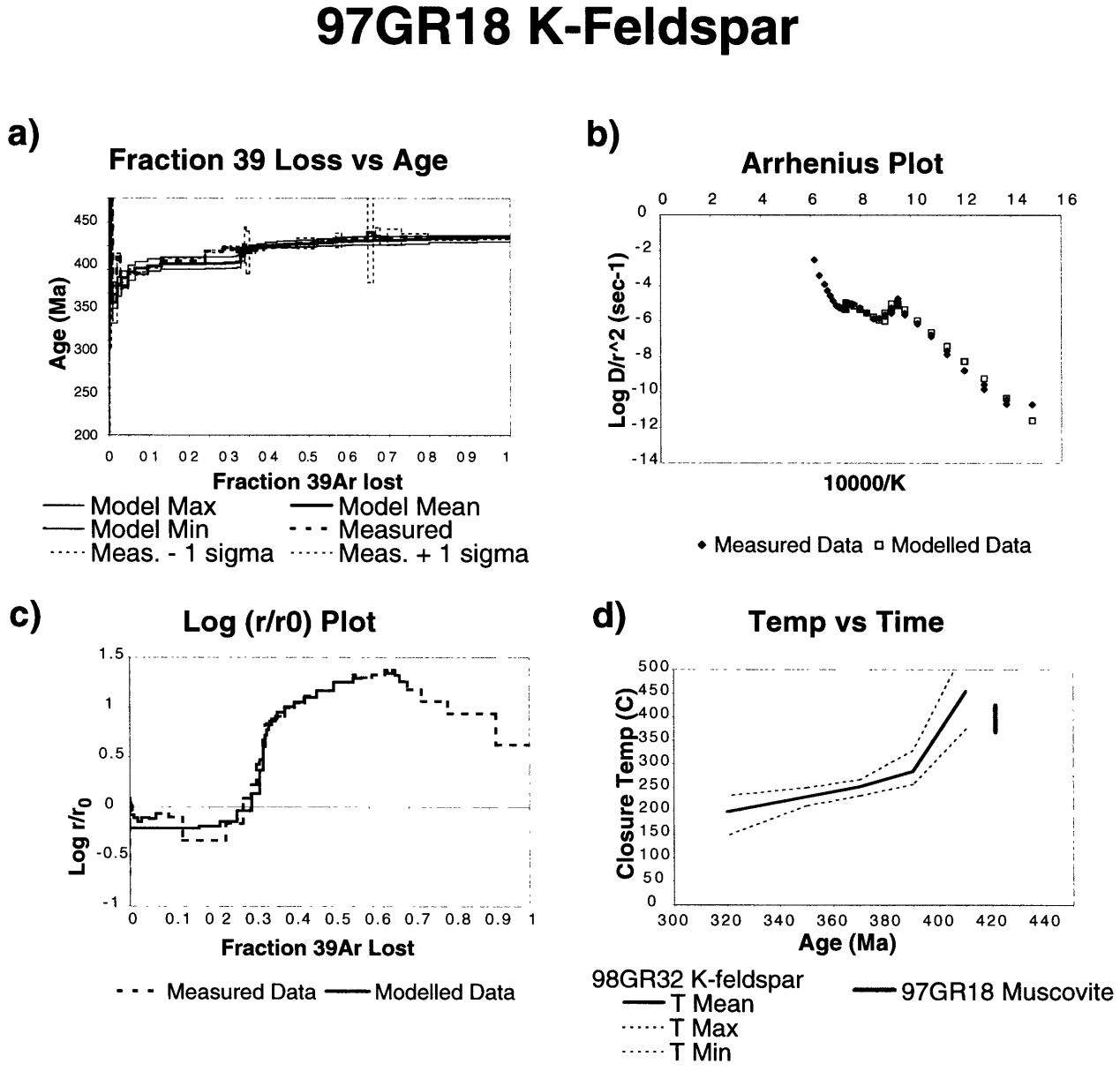
97GR18 K-Feldspar
a)
Fraction 39 Loss vs Age
Age (Ma)
Fraction 39Ar lost
Model Max
Model Mean
Model Min
Measured
Meas. - 1 sigma
Meas. + 1 sigma
b)
Arrhenius Plot
Log D/r^2 (sec-1)
10000/K
Measured Data
Modelled Data
c)
Log (r/r0) Plot
Log r/r0
Fraction 39Ar Lost
Measured Data
Modelled Data
d)
Temp vs Time
Closure Temp (C)
Age (Ma)
98GR32 K-feldspar
T Mean
T Max
T Min
97GR18 Muscovite

Figure 9

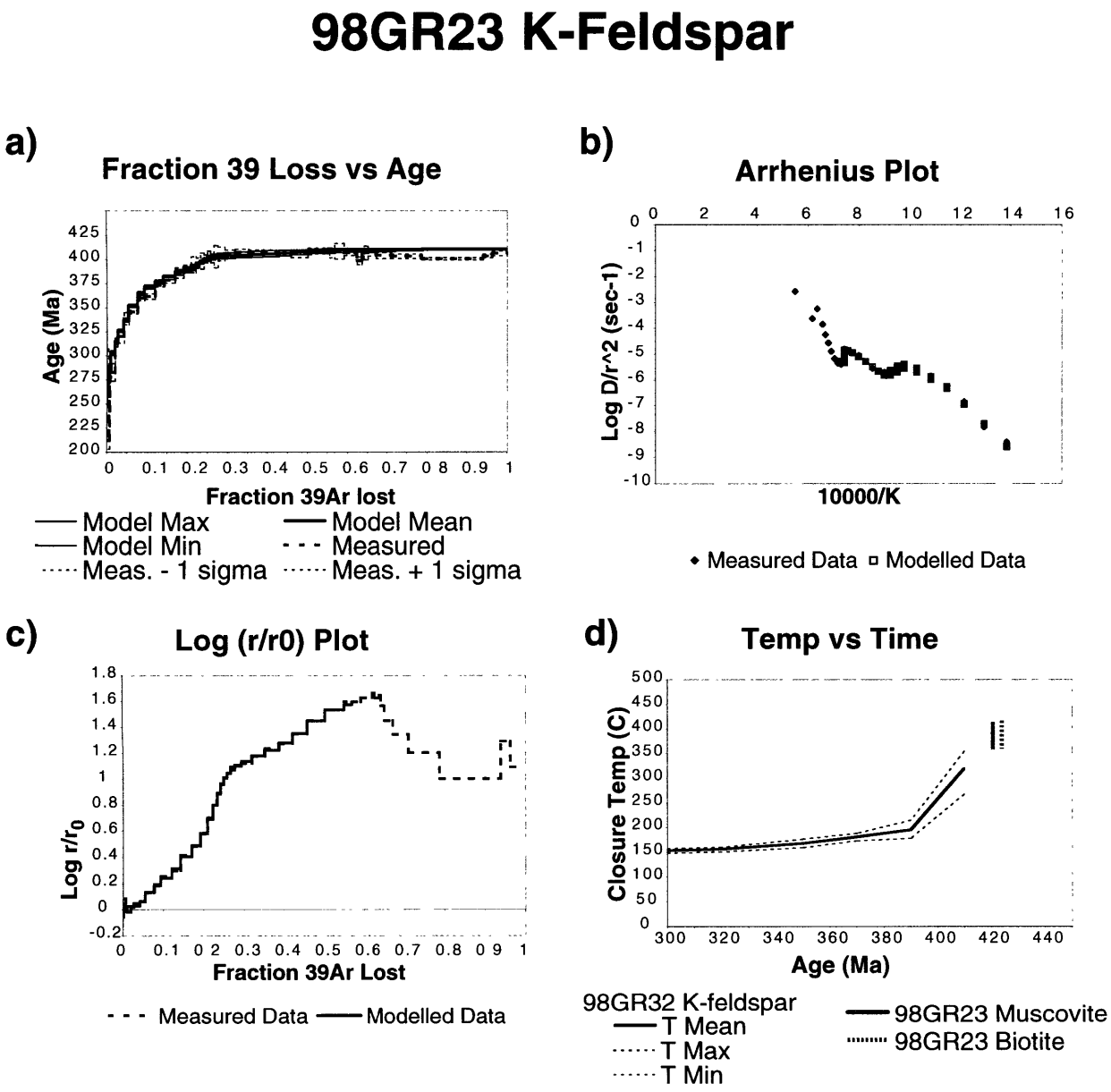
98GR23 K-Feldspar
a)
Fraction 39 Loss vs Age
Age (Ma)
Fraction 39Ar lost
Model Max
Model Mean
Model Min
Measured
Meas. - 1 sigma
Meas. + 1 sigma
b)
Arrhenius Plot
Log D/r^2 (sec-1)
10000/K
Measured Data
Modelled Data
c)
Log (r/r0) Plot
Log r/r0
Fraction 39Ar Lost
Measured Data
Modelled Data
d)
Temp vs Time
Closure Temp (C)
Age (Ma)
98GR32 K-feldspar
T Mean
T Max
T Min
98GR23 Muscovite
98GR23 Biotite

Figure 10

98GR28 K-Feldspar

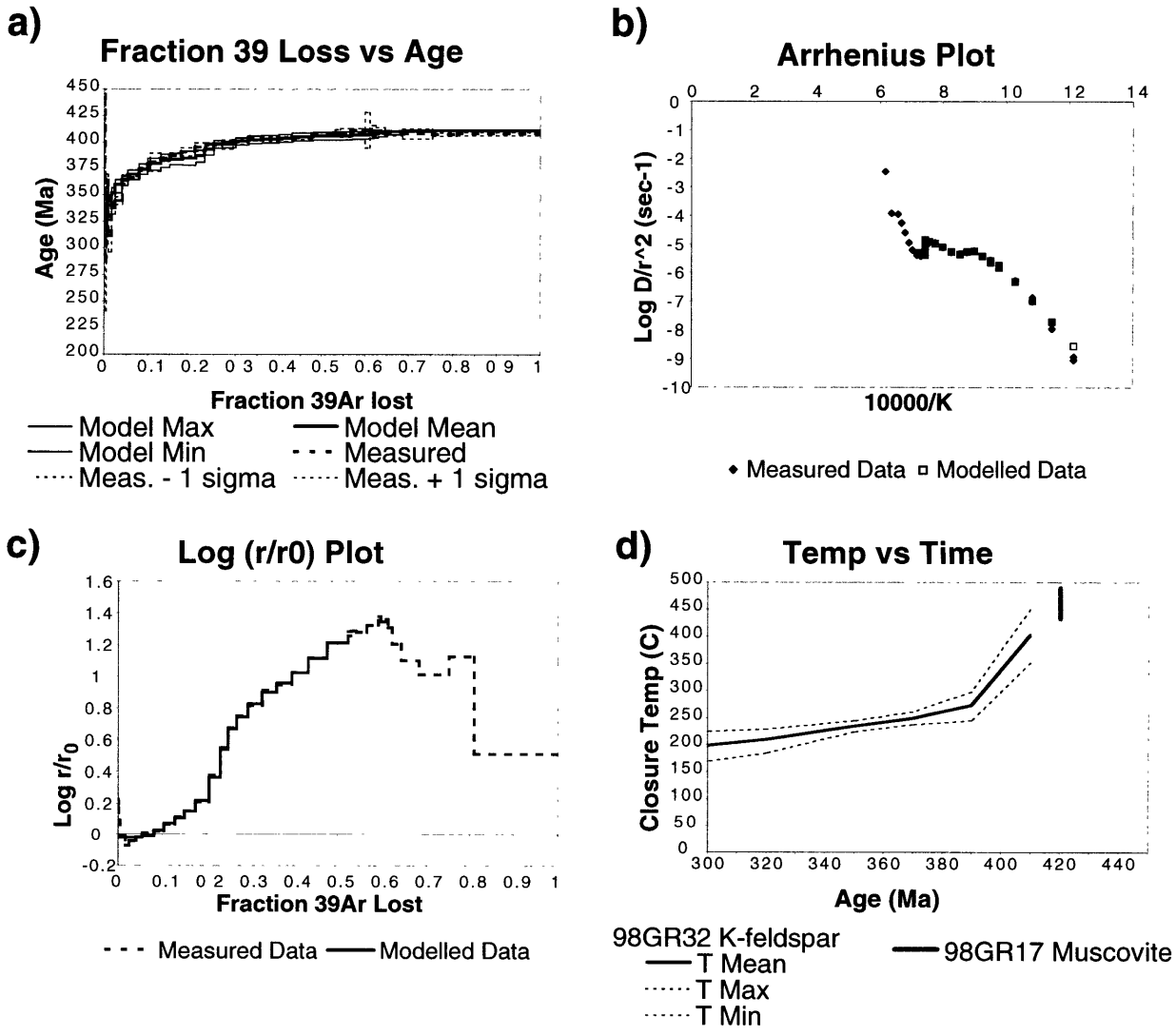

Figure 11

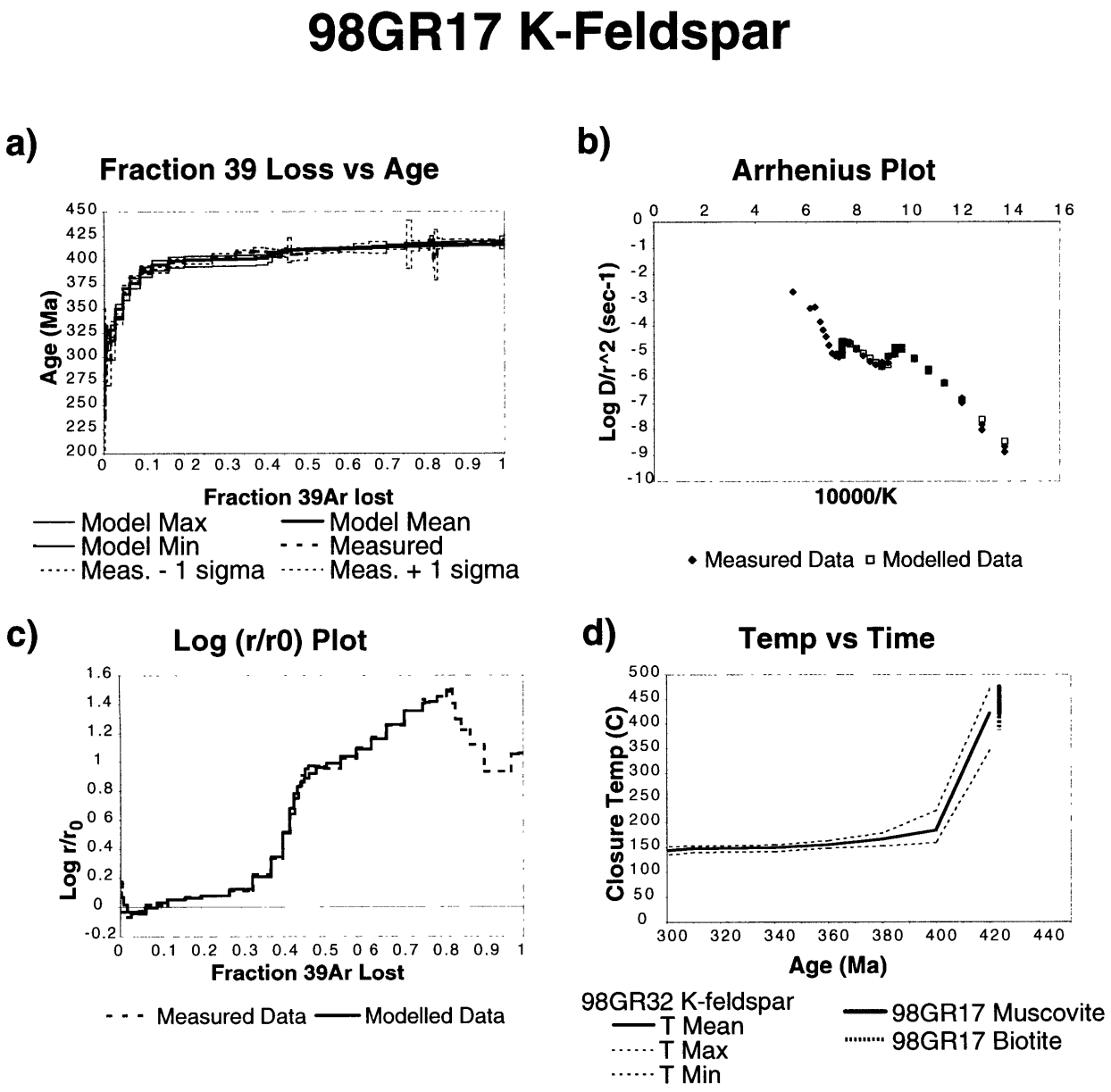
98GR17 K-Feldspar
a)
Fraction 39 Loss vs Age
Age (Ma)
Fraction 39Ar lost
Model Max
Model Mean
Model Min
Measured
Meas. - 1 sigma
Meas. + 1 sigma
b)
Arrhenius Plot
Log D/r^2 (sec-1)
10000/K
Measured Data
Modelled Data
c)
Log (r/r0) Plot
Log r/r0
Fraction 39Ar Lost
Measured Data
Modelled Data
d)
Temp vs Time
Closure Temp (C)
Age (Ma)
98GR32 K-feldspar
T Mean
T Max
T Min
98GR17 Muscovite
98GR17 Biotite

Appendix

K-feldspar Heating Schedules

98GR36

Temperature	Duration	Temperature	Duration
400 (C)	20	900 (C)	25
400 (C)	36	940 (C)	25
450 (C)	20	980 (C)	25
450 (C)	36	1020 (C)	25
500 (C)	28	1050 (C)	25
500 (C)	36	1075 (C)	25
550 (C)	28	1075 (C)	40
550 (C)	36	1075 (C)	80
600 (C)	28	1075 (C)	150
600 (C)	36	1100 (C)	20
650 (C)	28	1100 (C)	40
650 (C)	36	1100 (C)	80
700 (C)	28	1100 (C)	120
700 (C)	36	1125 (C)	20
750 (C)	28	1125 (C)	40
750 (C)	36	1150 (C)	15
780 (C)	28	1175 (C)	15
780 (C)	36	1200 (C)	15
810 (C)	28	1225 (C)	15
810 (C)	36	1250 (C)	15
840 (C)	28	1300 (C)	15
840 (C)	36	1350 (C)	15
870 (C)	28		

97GR18

Temperature	Duration	Temperature	Duration
400 (C)	20	900 (C)	25
400 (C)	36	940 (C)	25
450 (C)	20	980 (C)	25
450 (C)	36	1020 (C)	25
500 (C)	28	1050 (C)	25
500 (C)	36	1075 (C)	25
550 (C)	28	1075 (C)	40
550 (C)	36	1075 (C)	80
600 (C)	28	1075 (C)	150
600 (C)	36	1100 (C)	20
650 (C)	28	1100 (C)	40
650 (C)	36	1100 (C)	80
700 (C)	28	1100 (C)	120
700 (C)	36	1125 (C)	20
750 (C)	28	1125 (C)	40
750 (C)	36	1150 (C)	15
780 (C)	28	1175 (C)	15
780 (C)	36	1200 (C)	15
810 (C)	28	1225 (C)	15
810 (C)	36	1250 (C)	15
840 (C)	28	1300 (C)	15
840 (C)	36	1350 (C)	15
870 (C)	28		

98GR23

Temperature	Duration	Temperature	Duration
400 (C)	20	900 (C)	25
400 (C)	36	940 (C)	25
450 (C)	20	980 (C)	25
450 (C)	36	1020 (C)	25
500 (C)	28	1050 (C)	25
500 (C)	36	1075 (C)	25
550 (C)	28	1075 (C)	40
550 (C)	36	1075 (C)	80
600 (C)	28	1075 (C)	150
600 (C)	36	1100 (C)	20
650 (C)	28	1100 (C)	40
650 (C)	36	1100 (C)	80
700 (C)	28	1100 (C)	120
700 (C)	36	1125 (C)	20
750 (C)	28	1125 (C)	40
750 (C)	36	1150 (C)	15
780 (C)	28	1175 (C)	15
780 (C)	36	1200 (C)	15
810 (C)	28	1225 (C)	15
810 (C)	36	1250 (C)	15
840 (C)	28	1300 (C)	15
840 (C)	36	1350 (C)	15
870 (C)	28	1550 (C)	15

98GR28

Temperature	Duration	Temperature	Duration
400 (C)	20	980 (C)	25
400 (C)	36	1020 (C)	25
450 (C)	20	1050 (C)	25
450 (C)	36	1075 (C)	25
500 (C)	28	1075 (C)	40
500 (C)	36	1075 (C)	80
550 (C)	28	1075 (C)	150
550 (C)	36	1100 (C)	20
600 (C)	28	1100 (C)	40
600 (C)	36	1100 (C)	80
650 (C)	28	1100 (C)	120
650 (C)	36	1125 (C)	20
700 (C)	28	1125 (C)	40
700 (C)	36	1150 (C)	15
750 (C)	28	1175 (C)	15
750 (C)	36	1200 (C)	15
780 (C)	28	1225 (C)	15
780 (C)	36	1250 (C)	15
810 (C)	28	1300 (C)	15
840 (C)	28	1350 (C)	15
870 (C)	28		
900 (C)	25		
940 (C)	25		

98GR17

Temperature	Duration	Temperature	Duration
400 (C)	20	900 (C)	25
400 (C)	36	940 (C)	25
450 (C)	20	980 (C)	25
450 (C)	36	1020 (C)	25
500 (C)	28	1050 (C)	25
500 (C)	36	1075 (C)	25
550 (C)	28	1075 (C)	40
550 (C)	36	1075 (C)	80
600 (C)	28	1075 (C)	150
600 (C)	36	1100 (C)	20
650 (C)	28	1100 (C)	40
650 (C)	36	1100 (C)	80
700 (C)	28	1100 (C)	120
700 (C)	36	1125 (C)	20
750 (C)	28	1125 (C)	40
750 (C)	36	1150 (C)	15
780 (C)	28	1175 (C)	15
780 (C)	36	1200 (C)	15
810 (C)	28	1225 (C)	15
810 (C)	36	1250 (C)	15
840 (C)	28	1300 (C)	15
840 (C)	36	1350 (C)	15
870 (C)	28	1550 (C)	15

6. Cyclicity between thrusting and normal faulting in the East Greenland Caledonides

Arthur P. White*, Kip V. Hodges*

** Department of Earth, Atmospheric and Planetary Sciences, Massachusetts Institute of Technology, Cambridge, MA, 02139,USA. apwhite@mit.edu Tel (617)-253-8445 fax (617) 252-1800*

Abstract

Syn- and post-orogenic extension are now recognized as important components of the deformation during Caledonian orogenesis in central East Greenland (71°-74.5° N). Here, we present a new tectonic model reconstructing the sequence of events, with an emphasis on the role of extension both during and after the Baltica-Laurentia collision. We suggest that the temporal and spatial relationships between thrusts and normal faults imply that there was a fundamental cyclicity between crustal thickening and thinning that has only been observed in one other orogen in the world. Furthermore, the fact that all significant episodes of extension were restricted to a relatively small region of the orogen for a long time-period (ca. 75 Ma), frequently reactivating earlier faults, implies that the original geometry of normal faulting may have formed an inherent weakness in the middle and upper crust that exerted control on subsequent exhumation. Given the links between topographic gradients and synorogenic normal faults in active orogens, we suggest that the early topography formed during initial orogenesis may have ultimately determined the future location of middle and upper crustal extension, both during and

after the Baltica-Laurentia collision, implying that location and geometry of subsequent Mesozoic extension that formed the North Sea basin may have been inherited.

Introduction

When McClay et al. (1986) first suggested that the Devonian basins in East Greenland formed in response to the collapse of an overthickened Caledonian crustal welt, they did not know that the most significant orogen-parallel thrust fault was in actuality a complex system of overlapping normal faults (Hartz and Andresen, 1995). These faults, collectively referred to as the Fjord Region Detachment (FRD; Figure 1) were active during discrete episodes both during and after the Baltica-Laurentia collision at ca. 430-357 Ma (e.g. Andresen et al., 1998; Hartz, 2001; White and Hodges, submitted; White et al., in press). Collectively, the structures of the FRD system account for a minimum of ~34 km of tectonostratigraphic throw (White and Hodges, in preparation-b). Moreover, we have learned from observations along the FRD that the East Greenland Caledonides provide an unusually long-lived view into the evolution of extensional faulting during and after orogenesis, yielding insights that may be of relevance to other inactive orogens with less-complete preservation, or other active orogens that are still evolving. In this paper we focus upon the "big-picture" implications of the past five years of our investigations, which lead us to propose a new tectonic model for the East Greenland Caledonides.

Geologic Background

The Caledonides were formed as a two-sided fold-and-thrust belt when Baltica subducted beneath Laurentia during the Middle to Late Silurian (Andresen and Steltenpohl, 1994; Gee, 1975; Hodges et al., 1982; Sturt and Thon, 1978). Remnants of

east-verging thrusts are now preserved in Scandinavia, Ireland and Scotland. However, in central East Greenland (71° to 74.5° N) there are a series of thrust-bounded tectonic windows that expose Archean to Neoproterozoic metamorphic gneiss complexes and indicate that material was translated westward (e.g. Christoffersen, 1984; Elvevold et al., 2000; Escher and Jones, 1999; Haller, 1971; Leslie and Higgins, 1999). These thrusts are truncated by a prominent system of N-S striking, east-dipping normal faults called the Fjord Region Detachment (FRD; Hartz and Andresen, 1995) which separate into two significant splays just south of 73° N: the structurally lower and western of the two faults is called the Høgedal detachment, and the upper is the Tindern detachment (White et al., in press).

In order to maximize the potential of our investigations, we have been working within the Forsblad-fjord-Alpefjord-Segelsällskapets-fjord region (72.5° N) which comprises a transect that spans all three allochthonous units juxtaposed by activity on the FRD. From west to east and structurally lowest to highest, these are the amphibolite facies Archean-Paleoproterozoic Gletscherland Complex orthogneisses of the Hagar-Niggli Spids allochthon, the amphibolite facies Neoproterozoic Krummedal Sequence paragneisses of the Høgedal allochthon, and low-grade to unmetamorphosed sedimentary rocks of the Eleonore Bay Supergroup that comprise the Tindern allochthon (White et al., in press).

Reconstructing the tectonic evolution of the central East Greenland Caledonides

Although rocks from the Hagar-Niggli Spids allochthon record multiple episodes of pre-Caledonian deformation and metamorphism, all three allochthons preserve a complex, polyphase deformational and metamorphic history that represents the

cumulative affects of activity during the Caledonian orogeny (White and Hodges, in preparation-b). The combination of our previously reported structural data with U-Pb and $^{40}Ar/^{39}Ar$ constraints and P-T data (White and Hodges, in preparation-a; White and Hodges, in preparation-b; White and Hodges, in preparation-c; White et al., in press) form the basis for proposing the following new tectonic model to describe the evolution of extension during and after Caledonian orogenesis (Figure 2).

Initial Caledonian crustal thickening and orogen parallel shear

At some time prior to 425 Ma, the Laurentian crust began to thicken in response to sinistrally oblique Baltica-Laurentia plate convergence (White et al., in press). Although D_1 thrust faults are not preserved in the study area, they are inferred from the regional mapping. Proterozoic sedimentary rocks of the Krummedal Sequence that had served as the depositional base for the Eleonore Bay Supergroup were buried at this time. Semi-quantitative petrographic and quantitative thermobarometric data reported by White and Hodges (in preparation-b) suggest that ambient pressures in the Krummedal Sequence increased distinctly during M_1 metamorphism, followed by significant increases in temperature during M_2 metamorphism, to reach peak metamorphic conditions of ~785° C at ~10.5 kb. These numbers imply that D_1 and D_2 crustal thickening were collectively responsible for at least ~16 km of burial (White and Hodges, in preparation-b). Furthermore, peak metamorphic conditions are consistent with a simple 20°C/km geothermal gradient and 4 km/kb lithostatic gradient. Altogether these data imply that burial was accompanied or followed by near-complete thermal equilibration during M_2, prior to any subsequent exhumation. In addition, structural data discussed by White et al. (in press) indicate that M_2 metamorphism accompanied significant orogen-parallel shear (D_2), providing independent evidence of the importance of transpressional

deformation during the constrictional phase of the Caledonian orogeny in east Greenland (e.g. Holdsworth and Strachan, 1991; Larsen and Bengård, 1991; Strachan et al., 1991; Strachan et al., In Press; Torsvik et al., 1996).

The exact age of peak metamorphism is unclear; however eclogite facies metamorphism in NE Greenland has been dated using Sm-Nd to ca. 439 Ma (Brueckner et al., 1998). In the Forsblad Fjord region, the only constraint on the timing of peak metamorphism is a syn-M_2 leucosome that was dated at ca. 425 Ma (White et al., in press). M_1 is at least slightly older. Attempts to date M_1 monazite inclusions using the electron microprobe confirm that they are Caledonian (White and Hodges, in preparation-b); however, calibration difficulties have limited precise age determinations.

Initial phases of extension: synorogenic activity along the Tindern detachment

At some time between 425-424.5 Ma, the Tindern detachment splay of the Fjord Region Detachment system became active (White et al., in press), possibly in response to the gravitational collapse of high topographic gradients formed during crustal thickening (e.g. Burchfiel *et al.*, 1992). U-Pb and 40Ar/39Ar geochronologic and major element partitioning thermobarometric constraints indicate that this orogen-scale normal fault was responsible for ~13 km of vertical exhumation over a ca. 2 My period (White and Hodges, in preparation-a; White and Hodges, in preparation-b; White and Hodges, in preparation-c; White et al., in press). The superposition of deformational fabrics along with petrographic and thermobarometric constraints indicate that decompression was synkinematic with respect to the development of D_3 fabrics along the Tindern detachment and D_2 fabrics ~14 km structurally beneath the fault. (White and Hodges, in preparation-b). This implies that movement along the Tindern detachment was coeval with continued

orogen-parallel shear associated with plate collision. Therefore, the Tindern detachment must have acted as an important decoupling horizon between upper crustal thinning and middle crustal thickening.

Continued crustal thickening and upper-crustal extension:

Following two million years of rapid displacement along the Tindern detachment (rates of exhumation as fast as 6.5 mm/yr; White and Hodges, in preparation-c), extensional strain continued to be partitioned within the upper-crustal hanging-wall of the detachment on successive generations of high-angle (D_3) and low-angle (D_{4a}) west-dipping faults. These structurally higher features were responsible for an additional 5 km (White and Hodges, in preparation-c) of exhumation and about 22% crustal extension. Multi-domain diffusion modeling of K-feldspars indicates that this extension occurred over a 25 million year time-period, ending at ca. 400 Ma.

Although the most recent structural discontinuity between the Hagar-Niggli Spids and Høgedal allochthons reflects normal-sense slip on the Høgedal detachment, the metamorphic histories of these allochthons imply that they were originally separated by a major thrust fault that has been excised by the FRD (White et al., in press). This thrust was responsible for westward transport of Krummedal Sequence rocks, which were metamorphosed at amphibolite facies at ca. 425 Ma, over Hagar-Niggli Spids units which experienced only a low-temperature metamorphic overprint at that time. Subsequent east-directed displacement on the Høgedal detachment juxtaposed rocks of the hanging wall of the older thrust against rocks of its footwall, leading to the present-day structural configuration. $^{40}Ar/^{39}Ar$ geochronologic constraints suggest that Caledonian activity on the Høgedal detachment occurred between ca. 417 and ca. 380 Ma (White and Hodges,

submitted), bracketing the age of thrusting to between ca. 425 Ma and the time that activity began on the Høgedal detachment (as early as 417 Ma). Additional evidence for deformational activity in the Høgedal allochthon subsequent to 425-423 Ma Tindern detachment slip (D_3) comes from $^{40}Ar/^{39}Ar$ cooling ages of 423-411 Ma on retrograde muscovite deformed during D_{4b}. Thus, it is likely that movement along the inferred thrust fault was coeval with upper-crustal extension in the Tindern allochthon (White and Hodges, in preparation-c) sometime before ca. 400 Ma.

Post-orogenic extension along the Høgedal Detachment

$^{40}Ar/^{39}Ar$ data from biotite, K-feldspar and pseudotachylite indicate that the Høgedal Splay of the Fjord Region Detachment system had become active as early as 417 Ma and that slip persisted until at least 380 Ma. (White and Hodges, submitted). Allowing for movement along the excised thrust to have occurred at geologically reasonable rates, it is likely that the Høgedal detachment was mostly active after the Baltica-Laurentia collision had stopped. This inference is further supported by an *in situ* $^{40}Ar/^{39}Ar$ UV laser microprobe analysis on pseudotachylite from a late brittle shear-zone in the detachment that yielded an age of ca. 357 Ma (White and Hodges, submitted). This implies that the fault was reactivated during formation of the Devonian basins and deposition of the Old Red Sandstone. North of Kempes Fjord, where the Høgedal and Tindern detachments merge, the FRD system is a simpler feature, juxtaposing the Eleonore Bay Supergroup and the Archean-Paleoproterozoic basement orthogneisses of the Gletscherland Complex with an estimated tectonostratigraphic throw of ~34 km (Vold, 1997). This implies that the Høgedal detachment accommodated a cumulative throw of ~16 km (White and Hodges, submitted; White and Hodges, in preparation-b).

Devonian extension and deposition of conglomerates in the Forsblad Fjord Region

Field observations in the upper-crustal section of the Tindern allochthon indicate that there is a sinistral strike-slip fault complex there that cuts Devonian conglomerates that sit unconformably on top of the Eleonore Bay Supergroup. This fault complex consists of E-W striking, N-S-dipping, high-angle normal faults that sole into N-NW to S-SE striking left-lateral strike-slip faults (White and Hodges, in preparation-c). These structures extend westwards and structurally downwards, towards the Høgedal detachment, from which we infer that they soled into the Høgedal detachment at depth, a notion that is consistent with the available geochronologic constraints on these structures. Thus it appears that the Høgedal detachment served as a crucial extensional fault during the latter-portions of orogenesis and during the period traditionally associated with post-orogenic gravitational collapse, deposition of the Old Red Sandstones, and formation of the Devonian basins. Furthermore, the presence of a deep-crustal W-dipping seismic reflector has been interpreted to suggest that there was a deep-seated, W-dipping crustal-scale low-angle normal fault active during the Devonian (Schlindwein and Jokat, 2000). In this case, the Høgedal detachment likely soled into this deeper structure.

Cyclicity between thrusting and normal faulting during orogenesis

We have argued that the early stages of crustal thickening due to the Baltica-Laurentia collision were followed by rapid thinning associated with movement along the Tindern detachment. This was followed by continued thickening along a structurally deeper thrust (White et al., in press) and coeval thinning of the upper crust at much slower rates. Subsequent to this activity, extension was re-established along the FRD on a structurally deeper splay, the Høgedal detachment, and continued into the period of post-

orogenic collapse traditionally associated with the formation of the Devonian basins. Thus, our data imply a fundamental cyclicity between thrusting and normal faulting that began during collisional orogenesis and ended with the termination of the Baltica–Laurentia collision. The alternation between thrusting and normal faulting during orogenesis has only been previously reported in the Annapurna region of the Himalayas (Hodges et al., 1996). However, this behavior is a tacit assumption in many geodynamic models invoked to explain synkinematic extensional faulting in active orogens such as the Himalayas, that are premised on a simple force-balance model between the plate-forces that drive orogenesis, and the gravitational forces that drive extension (e.g. Royden, 1996). Hodges (1998) and Hodges et al. (in press), argued that there may be a natural tendency for orogenic systems to evolve toward a dynamical steady-state defined by energy accumulative (e.g. crustal thickening) and energy dissipative (e.g. crustal thinning) processes. By analogy with other dynamical systems, it would not be surprising if orogenic systems near steady-state exhibited a form of oscillatory behavior characterized by alternations between periods dominated by energy accumulation and other periods dominated by energy dissipation. The apparently cyclic nature of contraction and extension in both the Himalayas and the Greenland Caledonides may be a signature of such behavior.

Links between paleotopography and North Sea basin formation

Burchfiel and Royden (1985) proposed that there is a link between crustal extension during orogenesis and the gravitational collapse of high topographic gradients formed during crustal thickening, a notion that has been supported by a considerable amount of evidence since 1985. The implication of their work is that the location of the Tindern detachment may have been influenced by Caledonian paleotopography. In 1986,

McClay et al. proposed that extension in East Greenland, might have preferentially occurred on previous thrust faults; however, they did not have access to the complete extensional record. As argued in this paper, the Fjord Region detachment was responsible for at least ~34 km of exhumation over a total time-period of ca. 75 Ma. Although there is another significant Devonian-aged fault called the "Western Fault Zone", it has been argued from kinematic indicators that this fault was predominantly a left-lateral strike-slip shear zone (Larsen and Bengård, 1991). Hartz and Andresen (1995) suggested that this fault was a reactivated normal fault related to extension along the FRD system; unfortunately, the amount of dip slip that it may have accommodated remains unconstrained. In any event, we argue that most extension in the middle and upper crust of central East Greenland up to the time that the Devonian basins were forming was accommodated by movement along the FRD system. While our data do not preclude the idea that activity along the FRD system reactivated earlier thrusts, they provide evidence that an inherent weakness developed after early activity along the Tindern detachment that played a fundamental role in strain partitioning during later extensional deformation. This model is complicated by seismic data that reveal the presence of a laterally extensive, deep-crustal, W-dipping reflector. This structure has been interpreted as a significant, late-Caledonian extensional shear zone (Schlindwein and Jokat, 2000); however, there are no geochronologic constraints on the timing of this fault, nor geologic constraints on the amount of displacement. Assuming that this is a large décollement, it indicates that the extension within the lower crust was accommodated along a different structure from the middle and upper crust. Furthermore, the Fjord Region Detachment may have soled into this deep-crustal structure; however, the presence of the W-dipping reflector does not alter the fact that most middle and upper-crustal extension was accommodated along the FRD. Clearly the relative timing between lower, middle and

upper crustal extension may have important implications to the partitioning of strain throughout the crust. In any event, our arguments suggest that the early paleotopography established during the initial stages of orogenesis played a crucial role in determining the location and geometry of the later middle- and upper-crustal extension, including the site of eventual post-collisional collapse and formation of the Devonian basins, which as McClay et al. (1986) suggested, may have exerted an integral control on the geometry of Mesozoic extension and formation of the North Sea basin. Thus, the position of rifting associated with the opening of the present-day north Atlantic ocean may have been inherited from crustal anisotropies that developed more than 425 Ma in response to paleotopography at that time.

Acknowledgements

This research was part of a collaborative effort between the Department of Earth, Atmospheric and Planetary Sciences at MIT and the University of Oslo in Norway. Funding for this study was provided by National Science Foundation grant EAR 930072 (to K.V. H.). We wish to thank the Greenland Geological Survey, Danish Polar Center, Sirius Patrol, A. Andresen, E. Hartz, N. Henriksen, J. Hurtado, L. Schoenbohm, and J. Kaufman for logistical assistance.

References:

Andresen, A., Hartz, E.H., and Vold, J., 1998, A late orogenic extensional origin for the infracrustal gneiss domes of the East Greenland Caledonides (72-74 N): Tectonophysics, v. 285, p. 353-369.

Andresen, A., and Steltenpohl, M.G., 1994, A reevaluation of nappe sequences in the Ofoten-Troms region, north Norwegian Caledonides: Implications for terrane accretion, ophiolite obduction, and polyorogenic evolution: Tectonophysics, v. 231, p. 59-70.

Brueckner, H.K., Gilotti, J.A., and Nutman, A., 1998, Caledonian Eclogite-facies metamorphism of Early Proterozoic protoliths from the north-east Greenland Eclogite Province: Contributions to Mineralogy and Petrology, v. 130, p. 103-120.

Burchfiel, B.C., Chen, Z., Hodges, K.V., Liu, Y., Royden, L.H., Deng, C., and Xu, J., 1992, The South Tibetan Detachment System, Himalayan Orogen: Extension Contemporaneous With and Parallel to Shortening in a Collisional Mountain Belt: Boulder, CO, Geological Society of America, 41 p.

Burchfiel, B.C., and Royden, L.H., 1985, North-south extension within the convergent Himalayan region.: Geology, v. 13, p. 679-682.

Christoffersen, M., 1984, Scoresby Sund: Denmark, Grønlands Geologiske Undersøgelse.

Elvevold, S., Escher, J.C., Frederiksen, K.S., Friderichsen, J.D., Gilotti, J.A., Henriksen, N., Higgins, A.K., Jepsen, H.F., Jones, K.A., Kalsbeek, F., Kinny, P.D., Leslie, A.G., Robertson, S., Smith, M.P., Thrane, K., and Watt, G.R., 2000, Tectonic architecture of the East Greenland Caledonides 72° - 74°30' N, Danmarks og Grønlands Gelogiske Undersøgelse Rapport, Volume 88: Denmark, Geological Survey of Denmark and Greenland, p. 34.

Escher, J.C., and Jones, K.A., 1999, Caledonian geology of Frænkel Land and adjacent areas (73°00'-73°30'N), East Greenland, *in* Higgins, A.k., and Frederiksen, K.S., eds., Geology of East Greenland 72°-75°, mainly Caledonian: preliminary reports from the 1998 expedition: Denmark, Danmarks og Grønlands Geologiske Undersøgelse Rapport.

Gee, D.G., 1975, A tectonic model for the central part of the Scandinavian Caledonides: American Journal of Science, v. 275A, p. 468-515.

Haller, J., 1971, Geology of the East Greenland Caledonides: New York, Interscience Publishers, 413 p.

Hartz, E., 2001, Syncontractional extension and exhumation of deep crustal rocks in the east Greeland Caledonides: Tectonics, v. 20, p. 58-77.

Hartz, E., and Andresen, A., 1995, Caledonian sole thrust of central East Greenland: A crustal-scale Devonian extensional detachment?: Geology, v. 23, p. 637-640.

Henriksen, N., and Higgins, A.K., 1976, East Greenland Caledonian fold belt, *in* Escher, A., and Watt, W.S., eds., Geology of Greenland: Copenhagen, DK, The Geological Survey of Greenland, p. 183-246.

Hodges, K.V., Bartley, J.M., and Burchfiel, B.C., 1982, Structural evolution of an A-type subduction zone, Lofoten-Rombak area, northern Scandinavian Caledonides: Tectonics, v. 1, p. 441-462.

Hodges, K.V., Parrish, R.R., and Searle, M.P., 1996, Tectonic evolution of the central Annapurna Range, Nepalese Himalayas: Tectonics, v. 15, p. 1264-1291.

Hodges, K.V., Treloar, P.J.e, and O'Brien, P.J.e, 1998, The thermodynamics of Himalayan orogenesis: What drives metamorphism and metamorphic relations?: Geological Society Special Publications, v. 138, p. 7-22.

Holdsworth, R.E., and Strachan, R.A., 1991, Interlinked system of ductile strike slip and thrusting formed by Caledonian sinistral transpression in northeastern Greenland: Geology (Boulder), v. 19, p. 510-513.

Koch, L., and Haller, J., 1971, Geologic map of East Greenland 72°-76° N.Lat. (1:250,000).: Meddelelser om Grønland, v. 183, p. 1-26.

Larsen, P.H., and Bengård, H.J., 1991, The Devonian basin initiation in East Greenland: A result of sinestral wrench faulting and Caledonian extensional collapse: Journal of the Geological Society of London, v. 148, p. 355-368.

Leslie, A.G., and Higgins, A.K., 1999, On the Caledonian (and Grenvillian) geology of Bartholin Land, Ole Rømer Land and adjacent nunataks, East Greenland, *in* Higgins, A.k., and Frederiksen, K.S., eds., Geology of East Greenland 72°-75°, mainly Caledonian: preliminary reports from the 1998 expedition: Denmark, Danmarks og Grønlands Geologiske Undersøgelse Rapport, p. 220.

McClay, K.R., Norton, M.G., Coney, P., and Davis, G.H., 1986, Collapse of the Caledonian orogen and the Old Red Sandstone: Nature, v. 323, p. 147-149.

Peucat, J.J., Tisserant, D., Caby, R., and Clauer, N., 1985, Resistance of zircons to U-Pb resetting in a prograde metamorphic sequence of Caledonian age in East Greenland: Canadian Journal of Earth Sciences, v. 22, p. 330-338.

Royden, L., 1996, Coupling and decoupling of crust and mantle in convergent orogens; implications for strain partitioning in the crust: Journal of Geophysical Research, B, Solid Earth and Planets, v. 101, p. 17,679-17,705.

Schlindwein, V., and Jokat, W., 2000, Post-collisional extension of the East Greenland Caledonides; a geophysical perspective: Geophysical Journal International, v. 140, p. 559-567.

Smith, M.P., and Robertson, S., 1999, The Nathorst Land Group (Neoproterozoic) of East Greenland - lithostratigraphy, basin geometry and tectonic history, *in* Higgins,

A.k., and Frederiksen, K.S., eds., Geology of East Greenland 72°-75°, mainly Caledonian: preliminary reports from the 1998 expedition: Denmark, Danmarks og Grønlands Geologiske Undersøgelse Rapport, p. 220.

Strachan, R.A., Dallmeyer, R.D., Holdsworth, R.E., and Jepsen, H.F., 1991, New evidence for regional sinistral displacements within the Northeast Greenland Caledonides: Anonymous. Gsa Northeastern Section, 26th annual meeting; Southeastern Section, 40th annual meeting. Abstracts with Programs Geological Society of America, v. 23, p. 135.

Strachan, R.A., Martin, M.W., and Friderichsen, J.D., In Press, Evidence for contemporaneous yet contrasting styles of granite magmatism during extensional collapse of the northeast Greenland Caledonides: Tectonics.

Sturt, B.A., and Thon, A., 1978, An ophiolite complex of probable early Caledonian age discovered on Karmoy: Nature (London), v. 275, p. 538-539.

Torsvik, T.H., Smethurst, M.A., Meert, J.G., Van der Voo, R., McKerrow, W.S., Brasier, M.D., Sturt, B.A., and Walderhaug, H.J., 1996, Continental break-up and collision in the Neoproterozoic and Palaeozoic; a tale of Baltica and Laurentia: Earth-Science Reviews, v. 40, p. 229-258.

Vold, J., 1997, Et studie av den tectonomatemorphe utviklingen av gneisserne i liggblokken til "The Fjord Region Detachment Zone" på Kap hedlund, sentrale Øst Grønland [Cand. Scient Thesis thesis]: Oslo, University of Oslo.

White, A., and Hodges, K., submitted, Multi-stage dxtensional evolution of the central East Greenland Caledonides: .

White, A.P., and Hodges, K.V., in preparation-a, 40Ar/39Ar constraints from K-feldspar on late Caledonian normal faulting and formation of the Devonian basins in East Greenland: .

White, A.P., and Hodges, K.V., in preparation-b, Pressure-temperature-time evolution of the Central East Greenland Caledonides: quanitative constraints on crustal thickening and synorogenic extension: .

White, A.P., and Hodges, K.V., in preparation-c, The role of upper crustal extension in the evolution of the central East Greenland Caledonides: .

White, A.P., Hodges, K.V., Martin, M.V., and Andresen, A., in press, Geologic constraints on middle-crustal behaviour during synorogenic extension in the East Greenland Caledonides: International Journal of Earth Science.

Figure Captions:

Figure 1: Simplified tectonic map of the central fjord region of the East Greenland Caledonides interpreted after Koch and Haller (1971), Henriksen and Higgins (1976), Peucat *et al.* (1985), Andresen *et al.* (1998a), White *et al.* (in press), Smith and Robertson (1999), Leslie and Higgins (1999), Escher and Jones (1999). The following abbreviations have been used: Forsblad Fjord (FF); Segelsällskapets Fjord (SF); Alpefjord (AF); Kaiser Franz Joseph's Fjord (KFJF); Kong Oscar's Fjord (KOF); Furesø (F); Eleonore Sø (ES); Målebjorg (M); Niggli Spids (NS); Charcot Land (CL); Western Fault Zone (WFZ). *N.B.* Gåseland lies south to the south from this map. Box indicates study area. Question marks indicate unknown or enigmatic contacts, unexplained by past work in the region. We have interpreted the above thrust geometries based on correlations between the preliminary age relationships and fault contacts reported by the Greenland Geological Survey in 1999 and the earlier work of L. Koch, J. Haller and others as referenced above.

Figure 2: Schematic cartoon cross-section through the Forsblad Fjord region depicting reconstructed tectonic evolution of the central East Greenland Caledonides. Note, while the figure is not drawn to scale, the horizontal axis is roughly equivalent to

ca. 200 km. Also note that if ages are provided in a given frame's title, the dates indicate the tightest geochronologic brackets available on the timing of deformation. In some instances, there are ambiguities that arise from the structural relationships between multiple geochronologic constraints, such as the frame depicting the incipient Høgedal detachment. In this frame, deformation may have ceased earlier than the bracket indicates if activity on the Høgedal detachment began during the earliest period allowable by geochronologic constraints (as early as ca. 417 Ma). On the other hand, upper crustal extension apparently continued until ca. 400 Ma, which suggests that if the Høgedal detachment activated earlier than this time, crustal thickening must have stopped and activity on the Høgedal detachment was coeval with that of upper-crustal thinning. Note location of a deep W-dipping normal fault in the final frame is inferred from the work of Schlindwein and Jokat (2000), while the position of the Western Fault Zone (WFZ) is taken from Larsen and Bengård (1991) and the subsequent graben-horst structures from Hartz (1998).

Figure 1

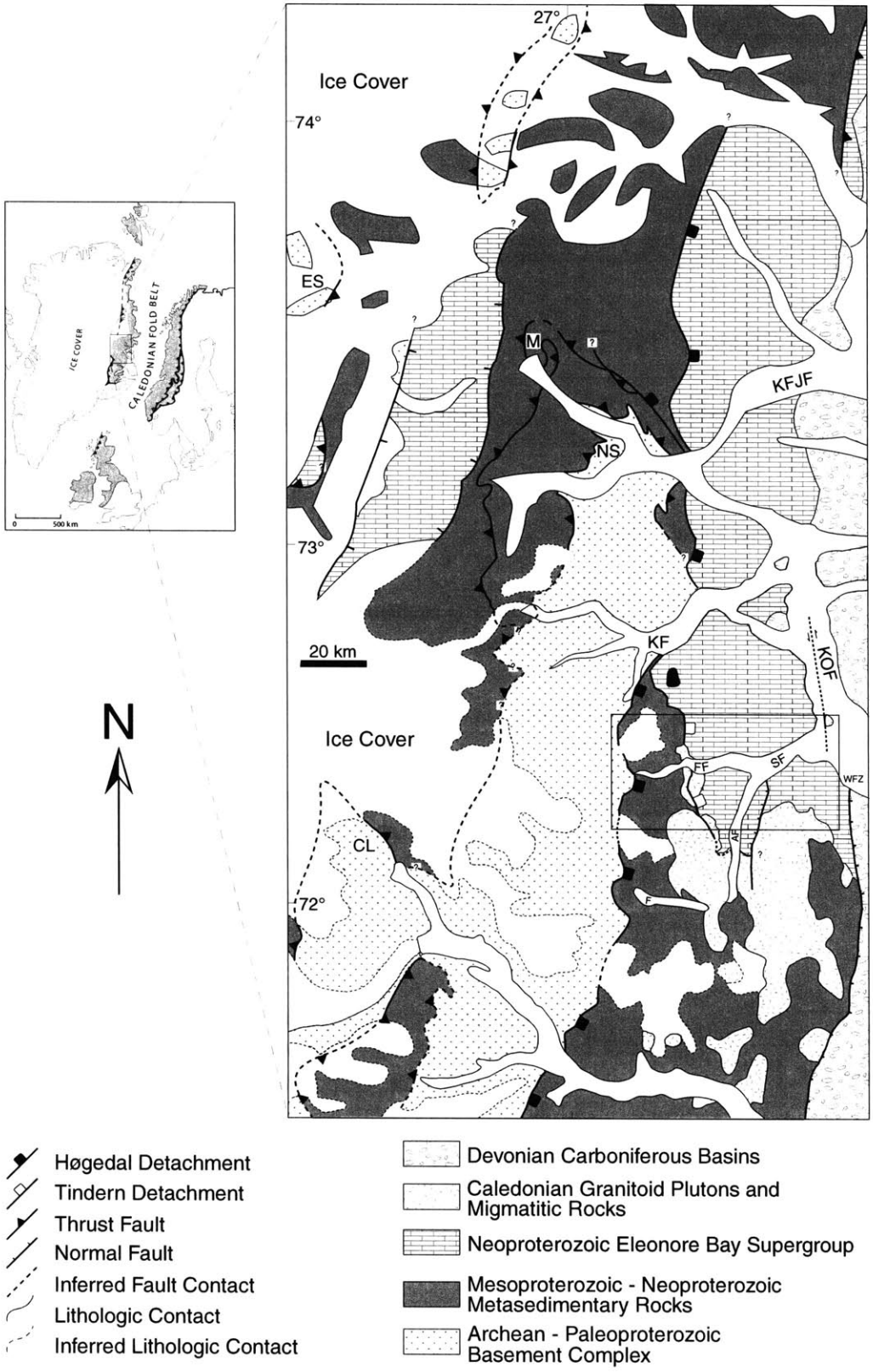
27°
Ice Cover
74°
ES
M
KFJF
NS
73°
20 km
KF
KOF
Ice Cover
FF
SF
WFZ
CL
72°
F
ICE COVER
CALEDONIAN FOLD BELT
0
500 km
N
Høgedal Detachment
Tindern Detachment
Thrust Fault
Normal Fault
Inferred Fault Contact
Lithologic Contact
Inferred Lithologic Contact
Devonian Carboniferous Basins
Caledonian Granitoid Plutons and Migmatitic Rocks
Neoproterozoic Eleonore Bay Supergroup
Mesoproterozoic - Neoproterozoic Metasedimentary Rocks
Archean - Paleoproterozoic Basement Complex

Figure 2

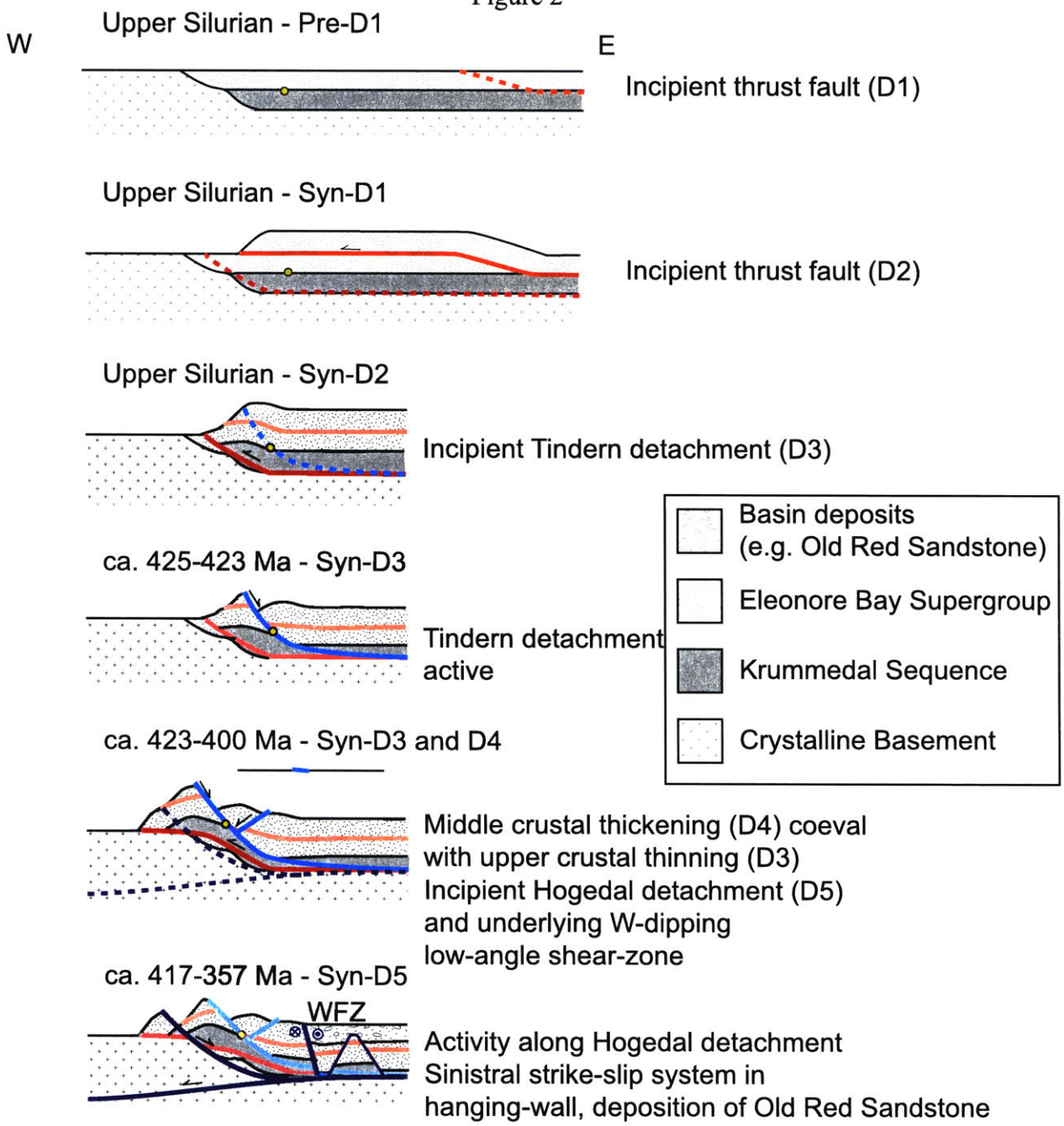

Note - schematic cross-sections not to scale. Horizontal axis represents ~ 200 km.

- Marker-point represents intersection between Tindern detachment and Forsblad Fjord at the present time.

SHORT DISCUSSION OF THESIS FINDINGS WITH RESPECT TO DYNAMICAL MODELS OF OROGENESIS

As is so often the case, the start does not predict the finish; the body of work presented in this thesis extends much further than the original aims as stated in the introduction. However, it is worth briefly returning to the beginning, and discussing the implications of the thesis data with respect to the four testable hypotheses originally proposed as the basis for our work in East Greenland. First, it is important to note that although this thesis presents good evidence for crustal thickening, no thrust faults were mapped in the field, precluding some of the work envisioned in the original thesis proposal. In spite of this, it is clear from the relative and absolute age of fabrics related to crustal thickening and thinning that normal faulting played a significant role during Caledonian orogenesis, both during and after the Baltica-Laurentia collision.

Second, the relative and absolute age constraints on the formation of anatexites and leucogranites indicate that melting was coeval with crustal thickening and slip along the Tindern detachment. Petrographic observations indicate that initial melting occurred during prograde metamorphism as pressure-temperature conditions exceeded first the granite minimum-melting conditions and then the muscovite dehydration reaction curve during crustal thickening. There has been no work to investigate whether this was linked to increased radioactive heat production; however, the fact that pressure increases during crustal thickening were followed by thermal equilibration is consistent with this idea. There is no strong evidence for decompression-related dehydration-reaction melting presented in the petrography discussed in Chapter 4; however, the presence of large, synkinematic, undeformed granite plutons (e.g. Klosterbjerg Granite) in the hanging-wall

of the Tindern detachment remain enigmatic and suggest that there may have been ponding of decompression-related melting associated with slip on that fault.

Third, pressure-temperature-time reconstructions from the Høgedal allochthon provide evidence that decompression was nearly isothermal at structural depths around 4.5 km beneath the Tindern detachment. This is consistent with predictions that suggest material in the footwall should decompress along an adiabat, so long as it is far enough from the hanging-wall to be insulated from any refrigerative effects during movement. However, it was not possible to determine the P-T-t path in the immediate footwall of the allochthon because samples from that region failed the necessary criteria for thermobarometry. Also, it was not possible to determine the P-T-t path near the inferred, underlying thrust because it has been excised by the Høgedal detachment.

Fourth, and most important of all the testable hypotheses, there is strong evidence to suggest that the East Greenland Caledonides experienced alternating crustal thickening and thinning as discussed in Chapter 6. Furthermore, the data suggest that both modes of deformation were active at different structural levels at the same time. This cyclical behavior is robust evidence in favor of dynamical models in which there are alternating periods of domination between the plate-forces that drive crustal thickening and the gravitational forces that drive crustal-thinning. Overall, the fact that these phenomena have been documented in East Greenland, indicates that there may be a more universal applicability of this dynamical model to other continent-continent collisions; however, more evidence from more orogens will be needed to refine and reform our understanding of these complex processes.

FUTURE WORK

The body of work presented in this thesis represents an initial attempt to resolve the complex polyphase Caledonian deformation preserved in central East Greenland; as such, there are many unresolved issues, some that are directly relevant to the arguments developed in this thesis and others that represent new avenues for future exploration.

Further investigation is needed to clarify the following issues. First, the U-Pb chemical ages on monazite used to constrain the earliest phases of deformation and metamorphism in the Krummedal Sequence, as discussed in Chapter 4, need to be calibrated and/or validated with conventional U-Pb TIMS data on monazite from the same sample. This work is currently in progress. However, the data are related to a more fundamental problem that arises from the apparent lack of published geochronologic constraints on the initial timing of the Baltica-Laurentia collision as experienced in East Greenland. The difficulty with pin-pointing this event is the fact that most melts crystallized around the time that synorogenic extension began. However, it is clear that more work can be performed on constraining the age of early prograde metamorphism, which would help to elucidate this problem.

In addition, a post-D_3 thrust fault placed the Krummedal Sequence gneisses onto the Gletscherland Complex, prior to slip on the Høgedal detachment. The arguments to justify this fault hinge on the age of high-temperature metamorphism in the footwall of the Høgedal detachment. The geochronologic data that constrain the timing of this metamorphism include U-Pb SHRIMP analyses of zircon or older Rb-Sr whole rock isochrons and errorchrons. In lieu of actually finding and mapping this thrust fault in outcrop, a whole suite of modern, conventional U-Pb-monazite and xenotime ages as well

as $^{40}Ar/^{39}Ar$ analyses at multiple structural levels beneath the Høgedal detachment would serve as the next best test to determine the validity of these arguments.

Moreover, the timing of upper-crustal extension can be further constrained by dating the mafic dikes in the Upper Eleonore Bay Supergroup that intrude the sedimentary rocks and are displaced by brittle normal faults. Also, it may be possible to further constrain activity on the Fangsthyttegletscher fault with additional geochronologic data from a granite pluton that it deformed.

Beyond this short list of some of the specific problems that have not been answered by this thesis, there are several broader questions that are worth raising. The first relates to the so-called "Western Fault Zone" that is discussed by (Larsen and Bengård, 1991). This significant, left-lateral, strike-slip fault zone has been invoked as one of the major Devonian structures responsible for the opening of the basins and deposition of the conglomerates. Given the late-aged deformation on the underlying Høgedal detachment, it is clearly very important to determine the relationship between these two structures.

Another area ripe for future research involves the large quantity of melt preserved within the Krummedal Sequence that is clearly related to Caledonian tectonic activity. What caused this melt to form, where did it come from, and what were the physical channels of migration? The petrographic observations presented in Chapter 4 indicate that melting of the metasedimentary rocks may have occurred in response to increased temperatures during crustal thickening and dehydration reaction melting during decompression — this is supported by the work of (Watt and Kinny, 1998) and (Watt et al., 2001); however, the fact is that the source region for this melt has not been clearly

established, and may only be revealed with trace-element geochemical analyses. Furthermore, the generation of large, undeformed plutons in the hanging wall of the Tindern detachment, that are the same age as activity on that fault, remain a mystery. For that matter, what is the source region of that melt? This is fundamental question in central East Greenland where the base of the Eleonore Bay Supergroup is frequently marked by both a tectonic unconformity and the intrusion of these "post-orogenic" granite plutons.

Another realm for future work in East Greenland is the polydeformed crystalline basement that lies beneath the Fjord Region Detachment such as the Gletscherland Complex. These rocks have been all-but-dismissed in this thesis because their age precludes the application of any deformational and/or metamorphic data to Caledonian events. However, these rocks represent one of the rare and valuable pieces of Archean-Paleoproterozoic real-estate that has not been properly explored in the modern age of geochronology, metamorphic petrology, and trace-element geochemistry. An entire thesis would be well-devoted to the difficult task of resolving some of this complexity.

Finally, the data presented in this thesis indicate that the earliest phases of deformation and metamorphism preserved in the Krummedal Sequence gneisses of Forsblad Fjord were Caledonian. Thus, the fact that U-Pb SHRIMP data indicate that zircon in correlative rocks north of the field area experienced a thermal overprint at ca. 1 Ga (Kalsbeek et al., 1998), does not constrain the deformation and metamorphism in those rocks to that time period (as argued recently by the Greenland Geological Survey) because of problems of inheritence. However, if one billion-year-old metamorphic monazite and/or xenotime were found in textural context that constrains deformation to be pre-Caledonian, this would resolve the conflict.

Reference:

Larsen, P.H., and Bengård, H.J., 1991, The Devonian basin initiation in East Greenland: A result of sinistral wrench faulting and Caledonian extensional collapse: Journal of the Geological Society of London, v. 148, p. 355-368.

Watt, G.R., and Kinny, P.D., 1998, Caledonian migmatization and granite formation in the northern Gåsefjord-Stauning Alper migmatite and granite zone, East Greenland, *in* Higgins, A.K., and Frederiksen, K.S., eds., Caledonian geology of East Greenland 72°-74° N: preliminary reports from the 1997 expedition, Volume 28: Denmark, Danmarks og Grønlands Geologiske Undersøgelse rapport.

Watt, G.R., Kinny, P.D., and Friderichsen, J.D., 2001, U-Pb geochronology of Neoproterozoic and Caledonian tectonothermal events in the East Greenland Caledonides: Journal of the Geological Society of London, v. 157, p. 1031-1048.

Appendix Thesis Proposal: General Exam Paper #1

Dynamic interactions between thrusting and normal faulting within the East Greenland Caledonides: could they be a Himalayan prototype?

Introduction

Le Chatelier's principle for a closed system states that, "If an external stress is applied to a system at equilibrium, the system will adjust itself in such a way as to partially offset the stress" (Chang, 1988). In accordance with this principle, gravity and heat loss work together to dissipate energy through the dynamic interaction of orogen convergence and orogen collapse. This has been a source of study for the past 13 years in the modern Himalayas. As India collides with Asia, compression has thrust the structurally deeper Greater Himalayan Sequence southwards (along the Main Central Thrust) on top of the shallower Lesser Himalayan Sequence (as illustrated in Figure 1). While this has been happening, the northern boundary of the Greater Himalayan Sequence records unloading along the South Tibetan Detachment (Burchfiel and Royden, 1985; Burchfiel et al., 1992). Geochronological constraints on kinematics and timing of these faults demonstrates their synchroneity on short timescales over millions of years (e.g. Hodges et al., 1996). Even though the Himalayan orogen is not in a closed system equilibrium, Le Chatalier's principle can still be applied to suggest thrusting and normal faulting work in consort to drive the orogen towards a state of minimum entropy (Hodges, submitted). This fundamental and interesting phenomenon has been documented extensively throughout the Himalayas, but it has not been directly observed in any other mountain range. In addition, the timing and interaction of these thrusts and

detachments beneath their surface exposures in the Himalayas remains a mystery. For this reason, the East Greenland Caledonides (70° N to 82° N) present a unique and exciting opportunity to investigate this theory of dynamic compensation. This approximately 400 My old, two sided orogen involved the subduction of Baltica beneath Laurentia (present day Scandinavia, UK, Ireland, Greenland, and North America), illustrated in Figure 2. This orogen has regional dimensions and geometries on the order of the modern Himalayas; and it has been exhumed just enough that interactions between thrusts and normal faults at depth may be exposed. Reconnaissance work within the area (72° N to 72.5° N) this past summer suggests that structures, textures and mineral assemblages are ideal for testing hypotheses generated from findings in the Himalayas.

There are three empirical observations from Himalayan tectonics which I propose to look for in East Greenland. First, timing of thrust and normal fault kinematics should be roughly synchronous over the entire period of orogenic deformation. This has been documented for example in transects across southern Tibet (Hodges et al., 1993) and Annapurna (Hodges et al., 1996). Second, specific cause-and-effect relationships between anatectic leucogranites, migmatitic leucosomes and faulting exist and should be recorded in the rock record as seen in the Himalayas (e.g. Burchfiel et al., 1992; Hollister and Crawford, 1986; Harris and Massey, 1994; Hodges, submitted). And third, there are predictable PTt histories which should be preserved in the exhumed wedge bound by thrust and detachment systems, as seen for example in a transect across the Greater Himalayan sequence in southern Tibet (Hodges et al., 1993). If dynamic compensation is truly a phenomenon universal to all mountain ranges, then these characteristics, with some expected variability, should be present in orogens everywhere. Testing this has proved more difficult than expected in many modern settings due to oblique convergence

during orogenesis. It is fortuitous that India and Asia converge so directly to form the Himalayas. And for this reason also, though there is some transpression recorded in the East Greenland Caledonides (e.g. Larsen and Bengård, 1991; Strachan et al., 1992), their relatively simply north-south trending contractional features suggest they will provide a similar testing ground.

To investigate these hypotheses predicted by the Himalayan, dynamic compensation model, I propose a field study of the Forsblad Fjord region (72° to 72.75° N) which cuts perpendicularly across the East Greenland Caledonides (Figure 3). Views along this fjord's walls expose a spectacular cross section of the regional metamorphism and deformation. In particular, prior structural work in this fjord and nearby regions (Haller, 1970; Caby, 1976; Higgins et al., 1981; Rex and Gledhill, 1981), though a matter of current debate (Andresen et al., 1998), suggests that it crosscuts an orogen-parallel, west verging thrust fault system which is in close proximity to an east verging detachment system. The structural relationships between these faults and the migmatitic, metasedimentary, amphibolite facies rocks which they bound look suspiciously like the Main Central Thrust and South Tibetan Detachment systems which sandwich the Greater Himalayan Zone. If this comparison proves relevant, then this fjord will be an excellent place to examine dynamic compensation models at a deeper crustal depth than can be done in the Himalayas. On the other hand, if this comparison is not fair, then Forsblad fjord still presents an exciting opportunity to explore extensional faulting at depth. For further discussion, it will be useful to briefly summarize and place the regional geology of the Scandinavian and Greenland Caledonides into a simple Himalayan tectonic framework.

Regional Geology of the Scandinavian and East Greenland Caledonides:

Characterized as a two sided orogen, Baltica is thought to have slid beneath Laurentia in an A-type subduction during the middle to upper Silurian to lower Devonian (Hodges et al., 1982, Henriksen, 1985). This extended event formed linear trending complementary fold and thrust belts, one side with thrusts verging to the east and the other side with thrusts verging to the west (inset of Figure 3). The East Greenland Caledonides represent the half with thrusts verging to the west, while the Scandinavian Caledonides represent the half with thrusts verging to the east. Modern plate reconstructions suggest that these orogens are not complementary. Instead, the opening of the Atlantic Ocean along with additional plate motions has separated the Scandinavian Caledonides from its true counterpart, the West Shetland and Hebrides shelves, and has hidden the East Greenland Caledonides' counterpart beneath the Barents Sea (Ziegler, 1985). However, for this comparison it is acceptable to assume that the Caledonides of Scandinavia reasonably represent what East Greenland's counterpart would be like if they could be examined.

The record of multiple events of deformation and metamorphism within the Scandinavian Caledonides has made its reconstruction complicated. Tectonostratigraphers have divided the orogen into four north-south trending allochthons (Gee and Sturt, 1985). Composed of piles upon piles of nappe sequences, each allochthon has been thrust up and to the east. Evidence to support the notion that Baltica subducted beneath Laurentia (comparative to India's subduction beneath Asia) and not the other way around hinges on field observations of a north-south trending Caledonian age continental arc (Gee, 1975; Hodges et al., 1982; Andresen and Steltenpohl, 1994). In addition to repeated thrust sequences, evidence for normal faulting and Devonian basin

formation has also been identified and hypothesized to record orogen collapse (Cashman, 1990; Northrup and Burchfiel, 1993; Gee et al., 1994; Rykkelid and Andresen, 1994). At the present, exposure of a clearly orogen-parallel detachment has not been recognized in Scandia. Some workers suggest that this structure may be just offshore to the west (Coker et al., 1994). To put this into our Himalayan framework, the Scandinavian Caledonides might best be viewed as a counterpart to the high Himalayas.

On the other hand, detailed mapping in the East Greenland Caledonides from 1947 to 1958, under Lauge Koch's supervision, also revealed an intricate series of metamorphic complexes (Haller, 1970; Higgins et al., 1981; Peucat et al., 1985; Henriksen, 1985; more references) structurally overlain by Precambrian, Cambrian, and younger unmetamorphosed, sedimentary sequences. This pile of nappes is similar in many ways to the intricate nappes of Scandinavia. Metamorphism and deformation of these north-south trending structures, seen on Figure 1, was originally thought to be solely of Caledonian origin (Backlund, 1930, Wegmann, 1935). Contacts separating migmatitic basement crystalline rocks cropping out on the western edge of the orogen from their neighboring migmatitic metasedimentary gneisses to the east were generally mapped as thrust faults (Haller, 1970; Henriksen and Higgins, 1976). However, more recent research by the Greenland Geological Survey over the past 20 years has suggested that multiple events may have contributed to this metamorphism and deformation which has been recorded in East Greenland (Henriksen and Higgins, 1976; Rex et al., 1976; Rex and Gledhill, 1981). And, since the recognition of major extensional features in the Himalayas, previously mapped normal faults have been remapped to connect into one another along a regional north-south trending zone just east of the main thrust fault system (e.g. Peucat et al., 1985; Larsen and Bengård, 1991; Strachan, 1994; Hartz and

Andresen, 1995; Andresen et al., 1998), as seen in Figure 1. Therefore, to put the East Greenland Caledonides into a Himalayan tectonic picture, they might best represent thrusting and collapse near the back side of the Tibetan plateau. This analogy does not need to be exactly correct. More important is the observation of extension within a compressional environment. This is why the Forsblad Fjord region, where prior mapping depicts these detachment systems side-by-side with thrusts in an overall compressional environment, makes such a good location for this project. Please note that future comparisons between East Greenland and the Himalayas in this paper will make use of observations from the high Himalayas because this is the type locality for normal faulting in a compressional environment.

Testing Hypothesis #1: Timing and Kinematics of Faulting

Predictions from Himalayan tectonics suggest thrust faulting associated with orogen formation should be accompanied by coeval normal faulting as summarized schematically in Figure 1. As compression during convergence thrusts the Greater Himalayan Sequence upwards and southwards, the Tibetan Sequence drops back down to the north when the mountain range grows too high. Meanwhile, thrusting continues to drive the Greater Himalayan Sequence upwards, creating a dynamic relationship between thrusting and normal faulting. The interaction of these faults at depth has not been observed and remains purely speculative at this point; this proposed research may provide some empirical insights into these fault geometries at depth. For now, one suggested option is that these faults continue on down to separately root in a ductile zone of the crust, while an alternative option suggests that these faults merge together at depth onto a

single, shared fault surface. In either scenario, observations from near-surface Himalayan exposures have shown that these faults must move synchronously over millions of years. This has been demonstrated using U-Pb geochronological constraints from granitic bodies in the Himalayas (Schärer et al., 1986; Parrish et al., 1992; Hodges et al., 1996).

To test this prediction of coeval faulting in the Forsblad Fjord region, the timing and kinematics of fault zones dividing the local tectonostratigraphy need to be worked out. Relevant formations can be divided into a sandwich of three north-south trending units comparative to the Lesser Himalayan zone, Greater Himalayan zone and Tibetan sequence. Analogous to the Greater Himalayan Zone, the amphibolite facies Krummedal supracrustal sequence lies fault bounded between the Gletscherland migmatite complex to the west (Lesser Himalayan Zone counterpart) and the Eleonore Bay Supergroup Sequence to the east (Tibetan Sequence counterpart), illustrated on a simplified map in Figure 4.

Structurally lowest in this regional tectonostratigraphy lies the crystalline basement called the Gletscherland migmatite complex (Haller, 1971; Henriksen and Higgins, 1976). This composite of granites, gneisses and amphibolites is characterized by clusters of small migmatitic bodies all swirled around together. The only available dates have been yielded from early Rb-Sr and K-Ar analyses and suggest an Archean age with Caledonian overprinting (Rex et al., 1977; Rex and Gledhill, 1981). This formation is bounded to the north and the west by conformable zones of supracrustal rocks (Henriksen and Higgins, 1976), and to the east by a mylonitic zone several meters thick. In most places this mylonitic zone has been mapped as a west verging thrust fault (Haller, 1971; Higgins et al., 1981). However, current work by Andresen et al., 1998, as well as reconnaissance work this past summer, suggests that the most recent sense of shear

indicators (e.g. east verging asymmetric boudins, east verging folds, rotated garnets with tails, and east plunging lineations) recorded within this contact zone in Forsblad Fjord show normal fault motion, down to the east. For this reason it is drawn as a detachment (it extends up into the brittle zone) in figure 4. But it is important to note that while Andresen argues that this contact has been mapped fundamentally incorrectly as a thrust fault and really is a detachment, I clearly saw shear sense indicators verging to the west (thrust motion) in Forsblad Fjord being overwritten by shearing associated with this detachment. Therefore, it seems more than likely that there is also an older thrust fault zone which may crop out differently in other places depending on the structural depth of exposure. This has implications which I will discuss shortly.

The Krummedal supracrustal sequence is the next unit structurally up and to the east along the fjord. This repetitive collection of amphibolite grade, banded biotite-garnet gneisses, has a compositional layering which strikes north-south and dips moderately to steeply eastward. The sequence contains abundant leucosomes and is frequently intruded by anatectic leucogranites. There are also frequent garnet-hornblende bearing calc-silicate lenses and garnet-amphibole bearing amphibolite lenses scattered throughout the sequence. Kyanite and sillimanite are common, and Higgins et al., 1981, write that they observe a decrease in proportion of kyanite eastward which is accompanied by an increase in proportion of sillimanite. This seems reasonable but I still need to confirm this in my own suite of thin sections. Suspect early Rb-Sr dates yielded from this sequence suggest a Proterozoic provenance for deformation and metamorphism overwritten by Caledonian orogenesis (Rex et al., 1976; Rex et al., 1977; Rex and Gledhill, 1981). However, my own preliminary U-Pb dates for monazites in leucogranite intrusions within

this sequence are early Silurian. These match with other dates mentioned by Andresen et al., 1998.

The eastern contact between the Krummedal supracrustal sequence and the weakly metamorphosed Eleonore Bay Supergroup is marked by a sharp break in metamorphic grade and intrusion of a large, foliated, biotite granite. This granite contains enclaves of both Krummedal and Eleonore Bay lithologies (seen last summer). Structures below the contact do not continue above. In addition, a marked mylonitic foliation was visible within the intruding biotite granite which strikes parallel to the Krummedal sequence - Eleonore Bay Supergroup contact and has top-to-the-east shear-sense indicators. All these observations suggest this is a detachment as previously mapped by Higgins et al., 1981. Sitting above this contact is a very thick sequence of slightly metamorphosed to completely unmetamorphosed Proterozoic to Ordovician sediments called the Eleonore Bay Supergroup.

Although large regional, geologic maps already exist, there are still debates regarding some fault system kinematics as mentioned above. Therefore, I plan to carefully remap all fault contacts with close attention to visible shear sense indicators within the Forsblad Fjord Region, including exposures in both inner Alpefjord and Kempes Fjord which are nearby to the south and north. Then I propose using U-Pb geochronology (technique discussed in Laboratory Methods appendix) on samples from granitic bodies chosen for their ability to constrain timing of motion along the fault contacts. For example, the mylonitic fabric within the biotite granite discussed above suggests intrusion before the last shearing event within the eastern detachment. This implies that a crystallization age for this granite dates the maximum age for the most recent motion along the fault. I have already done a preliminary U-Pb analysis on 4

monazite crystals from this granite. The $^{207}Pb/^{206}Pb$ date for the most concordant crystal (1% discordancy) was 424.6 ± 1.0 Ma. This represents the best current estimate for the date that the fault last moved. Similar U-Pb constraints can be placed on the western brittle detachment zone as well. Additionally, pseudotachylytes from within the brittle fault zone were sampled during last summer's reconnaissance trip. These glass melts, which formed during faulting, can be directly dated using ^{40}Ar-^{39}Ar with the laser spot fusion technique.

More complicated to constrain will be the thrust fault since it appears overprinted by successive stages of normal faulting. However, if the Krummedal supracrustal sequence turns out to be Caledonian in age as implied by another preliminary U-Pb analysis on a leucogranite intrusion, then dating truncated plutonic bodies displaying thrust sense of shear in the hanging wall of this fault, which is significantly older than the footwall, will provide a maximum age of thrusting. Furthermore, I hope to directly date deformational fabrics which display thrust sense of shear. This will be complicated by any overprinting due to normal faulting. Therefore, samples will be chosen on the basis of detailed petrographic studies of their microtextural features to determine whether they adequately represent periods of peak metamorphism during thrusting (e.g. no microtextural retrograde metamorphism or overprinting of shear indicators by normal faulting). Then using the technique discussed by Gromet, 1991, on samples with mineral assemblages such as Pl-Hbl-Kfs-Spn-Ap (mineral abbreviations after Kretz, 1983), the U-Pb, Sm-Nd and Rb-Sr isotope systems can be applied in consort to constrain the age of recrystallization of minerals within the deformational fabric. This will provide an age of peak metamorphism of deformation associated with thrusting, thus an approximate minimum age of thrusting itself.

Finally, important kinematic information associated with the normal fault systems in this region can be gleaned from studying the cooling history of their footwall rocks. Using ^{40}Ar-^{39}Ar on a series of minerals with different closure temperatures such as Ksp, Bt, Ms and Hbl, (Dodson, 1973; Hodges, 1991) the rate of cooling within a sample can be determined. If cooling is rapid, it suggests the sample has been unroofed quickly. So assuming a geothermal gradient, e.g. 30° C/km, an unroofing rate can be calculated for the sample. This will be important for understanding kinematics of these faults. Therefore, I propose to examine the cooling history for a suite of samples from below the base of the western detachment all the way across the Krummedal supracrustal sequence to just below the base of the eastern detachment (^{40}Ar-^{39}Ar technique discussed in Laboratory Methods appendix). Most of these samples have already been gathered during last summer's trip, and contain sufficient amounts of all the necessary minerals described above to analyze.

Combining this information with geochronological constraints on fault motion, hypothesis #1 can be directly tested to determine direction of motion along all fault systems which crop out in the Forsblad Fjord region, and whether these fault systems really moved at the same time as predicted by dynamic compensation in the Himalayas. Furthermore, if the brittle detachment to the west really overprints a thrust fault as suggested earlier, then this detachment may actually be moving along the same surface as the original thrust. This has important ramifications to the original model of dynamic compensation. Heretofore, there has been no direct observation of the interaction between thrusting and normal faulting at depth as described above. However, if this detachment reactivates the thrusting surface, then depending on the synchroneity of these two faults,

this may provide empirical evidence that lower crustal geometries of faulting in the second scenario mentioned earlier may be closer to accurate.

Testing Hypothesis #2: The Role of Anatexis During Faulting

There are specific cause and effect relationships between anatexis and faulting which have been observed in the Himalayas. Two main models have been developed there to explain the role of anatectic melting during orogenesis. The first model suggests that anatectic melting occurs (because of crustal thickening and increased amounts of radioactive heat production) at deep structural levels which weakens the crust and nucleates thrusting (Hollister and Crawford, 1986; Hollister, 1993; Hollister et al., 1995). The second model agrees that there may be a relationship between leucosome formation and thrusting, but suggests that leucogranite bodies are formed by decompression melting due to normal faulting (Hodges, 1990; Harris and Massey, 1994; Hodges, submitted). These models depend on a suite of structural, petrologic, geochemical and geochronological observations which can just as easily be tested in the East Greenland Caledonides.

As mentioned earlier, the Krummedal supracrustal sequence is rife with migmatitic bodies from small leucosomes no larger than a pencil to leucogranites 10s of meters thick. The first question to ask is do these leucosomes and leucogranites have the same origin, and is their source the surrounding meta-pelites? In the Himalayas, the leucosomes in pelitic gneisses (like the Krummedal sequence) typically contain the mineral assemblage Qtz+Kfs+Pl+Ms±Bt±Tur±Grt±Sil and sometimes Ky (Hodges et al., 1996; Hodges, submitted), while the leucogranites contain either Qtz+Kfs+Pl+Bt±Tur or Qtz+Kfs+Pl+Ms+Tur±Crd (Hodges et al., 1993; Inger and Harris, 1993; Harris and

Massey, 1994; Guillot and Le Fort, 1995; Scalliet et al., 1995; Searle et al., 1997). Recent trace element modeling has suggested that some Himalayan leucosomes have not melted from their immediate surroundings (Harris and Massey, 1994) but predate Himalayan tectonics. Applying this reasoning to Greenland, I propose to petrologically examine a suite of leucosome and leucogranite thin sections both under the microscope and the electron microprobe to determine their mineral assemblages. Then taking a representative sample of the leucosomes and the leucogranites, I propose to use Sm-Nd and U-Pb geochemistry to test whether their source regions could be the surrounding meta-pelites. This can be done easily by first dating each granitic body with U-Pb, then determining the Sm-Nd isotopic ratios from both the granitic bodies and their surrounding metasediments. If evolutionary curves from both migmatite and country rock intersect at the same age yielded by the U-Pb system, this suggests that the granitic body being analyzed may have melted directly from the surrounding metasediments. In addition, testing both leucosomes and leucogranites will also show whether these two types of granitic bodies have the same origin.

Next, the structural and timing relationship between these migmatitic bodies and regional fault systems needs to be unraveled. In the Himalayas, the earliest shearing fabrics associated with movement on the Main Central Thrust system have been demonstrated to be synmetamorphic with respect to anatectic melting (Hodges and Silverberg, 1988; Hubbard and Harrison, 1989; Parrish and Hodges, 1993; Hodges et al., 1996). Meanwhile, the earliest phases of anatexis predate the Main Central Thrust by 2 -3 my (Hodges et al., 1996; Coleman, submitted). In addition, when leucogranites can be traced down to the approximate structural level of the basal South Tibetan Detachment system, some exhibit extensional shear associated with these basal detachments (e.g.

Burg et al., 1984; Searle and Fryer, 1986; Burchfiel et al., 1992; Hodges et al., 1994) and some exhibit direct truncation along their ceilings by these detachments (e.g. Burchfiel et al., 1992; Searle et al., 1997). Later stage leucogranites intrude these basal detachments and are truncated by more recent, structurally higher movements along the South Tibetan Detachment system (Burchfiel et al., 1992; Guillot et al., 1993; Hodges et al., 1996). Looking for similar relationships within the Forsblad Fjord region is a matter of attentive mapping within the upper Gletscherland complex and Krummedal sequence and a few well placed geochronologic constraints therein. If these relationships are different, then the question will be what is the role of anatexis in the East Greenland Caledonides and why is it different than in the Himalayas? If similar relationships are observed, then the question will be what new information can be learned from looking at anatectic melting at a deeper crustal level? This study may provide particularly interesting new knowledge if it turns out that Forsblad Fjord exposes a depth where thrusting and normal faulting occur along the same surface (i.e. the contact between the Gletscherland Migmatite Complex and the Krummedal supracrustal sequence).

Testing Hypothesis #3: Pressure-Temperature-Time Histories

Work in the Himalayas suggests there are characteristic pressure-temperature-time (PTt) histories associated with orogens undergoing dynamic compensation. In particular, decompression and related cooling histories associated with tectonic denudation should be recorded by retrograde metamorphism. Simultaneous and rapid motion on both thrust and normal fault systems leads to the prediction of distinctly separate PTt histories within the wedge of rocks bound between them. In the center of the wedge, rapid tectonic exhumation should record nearly isothermal decompression

(approximately along an adiabat). Near the top and bottom of the wedge, similar rates of tectonic exhumation should record decompression relative to structural position. However cooling will not be adiabatic due to refrigerative effects as colder material is faulted next to the warm material inside the wedge. It is important to note that these predictable PTt paths will only be recorded if tectonic denudation is fast enough to prevent thermal equilibration of rocks within the wedge; and this depends on the thermal conductivity of the rocks themselves. Otherwise, their cooling histories will reflect upward motion through a geotherm.

This theory has been tested in southern Tibet by Hodges et al., 1993. There, they found that samples from roughly 4 - 6 km above the Main Central Thrust (base of the Greater Himalayan Sequence) recorded decompression and cooling of ca. 150° C. While samples (7-8 km) beneath the detachment (middle of the Greater Himalayan Sequence) recorded decompression and adiabatic cooling. However, this model can just as easily be tested in the East Greenland Caledonides. Thus, I propose examining samples from five localities, one from about 8 km west of the brittle detachment (Gletscherland Migmatite Complex), one just west of this same detachment, one from the base of the Krummedal Supracrustal Sequence, one from the middle of this sequence and one from the top of this sequence just west of the eastern ductile detachment. Next, I will take a close look at the petrology of these samples to determine whether the necessary criteria for thermobarometry are met (e.g. local, ionic solution equilibrium is maintained, reactions of geothermometers and geobarometers occur synchronously, garnet zoning is product of continuous reaction, etc.). Finally quantitative thermobarometry using GARB and GASP (Hodges, 1991), mineral zoning in garnets (Spear, 1993) and U-Pb geochronologic constraints can be all combined to reconstruct the PTt histories of these rocks (techniques

discussed in methods section). As an additional prediction from the metamorphic history, all amphibolite grade metamorphism should be related to the detachment (preliminary date ca. 424.6 ± 1.0), and thus should also be Caledonian in age. This will be testable using Gromet's method for dating deformation fabrics as mentioned above.

Conclusion

Through detailed mapping in the Forsblad Fjord region and an aggressive approach towards geochronology, petrology and quantitative thermobarometry as outlined above, I hope to test the viability of dynamic compensation as defined in the Himalayas. The East Greenland Caledonides provide a unique *"natural laboratory"* because of their tremendous exposure at deeper crustal levels which is not possible in modern orogens. This field area may even show the overlapping interaction between thrusting and normal faulting at depth, now only speculated upon in the Himalayas. However, if this scenario does not pan out, this proposed research will still substantially increase knowledge of extension within compressional environments at deeper crustal levels and ultimately aid in the fundamental understanding of orogenesis.

Appendix:

Laboratory Methods

U-Pb: All U-Pb analyses will be conducted on the solid source MIT thermal ionization mass spectrometer. Zircons will be air abraded and dissolved in HF at a temperature of 220° C. Monazite and xenotime will be washed in acetone and dissolved in HCl at a temperature of 180° C. Samples will be spiked with ^{205}Pb-^{233}U-^{235}U. Then Pb

and U will be separated using anion-exchange chemistry resulting from the incremental addition of HCl and H_20. These separates will be mounted with phosphoric acid on Re filaments and electrically ionized.

For successful use as a geochronometer this technique requires four basic assumptions to be fulfilled. First, the mineral to be analyzed must have been in a closed system with respect to U, Th, Pb and all intermediate daughter products throughout its history. Second, initial Pb isotope ratios must be accurately estimated for age calculation. Third, the decay constants must be correct. And fourth, U isotopic compositions cannot be fractionated (basic assumptions after Faure, 1986). Since almost none of these assumptions are ever fully met, each must be corrected for as follows: first, to recognize potential effects due to open system behavior, both $^{206}Pb^*/^{238}U$ and $^{207}Pb^*/^{235}U$ are determined and plotted up on a concordia diagram. This provides a method to assess the amount of open system behavior (i.e. Pb, U loss and/or gain). Reasons for this open system behavior vary, but can be associated with metamorphism, continuous diffusion of Pb and chemical weathering (Faure, 1986). Essentially, samples with no open system behavior will plot on concordia, i.e. both ages calculated from decay of ^{238}U to ^{206}Pb and ^{235}U to ^{207}Pb agree. However, if samples do not plot on concordia, a best estimate from the discordant age may still be possible to obtain. In addition, to minimize potential late stage overgrowths on the rim of zircon grains, these minerals will be abraded slightly (as mentioned above). Second, estimation of initial Pb isotopes will be based on the Stacy-Kramers common lead, 2 stage growth model (Stacey and Kramers, 1975). Third, decay constants to be used will be the accepted values as defined by Steiger and Jäger, 1977. Though these may not be 100% accurate, the adherence to these accepted standards allows comparison between results from this study and other U-Pb data in the literature.

Finally, isotopic fraction will be corrected on the basis of whichever of the following method yields the lowest standard deviation in $^{207}Pb/^{204}Pb$ and $^{206}Pb/^{204}Pb$ ratios, linear correction, power law correction or exponential correction.

In addition to these issues, another point to consider is age inheritance. Since most minerals of interest, such as zircon, have extremely high closure temperatures, >700° C, they are likely to retain original crystallization ages in their cores after metamorphism. Therefore, to date these deformational, metamorphic fabrics in the Krummedal Sequence, it will be best to use monazite and xenotime which have been demonstrated to typically grow during metamorphism (Hawkins and Bowring, 1997) despite their high closure temperatures, as opposed to zircon which grows prodigiously during any kind of plutonism.

^{40}Ar-^{39}Ar: Mineral separates will be prepared in an acetone bath and then sent to be irradiated at the McMaster reactor in Ontario, Canada. This procedure enables ^{39}Ar to be used as a proxy for ^{39}K with the introduction of a correction (J) factor based on the irradiation history. A monitor of known age must also be irradiated in order to solve for this J factor. Then gas will be released from samples either using a furnace step heating method or laser spot fusion procedure. All analyses will be conducted on a Mass Analyser Products (MAP) 215-50 rare gas mass spectrometer.

The application of this technique to determine a cooling history depends upon the availability of a variety of minerals with different closure temperatures such as Hbl, Bt, Ms and Ksp. The functionality of this method depends upon the mineral being in closed system behavior with respect to K and Ar. This criteria is not always met. If

excess Ar has been retained uniformly throughout the crystal, it may be impossible to detect. Otherwise, stepwise heating of the irradiated samples, either in a furnace or with the laser, will provide a spectrum of dates anomalously old at low temperatures and without reliable plateaus at higher temperatures. If Ar has been lost from the sample, stepwise heating may reveal a plateau date equal to or slightly younger than the time of crystallization. Unlike U-Pb, there is no test of concordance. However, the big advantage of stepwise heating is that anomalous domains within the crystal may be recognized and discarded from the overall data set.

Additional concerns regard accurate decay constants, introduction of atmospheric argon into the mass spectrometer and correct estimation of initial $^{40}Ar/^{36}Ar$ ratios (a measure of inherited ^{40}Ar). As with U-Pb, the decay constants to be used are those published by Steiger and Jäger, 1977; and introduction of atmospheric argon can be corrected for by running a blank after each sample. Furthermore, fractionation problems are eliminated by using a gas source mass spectrometer. However, estimating initial Ar ratios can make a big difference in model ages depending on how much radiogenic Ar is in the sample. Typically, this initial ratio is assumed to be the $^{40}Ar/^{36}Ar$ ratio of atmosphere (295.5). To see how much effect an incorrect estimation of this initial ratio will have on the calculated age, $^{39}Ar/^{40}Ar$ vs. $^{36}Ar/^{40}Ar$ is plotted for a variety of plateau segments (temperature increments) of a stepwise heating run on an inverse isotope correlation diagram. On this kind of plot, the reciprocal of the x intercept yields the age. And the comparison of the reciprocal of the y intercept with present day atmosphere $^{40}Ar/^{36}Ar$ (295.5) shows how strong the effect of the initial $^{40}Ar/^{36}Ar$ will have on the model age. It can be easily seen from this diagram that if the sample consists mostly of radiogenic Ar, then it plots close to the x axis, and the initial $^{40}Ar/^{36}Ar$ ratio will have

almost no effect on the x intercept. So older rocks such as the metasedimentary migmatitic gneisses which make up the Krummedal supracrustal sequence, which should have lots of radiogenic Ar, should not be very dependent on the initial $^{40}Ar/^{36}Ar$ ratio.

Thermobarometry: This paper proposes to determine P-T paths by combining GARB with GASP and employing in-depth studies of garnet zoning. GARB is a geothermometer which depends on the exchange of Fe and Mg between biotite and garnet:

$$Fe_3Al_2Si_3O_{12} + KMg_3AlSi_3O_{10}(OH)_2 = Mg_3Al_2Si_3O_{12} + KFe_3AlSi_3O_{10}(OH)_2$$

Almandine + Phlogopite = Pyrope + Annite

First, detailed petrology of the sample must be done to determine whether the reaction textures of the biotite and garnet indicate that they formed at approximately the same time. This might be suggested by inclusions of biotite within the garnet, or the presence of touching grains. Then, assuming ideal ionic solution behavior (Spear, 1993) between the biotite and garnet, the activities of Almandine, Phlogopite, Pyrope and Annite can all be measured with the electron microprobe and used to calculate an equilibrium constant. Next, since this equilibrium constant has a tremendously small pressure dependence, charts determined from experimental petrology (e.g. Ferry and

Spear, 1978; Hodges and Spear, 1982; Berman, 1990) can be used to figure out the temperature at which the exchange reaction occurred.

On the other hand, GASP can be used to identify the pressure at which the following reaction occurs:

$$3CaAl_2Si_2O_8 = Ca_3Al_2Si_3O_5 + SiO_2$$

Anorthite = Grossular + Kyanite + Quartz

Again, using detailed petrology to determine whether the different minerals involved were in equilibrium and assuming ideal ionic solution behavior, the electron microprobe can be employed to measure the activity of the anorthite, grossular, quartz, and aluminosilicate minerals. From this, the equilibrium constant can be calculated. And then taking advantage of the steep temperature dependence of the equilibrium constant for this reaction, the pressure can be looked up on charts already constructed from experimental petrology (e.g. Ghent, 1976; Hodges and Spear, 1982; Hodges and Royden, 1984; Koziol and Newton, 1989).

In order for GARB and GASP to be used together to give pressure and temperature at the same time, reaction textures must be examined under a microscope to determine whether ionic solution equilibration for both sets of minerals was occurring simultaneously. Furthermore, it must be noted that the pressure and temperature yielded by these thermobarometers may not represent peak metamorphism as recorded by

geochronometers for the same sample. However, GARB and GASP can still be used to get a more detailed picture with relative timing (t), through the Gibbs approach to garnet zoning as described by Spear and Selverstone, 1983. In this method, the electron microprobe is used to measure activities of each component of garnet present in a traverse from core to rim of a single garnet grain. Then making the assumption that this garnet grew in ionic equilibrium with a coexisting matrix of biotite, plagioclase, silica and aluminosilicate, GARB and GASP can be used to calculate P and T from core to rim. This technique involves four main assumptions. First and foremost, at each point along the zoning profile, local equilibrium is maintained at the rim of garnet growth and represents a frozen equilibrium composition. Second, a continuous reaction is responsible for all zoning produced during garnet growth. Third, mineral assemblages present during garnet growth and the reactions responsible for this growth are known, e.g. GARB and GASP. Fourth, Diffusion has not modified zoning during or after garnet growth (after assumptions listed by Spear, 1993). The first three of these assumptions can be reasonably well addressed with careful petrography, looking at reaction textures and spatial relationships between the minerals. The fourth assumption is more difficult to satisfy. Diffusion is highly temperature sensitive, and this assumption may be violated at temperatures greater than 550° C (Spear, 1993) making results more complicated to evaluate. But if these requirements can all be met, then the Gibbs method is a powerful tool to model PTt paths. Furthermore, though not discussed here, there are many other exchange reactions which can be used as thermobarometers in exactly the same way if the necessary mineral assemblages are present.

Reference List

Andresen, A., E.H. Hartz, and J. Vold, A late orogenic extensional origin for the infracrustal gneiss domes of the East Greenland Caledonides (72--74 N), *Tectonophysics, 285*, 353-369, 1998.

Andresen, A., and M.G. Steltenpohl, A reevaluation of nappe sequences in the Ofoten-Troms region, north Norwegian Caledonides: Implications for terrane accretion, ophiolite obduction, and polyorogenic evolution, *Tectonophysics, 231*, 59-70, 1994.

Backlund, H.G., Contributions to the geology of Northeast Greenland, *Meddelser om Grønland, 74*, 207-296, 1930.

Berman, R.G., Mixing properties of Ca-Mg-Fe-Mn garnets, *American Mineralogist, 75*, 328-344, 1990.

Burchfiel, B.C., Z. Chen, K.V. Hodges, Y. Liu, L.H. Royden, C. Deng, and J. Xu, *The South Tibetan Detachment System, Himalayan Orogen: Extension Contemporaneous With and Parallel to Shortening in a Collisional Mountain Belt*, 41 pp., Geological Society of America, Boulder, CO, 1992.

Burchfiel, B.C., and L.H. Royden, North-south extension within the convergent Himalayan region., *Geology, 13*, 679-682, 1985.

Burg, J.P., M. Brunel, D. Gapais, G.M. Chen, and G.H. Liu, Deformation of leucogranites of the crystalline Main Central Sheet in southern Tibet (China), *Journal of Structural Geology, 6*, 535-542, 1984.

Caby, R., Investigations on the lower Eleonore Bay group in the Alpefjord region, central East Greenland, *Rapport Grønlands geologiske Undersøgelse, 80*, 102-106, 1976.

Cashman, P.H., Evidence for extensional deformation during a collisional orogeny, Rombak window, North Norway, *Tectonics, 9*, 859-886, 1990.

Chang, R., *Chemistry*, 1046 pp., McGraw-Hill Publishing Co., New York, 1988.

Coker, J.E., M.G. Steltenpohl, A. Andresen, and M.J. Kunk, An 40Ar/39Ar thermochronology of the Ofoten-Troms region: Implications for terrane

amalgamation and extensional collapse of the northern Scandinavian Caledonides, *Tectonics, 14*, 435-447, 1994.

Coleman, M.E., U-Pb constraints on Oligocene-Miocene deformation and anatexis, Marsyandi Valley, central Nepalese Himalaya, *American Journal of Science*, submitted.

Dodson, M.H., Closure temperature in cooling geochronological and petrological systems, *Contributions to Mineralogy and Petrology, 40*, 259-274, 1973.

Faure, G., *Principles of isotope geology*, 282-308 pp., John Wiley & Sons, Columbus, Ohio, 1986.

Ferry, J.M., and F.S. Spear, Experimental calibration of the partitioning of Fe and Mg between biotite and garnet., *Contrib. Mineral. Petrol., 66*, 113-117., 1978.

Gee, D.G., A tectonic model for the central part of the Scandinavian Caledonides, *American Journal of Science, 275A*, 468-515, 1975.

Gee, D.G., M. Lobkowicz, and S. Singh, Late Caledonian extension in the Scandinavian Caledonides; the Roragen detachment revisited, *Tectonophysics, 231*, 139-155, 1994.

Ghent, E.D., Plagioclase-garnet-Al2SiO5-quartz: a potential geobarometer-geothermometer, *Am. Min., 61*, 710-714, 1976.

Gromet, L.P., Direct dating of deformational fabrics, in *Applications of Radiogenic Isotope Systems to Problems in Geology*, edited by L. Heaman and J.N. Ludden, pp. 167-189, Mineralogical Association of Canada, Toronto, 1991.

Guillot, S., and P. Le Fort, Geochemical constraints on the bimodal origin of High Himalayan leucogranites, *Lithos, 35*, 221-234, 1995.

Guillot, S., A. Pêcher, P. Rochette, and P. Le Fort, The emplacement of the Manaslu granite of Central Nepal: field and magnetic susceptibility constraints, in *Himalayan Tectonics*, edited by P.J. Treloar and M.P. Searle, pp. 413-428, Geological Scoiety Special Publication, 47, London, 1993.

Haller, J., Tectonic map of East Greenland (1:500,000). An account of tectonism, plutonism, and volcanism in East Greenland, *Meddelelser om Grønland, 171*, 1-286, 1970.

Haller, J., *Geology of the East Greenland Caledonides*, 413 pp., Interscience Publishers, New York, 1971.

Harris, N., and J. Massey, Decompression and anatexis of Himalayan metapelites, *Tectonics, 13*, 1537-1546, 1994.

Hartz, E., and A. Andresen, Caledonian sole thrust of central East Greenland: A crustal-scale Devonian extensional detachment?, *Geology, 23*, 637-640, 1995.

Hawkins, D.P., and S.A. Bowring, U-Pb systematics of monazite and xenotime: case studies from the Paleoproterozoic of the Grand Canyon, Arizona, *Contributions to Mineralogy and Petrology, 127*, 87-103, 1997.

Henriksen, N., The Caledonides of central East Greenland 70 degrees -76 degrees N, in *The Caledonide Orogen — Scandinavia and Related Areas*, vol. 2, edited by D.G. Gee and B.A. Sturt, pp. 1095-1113, John Wiley & Sons, Chichester, U.K., 1985.

Henriksen, N., and A.K. Higgins, East Greenland Caledonian fold belt, in *Geology of Greenland*, edited by A. Escher and W.S. Watt, pp. 183-246, The Geological Survey of Greenland, Copenhagen, DK, 1976.

Higgins, A.K., J.D. Friderichsen, and T. Thyrsted, Precambrian metamorphic complexes on the East Greenland Caledonides (72° -74° N) - their relationships to the Eleonore Bay Group, and Caledonian orogenesis, *Rapport Grønlands geologiske Undersøgelse, 104*, 1-82, 1981.

Hodges, K.V., Tectonic denudation and anatectic melting in compressional settings, *EOS, 71*, 1618, 1990.

Hodges, K.V., Pressure-Temperature-Time Paths, *Annual Reviews of Earth and Planetary Science, 19*, 207-236, 1991.

Hodges, K.V., Thermodynamics of the Himalayan orogenesis, , submitted.

Hodges, K.V., J.M. Bartley, and B.C. Burchfiel, Structural evolution of an A-type subduction zone, Lofoten-Rombak area, northern Scandinavian Caledonides, *Tectonics, 1*, 441-462, 1982.

Hodges, K.V., B.C. Burchfiel, L.H. Royden, Z. Chen, and Y. Liu, The metamorphic signature of contemporaneous extension and shortening in the central Himalayan orogen: Data from the Nyalam transect, southern Tibet, *Journal of Metamorphic Geology, 11*, 721-737, 1993.

Hodges, K.V., W.E. Hames, W.J. Olszewski, B.C. Burchfiel, L.H. Royden, and Z. Chen, Thermobarometric and $^{40}Ar/^{39}Ar$ geochronologic constraints on Eohimalayan metamorphism in the Dinggyê area, southern Tibet, *Contributions To Mineralogy and Petrology, 117*, 151-163, 1994.

Hodges, K.V., R.R. Parrish, and M.P. Searle, Tectonic evolution of the central Annapurna Range, Nepalese Himalayas, *Tectonics, 15*, 1264-1291, 1996.

Hodges, K.V., and L.H. Royden, Geologic thermobarometry of retrograded metamorphic rocks: an indication of the uplift trajectory of a portion of the northern Scandinavian Caledonides, *Journal of Geophysical Research, 89*, 7077-7090, 1984.

Hodges, K.V., and D.S. Silverberg, Thermal evolution of the Greater Himalaya, Garhwal, India, *Tectonics, 7*, 583-600, 1988.

Hodges, K.V., and F.S. Spear, Geothermometry, geobarometry and the Al_2SiO_5 triple point at Mt. Moosilauke, New Hampshire, *American Mineralogist, 67*, 1118-1134, 1982.

Hollister, L.S., The role of melt in the uplift and exhumation of orogenic belts, *Chemical Geology, 108*, 31-48, 1993.

Hollister, L.S., and M.L. Crawford, Melt-enhanced deformation: A major tectonic process, *Geology, 14*, 558-561, 1986.

Hollister, L.S., R. Kundig, S. Schmid, D. Grujic, T. Pavlis, and C. Davidson, Tectonic transport of heat and melt within the High Himalayan Crystallines of Bhutan, in *10th Himalaya-Karakoram-Tibet Workshop Abstract Volume*, edited by D.A.

Spencer, J.-P. Burg and C. Spencer-Cervato, Mitteilungen aus dem Geologischen Institut der ETH und der Universität Zürich, No. 298, Zürich, 1995.

Hubbard, M.S., and T.M. Harrison, 40Ar/39Ar age constraints on deformation and metamorphism in the Main Central thrust zone and Tibetan Slab, eastern Nepal Himalaya, *Tectonics, 8*, 865-880, 1989.

Inger, S., and N. Harris, Geochemical constraints on leucogranite magmatism in the Langtang Valley, Nepal Himalaya, *Journal of Petrology, 34*, 345-368, 1993.

Koziol, A.M., and R.C. Newton, Grossular activity-composition relationships in ternary garnets determined by reversed displaced-equilibrium experiments, *Contrib. Mineral. Petrol., 103*, 423-433, 1989.

Kretz, R., Symbols for rock-forming minerals, *American Mineralogist, 68*, 277-279, 1983.

Larsen, P.H., and H.J. Bengård, The Devonian basin initiation in East Greenland: A result of sinestral wrench faulting and Caledonian extensional collapse, *Journal of the Geological Society of London, 148*, 355-368, 1991.

Northrup, C.J., and B.C. Burchfiel, Emplacement of the Scandinavian allochthon, Scandinavian Caledonides: A-type subduction, syn-collisional extension, or both?, *Geological Society of America Abstracts with Programs, 25*, A-340, 1993.

Parrish, R.R., and K.V. Hodges, Miocene (22 ±1 Ma) metamorphism and two-stage thrusting in the Greater Himalayan sequence, Annapurna Sanctuary, Nepal, *Geological Society of America Abstracts with Programs, 25*, A174, 1993.

Parrish, R.R., K.V. Hodges, and A. Macfarlane, U-Pb geochronology of igneous and metamorphic rocks near the Main Central Thrust in the Langtang area, central Nepal Himalaya, in *7th Himalaya-Tibet-Karakoram Workshop Abstracts*, edited by M.P. Searle and P.J. Treloar, pp. 67-68, Oxford, U.K., 1992.

Peucat, J.J., D. Tisserant, R. Caby, and N. Clauer, Resistance of zircons to U-Pb resetting in a prograde metamorphic sequence of Caledonian age in East Greenland, *Canadian Journal of Earth Sciences, 22*, 330-338, 1985.

Rex, D.C., A. Gledhill, and A.K. Higgins, Precambrian Rb-Sr isochron ages from the crystalline complexes of inner Forsblads Fjord, East Greenland fold belt, *Rapport Grønlands geologiske Undersøgelse, 85*, 122-126, 1977.

Rex, D.C., and A.R. Gledhill, Isotopic studies in the East Greenland Caledonides (72°-74°N) — Precambrian and Caledonian ages, *Rapport Grønlands geologiske Undersøgelse, 104*, 47-72, 1981.

Rex, D.C., A.R. Gledhill, and A.K. Higgins, Progress report on geochronological investigations in the crystalline complexes of the East Greenland Caledonian fold belt between 72°N and 76°N, *Rapport Grønlands geologiske Undersøgelse, 80*, 127-133, 1976.

Rykkelid, E., and A. Andresen, Late Caledonian extension in the Ofoten area, northern Norway, *Tectonophysics, 231*, 157-169, 1994.

Scalliet, B., M. Pichavant, and J. Roux, Experimental crystallization of leucogranite magmas, *Journal of Petrology, 36*, 663-705, 1995.

Schärer, U., R. Xu, and C. Allegre, U-(Th)-Pb systematics and ages of Himalayan leucogranites, South Tibet, *Earth. Planet. Sci. Lett., 77*, 35-48, 1986.

Searle, M.P., and B.J. Fryer, Garnet, tourmaline, and muscovite-bearing leucogranites, gneisses and migmatites of the Higher Himalaya from Zanskar, Kulu, Lahoul and Kashmir, in *Collision Tectonics: Geological Society of London Special Publication 19*, edited by M.P. Coward and A.C. Ries, pp. 185-201, 1986.

Searle, M.P., R.R. Parrish, K.V. Hodges, A. Hurford, M.W. Ayers, and M.J. Whitehouse, Shisha Pangma leucogranite, South Tibetan Himalaya: Field relations, geochemistry, age, origin, and emplacement, *Journal of Geology, 105*, 295-317, 1997.

Spear, F.S., *Metamorphic Phase Equilibria and Pressure-Temperature-Time Paths*, 799 pp., Mineralogical Society of America, Washington, D.C., 1993.

Spear, F.S., and J. Selverstone, Quantitative P-T paths from zoned minerals: theory and tectonic applications., *Contrib. Mineral. Petrol., 83*, 348-357, 1983.

Stacey, J.S., and J.D. Kramers, Approximation of terrestrial isotope evolution by a two-stage model, *Earth and Planetary Science Letters, 26*, 207-221, 1975.

Steiger, R.H., and E. Jäger, Subcommission on geochronology: convention on the use of decay constants in geo- and cosmochronology, *Earth and Planetary Science Letters, 36*, 359-362, 1977.

Strachan, R.A., Evidence in North-East Greenland for Late Silurian - Early Devonian regional extension during the Caledonian orogeny, *Geology, 22*, 913-916, 1994.

Strachan, R.A., R.E. Holdsworth, J.D. Friderichsen, and H.F. Jepsen, Regional Caledonian structure within an oblique convergence zone, Dronning Louise Land, NE Greenland, *Journal of the Geological Society of London, 149*, 359-371, 1992.

Wegmann, C.E., Preliminary report on the Caledonian orogeny in Christian X's Land (North-East Greenland), *Meddelelser om Grønland, 128*, 145-156, 1935.

Ziegler, P.A., Late Caledonian framework of western and central Europe, in *The Caledonide Orogen — Scandinavia and Related Areas*, vol. 1, edited by D.G. Gee and B.A. Sturt, pp. 3-18, John Wiley & Sons, Chichester, U.K., 1985.